

# UVM ScholarWorks

## **VO(dtpa) Complexes Immobilized on Mesoporous Silica: Structural Characterization and Mechanistic Investigation of Sulfide and Alkene Oxidation Reactions**

Item Type	dissertation;article
Authors	Taft, Jenna R.
Download date	2026-06-07 14:11:33
Link to Item	<a href="https://hdl.handle.net/20.500.14849/4956">https://hdl.handle.net/20.500.14849/4956</a>

VO(dtpa) COMPLEXES IMMOBILIZED ON MESOPOROUS SILICA:  
STRUCTURAL CHARACTERIZATION AND MECHANISTIC  
INVESTIGATION  
OF SULFIDE AND ALKENE OXIDATION REACTIONS

A Dissertation Presented

by

Jenna R. Taft

to

The Faculty of the Graduate College

of

The University of Vermont

In Partial Fulfillment of the Requirements  
for the Degree of Doctor of Philosophy  
Specializing in Chemistry

January, 2019

Defense Date: September 13, 2018  
Dissertation Examination Committee:

Christopher C. Landry, Ph.D., Advisor  
Juan Vanegas, Ph.D., Chairperson  
Matthew D. Liptak, Ph.D.  
Adam C. Whalley, Ph.D.  
Adrian Del Maestro, Ph.D.

Cynthia J. Forehand, Ph.D., Dean of the Graduate College

## ABSTRACT

It was recently shown that V-doped acid-prepared mesoporous silica (APMS) nanoparticles are active catalysts for the oxidation of the mustard gas analogue 2-chloroethyl ethyl sulfide (CEES) under ambient conditions in the presence of aldehydes, using O<sub>2</sub> from air as the oxidation source. However, the vanadium ion leached from the surface when water was present, leading to decreased catalytic activity. Therefore, in this work, the environment around the vanadium is changed, using diethylenetriamine pentaacetic acid (dtpa) as a ligand and anchoring it to the surface of a mesoporous silica nanoparticle, to investigate its effect on vanadium's ability to perform oxidation reactions.

VO(dtpa)-APMS was synthesized by covalently linking the multi-dentate chelator dtpa onto the surface through peptide coupling of one of the acetate groups to aminopropyltriethoxysilane (APTES), condensing the dtpa-APTES molecule onto the mesoporous silica surface, and then exchanging a vanadyl salt into the resulting solid. Physical characterization of the material confirmed that the substrate retained its porosity after modification, and that the vanadium did not leach from the solid, in contrast to samples that did not contain dtpa. Solid-state EPR spectroscopy, combined with ongoing computational modeling, indicated that the vanadium was in a distorted five-coordinate environment.

Various vanadium catalysts have been shown to oxidize alkanes, alkenes, alcohols and aromatic compounds. To further understand the catalyst's ability to perform oxidation reactions, mechanisms of sulfides and alkenes were studied. Two model substrates were chosen for the investigation: CEES and *cis*-cyclooctene. The catalytic system effectively oxidizes CEES at room temperature in less than 15 minutes and *cis*-cyclooctene at 47 °C within 3 hours, using a peroxyacid generated *in situ* as the oxidant source. Kinetic experiments demonstrated that the mechanism of the sulfide reaction changed at higher temperatures, while the alkene reaction did not. In each reaction, a partial negative charge on the peroxyacid during the oxidation process was indicated. The confirmation of radical formation in the mechanism was experimentally shown by the appearance of an induction period when diphenylamine, a radical trap, was introduced into the reaction.

VO(dtpa)-APMS performs two catalytic oxidations: the oxidation of propionaldehyde to make the peroxyacid and the oxidation of alkenes or sulfides. In the first reaction, O<sub>2</sub> binds to the vanadium complex to form a superoxo  $\eta^1$ -bound O<sub>2</sub> radical. This species leads to the formation of peroxyacid through a radical process. The peroxyacid produced in this manner can then react with a sulfide or an alkene in a process also catalyzed by the VO(dtpa) complex. The peroxyacid coordinates with the vanadium center. Upon coordination, the sulfide or alkene directly reacts with the oxygen of the peroxyacid while the peroxyacid is being deprotonated. A 6-coordinate catalyst intermediate is formed prior to the release of the oxidation product and propionic acid to regenerate the VO(dtpa) complex.

## ACKNOWLEDGEMENTS

Thank you to my advisor, Professor Christopher Landry, for all his guidance throughout my time in graduate school. Thank you to my defense committee, especially Professor Adam Whalley for creating an environment where I always felt welcome to ask for help and talk about science.

Thank you to the many members of the Landry group: Dr. Daniel DePuccio for setting an example as the best graduate student; Dr. Alden Clemments for helping me think critically; Dr. Brendon Miller for welcoming into the group and always helping when asked; Michelle DiPinto for always being a sympathetic ear; Bobby Tracy for bringing joy to the group through Disney music and a portable speaker.

Thank you Dr. Morgan Cousins and Dr. Ramya Srinivasan for being my core support! Thank you to the rest of Team Vortex, especially Dr. Robert Miller and soon to be Dr. Matthew Luedtke.

Thank you to my family: Lawrence and Lynn Taft and Lauren, Collin, Bennett and Gavin Fleury. Your understanding of my degree was priceless. Thank you for all the love and support. Most importantly, thank you to my husband **Craig Baden**. Your loving support was incalculable. You enabled me to be the best I could be throughout this time. **I love you.**

## TABLE OF CONTENTS

	Page
ACKNOWLEDGEMENTS .....	ii
LIST OF TABLES .....	vi
LIST OF FIGURES .....	vii
CHAPTER 1: INTRODUCTION .....	1
1.1 Immobilization of Homogeneous Catalysts onto Silica Supports .....	1
1.2 Mesoporous Silica .....	5
1.2.1 Covalent Tethering to Silica Surface .....	8
1.3 Oxidation Reactions Performed by Heterogeneous Vanadium Catalysts .....	11
1.3.1 Sulfide Oxidation .....	11
1.3.2 Oxidation of Alkenes .....	17
1.3.3 Diethylenetriaminepentaacetic acid .....	23
1.4 Instrumental Techniques .....	27
1.4.1 Nitrogen Physisorption .....	27
1.4.2 Electron Paramagnetic Resonance (EPR) .....	29
1.5 References .....	36
CHAPTER 2: VO(dtpa) IMMOBILIZED ON MESOPOROUS SILICA: STRUCTURAL CHARACTERIZATION AND SULFIDE OXIDATION .....	59
2.1 Introduction .....	59
2.2 Experimental Section .....	63
2.2.1 Materials and methods .....	63
2.2.2 Synthesis of Acid Prepared Mesoporous Spheres (APMS) .....	64
2.2.3 Synthesis of dtpa-APMS .....	64
2.2.4 Chelation of Vanadium to dtpa-APMS and exchange vanadium APMS (V-APMS-exch) .....	65
2.2.5 Synthesis of incipient wetness prepared vanadium APMS (V-APMS-incip) .....	65
2.2.6 Catalytic oxidation of sulfide to sulfoxide .....	66
2.2.7 Determination of leaching .....	66
2.2.8 Recycling of the catalyst .....	66
2.3 Results and Discussion .....	67
2.3.1 Physical characterization of materials containing grafted DTPA and vanadyl DTPA complexes .....	67
2.3.2 Comparison of the properties of materials containing grafted vanadyl complexes and exchange vanadium species .....	74

2.3.3	CEES oxidation.....	75
2.4	Conclusion.....	77
2.5	References .....	78
<b>CHAPTER 3: MECHANISTIC INVESTIGATION OF SULFIDE OXIDATION WITH PEROXYACID AND AN IMMOBILIZED VANADYL COMPLEX .....</b>		
3.1	Introduction .....	85
3.2	Experimental Section .....	88
3.2.1	Materials and methods .....	88
3.2.2	Synthesis of Acid Prepared Mesoporous Spheres (APMS) .....	88
3.2.3	Synthesis of dtpa-APMS.....	89
3.2.4	Chelation of vanadium to dtpa-APMS.....	89
3.2.5	Catalytic oxidation of CEES .....	90
3.2.6	Eyring Plot catalysis .....	90
3.2.7	Hammett Plot catalytic experiments .....	91
3.3	Results .....	91
3.4	Discussion .....	97
3.5	Conclusion.....	103
3.6	References .....	105
<b>CHAPTER 4: OXIDATION OF CYCLOALKENES USING VO(dtpa) IMMOBILIZED ON A POROUS SILICA SUBSTRATE .....</b>		
4.1	Introduction .....	115
4.2	Experimental Section .....	118
4.2.1	Materials and methods .....	118
4.2.2	Synthesis of (VO)dtpa-APMS .....	118
4.2.3	Catalytic oxidation of cycloalkene to cycloalkene oxide .....	118
4.2.4	Eyring Plot catalysis .....	119
4.2.5	Hammett Plot catalytic experiments .....	120
4.3	Results and Discussion.....	120
4.3.1	Investigation of reaction mechanism using <i>cis</i> -cyclooctene .....	121
4.3.2	Exploration of the reaction scope using other cyclic alkenes .....	127
4.4	Conclusion.....	131

4.5 References .....	132
CHAPTER 5: CONCLUSIONS .....	140
5.1 Conclusions .....	140
COMPREHENSIVE BIBLIOGRAPHY .....	143
SECTION A. CHAPTER 3 APPENDIX.....	179
A.1 Calculating k for Eyring Plots .....	179
A.2 Calculating k for Hammett Plots .....	180
A.3 Sterics and comparison of sulfide versus sulfoxide .....	181

## LIST OF TABLES

	Page
Table 2.1. Physical Characterization of the Porous Solids .....	70
Table 2.2. Comparison of Physical Properties and Vanadium Retention Capabilities of V-APMS Materials .....	75
Table 2.3. Kinetic Data for the Oxidation of CEES in HFE-7100 Under Ambient Conditions. ....	76
Table 3.1. Entropy and Enthalpy of Reaction.....	95
Table 4.1. Comparison of Reaction Rates for the Oxidation of Various Cycloalkenes ..	128
Table A1. Kinetic Data for Eyring Plot of the Oxidation of CEES Using Aldehyde/O <sub>2</sub> as an Oxidant .....	179
Table A2. Kinetic Data for Eyring Plot of the Oxidation of CEES Using <sup>t</sup> BuOOH as an Oxidant .....	180
Table A3. Kinetic Data for Hammett Plot Data .....	181
Table A4. Steric Effects .....	181

## LIST OF FIGURES

	Page
Figure 1.1. Examples of sol-gel processing. Adapted from ref. 35. ....	5
Figure 1.2 Pathway b represents cooperative self-assembly mechanisms for the synthesis of MCM-41. From ref. 39... ..	7
Figure 1.3. Vanadium Schiff base catalysts on MCM-41 silica supports. Adapted from ref. 104, 98, and 93.. ..	13
Figure 1.4. Novel vanadium catalysts supported on silica for the oxidation of sulfides. Adapted from ref. 100, 97, 92.....	14
Figure 1.5. Mechanism of CEES oxidation using V-APMS and <sup>t</sup> BuOOH. Taken from ref. 54. ....	15
Figure 1.6. Proposed structures of two dtpa complexes of vanadium. From refs 176 and 177.....	26
Figure 1.7. Gas adsorption and desorption during N <sub>2</sub> physisorption measurement.....	28
Figure 1.8. Type IV isotherm derived from N <sub>2</sub> physisorption on mesoporous silica.....	29
Figure 1.9. Diagram showing the splitting of electron spin energies in a magnetic field. Adapted from ref 188.....	31
Figure 1.10. Diagram relating the local symmetry of samples to typical EPR spectra. From ref 189. ....	32
Figure 1.11. Diagram showing the splitting of an electron spin energies ( $M_s = \pm \frac{1}{2}$ $S = \frac{1}{2}$ ) in a magnetic field interacting with a $I = \frac{1}{2}$ nuclear moment. The dotted line represents transitions in the beginning of hyperfine coupling. The blue arrows represent the additional EPR spectrum lines produced.....	33

Figure 1.12. The relative energy levels of 3d orbitals from two common geometries of $\text{Mo}^{5+}$ ( $4d^1$ ). The electron circulations associated with the orbital contributions to each of the three g values are shown by the rings. From ref 189.....	35
Figure 2.1. Scanning electronic microscope (SEM) image of VO(dtpa)-APMS .....	68
Figure 2.2. Characterization of materials by solid-state NMR. (A) $^{29}\text{Si}$ CPMAS NMR spectra of rehydrated APMS (red) and the same material after dtpa silane was grafted (blue). (B) $^{13}\text{C}$ CPMAS NMR spectrum of the grafted material (blue) and pure dtpa (green).....	71
Figure 2.3. EPR spectra of the immobilized VO(dtpa) complex. The experimental data is shown in black, and the simulated spectrum used to derive g and A tensors is shown in green. Tensors calculated from EasySpin: $g_{\perp} = 1.98$ , 1.99, $g_{\parallel} = 1.93$ ; $A_x = -200.8$ , $A_y = -71.43$ , $A_z = -515.4$ . .....	73
Figure 2.4. Potential geometry of VO(dtpa) based on computational studies .....	74
Figure 2.5. Progress of the oxidation of CEES using VO(dtpa)-APMS as the catalyst, monitored by gas chromatography. R is an internal reference and * is an impurity.....	76
Figure 3.1. Radical trap experiments using diphenylamine.....	93
Figure 3.2. Eyring Plot from kinetic temperature runs of the oxidation of CEES with a. aldehyde/ $\text{O}_2$ as oxidant b. $^t\text{BuOOH}$ as oxidant. ....	95
Figure 3.3. Hammett Plot for methyl phenyl sulfide, 4-fluorophenyl methyl sulfide, 4-bromophenyl methyl sulfide, and 4-methoxythioanisole .....	97
Figure 4.1 a. Eyring Plot of <i>cis</i> -cyclooctene oxidation using VO(dtpa)-APMS <i>in situ</i> generated peroxyacid. b. Hammett Plot for 4-methoxystyrene, p-methylstyrene, 4-fluorostyrene, and styrene.....	123
Figure A1. The oxidation of diphenyl sulfide (blue) versus the oxidation of diphenyl sulfoxide (grey).....	181

## CHAPTER 1: INTRODUCTION

### 1.1 Immobilization of Homogeneous Catalysts onto Silica Supports

More than 85% of chemical products are made using catalysts. Therefore, developing new catalytic systems and understanding catalytic mechanisms is of vital importance to the field of chemistry.<sup>1,2</sup> A catalyst is a substance that increases the rate of a chemical reaction without itself being consumed.<sup>3</sup> There are two types of catalysts: homogeneous and heterogeneous. A homogeneous catalyst is a catalyst that is soluble in the reaction mixture, or the catalyst is in the same phase as the reactant. One of the oldest examples of a homogeneous catalyst that is still used commercially is  $\text{HCo}(\text{CO})_4$  for hydroformylation.<sup>4</sup> The process consists of reacting terminal alkenes with hydrogen gas at high pressure and the resulting products are aldehydes.<sup>4</sup> A heterogeneous catalyst is a catalyst that is of a different physical state than the chemical reactants it is catalyzing. An example of a heterogeneous catalyst that is used in industrial manufacturing is  $\text{Fe}_3\text{O}_4$  on  $\text{Al}_2\text{O}_3$  supports for the Haber-Bosch process,  $\text{NH}_3$  synthesis.<sup>3,5</sup> For industrial manufacturing, heterogeneous catalysts are often preferred over homogeneous ones. Heterogeneous catalysts are used in 80-85 % of industrial processes.<sup>6</sup> The main drawback to the use of homogeneous catalysts in large-scale industrial processes is that they cannot be easily recycled or separated from the products.<sup>1,7,8</sup> In contrast, using heterogeneous catalysts leads to decreased solvent purification waste,<sup>9,10</sup> and they can be used in continuous flow operations manufacturing.<sup>1</sup>

It is possible to combine the desirable properties of homogeneous and heterogeneous catalysts by "heterogenizing" homogeneous catalysts; that is, by

immobilizing a homogeneous catalyst onto an inert solid support.<sup>11</sup> Because heterogeneous catalytic reactions occur at the solid surface, in many cases the solid support is highly porous or consists of nanoparticles, to maximize the surface area and therefore, the reactivity of the overall process. Examples include zeolite Y,<sup>12</sup> boehmite nanoparticles,<sup>13</sup> carbon nanotubes,<sup>14</sup> mesoporous carbon,<sup>15</sup> graphene oxide,<sup>16</sup> magnetic nanoparticles,<sup>17</sup> polymers,<sup>18</sup> silica gel,<sup>19</sup> and mesoporous silica.<sup>10,20-22</sup>

The most common ways to immobilize homogeneous catalysts are adsorption, encapsulation, electrostatics, and covalent tethering.<sup>7</sup> A recent example of the adsorption method was demonstrated by Brookhart, Goldman, and Scott.<sup>23</sup> Iridium chelated with the pincer ligands 1,3,5-tri(<sup>t</sup>butylphosphinite)benzene and 1,3-bis[di(<sup>t</sup>butyl)phosphinomethyl]-5-dimethylaminobenzene was adsorbed onto the surface of commercially purchased  $\gamma$ -Al<sub>2</sub>O<sub>3</sub>, which has Lewis acidic sites. By using ligands with pendant basic functional groups, the complexes could adsorb to the surface through Lewis acid/base interactions. The immobilized iridium pincer complex was found to be a very active heterogeneous catalyst, with turnover numbers of up to 7000 for the transfer of hydrogen from cyclooctane to <sup>t</sup>butylethylene.<sup>23</sup>

Encapsulation is also referred to as the “ship in a bottle” method, and is often used when the support is porous with small pore openings and larger internal cavities, as is the case with many zeolites.<sup>24</sup> Ichihashi synthesized a copper catalyst through an encapsulation method with zeolite Y for the oxidation of benzene with molecular oxygen.<sup>25</sup> An ion exchange with Cu<sup>2+</sup> and zeolite Y was the first step of the synthesis. The copper zeolite material was then reacted with the ligands picolinic acid, 2-pyridin carbonic acid or

quinaldic acid. The copper complex that forms inside the pore is too large to diffuse out of the zeolite. These catalysts successfully oxidized benzene to phenol with molecular oxygen, and produced more phenol than copper zeolites prepared through simple ion exchange, due to the retention of copper in the encapsulated catalyst.<sup>25</sup>

An example of the immobilization of a homogeneous catalyst by electrostatics can be seen in work by Stanford, in which a catalyst for the hydrogenation of 1-octene was developed.<sup>26</sup> The solid support was a metal-organic framework, ZJU-28 (ZJU-28 =  $(\text{Me}_2\text{NH}_2)_3[\text{In}_3(\text{BTB})_4] \cdot 12 \text{ DMF} \cdot 22 \text{ H}_2\text{O}$ , where BTB = 1,3,5-Tris(4-benzoate) benzene).<sup>27</sup> A rhodium complex,  $[\text{Rh}(\text{dppe})\text{COD}]\text{BF}_4$  (dppe = 1,2-bis(diphenylphosphino)ethane; COD = 1,5-cyclooctadiene) was bound to the solid through ion exchange with  $\text{H}_2\text{NMe}_2^+$  remaining in the support material due to synthesis.<sup>26</sup> The heterogeneous catalyst outperformed the support-free catalyst in the reduction of 1-octene using  $\text{H}_2$ , which was attributed to the enhanced stability of the heterogeneous catalyst. For example, the heterogeneous catalyst was recycled four times with minimal loss of activity.<sup>26</sup>

Covalent tethering is often performed by using a silane as a "linker" between the solid support and a transition metal complex that will act as the catalyst.<sup>7</sup> Any number of traditional chemical reactions, including peptide bond formation, sulfide bridge formation, "click" chemistry, or others can be used in the attachment (also called "grafting") process. Obviously, the selection of a robust bond formation reaction relative to the catalytic conditions that will be used is a primary consideration. An interesting example of covalent tethering is work done by Baïke, Dong and Soo.<sup>28</sup> They designed a versatile anchoring

strategy in which they "photoclicked" (photochemically grafted by UV radiation) maleimide groups from salicylaldehyde ligands used to complex  $\text{Ni}^{2+}$  onto solid oxide supports by reaction with surface hydroxyl groups.<sup>28</sup> The solid supports were  $\text{SiO}_2$ ,  $\text{TiO}_2$ ,  $\text{CeO}_2$ , and  $\text{WO}_3$  nanoparticles. These catalysts oxidized alkenes with  $\text{NaClO}$  as an oxidant. As an example of their reactivity, after 5 hours, the  $\text{Ni}^{2+}$  complex supported on  $\text{TiO}_2$  oxidized 84% of *cis*-cyclooctene to cyclooctene oxide with 42% selectivity towards the epoxide product.

Mesoporous silica is a desirable support material because it is low-cost and easy to synthesize, has high thermal stability,<sup>29</sup> is optically transparent,<sup>29</sup> and more robust than polymer supports in organic solvents.<sup>22</sup> "Mesoporous" implies pore diameters between 20 and 500 Å, which are large enough to allow many catalysts to be immobilized in the pores and to allow significant molecular diffusion (unlike microporous silica such as zeolites, with pore diameters less than 20 Å),<sup>30</sup> but are still small enough to provide significant surface area (unlike macroporous silica, with pore diameters larger than 500 Å).<sup>31</sup> For reasons that will be explained later in this chapter, the pore diameters of mesoporous silica can be controlled by the choice of reactants and by synthetic conditions, allowing the accommodation of a variety of catalysts.<sup>32</sup> Although all four of the above immobilization methods have been used with mesoporous silica supports, covalently anchoring catalysts within the pores of silica is a preferable option because it inhibits leaching of the catalyst into the reaction system and it enables more synthetic control of the amount of catalyst loaded onto the support.<sup>22</sup> This gives an additional measure of synthetic control of the catalytic process.

## 1.2 Mesoporous Silica

Mesoporous silica is prepared by a precipitation method based on sol-gel synthesis, and it typically produces a micro or nanoparticulate material. Sol-gel synthesis was first described by Graham's work on the properties of silicic acid.<sup>33</sup> The term sol-gel is derived from the term sol, which is used to describe a colloidal dispersion of particles in a liquid, and gel, which is used to describe a substance that contains a continuous solid skeleton enclosing a continuous liquid phase.<sup>34</sup> Thus, drying of sols produces gels. In general, the sol-gel synthetic process consists of dispersion of a metal alkoxide precursor into an aqueous solution, where it undergoes hydrolysis and condensation to form a stable colloidal suspension (a sol). At this point, processing the sol into various forms followed by drying leads to a variety of materials, such as bulk solid, powders, fibers, thin films, and others (Figure 1.1).<sup>34,35</sup>

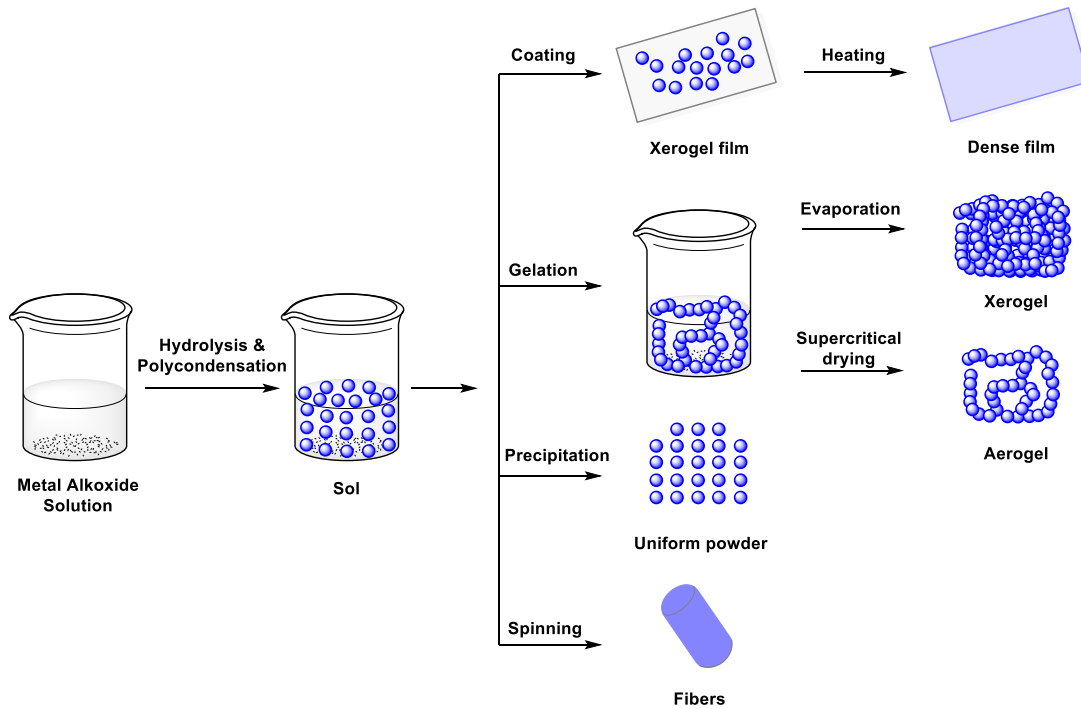
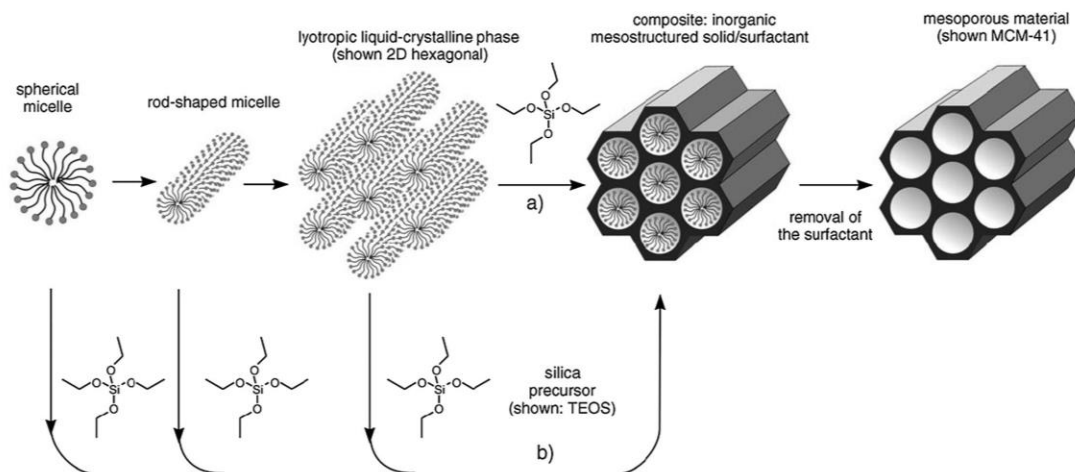


Figure 1.1. Examples of sol-gel processing. Adapted from ref. 35.

Much of modern silica nanoparticle synthesis grew from the foundation laid by Stöber,<sup>36</sup> who first showed how to synthesize spherical silica nanoparticles from colloidal solutions with high monodispersity and flexible control of particle size.<sup>36</sup> Uniformity and shape are often important aspects of a heterogeneous catalyst because different surface sites can display different catalytic activity;<sup>37</sup> thus, controlling properties is important when preparing supports for heterogeneous catalytic processes.

Mesoporous silica was first defined in 1992, after the synthesis of the "MCM" family of porous solids prepared at Mobil Corporation.<sup>38</sup> These materials are synthesized through a combination of a sol-gel process and a templating process called liquid crystal templating (**Figure 1.2**).<sup>39</sup> Both Stöber particles and MCM porous materials are made by the base catalyzed hydrolysis of silicate monomers.<sup>36,38,40</sup> Unlike the Stöber method, where small nuclei of silica are rapidly formed and then particle growth continues by condensation,<sup>41</sup> liquid crystal templating consists of metal alkoxide precursors condensing around cationic surfactant micelles. For the synthesis of the MCM-41, the surfactant micelles and the silicate anions undergo cooperative self-assembly,<sup>42,43</sup> in which the self-assembly of the rod-shaped micelles is mediated by the presences of silicate anions (**Figure 1.2**).<sup>42,44</sup>



**Figure 1.2.** Pathway b represents cooperative self-assembly mechanisms for the synthesis of MCM-41. From ref. 39.

If the surfactant to silica ratio is increased, two other materials of the MCM family can be produced: cubic (MCM-48) and lamellar (MCM-50).<sup>42,45</sup> The pore structure of these materials is very regular and the pore size distribution is quite narrow, as with zeolites, but the pores are significantly larger, with diameters between 20 and 100 Å.<sup>45</sup> MCM-41 consists of non-intersecting unidirectional hexagonal pore channels.<sup>46</sup> The largest pore diameter that can be reasonably prepared by the MCM synthesis method limited by the size of the surfactant; adding "swelling agents" such as mesitylene, which enlarges the micelle diameter during synthesis, is limited in utility due to thermal and solubility considerations. Several years after MCM materials were prepared, a related family of mesoporous materials were prepared at the University of California at Santa Barbara.<sup>47</sup> These materials, called "SBA" materials, have much larger pore diameters than MCM materials due to the use of ether triblock copolymers as pore templating agents during synthesis. They have pore diameters from approximately 40 to 300 Å.<sup>45</sup> In contrast to MCM materials and

materials prepared by the Stöber method, SBA materials are prepared in acidic solution, which is necessary to protonate the ether polymers and provide an electrostatic interaction with the growing silica colloidal network.

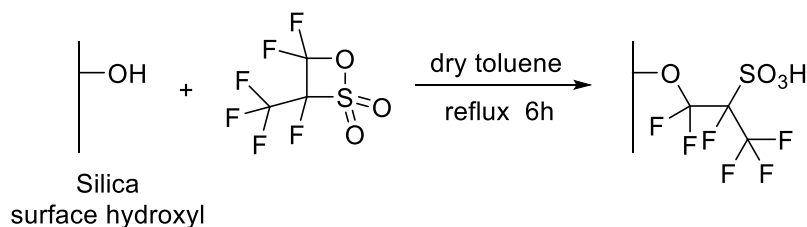
One problem with using acidic conditions for the synthesis of silica is that it is difficult to control the morphology and monodispersity of the resulting solid, as is observed in the synthesis of SBA materials. In 1999, Acid Prepared Mesoporous Spheres (APMS) were developed by Landry.<sup>48,49</sup> The pores of APMS have a narrow size distribution, and the particles are reasonably monodisperse and spherical with diameters between 0.5 and 5  $\mu\text{m}$ . Initially, the materials were used both as catalyst supports and as packing materials for HPLC techniques, particularly chiral HPLC where the narrow pore size distribution gave a significant advantage over traditional macroporous HPLC packing materials.<sup>49,50</sup>

Although it was initially designed as a catalyst and catalytic support,<sup>51-55</sup> mesoporous silica is increasingly being used in other applications such as drug delivery,<sup>56-60</sup> molecular adsorption,<sup>61-63</sup> and biomedical imaging.<sup>64,65</sup>

### 1.2.1 Covalent Tethering to Silica Surface

Silica is a highly versatile material for many applications because it is simply and easily modified with a variety of organic moieties. There are several ways to graft organic materials to silica. One example is the chlorination of the surface hydroxyls with carbon tetrachloride or sulfuryl chloride.<sup>66</sup> From the chlorinated surface, Grignard reagents can be used to attach many different functional groups.<sup>66</sup> For example, fluorinated sultones (i.e. 1,2,2-trifluoro-2-hydroxy-1-trifluoromethylethane sulfonic acid sultone) have been shown to form covalent bonds with surface silanols through sultone ring opening (**Scheme 1.1**).<sup>67</sup>

The drawback of this method is that hydrolysis can occur at the Si-O-CF<sub>2</sub> bond.<sup>67,68</sup> Chlorosilanes can be used in the presence of a base to afford a Si-O-Si connection between the silane and the silica surface; similarly, disilazanes react with silanol groups to form bonds with the surface. However, both types of silanes must be handled in air- and water-free environments, limiting their practical utility.



**Scheme 1.1.** Sultone reaction with silica surface hydroxyls. Taken from ref. 67.

Trialkoxysilanes are by far the simplest and most common compounds used for modification of the silica surface.<sup>66,68,69</sup> They are stable and simple to use, and are available with a variety of organic functionalities. Much like the process by which silica itself can be prepared by condensation with tetraalkoxysilanes, trialkoxysilanes react with surface silanol groups on the nanoparticles at advanced temperatures to form Si-O-Si bonds and release alcohol. Trialkoxysilanes can also be simply added to the initial reaction mixture used to form the nanoparticles themselves, condensing throughout the nanoparticles in a co-condensation process. Although simpler and easier, there is less control over the location and loading of the silane groups within the nanoparticle, and the surfactant template must be removed by extraction, which is often incomplete. Whatever the method of attachment, alkoxy silanes are available for a range of attachment processes. For

example, (3-aminopropyl)triethoxysilane (APTES) yields amine groups that can be used in subsequent peptide or urea bond-forming reactions.<sup>70</sup> Condensation of (3-mercaptopropyl)trimethoxysilane (MPTMS) gives a thiol-terminated surface that is useful for reactions with other thiols to form reversible disulfide bonds, or with maleimides to make permanent sulfide attachments. Azido and alkynyl silanes can participate in click reactions to attach organic groups,<sup>71</sup> and silanes terminated with glycidyloxy groups can participate in epoxide ring opening reactions.<sup>69</sup>

Using a trialkoxysilane as the grafting agent lends flexibility to the synthetic process. For example, the silane could be grafted to the silica nanoparticle, and then a fully complete metal complex could be connected to the surface through it. Alternatively, the complex could be attached to the silane first, and then the silane-bound complex could be condensed onto the nanoparticle. It is also possible to react just the ligands of the catalytic complex with the silane (either before or after grafting), inserting the metal after the ligands have been attached. The benefit of using one method over another depends on the features of the catalytic system—the catalyst loading desired, pore diameter, solvent, etc. For example, for the reactions described in this dissertation, we determined that the best method for our reactions is to first attach the ligand to the trialkoxysilane and condense it to the surface in a second step. The metal was bound to the ligand in a final step, yielding the fully catalytic material. A prime consideration was that an aminosilane/peptide bond strategy was being used and the peptide bond formation was incomplete. This meant that if the aminosilane was grafted first, there were a large number of unreacted amine groups

remaining on the nanoparticle surface that could bind the metal and participate in unwanted side reactions during the catalytic process.

### 1.3 Oxidation Reactions Performed by Heterogeneous Vanadium Catalysts

Since the early 1900s, catalysts containing vanadium have been shown to catalyze many chemical reactions. Complexes containing the vanadyl (V=O) group are of particular focus in oxidation of a variety of structures, such as alkanes, alkenes, alcohols, sulfides, and aromatic compounds, and they can also perform halogenations and carboxylations.<sup>72-74</sup> While much of this work involved homogeneous systems,<sup>75-81</sup> two types of vanadium-based heterogeneous catalysts have been identified. The first type includes traditional heterogeneous catalysts, in which vanadium is part of, or is the main component of, the solid itself.<sup>53-55,82-91</sup> The second type is a hybrid catalyst in which the vanadium is attached to a solid support through organic linkers.<sup>13,16,17,92-101</sup> The vanadium in the latter type could be ionic, or it could be complexed.

#### 1.3.1 Sulfide Oxidation

The catalytic oxidation of sulfides ( $R_2S$ ) to sulfoxides ( $R_2SO$ ) and sulfones ( $R_2SO_2$ ) by vanadium is of general chemical interest. For example, asymmetric sulfide oxidation, an oxidation technique in which the desired products are enantiomerically pure sulfoxides, is useful in synthetic organic chemistry,<sup>93,94,102,103</sup> and oxidation of sulfides is also important in the pharmaceutical<sup>100</sup> and petrochemical industries.<sup>104,105</sup> The toxic character of some chemicals, such as bis(2-chloroethyl)sulfide, also called sulfur mustard or mustard gas, can be eliminated by vanadium-catalyzed sulfur oxidation.<sup>53-55,106-110</sup> Most of the

research on heterogeneous catalysts for sulfide oxidation has been focused on their usefulness in environmentally friendly chemical systems for industry.<sup>82,85,87,92,95-98</sup>

There are some interesting examples of heterogeneous vanadium catalysts with mesoporous silica supports. There are a few examples of vanadium Schiff base catalysts supported on MCM-41.<sup>94,98,104</sup> The Schiff base ligands for these catalysts were salicylaldehyde,<sup>104</sup> 3,4-dihydroxybenzaldehyde,<sup>98</sup> and a modified 2,6-diformyl-4-<sup>t</sup>butylphenol<sup>94</sup> (**Figure 1.3**). Each Schiff base was covalently tethered to amine functionalized MCM-41. All three examples used a VO<sup>2+</sup> vanadium source, either VO(acac)<sub>2</sub><sup>98,104</sup> or VOSO<sub>4</sub> • 4 H<sub>2</sub>O.<sup>94</sup> In one study, H<sub>2</sub>O<sub>2</sub>, <sup>t</sup>BuOOH, and cumene hydroperoxide (CHP) were all investigated as oxidants.<sup>94</sup> At room temperature using H<sub>2</sub>O<sub>2</sub> as the oxidant, the oxidation of methyl phenyl sulfide was 65% complete after 6 hours, with 88% selectivity for the sulfoxide over the sulfone. CHP was a more active oxidant, giving a 95% yield and 98% sulfoxide selectivity after 6 hours at room temperature. In the second reaction cycle, the yield dropped to 73% with 70% sulfoxide selectivity; therefore, it was evident that more work needed to be done to optimize recyclability. The catalyst in one of the other studies, showed improved recyclability, with a loss of only 10% in yield after 5 cycles.<sup>98</sup> This catalytic system used urea hydrogen peroxide and was 95% complete after 8 hours.

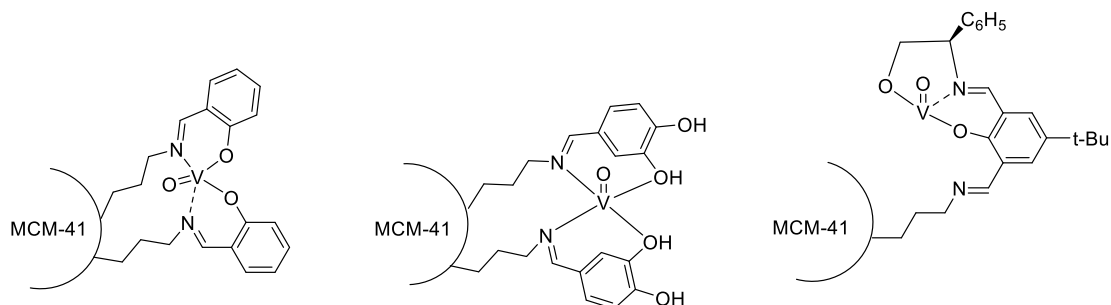


**Figure 1.3.** Vanadium Schiff base catalysts on MCM-41 silica supports.  
Adapted from ref. 104, 98, and 93.

Three examples of non-Schiff base vanadium catalysts supported on silica are novel catalysts using modified chitosan,<sup>100</sup> L-cysteine<sup>97</sup> and 2-amino-2-methyl-1,3-propanediol<sup>92</sup> as ligands (**Figure 1.4**). Nikoorazm<sup>97</sup> and Tamoradi<sup>92</sup> both used  $\text{VO}^{2+}$  sources, specifically  $\text{VO}(\text{acac})_2$ . Shen used  $\text{NH}_4\text{VO}_3$  as a vanadium source.<sup>100</sup> All three examples optimized reaction conditions with methyl phenyl sulfide and  $\text{H}_2\text{O}_2$  as the main oxidant. Of the conditions investigated for Shen's catalyst, a mixture of methanol and water afforded the best catalysis at room temperature, yielding 86% methyl phenyl sulfoxide after 12 hours. If the reaction was cooled to 0 °C and acetic acid was added, the yield increased to 93%. The increase in yield was due to better solubility of the reactants with the acetic acid. The catalyst was recycled up to 5 times with only a 3% loss in yield.<sup>100</sup> Tamoradi's catalyst is more active than Shen's, producing 98% yield of methyl phenyl sulfoxide after 55 min, solvent-free with  $\text{H}_2\text{O}_2$  as the oxidant. The catalyst was able to be recycled 4 times with no loss in yield.<sup>92</sup> Finally, Nikoorazm's catalyst is more active than both Tamoradi's and Shen's with a 98% yield of methyl phenyl sulfoxide after 35 min. The reaction was run neat and  $\text{H}_2\text{O}_2$  (30% in  $\text{H}_2\text{O}$ ) was added. The catalyst was recycled 7 times with only a 5% loss in yield.<sup>97</sup>

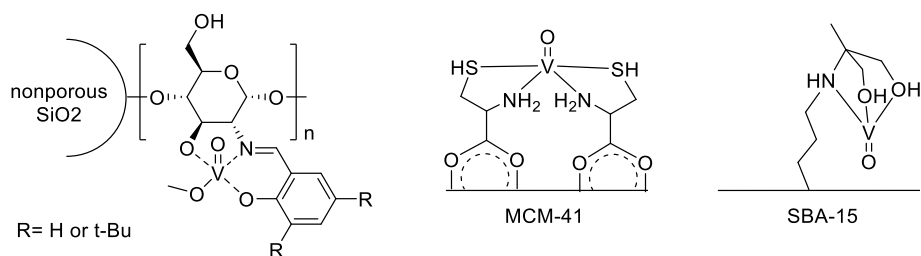


**Figure 1.4.** Novel vanadium catalysts supported on silica for the oxidation of sulfides. Adapted from ref. 100, 97, 92.

The Landry group recently developed a heterogeneous system for sulfide oxidation using vanadium-doped mesoporous silica nanoparticles, <sup>t</sup>BuOOH as the oxidant, and perfluorobutyl methyl ether (Novec™ 7100 Engineered Fluid, "HFE-7100") as the solvent.<sup>53-55</sup> This solvent was used because it readily solubilizes many chemicals that may be contaminants in commercial materials without damaging the materials themselves. The substrate used in testing this system was the mustard gas analogue 2-chloroethyl ethylsulfide (CEES or "half mustard"). The catalyst was prepared using the incipient wetness technique, with (NH<sub>4</sub>)VO<sub>3</sub> as the vanadium source and APMS as the inert support.<sup>54</sup> In a mechanistic study (**Figure 1.5**),<sup>54</sup> <sup>t</sup>BuOOH was found to bind in an η<sup>2</sup> manner, with a dative bond to the alkane oxygen. The sulfide attacked the terminal oxygen directly, without interacting with the vanadium atom itself. While the sulfoxide (CEESO) could also perform the same reaction, its interaction with the bound <sup>t</sup>BuOOH was much slower, so that in effect all of the sulfide in the system was consumed before the sulfoxide was converted to the sulfone (CEESO<sub>2</sub>).

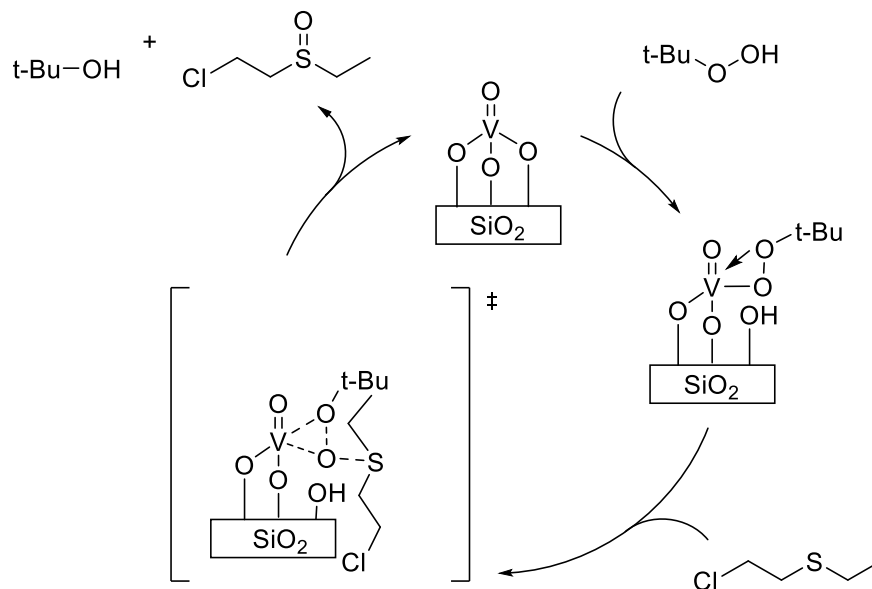
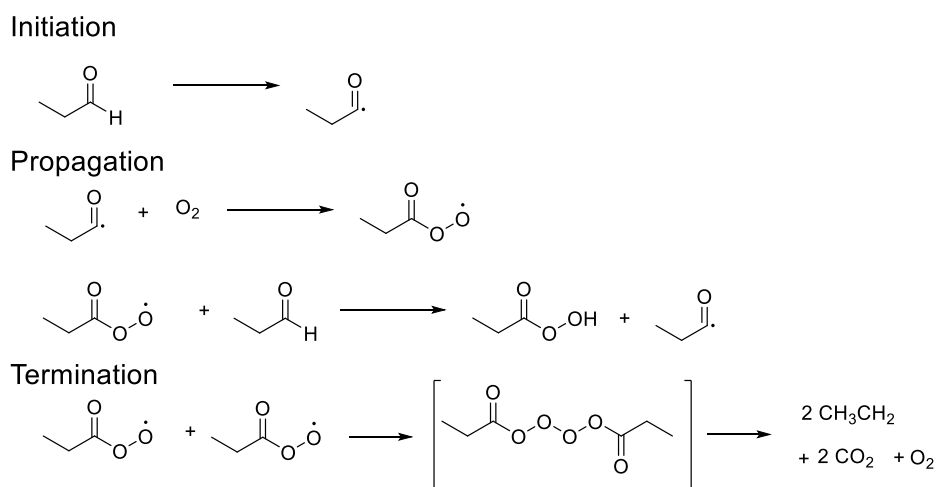


**Figure 1.5.** Mechanism of CEES oxidation using V-APMS and <sup>t</sup>BuOOH.  
Taken from ref. 54.

While oxidation of CEES with <sup>t</sup>BuOOH was effective, in a real world setting, using <sup>t</sup>BuOOH is not realistic due to its purchase and transportation costs. H<sub>2</sub>O<sub>2</sub> can be transported at weight percents below 3-8%, but transporting it at such low concentrations is also cost-prohibitive relative to the required reactivity, and although H<sub>2</sub>O<sub>2</sub> is also available at 30 wt%, it is considered hazardous at this concentration and has associated higher transportation costs. Additionally, it was found that when water was present in the V-APMS catalytic system, the vanadyl ion leached from the solid, leading to unwanted side reactions and significantly decreased reactivity. Consequently, other oxidants were tested as replacements for peroxides. Interestingly, the group found that aldehydes, either dissolved in HFE-7100 or used neat, served as an effective replacement for <sup>t</sup>BuOOH as the oxidant in this system.<sup>53</sup>

Depending on their conditions and chemical properties, aldehydes can undergo autoxidation with O<sub>2</sub> to form peroxyacid radicals and/or peroxyacids, as shown in **Scheme 1.2**.<sup>111,112</sup> The important step is the formation of an acyl radical, which then reacts with O<sub>2</sub> to form the peroxyacid radical. In general, this step is slow and thus aldehyde autoxidation does not take place to an appreciable extent under normal conditions. When a metal is present, it can catalyze this process and increase the rate of peroxyacid formation in two ways. For example, the metal can directly abstract the aldehyde hydrogen to produce the acyl radical, or it can bind O<sub>2</sub> and form metal-bound O<sub>2</sub> radicals, which then abstract the aldehyde hydrogen to form the acyl radical in a more indirect process.<sup>112,113</sup>



**Scheme 1.2.** Proposed mechanism of aldehyde autoxidation.

With this background, it was proposed that V-APMS was playing a dual catalytic role: first, it catalyzed the oxidation of aldehyde to peroxyacid, and then it used the peroxyacid generated *in situ* to catalytically oxidize CEES. Other examples of metal ions or metal oxides using *in situ* generated peroxyacid in sulfide oxidation include Co<sub>3</sub>O<sub>4</sub>,<sup>114</sup> Fe<sub>2</sub>O<sub>3</sub>,<sup>115</sup> MnO<sub>2</sub>,<sup>114,115</sup> Co<sup>2+</sup>,<sup>116,117</sup> Mn<sup>2+</sup>,<sup>117</sup> Ni<sup>2+</sup>,<sup>117</sup> Cu<sup>+</sup>,<sup>117</sup> or Cu<sup>2+</sup><sup>115</sup> as metal catalysts. In

terms of vanadium-catalyzed aldehyde oxidation, there are very few examples. Heteropolyacids with the general formula  $H_{3+n}[PMo_{12-n}V_nO_{40}] \cdot H_2O$  ( $n = 2, 3, 8$ ) have been shown to form peroxyacids from aldehydes using  $O_2$  as the oxidant.<sup>118</sup>

One problem with the previously reported system using V-APMS was that because the vanadium was distributed onto the porous silica support by ion exchange and calcination, under humid conditions or when water was a contaminant, the vanadium would leach from the solid, leading to decreased or no catalytic activity. Therefore, in this work, the environment around the vanadium is changed, using diethylenetriamine pentaacetic acid (dtpa) as a ligand and anchoring it to the surface of a mesoporous silica nanoparticle, to investigate its effect on vanadium's ability to perform oxidation reactions.

In addition to being useful for sulfide oxidation, the *in situ* generation of peroxyacids from aldehydes can also be used to oxidize alkenes, which makes the process more useful in synthetic organic chemistry. For example,  $Fe(AAEMA)_3$  (AAEMA = 2-(methacryloyloxy)ethyl acetoacetate) can oxidize a variety of alkenes using a sacrificial aldehyde and molecular oxygen.<sup>119</sup> Other examples of catalysts for alkene oxidation using *in situ* generated peroxyacid include cyclam complexes of  $Mn^{2+}$ ,  $Fe^{2+}$ ,  $Co^{2+}$ ,  $Cu^{2+}$ ,<sup>120</sup> as well as  $Mn^{3+}$  Schiff base complexes (derivations of salen ligands [salen = 2,2'-Ethylenebis(nitrilomethylidene)diphenol]),<sup>121</sup>  $Cu(OH)_2$ ,<sup>122</sup> and a silica-supported Ru catalyst.<sup>123</sup>

### 1.3.2 Oxidation of Alkenes

The formation of epoxides from alkenes is of interest due to the value of epoxides as intermediates in organic synthesis<sup>124</sup> and industrial chemistry.<sup>125</sup> Importantly, large-

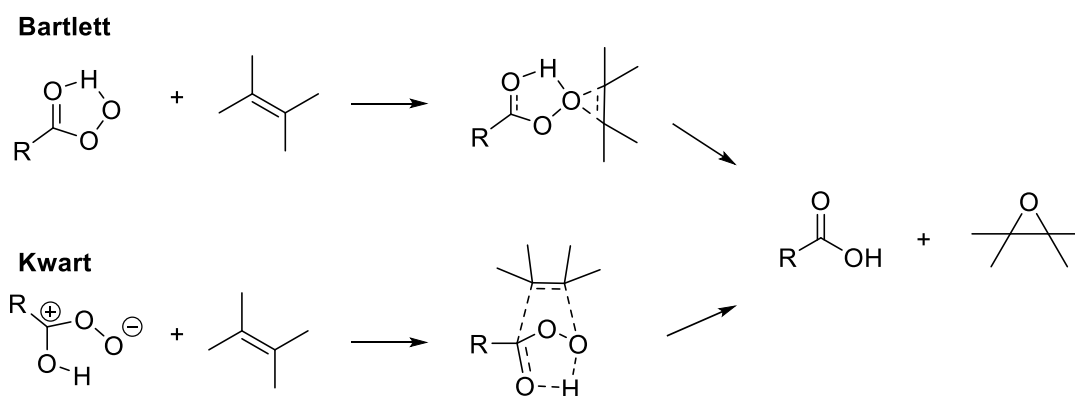
volume chemical products such as poly(ester)s and ethylene glycol are produced by processes involving epoxides.<sup>126</sup>

There are a few inorganic-organic hybrid vanadium catalytic systems that exist with silica supports. One example is a VO(acac)<sub>2</sub> covalently tethered to amine functionalized MCM-41.<sup>10</sup> The catalyst oxidized a variety of alkenes with <sup>t</sup>BuOOH as its oxidant and for comparison, it oxidized 90% of *cis*-cyclooctene, after 24 hours, at 60 °C.<sup>10</sup> Another example is a covalently tethered hydrazine Schiff base (derived from salicylaldehyde and benzhydrazide) on silica gel.<sup>19</sup> The Schiff base was tethered by reacting the carbonyl group on the base with an amine silane which was then grafted onto the silica gel.<sup>19</sup> The system used H<sub>2</sub>O<sub>2</sub> as an oxidant and sodium bicarbonate as co-catalyst in acetonitrile.<sup>19</sup> A variety of alkenes were investigated and the reactions took place at reflux (80 °C).<sup>19</sup> After 5 hours, 96% of *cis*-cyclooctene was oxidized.<sup>19</sup> Therefore, although the reactions were completed at elevated temperatures, the hydrazine Schiff base vanadium catalyst performed better than the immobilized VO(acac)<sub>2</sub> complex based on *cis*-cyclooctene. A final example is a Schiff base derived salicylaldehyde and diethylenetriamine covalently tethered to chloropropyl modified MCM-41.<sup>20</sup> The oxidant in this system is H<sub>2</sub>O<sub>2</sub> as an oxidant and sodium bicarbonate as co-catalyst.<sup>20</sup> After 8 hours, at room temperature, 82% *cis*-cyclooctene was oxidized.<sup>20</sup> Although this catalyst took longer than the hydrazine Schiff base complex, it was completed at room temperature and therefore a better system due to its mild conditions.

Two examples of reactions between peroxyacids and alkenes have been shown, although these examples do not involve metals. Bartlett has proposed a mechanism with a

five-membered ring in the transition state connected through the terminal oxygen atom of the acid and including the acidic hydrogen (**Scheme 1.3**).<sup>127,128</sup> Kwart proposed that the peroxyacid forms a zwitterion, which forms a transition state containing two fused five-membered rings.<sup>128</sup> There has been little work studying metal catalyzed oxidations of alkenes using peroxyacids, but there have been a few studies in which *in situ* generated peroxyacids have been used. These studies were briefly discussed in the previous section. Of the studies that provide insight into the mechanism of peroxyacid metal catalyzed oxidation of alkenes, the most similar to a vanadium based system is the investigation of transition metal cyclam complexes.<sup>120</sup> The catalytic oxidation of cyclohexene by  $\text{Mn}(\text{cyclam})^{2+}$  was investigated using isobutyraldehyde and  $\text{O}_2$  in acetonitrile. After 4 hours, the reaction yielding 33% cyclooctene oxide for  $\text{Mn}(\text{cyclam})^{2+}$  and 13% yield without a metal complex. This led to further investigation into how much the metal center is really participating in the oxidation. Geometric isomers of stilbene were investigated to deduce the participation of the metals. Peroxyacids are known to epoxidize *cis*-stilbene stereoselectively to give only the *cis*-stilbene oxide as product.  $\text{Mn}(\text{cyclam})^{2+}$  and  $\text{Mn}(\text{acac})_2$  both produced mixtures of *cis*-stilbene oxide and *trans*-stilbene oxide with the  $\text{O}_2$ /aldehyde system. This demonstrated the ligand does not affect the oxidation. In contrast, other metal complexes  $\text{Fe}(\text{cyclam})^{2+}$ ,  $\text{Co}(\text{cyclam})^{2+}$  and  $\text{Cu}(\text{cyclam})^{2+}$  demonstrated different product ratios. If the oxidant was not coordinating to the metal center, changing the metals should not affect the product distribution, but since the product distribution did change, it is evident the oxidant does coordinate to the metal. The researchers determined that in their system, the oxidant was more likely an acylperoxy radical due to the product

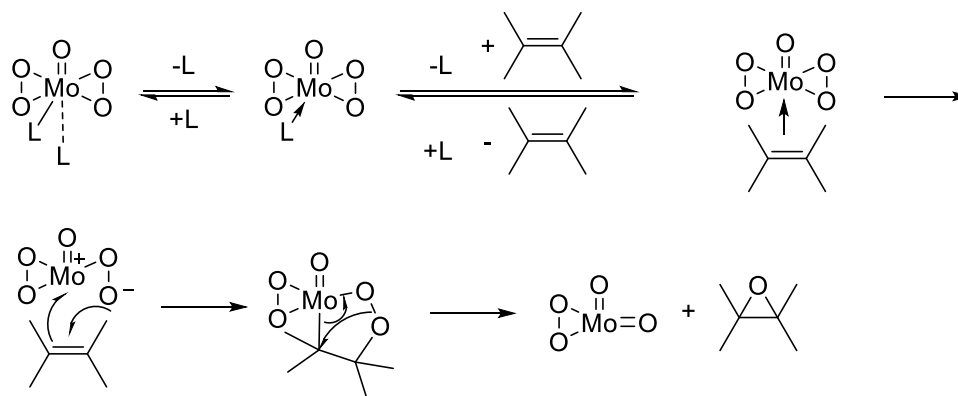
distribution of the *cis*- and *trans*- stilbene. Although this study was quite detailed, the researchers failed to illustrate how the peroxyacids were coordinating to the metal centers and whether the alkene was coordinating to the metal center or simply attacking the oxidant.



**Scheme 1.3.** Proposed alkene epoxidation mechanisms using peroxyacid oxidants.  
From ref. 127 and 128.

Two mechanisms have been proposed for the formation of epoxides from alkenes using metal-bound dioxygen species as the oxidant that illustrate how the oxidant and alkene bind to the metal catalyst. These mechanisms were illustrated using a Mo complex,  $[\text{Mo}(\text{O}_2)_2\text{O}]\text{L}_1\text{L}_2$  where  $\text{L}_1$  and  $\text{L}_2$  donor ligands such as pyridine, dimethylformamide (DMF), or hexamethylphosphoric triamide (HMPA).<sup>127</sup> Kinetic studies with the HMPA ligand illustrated that the rate determining step consisted of a reversible formation of a alkene-metal complex followed by an irreversible oxygen transfer to the alkene.<sup>127</sup> NMR studies monitored the displacement of the HMPA ligand during the oxidation reaction, indicating the alkene was coordinating to the metal center during the reaction.<sup>127</sup> Therefore, Mimoun proposed an inner-sphere mechanism in which the alkene coordinates directly to the metal, displacing a coordinating ligand and forming a five-membered metallocycle in

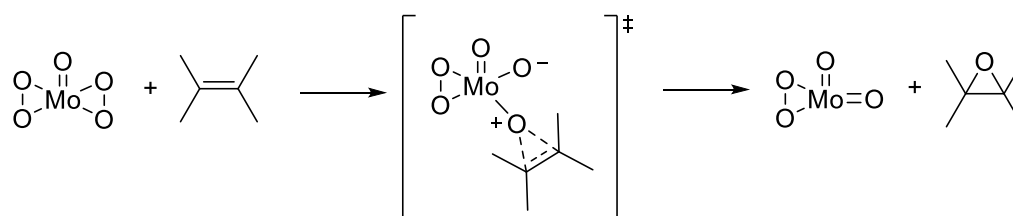
the transition state (**Scheme 1.4**).<sup>127,129,130</sup> This mechanism disagrees with Bartlett's mechanism (**Scheme 1.3**), but is consistent with a  $\pi$ - $\sigma$  rearrangement which occurs in most transition metal catalyzed transformations of alkenes.<sup>127</sup> Although this original work was completed with a  $\text{Mo}^{6+}$  catalyst, there was evidence that the mechanism was also applicable to a vanadium catalyzed epoxidation. Studies using  $\text{VO}(\text{acac})_2$  as a catalyst with  $^t\text{BuOOH}$  as an oxidant illustrated that the epoxidation products of allylic alcohols were highly stereo- and regioselective.<sup>131</sup> It was suggested that Mimoun's mechanism was the rationale behind this selectivity.<sup>127</sup>



**Scheme 1.4.** Proposed alkene epoxidation mechanisms by Mimoun. L = HMPA.  
Taken from ref. 127.

In contrast to work by Mimoun, Sharpless examined the same active catalyst,  $\text{MoO}_5 \cdot \text{HMPA}$ .<sup>132</sup>  $^{18}\text{O}$  labeling experiments demonstrated that the oxygen in the oxygen transfer to the alkene is the peroxo oxygen and not the oxo oxygen.<sup>132</sup> Although these results did not contradict Mimoun's mechanism, further investigation into the cyclic transition state led to evidence that did not support a 5-membered transition state. Bingham, Meakins, and Whitham developed an experimental method to determine cyclic transition states through structure-relative rate correlations.<sup>133</sup> Norbornene and cyclohexene are sensitive to the size

of their cyclic transition state during oxidation reactions. By comparing the rates of these two reactions, the size of the transition state can be deduced since the ratios of these substrates have been catalogued from reactions with catalysts that have known cyclic transition states.<sup>132</sup>  $\text{MoO}_5 \cdot \text{HMPA}$  demonstrated a ratio of rates of norbornene to cyclohexene that were similar to peracetic acid, which can react through a three membered transition state.<sup>132</sup> Therefore, an outer-sphere mechanism was proposed, where the alkene binds directly to one of the metal-bound oxygen atoms, forming a three-membered ring in the transition state (**Scheme 1.5**).<sup>130,132</sup> Sharpless went on to investigate the  $\text{VO}(\text{acac})_2$  catalyzed epoxidation of geraniol in  $^{18}\text{O}$  enriched water/dioxane with  $^t\text{BuOOH}$  as the oxidant.<sup>134</sup> These  $^{18}\text{O}$  labeling experiments demonstrated that oxygen atoms of allylic alcohols coordinate with the vanadium center, but the alkene portion does not.<sup>134</sup> The alkene still undergoes a three-membered transition state the same as the work originally proposed with  $\text{MoO}_5 \cdot \text{HMPA}$ .



**Scheme 1.5.** Proposed alkene epoxidation mechanisms by Sharpless.  
Taken from ref. 132.

The catalytic oxidation of sulfides using V-APMS and peroxyacids generated *in situ* from aldehydes is sufficiently new that there are no corresponding examples in the literature. However, the examples above will be used to inform the mechanistic studies

described later in this dissertation, in which the complex VO(dtpa) is immobilized onto mesoporous silica.

### 1.3.3 Diethylenetriaminepentaacetic acid

Multidentate ligands or chelating ligands are often used for their stabilizing effect of metal ions. This is known as the chelate effect: the thermodynamic stability of chelated complexes is greater than a complex containing the same corresponding number of monodentate ligands.<sup>135</sup> Chelating ligands can be categorized by "denticity", the number of donor atoms through which the ligand coordinates.<sup>135</sup> Some common bidentate ligands are 1,2-ethanediamine, acetylacetonate, oxalate, 2-2' bipyridine and 1,10-phenanthroline.<sup>135</sup> Some common multidentate ligands are 1,2,7-triazaheptane, 1,4,7,10-tetraazadecane, ethylenediaminetetraacetic acid and diethylenetriaminepentaacetic acid.<sup>135</sup>

The ligand diethylenetriaminepentaacetic acid, abbreviated "dtpa", belongs to a family of ligands for transition metal complexes consisting of acetate-modified alkylamines. The best-known member of this family is ethylenediaminetetraacetic acid, called edta, which is a strong chelator for a wide variety of metals. It is used commercially, in environmental remediation, and in biological applications.<sup>136-140</sup>

Because it has a large number of donor atoms, dtpa is particularly useful in the chelation of metals requiring larger coordination environments, such as f-block metals. This was the reason for initial studies many years ago on the clearance of yttrium and lanthanum from the human bloodstream.<sup>141</sup> Similarly, the most important commercial application of dtpa is in the first clinically available MRI contrast agent, Magnevist<sup>®</sup>, which uses a Gd(dtpa) complex.<sup>142</sup> Dtpa complexes are also used in other types of medical

imaging<sup>64,143-150</sup> and in radiopharmaceuticals<sup>151-155</sup> as well as in dual imaging drug delivery systems<sup>156-158</sup> and phototherapies.<sup>159-162</sup> The ability to chelate f-block metals has also led to its application in nuclear waste separation.<sup>163-165</sup>

There are somewhat fewer studies on d-block complexes of dtpa. These have mainly involved relatively recent catalytic studies using dtpa complexes of Cu and Pt. In one example,  $[\text{Cu}(\text{dtpa})]^{3-}$  was used for the amination of aryl bromides and iodides with aqueous  $\text{NH}_3$ .<sup>166</sup> Amination reactions are often performed in toxic organic solvents. To make a catalytic system that was low-cost and could be performed in water, water-soluble polyamino carboxylic acids such as ethylenediaminetetraacetic acid (edta) and dtpa, that are known to chelate transition metals, were investigated as ligands for  $\text{Cu}^{2+}$ . The  $[\text{Cu}(\text{dtpa})]^{3-}$  complex was made *in situ* during the amination reaction and was not characterized, but the reactions were completed in basic conditions and therefore  $[\text{Cu}(\text{dtpa})]^{3-}$  was most likely the active catalyst complex.  $[\text{Cu}(\text{dtpa})]^{3-}$  outperformed edta complexes, without the need for an inert atmosphere, producing high yields for a variety of aryl iodides and aryl bromides. Another study that was performed in aqueous solvents, involved a slightly more complex aqueous/organic two-phase system containing  $[\text{Pt}^0(\text{dtpa})]\text{Na}_5$  for the catalytic hydrogenation of polyunsaturated methyl esters of soybean oil.<sup>167</sup> A final example from the current year used silica-supported  $\text{Pt}^{4+}(\text{dtpa})$  complexes as catalysts for alkene hydrosilylation.<sup>168</sup>

With respect to vanadium, dtpa has been used in variety of applications, such as metal extraction,<sup>169-172</sup> measuring vanadium phytoavailability,<sup>173,174</sup> and for the chelation of vanadium in biological systems.<sup>175,176</sup> Some researchers have used dtpa to investigate

the stability constants for  $\text{VO}_2^+$  ions in solution,<sup>177</sup> and others have determined vanadium speciation using chelation with dtpa and capillary electrophoresis.<sup>178-180</sup> However, there have been no attempts to study oxidation or any other type of catalysis using vanadium complexes of dtpa and only three studies have even attempted to define the structure of these complexes.<sup>181-183</sup>

In the first example,  $\text{VO}_2(\text{dtpa})$  was prepared from  $\text{NH}_4\text{VO}_3$ .<sup>181</sup> Characterization by  $^{13}\text{C}$  and  $^{51}\text{V}$  NMR led these researchers to conclude that the vanadium had a hexacoordinate environment (**Figure 1.6a**), with two oxo ligands in adjacent coordination sites, acetate oxygen atoms in opposite positions, and nitrogen donors completing the coordination sphere. The assignment has precedence, as  $[\text{VO}_2(\text{H}_2\text{O})_4]^+$  is known to have an octahedral geometry,<sup>184</sup> allowing the  $\pi$  donating  $\text{O}^{2-}$  ligands to interact with the  $d_{xz}$ ,  $d_{yz}$  and  $d_{xy}$  orbitals of the vanadium ion. In another example using  $\text{V}_2(\text{SO}_4)_3$  as the vanadium source, FT-IR and UV/Visible spectroscopies were used to characterize the resulting dtpa complex of  $\text{V}^{3+}$  (**Figure 1.6b**).<sup>182</sup> The researchers proposed a heptacoordinate vanadium environment with no oxo ligands, one unbound acetate, four bound acetates, one labile bound  $\text{H}_2\text{O}$ , and two nitrogen atoms bound to the vanadium ion. Typically, heptacoordinate vanadium environments are a result of peroxo ligands.<sup>184</sup> Therefore, if the complex is considered without the coordination of the water, it is likely to adopt a trigonal antiprism or trigonal prism geometry as these are the common geometries of six coordinate non-oxo vanadium. The uncertainty and peculiarity of the geometry of the heptacoordinate complex makes it an unlikely to be of any aid in determining the geometry of  $\text{VO}(\text{dtpa})$ . In the third example, a  $\text{VO}(\text{dtpa})$  complex was prepared from  $\text{VO}(\text{SO}_4)$ , and EPR was used to conclude that the

resulting complexes deviated from axial symmetry.<sup>183</sup> Although they did not suggest a geometry, they concluded that the complex would have three unchelated acid groups because they observed second sphere water ligands when analyzing their proton relaxation profiles. Pentacoordinate geometries such as square pyramidal and trigonal bipyramidal environments are common for vanadyl complexes.<sup>184</sup> Therefore it is probable that it adopts one of these geometries.

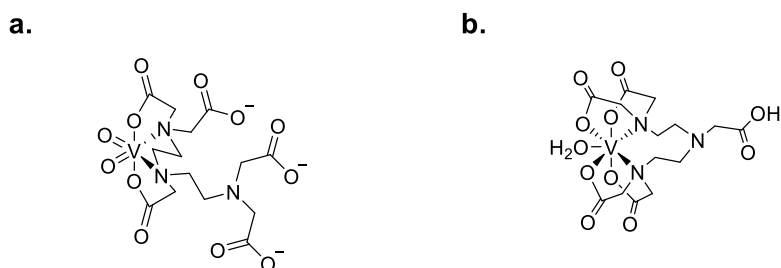


**Figure 1.6.** Proposed structures of two dtpa complexes of vanadium.  
From refs 176 and 177.

The lack of consistent structural analysis implies that there is room for improved and more detailed studies. In addition, the development of advanced computational tools allows experimental data to be supported by modeling. The detailed analysis of immobilized VO(dtpa) complexes is a key component of the work in this dissertation. Dtpa was chosen for our study not only because it is a good chelator, but also because the many acetate groups provide opportunities for linkage to the surface of a silica support, making it easy to immobilize.

## 1.4 Instrumental Techniques

### 1.4.1 Nitrogen Physisorption

Nitrogen physisorption is a technique from which the surface area ( $\text{m}^2/\text{g}$ ), pore diameter ( $\text{\AA}$ ) and pore volume ( $\text{cm}^3/\text{g}$ ) of porous solids can be obtained.<sup>185</sup> Physisorption describes the phenomenon of when an adsorbable gas, in this case nitrogen, is brought into contact with the surface of a solid (the adsorbent).<sup>185</sup> This phenomenon is schematically illustrated, with mesoporous silica as an example, in **Figure 1.7**. In the first step, nitrogen fills the pores of the material. When a monolayer of nitrogen molecules forms on the surface of the material, BET (Brunauer–Emmett–Teller) theory can be applied to calculate the surface area of the material.<sup>186</sup> BET Theory describes the relationship of monolayer molecular adsorption through the following equation (**Equation 1.1**):

$$\frac{1}{v\left[\left(\frac{p_0}{p}\right)-1\right]} = \left(\frac{c-1}{v_m c}\right)\left(\frac{p}{p_0}\right) + \left(\frac{1}{v_m c}\right) \quad (1.1)$$

where  $v$  represents the adsorbed gas quantity,  $p_0$  is saturation pressure of the gas,  $p$  is pressure of the gas,  $v_m$  is the volume of gas adsorbed when the entire adsorbent surface is covered, and  $c$  is the BET constant.<sup>186</sup> The data from this relationship can be plotted as a straight line with  $\frac{1}{v\left[\left(\frac{p_0}{p}\right)-1\right]}$  on the x axis and  $\frac{p}{p_0}$  on the y axis. The plot is called a BET plot.

<sup>187</sup> The slope of this plot ( $A$ ) and the y-intercept ( $I$ ) can be used to calculate  $v_m$  and  $c$  (the BET constant) in the following relationships (**Equation 1.2 and 1.3**):

$$v_m = \frac{1}{A+I} \quad (1.2)$$

$$c = 1 + \frac{A}{I} \quad (1.3)$$

Once  $v_m$  is known, the specific surface area ( $S_{\text{BET}}$ ) can be calculated through the following relationships (**Equation 1.4**):

$$S_{\text{BET}} = \left( \frac{v_m N \sigma}{V} \right) \left( \frac{1}{a} \right) \quad (1.4)$$

where  $N$  is Avogadro's number,  $\sigma$  is the adsorption cross section of the adsorbing species,  $V$  is the molar volume of adsorbate gas and  $a$  is the mass of the sample.<sup>187</sup>

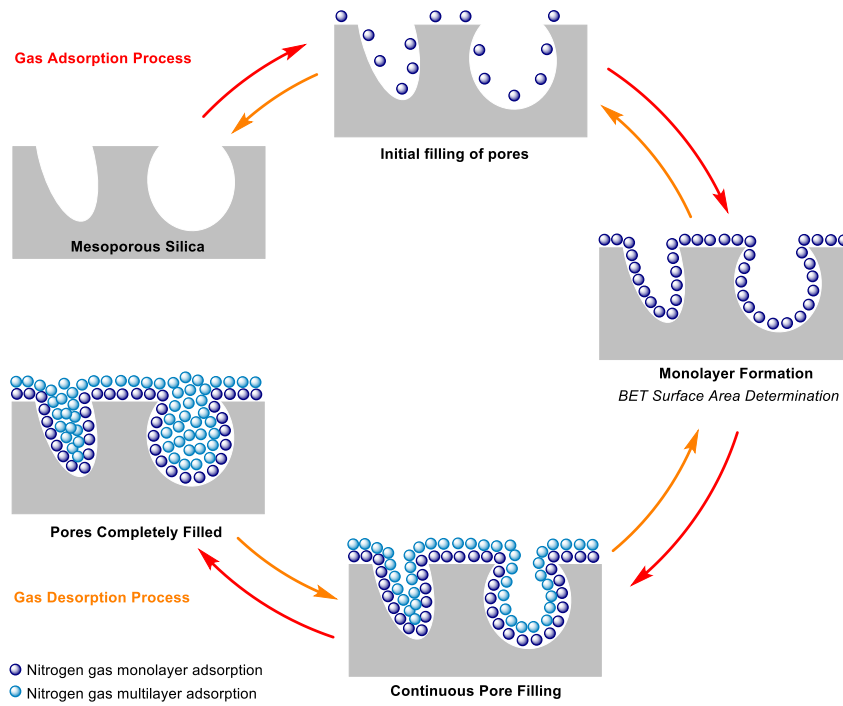


**Figure 1.7.** Gas adsorption and desorption during  $\text{N}_2$  physisorption measurement.

After the low-pressure filling of the pores and after the monolayer formation, the pores begin to fill in a multilayer fashion. This area represents capillary condensation of nitrogen (**Figure 1.7**). The data obtain in this step can be used to calculate the pore diameter by using a modified Kelvin equation,<sup>188,189</sup> called BJH (Barrett-Joyner-Halenda) method.<sup>190</sup> This method is the most popular for mesopore size analysis.<sup>191</sup> In the final step,

the highest partial pressure is at its maximum and all of the pores are filled with N<sub>2</sub>. It is at this point that the total pore volume is determined.<sup>186</sup>

The data collected in this technique results in a N<sub>2</sub> physisorption isotherm. IUPAC classifies isotherms into six different types.<sup>185</sup> The type of isotherm depends on the type of porous material being investigated. For mesoporous silica, a Type IV isotherm is observed (**Figure 1.8**). Each step in the N<sub>2</sub> physisorption process is evident in the isotherm. The surface area is determined at a P/P<sub>0</sub> of less than 0.3.<sup>187</sup> The pore diameter is determined at a P/P<sub>0</sub> greater than 0.3. Finally, the pore volume is calculated between a P/P<sub>0</sub> of 0.95-1.

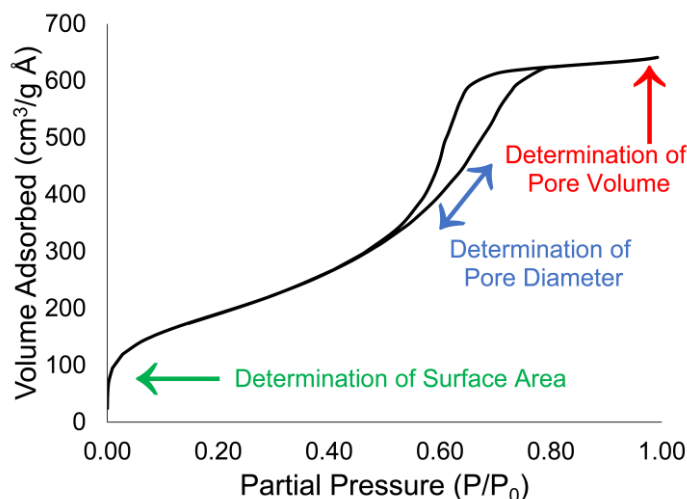


**Figure 1.8.** Type IV isotherm derived from N<sub>2</sub> physisorption on mesoporous silica.

#### 1.4.2 Electron Paramagnetic Resonance (EPR)

One focus of this dissertation is to characterize the geometry of the VO(dtpa) catalyst. Because there are no crystal structures in the literature of this complex, and because it is not possible to use X-ray diffraction methods to determine the structure after immobilization onto a silica support, other spectroscopic and computational techniques

were used to develop a structural understanding of the complex. Electron paramagnetic resonance (EPR), also called electron spin resonance or ESR, is the most significant of these techniques. EPR is similar to nuclear magnetic resonance (NMR), a much more commonly used experimental technique to study the structures of compounds, but instead of studying changes in nuclear spin in the presence of a magnetic field, EPR studies changes in electron spin. Therefore, the presence of an unpaired electron is a requirement for EPR.<sup>192-194</sup>

In the presence of a magnetic field, an unpaired electron has two electron spin energy levels (**Figure 1.9**). The relationship between the two energies can be expressed in the relationship below (**Equation 1.5**):

$$E = g\mu_B B_0 M_S \quad (1.5)$$

In this equation,  $B_0$  is the magnitude of the magnetic field,  $\mu_B$  is the Bohr magneton (a constant value of  $9.285 \times 10^{-21}$  erg  $G^{-1}$ ),  $M_S$  is the electron spin quantum number (+1/2 or -1/2) and  $g$  is a unitless proportionality factor, also referred to as the  $g$  tensor or the effective Zeeman factor.<sup>194</sup> A free electron has a proportionality factor of 2.00232 and electrons found in chemical systems deviate from that number due to their local environments. The total magnetic moment for an electron is the sum of the spin and orbital angular momentum.<sup>192</sup> These two angular momenta will each generate an intrinsic magnetic field.<sup>195</sup> The interaction of spin and orbital angular momentum is called spin-orbit coupling.<sup>195</sup> If the electron is interacting with a filled orbital, the  $g$  tensor will be above 2. This is because the coupling of the electron spin magnetic moment aids the applied field. If the unpaired electron is interacting with an unoccupied orbital, the  $g$  tensor will be below

2. This is because the coupling of the electron spin magnetic moment opposes the applied field.

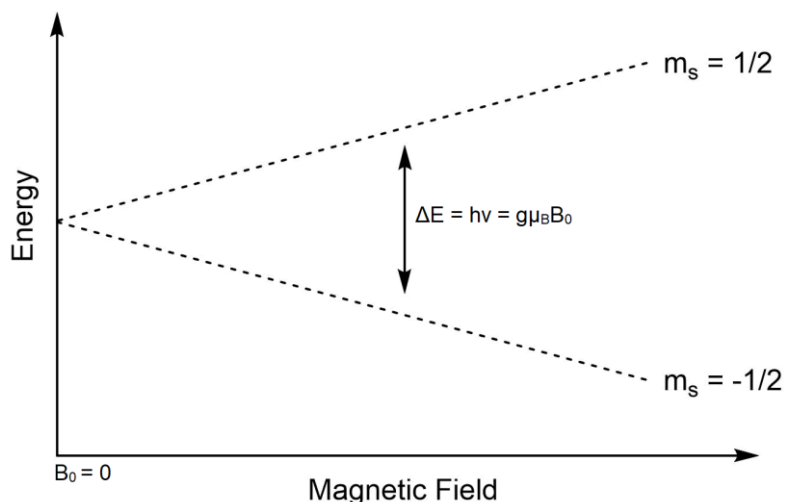


**Figure 1.9.** Diagram showing the splitting of electron spin energies in a magnetic field. Adapted from ref 188.

There are three types of local symmetry at the unpaired electron center: cubic, axial and rhombic.<sup>192</sup> There is directionality associated with a  $g$  tensor, and therefore it can be described in terms of the three Cartesian coordinates:  $g_x$ ,  $g_y$ , and  $g_z$ .<sup>193</sup> An isotropic system is defined as one in which the local environment of the unpaired electron is symmetric (cubic), so  $g_x = g_y = g_z$ . In this case, **Equation 1.5** is still valid. In an axial system, one of the tensors is unique  $g_{||}$ , and is called while the other two are called  $g_{\perp}$ . This adopts the following spin Hamiltonian (**Equation 1.6**):<sup>192</sup>

$$\hat{H} = \beta_e [g_{\perp}(B_x \hat{S}_x + B_y \hat{S}_y) + g_{||} B_z \hat{S}_z] \quad (1.6)$$

where  $\beta_e$  is the Bohr magneton,  $g_{\perp}$  is the  $g$  tensor perpendicular to the magnetic field,  $g_{||}$  is

the  $g$  tensor parallel to the magnetic field,  $\hat{S}_x$ ,  $\hat{S}_y$ , and  $\hat{S}_z$  are electron spin operators and  $B_x$ ,  $B_y$ , and  $B_z$  are the magnetic fields in each direction. Finally, in a rhombic system, all three tensors are unique from each other and therefore the following spin Hamiltonian must be applied (**Equation 1.7**):<sup>192</sup>

$$\hat{H} = \beta_e(g_x B_x \hat{S}_x + g_y B_y \hat{S}_y + g_z B_z \hat{S}_z) \quad (1.7)$$

For an EPR experiment, the electric field component interacts with the molecules and an absorption spectrum is obtained.<sup>192</sup> For absorption to occur, the energy of the quantum radiation must correspond to the separation between certain energy levels in the molecule and the static magnetic field must interact with a magnetic dipole in the molecule.<sup>192</sup> Therefore, a magnetic field is applied to split energy levels of the spin states (**Figure 1.9**). Then, a microwave energy is applied to the system to excite some of the unpaired electrons to a higher energy state. The absorption spectrum is integrated to afford an absorption derivative which is a typical EPR spectrum (**Figure 1.10**).

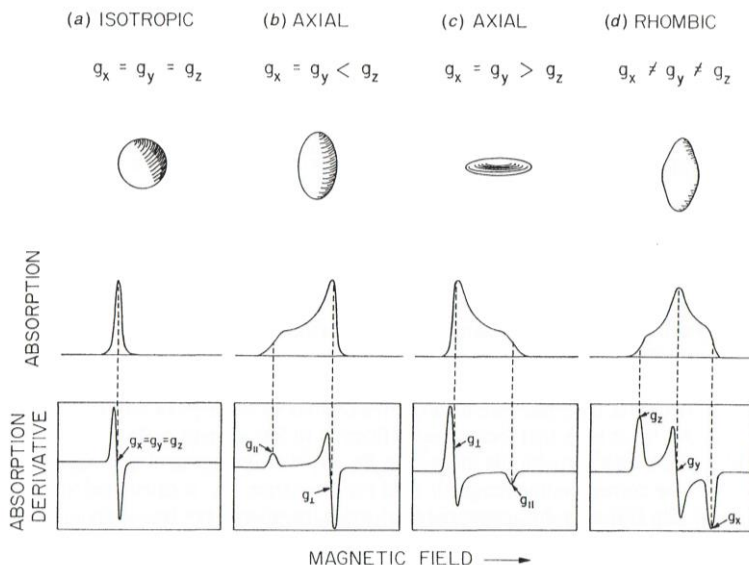


**Figure 1.10.** Diagram relating the local symmetry of samples to typical EPR spectra.  
From ref 189.

If the electron interacts with a neighboring nuclear dipole, hyperfine coupling is observed. In an isotropic system, this can be demonstrated in the following equation (Equation 1.6):

$$E = g\mu_B B_0 M_S + a M_S m_I \quad (1.6)$$

where  $m_I$  is the nuclear spin quantum number and  $a$  is the hyperfine constant, also called the a tensor.<sup>194</sup> Coupling of the electronic and nuclear spins can occur either by direct dipole-dipole interactions or by Fermi contact. The latter case only occurs when the electron is in an orbital with s character.<sup>194</sup> Figure 1.11 demonstrates the splitting of a  $S = \frac{1}{2}$  paramagnet interacting with a  $I = \frac{1}{2}$  nuclear moment.<sup>193</sup> This interaction leads to new energy splitting which translates to an EPR spectrum as additional lines. When coupling to a single nucleus that has a spin of  $n/2$ , there will be  $n + 1$  lines of splitting. Each of these lines should be of equal spacing and intensity. When coupling with multiple nuclei, the line distribution becomes binomial.<sup>194</sup>

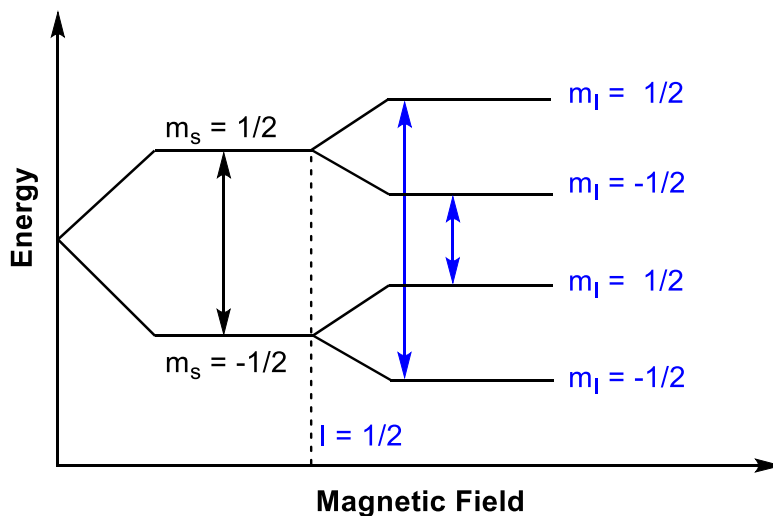


**Figure 1.11.** Diagram showing the splitting of an electron spin energies ( $M_s = \pm \frac{1}{2}$   $S = \frac{1}{2}$ ) in a magnetic field interacting with a  $I = \frac{1}{2}$  nuclear moment. The dotted line represents transitions in the beginning of hyperfine coupling. The blue arrows represent the additional EPR spectrum lines produced.

In order to use EPR to determine geometry, the spin-orbit interaction must be analyzed. Spin-orbit interaction is the mixture of a hypothetical pure spin ground state with an excited state.<sup>193</sup> This mixture causes a small orbital angular momentum to exist in the real ground state. This produces a local magnetic field. This new magnetic field interacts with the external magnetic field. This coupling is also referred to as rotational relationships.<sup>193</sup> The rotational relationships for real d orbitals are known and by using these known rotations in conjunction with potential orbital diagrams, a geometry can be determined.<sup>193</sup> This concept is depicted in **Figure 1.12** for a  $\text{Mo}^{5+}$  compound. The two common geometries for  $\text{Mo}^{5+}$  are compressed octahedron and dodecahedron. EPR can be used to determine which of these geometries is associated with a particular  $\text{Mo}^{5+}$  sample. The electron circulation that are associated with the orbital contributes are shown by the rings.<sup>193</sup> A large orbital rotational relationship produces a small deviation from a g tensor equal to 2, while a small orbital rotational relationship produces a large deviation from a g tensor equal to 2. Looking at the example in **Figure 1.12**, the values of the g tensors in relationship to each other will determine if the  $\text{Mo}^{5+}$  sample is compressed octahedron and dodecahedron.

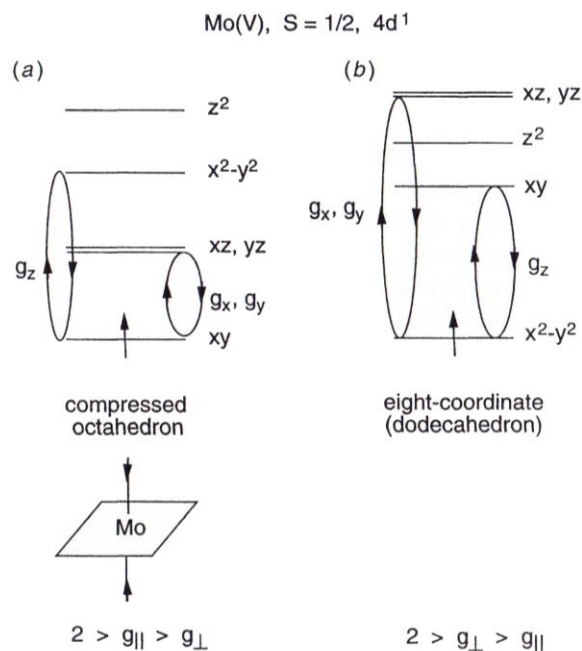


**Figure 1.12.** The relative energy levels of 3d orbitals from two common geometries of  $\text{Mo}^{5+}$  ( $4d^1$ ). The electron circulations associated with the orbital contributions to each of the three g values are shown by the rings. From ref 189.

In order to use rotational relationships, values of the g tensors and a tensors must be known. There are two main computational methods that can assist in the assignment of g tensors and a tensor from an EPR spectrum. The first is a modeling program called EasySpin,<sup>196</sup> which interfaces with MatLab software. Through EasySpin, spectrum simulations can be performed in which the program automatically determines spin Hamiltonian symmetry and can project the predicted spectra.<sup>196</sup> EasySpin computes g tensors and a tensors for a given EPR spectrum. The advantages of EasySpin are that being based in Matlab enables the program to have visually rich graphics and easy interfacing.<sup>196</sup> Also, the program has an extensive library for spin physics which are vital for EPR calculations.<sup>196</sup> The second computational program is ORCA.<sup>197,198</sup> ORCA is an extensive

computation tool that uses Hartree-Fock theory, density functional theory (DFT) and other quantum mechanical theories.<sup>197</sup> ORCA has a wide range of applicable functions but in terms of its use for EPR, ORCA can calculate zero-field splitting, g-tensors, hyperfine couplings, quadrupole tensors from Hartree-Fock, DFT and MR-CI (multireference configuration interaction).<sup>197</sup> EasySpin is a fitting software and does not have the option to input geometries to match with an EPR spectrum. Therefore, EasySpin is helpful if g tensors and a tensors are the only desired output. With ORCA, a suspected geometry can be optimized and g tensors and a tensors can then be calculated. ORCA can also interface with EasySpin so that once there is a known geometry with matching tensors calculated from ORCA, the spectrum can be simulated on EasySpin.

For work found in this dissertation, where the electronic geometry around the vanadium was unknown, EPR is a very valuable tool. The VO(dtpa) complex has V<sup>4+</sup> vanadium and therefore has a d<sup>1</sup> electron count. This makes the compound EPR active. By comparing the geometries of literature proposed vanadium dtpa complexes and common geometries for VO complexes, EPR can be used in conjunction with computational studies, to effectively identify the geometry of VO(dtpa).

## 1.5 References

1. Heveling, J. Heterogeneous Catalytic Chemistry by Example of Industrial Applications. *J. Chem. Educ.* **2012**, *89*, 1530-1536.
2. Roy, A.; Srivastava, A. K.; Singh, B.; Shah, D.; Mahato, T. H.; Srivastava, A. Kinetics of degradation of sulfur mustard and sarin simulants on HKUST-1 metal organic framework. *Dalton Trans.* **2012**, *41*, 12346-12348.

3. Hartwig, J. F., *Organotransition Metal Chemistry: From Bonding to Catalysis*. University Science Books: Sausalito, CA, 2010.
4. Adkins, H.; Krsek, G. Preparation of Aldehydes from Alkenes by the Addition of Carbon Monoxide and Hydrogen with Cobalt Carbonyls as Intermediates. *J. Am. Chem. Soc.* **1948**, *70*, 383-386.
5. Haber, F.; van Oordt, G. Über die Bildung von Ammoniak den Elementen. *Z. Anorg. Allg. Chem.* **1905**, *44*, 341-378.
6. Thomas, J. M. Handbook Of Heterogeneous Catalysis. 2., completely revised and enlarged Edition. Vol. 1–8. Edited by G. Ertl, H. Knözinger, F. Schüth, and J. Weitkamp. *Angew. Chem. Int. Ed.* **2009**, *48*, 3390-3391.
7. Maurya, M. R.; Kumar, A.; Costa Pessoa, J. Vanadium complexes immobilized on solid supports and their use as catalysts for oxidation and functionalization of alkanes and alkenes. *Coord. Chem. Rev.* **2011**, *255*, 2315-2344.
8. Gawande, M. B.; Monga, Y.; Zboril, R.; Sharma, R. K. Silica-decorated magnetic nanocomposites for catalytic applications. *Coord. Chem. Rev.* **2015**, *288*, 118-143.
9. Kosslick, H.; Mönnich, I.; Paetzold, E.; Fuhrmann, H.; Fricke, R.; Müller, D.; Oehme, G. Suzuki reaction over palladium-complex loaded MCM-41 catalysts. *Microporous Mesoporous Mater.* **2001**, *44-45*, 537-545.
10. Bhunia, S.; Koner, S. Functionalization of oxo-vanadium(IV) acetylacetonate over modified MCM-41: an efficient reusable catalyst for epoxidation reaction. *J. Porous Mater.* **2011**, *18*, 399-407.
11. Petrucci, M. G. L.; Kakkar, A. K. Heterogenizing homogeneous catalysis. *Adv. Mater.* **1996**, *8*, 251-253.
12. Modi, C. K.; Vithalani, R. S.; Patel, D. S.; Som, N. N.; Jha, P. K. Zeolite-Y entrapped metallo-pyrazolone complexes as heterogeneous catalysts: Synthesis, catalytic aptitude and computational investigation. *Microporous Mesoporous Mater.* **2018**, *261*, 275-285.

13. Mirzaee, M.; Bahramian, B.; Gholizadeh, J.; Feizi, A.; Gholami, R. Acetylacetonate complexes of vanadium and molybdenum supported on functionalized boehmite nano-particles for the catalytic epoxidation of alkenes. *Chem. Eng. J.* **2017**, *308*, 160-168.
14. Salavati-Niasari, M.; Badiei, A.; Saberyan, K. Oxovanadium(IV) salophen complex covalently anchored to multi-wall carbon nanotubes (MWNTs) as heterogeneous catalyst for oxidation of cyclooctene. *Chem. Eng. J.* **2011**, *173*, 651-658.
15. Dorbes, S.; Pereira, C.; Andrade, M.; Barros, D.; Pereira, A. M.; Rebelo, S. L. H.; Araújo, J. P.; Pires, J.; Carvalho, A. P.; Freire, C. Oxidovanadium(IV) acetylacetonate immobilized onto CMK-3 for heterogeneous epoxidation of geraniol. *Microporous Mesoporous Mater.* **2012**, *160*, 67-74.
16. Li, Z.; Wu, S.; Zheng, D.; Liu, H.; Hu, J.; Su, H.; Sun, J.; Wang, X.; Huo, Q.; Guan, J.; Kan, Q. Enhanced alkenes epoxidation reactivity of discrete bis(8-quinolinol)oxovanadium(IV) or bis(8-quinolinol)dioxomolybdenum(VI) tethered to graphene oxide by a metal-template/metal-exchange method. *Appl. Catal. A* **2014**, *470*, 104-114.
17. Hamidipour, L.; Farzaneh, F. Immobilized VOsalpr on modified Fe<sub>3</sub>O<sub>4</sub> nanoparticles as a magnetically separable epoxidation catalyst. *C. R. Chim.* **2014**, *17*, 927-933.
18. Hsiao, M.-C.; Liu, S.-T. Polymer Supported Vanadium Complexes as Catalysts for the Oxidation of Alkenes in Water. *Catal. Lett.* **2010**, *139*, 61-66.
19. Monfared, H. H.; Abbasi, V.; Rezaei, A.; Ghorbanloo, M.; Aghaei, A. A heterogenized vanadium oxo-aryylhydrazone catalyst for efficient and selective oxidation of hydrocarbons with hydrogen peroxide. *Transition Met. Chem.* **2012**, *37*, 85-92.
20. Parida, K. M.; Singha, S.; Sahoo, P. C. A facile method for promoting activities of vanadium-schiffbase complex anchored on organically modified MCM-41 in epoxidation reaction. *J. Mol. Catal. A: Chem.* **2010**, *325*, 40-47.

21. Kalilur Rahiman, A.; Shanmuga Bharathi, K.; Sreedaran, S.; Rajesh, K.; Narayanan, V. Cationic vanadyl porphyrin-encapsulated mesoporous Al/V-MCM-41 as heterogeneous catalysts for the oxidation of alkenes. *Inorg. Chim. Acta* **2009**, *362*, 1810-1818.
22. Kala Raj, N. K.; Deshpande, S. S.; Ingle, R. H.; Raja, T.; Manikandan, P. Heterogenized Molybdovanadophosphoric Acid on Amine-Functionalized SBA-15 for Selective Oxidation of Alkenes. *Catal. Lett.* **2004**, *98*, 217-224.
23. Huang, Z.; Brookhart, M.; Goldman, A. S.; Kundu, S.; Ray, A.; Scott, S. L.; Vicente, B. C. Highly Active and Recyclable Heterogeneous Iridium Pincer Catalysts for Transfer Dehydrogenation of Alkanes. *Adv. Synth. Catal.* **2009**, *351*, 188-206.
24. Corma, A.; Garcia, H. Supramolecular Host-Guest Systems in Zeolites Prepared by Ship-in-a-Bottle Synthesis. *Eur. J. Inorg. Chem.* **2004**, *2004*, 1143-1164.
25. Okemoto, A.; Ueyama, K.; Taniya, K.; Ichihashi, Y.; Nishiyama, S. Direct oxidation of benzene with molecular oxygen in liquid phase catalysed by heterogeneous copper complexes encapsulated in Y-type zeolite. *Catal. Commun.* **2017**, *100*, 29-32.
26. Genna, D. T.; Wong-Foy, A. G.; Matzger, A. J.; Sanford, M. S. Heterogenization of Homogeneous Catalysts in Metal–Organic Frameworks via Cation Exchange. *J. Am. Chem. Soc.* **2013**, *135*, 10586-10589.
27. Yu, J.; Cui, Y.; Wu, C.; Yang, Y.; Wang, Z.; O'Keeffe, M.; Chen, B.; Qian, G. Second-Order Nonlinear Optical Activity Induced by Ordered Dipolar Chromophores Confined in the Pores of an Anionic Metal–Organic Framework. *Angew. Chem. Int. Ed.* **2012**, *51*, 10542-10545.
28. Ghosh, D.; Febriansyah, B.; Gupta, D.; Ng, L. K.-S.; Xi, S.; Du, Y.; Baikie, T.; Dong, Z.; Soo, H. S. Hybrid Nanomaterials with Single-Site Catalysts by Spatially Controllable Immobilization of Nickel Complexes via Photoclick Chemistry for Alkene Epoxidation. *ACS Nano* **2018**, *12*, 5903-5912.
29. Jin, Y.; Li, A.; Hazelton, S. G.; Liang, S.; John, C. L.; Selid, P. D.; Pierce, D. T.; Zhao, J. X. Amorphous silica nanohybrids: Synthesis, properties and applications. *Coord. Chem. Rev.* **2009**, *253*, 2998-3014.

30. Everett, D. H. Manual of Symbols and Terminology for Physicochemical Quantities and Units, Appendix II: Definitions, Terminology and Symbols in Colloid and Surface Chemistry. *Pure Appl. Chem.* **1972**, *31*, 577-638.
31. Anwander, R. SOMC@PMS. Surface Organometallic Chemistry at Periodic Mesoporous Silica. *Chem. Mater.* **2001**, *13*, 4419-4438.
32. Ariga, K.; Vinu, A.; Hill, J. P.; Mori, T. Coordination chemistry and supramolecular chemistry in mesoporous nanospace. *Coord. Chem. Rev.* **2007**, *251*, 2562-2591.
33. Graham, T. XXXV.—On the properties of silicic acid and other analogous colloidal substances. *J. Chem. Soc.* **1864**, *17*, 318-327.
34. Brinker, C. J., Sol—Gel Processing of Silica. In *The Colloid Chemistry of Silica*, American Chemical Society: 1994; Vol. 234, pp 361-401.
35. Ullattil, S. G.; Periyat, P., Sol-Gel Synthesis of Titanium Dioxide. In *Sol-Gel Materials for Energy, Environment and Electronic Applications*, Pillai, S. C.; Hehir, S., Eds. Springer International Publishing: Cham, 2017; pp 271-283.
36. Stöber, W.; Fink, A.; Bohn, E. Controlled growth of monodisperse silica spheres in the micron size range. *J. Colloid Interface Sci.* **1968**, *26*, 62-69.
37. Zaera, F. Nanostructured materials for applications in heterogeneous catalysis. *Chem. Soc. Rev.* **2013**, *42*, 2746-2762.
38. Beck, J. S.; Vartuli, J. C.; Roth, W. J.; Leonowicz, M. E.; Kresge, C. T.; Schmitt, K. D.; Chu, C. T.-W.; Olson, D. H.; Sheppard, E. W.; McCullen, S. B.; Higgins, J. B.; Schlenker, J. L. A New Family of Mesoporous Molecular Sieves Prepared with Liquid Crystal Templates. *J. Am. Chem. Soc.* **1992**, *114*, 10834-10843.
39. Gibson, L. T. Mesosilica materials and organic pollutant adsorption: part A removal from air. *Chem. Soc. Rev.* **2014**, *43*, 5163-5172.

40. Beck, J. S.; Vartuli, J. C.; Kennedy, G. J.; Kresge, C. T.; Roth, W. J.; Schramm, S. E. Molecular or Supramolecular Templating: Defining the Role of Surfactant Chemistry in the Formation of Microporous and Mesoporous Molecular Sieves. *Chem. Mater.* **1994**, *6*, 1816-1821.
41. Li, W.; Zhao, D. Extension of the Stöber Method to Construct Mesoporous SiO<sub>2</sub> and TiO<sub>2</sub> Shells for Uniform Multifunctional Core-Shell Structures. *Adv. Mater.* **2013**, *25*, 142-149.
42. Kresge, C. T.; Roth, W. J. The discovery of mesoporous molecular sieves from the twenty year perspective. *Chem. Soc. Rev.* **2013**, *42*, 3663-3670.
43. Firouzi, A.; Kumar, D.; Bull, L. M.; Besier, T.; Sieger, P.; Huo, Q.; Walker, S. A.; Zasadzinski, J. A.; Glinka, C.; Nicol, J.; Margolese, D.; Stucky, G. D.; Chemelka, B. F. Cooperative organization of inorganic-surfactant and biomimetic assemblies. *Science* **1995**, *267*, 1138-1143.
44. Kresge, C. T.; Leonowicz, M. E.; Roth, W. J.; Vartuli, J. C.; Beck, J. S. Ordered mesoporous molecular sieves synthesized by a liquid-crystal template mechanism. *Nature* **1992**, *359*, 710.
45. Alatham, Z. A. A Review: Fundamental Aspects of Silicate Mesoporous Materials. *Materials* **2012**, *5*, 2874-2902.
46. Bhattacharyya, S.; Lelong, G.; Saboungi, M. L. Recent progress in the synthesis and selected applications of MCM-41: a short review. *J. Exp. Nanosci.* **2006**, *1*, 375-395.
47. Zhao, D.; Huo, Q.; Feng, J.; Chmelka, B. F.; Stucky, G. D. Nonionic Triblock and Star Diblock Copolymer and Oligomeric Surfactant Syntheses of Highly Ordered, Hydrothermally Stable, Mesoporous Silica Structures. *J. Am. Chem. Soc.* **1998**, *120*, 6024-6036.
48. Gallis, K. W.; Landry, C. C. Mesoporous Silica Production for Liquid Chromatography. U.S. Patent 6,334,988, August 20, 1999.
49. Gallis, K. W.; Araujo, J. T.; Duff, K. J.; Moore, J. G.; Landry, C. C. The Use of Mesoporous Silica in Liquid Chromatography. *Adv. Mater.* **1999**, *11*, 1452-1455.

50. Nassivera, T.; Eklund, A. G.; Landry, C. C. Size-exclusion chromatography of low-molecular-mass polymers using mesoporous silica. *J. Chromatogr. A* **2002**, *973*, 97-101.
51. Sorensen, A. C.; Landry, C. C. Complete reduction of 2-chloroethylethylsulfide by hydrodesulfurization using mo-doped mesoporous substrates. *Catal. Lett.* **2005**, *100*, 135-138.
52. Sorensen, A. C.; Fuller, B. L.; Eklund, A. G.; Landry, C. C. Mo-Doped Mesoporous Silica for Thiophene Hydrodesulfurization: Comparison of Materials and Methods. *Chem. Mater.* **2004**, *16*, 2157-2164.
53. Livingston, S. R.; Landry, C. C. Oxidation of a Mustard Gas Analogue Using an Aldehyde/O<sub>2</sub> System Catalyzed by V-Doped Mesoporous Silica. *J. Am. Chem. Soc.* **2008**, *130*, 13214-13215.
54. Livingston, S. R.; Kumar, D.; Landry, C. C. Oxidation of 2-chloroethyl ethyl sulfide using V-APMS. *J. Mol. Catal. A: Chem.* **2008**, *283*, 52-59.
55. Ringenbach, C. R.; Livingston, S. R.; Kumar, D.; Landry, C. C. Vanadium-Doped Acid-Prepared Mesoporous Silica: Synthesis, Characterization, and Catalytic Studies on the Oxidation of a Mustard Gas Analogue. *Chem. Mater.* **2005**, *17*, 5580-5586.
56. Wu, C.; Fan, W.; Chang, J. Functional mesoporous bioactive glass nanospheres: synthesis, high loading efficiency, controllable delivery of doxorubicin and inhibitory effect on bone cancer cells. *J. Mater. Chem. B* **2013**, *1*, 2710-2718.
57. Pang, J.; Zhao, L.; Zhang, L.; Li, Z.; Luan, Y. Folate-conjugated hybrid SBA-15 particles for targeted anticancer drug delivery. *J. Colloid Interface Sci.* **2013**, 31-39.
58. Vafaei, M.; Amini, M. M.; Najafi, E.; Sadeghi, O.; Amani, V. Modified nanoporous silicas for oral delivery of the water insoluble organotin compound: loading and release of methylphenyltin dichloride as an anti-tumor drug model. *J. Sol-Gel Sci. Technol.* **2012**, *64*, 411-417.

59. Cheng, K.; Blumen, S. R.; MacPherson, M. B.; Steinbacher, J. L.; Mossman, B. T.; Landry, C. C. Enhanced Uptake of Porous Silica Microparticles by Bifunctional Surface Modification with a Targeting Antibody and a Biocompatible Polymer. *ACS Appl. Mater. Interfaces* **2010**, *2*, 2489-2495.
60. Hillegass, J. M.; Blumen, S. R.; Cheng, K.; MacPherson, M. B.; Alexeeva, V.; Lathrop, S. A.; Beuschel, S. L.; Steinbacher, J. L.; Butnor, K. J.; Ramos-Niño, M. E.; Shukla, A.; James, T. A.; Weiss, D. J.; Taatjes, D. J.; Pass, H. I.; Carbone, M.; Landry, C. C.; Mossman, B. T. Increased efficacy of doxorubicin delivered in multifunctional microparticles for mesothelioma therapy. *Int. J. Cancer* **2011**, *129*, 233-244.
61. Zhao, A.; Samanta, A.; Sarkar, P.; Gupta, R. Carbon Dioxide Adsorption on Amine-Impregnated Mesoporous SBA-15 Sorbents: Experimental and Kinetics Study. *Ind. Eng. Chem. Res.* **2013**, *52*, 6480-6491.
62. Wang, X.; Ma, X.; Song, C.; Locke, D. R.; Siefert, S.; Winans, R. E.; Möllmer, J.; Lange, M.; Möller, A.; Gläser, R. Molecular basket sorbents polyethylenimine–SBA-15 for CO<sub>2</sub> capture from flue gas: Characterization and sorption properties. *Microporous Mesoporous Mater.* **2013**, *169*, 103-111.
63. Zukal, A.; Pastva, J.; Čejka, J. MgO-modified mesoporous silicas impregnated by potassium carbonate for carbon dioxide adsorption. *Microporous Mesoporous Mater.* **2013**, *167*, 44-50.
64. Steinbacher, J. L.; Lathrop, S. A.; Cheng, K.; Hillegass, J. M.; Butnor, K. J.; Kauppinen, R. A.; Mossman, B. T.; Landry, C. C. Gd-Labeled Microparticles in MRI: In vivo Imaging of Microparticles After Intraperitoneal Injection. *Small* **2010**, *6*, 2678-2682.
65. Duncan, A. K.; Klemm, P. J.; Raymond, K. N.; Landry, C. C. Silica Microparticles as a Solid Support for Gadolinium Phosphonate Magnetic Resonance Imaging Contrast Agents. *J. Am. Chem. Soc.* **2012**, *134*, 8046-8049.
66. Wight, A. P.; Davis, M. E. Design and Preparation of Organic–Inorganic Hybrid Catalysts. *Chem. Rev.* **2002**, *102*, 3589-3614.

67. Alvaro, M.; Corma, A.; Das, D.; Fornés, V.; García, H. Single-step preparation and catalytic activity of mesoporous MCM-41 and SBA-15 silicas functionalized with perfluoroalkylsulfonic acid groups analogous to Nafion®. *Chem. Commun.* **2004**, 956-957.
68. Corma, A.; Garcia, H. Silica-Bound Homogenous Catalysts as Recoverable and Reusable Catalysts in Organic Synthesis. *Adv. Synth. Catal.* **2006**, *348*, 1391-1412.
69. Zucca, P.; Sanjust, E. Inorganic Materials as Supports for Covalent Enzyme Immobilization: Methods and Mechanisms. *Molecules* **2014**, *19*, 14139-14194.
70. El-Faham, A.; Albericio, F. Peptide Coupling Reagents, More than a Letter Soup. *Chem. Rev.* **2011**, *111*, 6557-6602.
71. Erathodiyil, N.; Ying, J. Y. Functionalization of Inorganic Nanoparticles for Bioimaging Applications. *Acc. Chem. Res.* **2011**, *44*, 925-935.
72. da Silva, J. A. L.; da Silva, J. J. R. F.; Pombeiro, A. J. L. Oxovanadium complexes in catalytic oxidations. *Coord. Chem. Rev.* **2011**, *255*, 2232-2248.
73. Butler, A.; Clague, M. J.; Meister, G. E. Vanadium Peroxide Complexes. *Chem. Rev.* **1994**, *94*, 625-638.
74. Conte, V.; Coletti, A.; Floris, B.; Licini, G.; Zonta, C. Mechanistic aspects of vanadium catalysed oxidations with peroxides. *Coord. Chem. Rev.* **2011**, *255*, 2165-2177.
75. Romanowski, G.; Kira, J.; Wera, M. Vanadium(V) complexes with chiral tridentate Schiff base ligands derived from 1S,2R(+)-2-amino-1,2-diphenylethanol and with acetohydroxamate co-ligand: Synthesis, characterization and catalytic activity in the oxidation of prochiral sulfides and olefins. *J. Mol. Catal. A: Chem.* **2014**, *381*, 148-160.
76. Romanowski, G.; Kira, J.; Wera, M. Five- and six-coordinate vanadium(V) complexes with tridentate Schiff base ligands derived from S(+)-isoleucinol: Synthesis, characterization and catalytic activity in the oxidation of sulfides and olefins. *Polyhedron* **2014**, *67*, 529-539.

77. Grivani, G.; Tahmasebi, V.; Khalaji, A. D.; Fejfarová, K.; Dušek, M. Synthesis, characterization and crystal structure determination of a new vanadium(IV) Schiff base complex (VOL<sub>2</sub>) and investigation of its catalytic activity in the epoxidation of cyclooctene. *Polyhedron* **2013**, *51*, 54-60.
78. Azizi, T. S.; Gholamhossein, G.; Dehno, K. A. Six-coordinated vanadium(IV) complexes with tridentate task-specific ionic liquid Schiff base ligands: Synthesis, characterization and effect of ionic nature on catalytic activity. *Appl. Organomet. Chem.* **2018**, *32*, e4078.
79. Bikas, R.; Ghorbanloo, M.; Jafari, S.; Eigner, V.; Dusek, M. Catalytic oxidation of olefins and sulfides in the presence of hydrazone-oxidovanadium(V) complex containing VOCl<sub>2</sub><sup>+</sup> core. *Inorg. Chim. Acta* **2016**, *453*, 78-85.
80. Sutradhar, M.; Martins, L. M. D. R. S.; Guedes da Silva, M. F. C.; Pombeiro, A. J. L. Vanadium complexes: Recent progress in oxidation catalysis. *Coord. Chem. Rev.* **2015**, *301-302*, 200-239.
81. Kumar, R.; Chaudhary, N.; Sankar, M.; Maurya, M. R. Electron deficient nonplanar β-octachlorovanadylporphyrin as a highly efficient and selective epoxidation catalyst for olefins. *Dalton Trans.* **2015**, *44*, 17720-17729.
82. Kantam, M. L.; Neelima, B.; Reddy, C. V.; Chaudhuri, M. K.; Dehury, S. K. VO(acac)<sub>2</sub> Supported on Titania: A Heterogeneous Protocol for the Selective Oxidation of Sulfides Using TBHP. *Catal. Lett.* **2004**, *95*, 19-22.
83. Uematsu, T.; Miyamoto, Y.; Ogasawara, Y.; Suzuki, K.; Yamaguchi, K.; Mizuno, N. Molybdenum-doped [small alpha]-MnO<sub>2</sub> as an efficient reusable heterogeneous catalyst for aerobic sulfide oxygenation. *Catal. Sci. Technol.* **2016**, *6*, 222-233.
84. Uematsu, T.; Ogasawara, Y.; Suzuki, K.; Yamaguchi, K.; Mizuno, N. Platinum-supporting hollandite-type vanadium-chromium mixed oxides as efficient heterogeneous catalysts for deoxygenation of sulfoxides under atmospheric H<sub>2</sub> pressure. *Catal. Sci. Technol.* **2017**, *7*, 1912-1920.

85. Zolfigol, M. A.; Khazaei, A.; Safaiee, M.; Mokhlesi, M.; Rostamian, R.; Bagheri, M.; Shiri, M.; Kruger, H. G. Application of silica vanadic acid as a heterogeneous, selective and highly reusable catalyst for oxidation of sulfides at room temperature. *J. Mol. Catal. A: Chem.* **2013**, *370*, 80-86.
86. Fazaeli, R.; Mohagheghian, Z. Vanadium oxide supported on mesocellulose silica foams (MCF): An efficient and reusable catalyst for selective oxidation of sulfides. *Iran. Chem. Commun.* **2016**, *4*, 198-206.
87. Gregori, F.; Nobili, I.; Bigi, F.; Maggi, R.; Predieri, G.; Sartori, G. Selective oxidation of sulfides to sulfoxides and sulfones using 30% aqueous hydrogen peroxide and silica-vanadia catalyst. *J. Mol. Catal. A: Chem.* **2008**, *286*, 124-127.
88. Farzaneh, F.; Zamanifar, E.; Williams, C. D. V-MCM-41 as selective catalyst for epoxidation of olefins and trans-2-hexene-1-ol. *J. Mol. Catal. A: Chem.* **2004**, *218*, 203-209.
89. Neumann, R.; Levin-Elad, M. Vanadium silicate xerogels in hydrogen peroxide catalyzed oxidations. *Appl. Catal. A* **1995**, *122*, 85-97.
90. Tanaka, T.; Ooe, M.; Funabiki, T.; Yoshida, S. Formation of an epoxide intermediate in the photo-oxidation of alkenes over silica-supported vanadium oxide. *J. Chem. Soc., Faraday Trans. 1* **1986**, *82*, 35-43.
91. Chanquía, C. M.; Cánepa, A. L.; Winkler, E. L.; Rodríguez-Castellón, E.; Casuscelli, S. G.; Eimer, G. A. Nature of active vanadium nanospecies in MCM-41 type catalysts for olefins oxidation. *Mater. Chem. Phys.* **2016**, *175*, 172-179.
92. Tamoradi, T.; Ghadermazi, M.; Ghorbani-Choghamarani, A.; Molaei, S. Synthesis and characterization of oxo-vanadium complex anchored onto SBA-15 as a green, novel and reusable nanocatalyst for the oxidation of sulfides and oxidative coupling of thiols. *Res. Chem. Intermed.* **2018**.
93. Ben Zid, T.; Fadhli, M.; Khedher, I.; Fraile, J. M. New bis(oxazoline)-vanadyl complexes, supported by electrostatic interaction in Laponite clay, as heterogeneous catalysts for asymmetric oxidation of methyl phenyl sulfide. *Microporous Mesoporous Mater.* **2017**, *239*, 167-172.

94. Ben Zid, T.; Khedher, I.; Ksibi, Z.; Fraile, J. M. Vanadium-Schiff base complex covalently bonded on modified MCM-41 as catalyst for asymmetric oxidation of methyl phenyl sulfide. *J. Porous Mater.* **2016**, *23*, 507-516.
95. Norouzi, M.; Ghorbani-Choghamarani, A. Mild and highly efficient method for the oxidation of sulfides and protection of alcohols catalyzed by oxovanadium(IV) supported on modified magnetic nanoparticles as recyclable catalyst. *React. Kinet., Mech. Catal.* **2016**, *119*, 537-554.
96. Eftekhari-Sis, B.; Akbari, M.; Akbari, A.; Amini, M. Vanadium (V) and Tungsten (VI) Oxoperoxo-Complexes Anchored on Fe<sub>3</sub>O<sub>4</sub> Magnetic Nanoparticles: Versatile and Efficient Catalysts for the Oxidation of Alcohols and Sulfides. *Catal. Lett.* **2017**, *147*, 2106-2115.
97. Noori, N.; Nikoorazm, M.; Ghorbani-Choghamarani, A. Oxo-vanadium immobilized on L-cysteine-modified MCM-41 as catalyst for the oxidation of sulfides and oxidative coupling of thiols. *Microporous Mesoporous Mater.* **2016**, *234*, 166-175.
98. Nikoorazm, M.; Ghorbani-Choghamarani, A.; Noori, N. Oxo-vanadium(IV) Schiff base complex supported on modified MCM-41: a reusable and efficient catalyst for the oxidation of sulfides and oxidative S-S coupling of thiols. *Appl. Organomet. Chem.* **2015**, *29*, 328-333.
99. Fuerte, A.; Iglesias, M.; Sánchez, F.; Corma, A. Chiral dioxomolybdenum(VI) and oxovanadium(V) complexes anchored on modified USY-zeolite and mesoporous MCM-41 as solid selective catalysts for oxidation of sulfides to sulfoxides or sulfones. *J. Mol. Catal. A: Chem.* **2004**, *211*, 227-235.
100. Shen, C.; Qiao, J.; Zhao, L.; Zheng, K.; Jin, J.; Zhang, P. An efficient silica supported Chitosan@vanadium catalyst for asymmetric sulfoxidation and its application in the synthesis of esomeprazole. *Catal. Commun.* **2017**, *92*, 114-118.
101. Farzaneh, F.; Sadeghi, Y. Immobilized V-MIL-101 on modified Fe<sub>3</sub>O<sub>4</sub> nanoparticles as heterogeneous catalyst for epoxidation of allyl alcohols and alkenes. *J. Mol. Catal. A: Chem.* **2015**, *398*, 275-281.

102. Ben Zid, T.; Khedher, I.; Ghorbel, A. Chiral vanadyl salen catalyst immobilized on mesoporous silica as support for asymmetric oxidation of sulfides to sulfoxides. *React. Kinet., Mech. Catal.* **2010**, *100*, 131-143.
103. Bryliakov, K. P. Catalytic Asymmetric Oxygenations with the Environmentally Benign Oxidants H<sub>2</sub>O<sub>2</sub> and O<sub>2</sub>. *Chem. Rev.* **2017**, *117*, 11406-11459.
104. Gao, J.; Lu, L.; Zhou, W.; Gao, G.; He, M. Synthesis, characterization and sulfide oxidation activity of vanadyl Schiff base complexes anchored on MCM-41. *J. Porous Mater.* **2008**, *15*, 127-132.
105. Hulea, V.; Maciuca, A.-L.; Cojocariu, A.-M.; Ciocan, C.-E.; Dumitriu, E. New heterogeneous catalysts for mild oxidation of S-containing organic compounds. *C. R. Chim.* **2009**, *12*, 723-730.
106. Jing, D.; Jufang, H.; Yingnan, C.; Zhengguo, L.; Bo, Z.; Song, Y.; L., H. C.; Changwen, H. A Polyoxoniobate–Polyoxovanadate Double-Anion Catalyst for Simultaneous Oxidative and Hydrolytic Decontamination of Chemical Warfare Agent Simulants. *Angew. Chem. Int. Ed.* **2017**, *56*, 4473-4477.
107. Jung, H.; Lee, H. W.; Jeong, E. A. Enhanced thermal degradation of 2,2'-dichlorodiethyl sulfide (sulfur mustard, HD) with the presence of metal oxides. *Phosphorus Sulfur Silicon Relat Elem* **2016**, *191*, 1137-1141.
108. Liu, F.; Lu, Q.; Jiao, X.; Chen, D. Fabrication of nylon-6/POMs nanofibrous membranes and the degradation of mustard stimulant research. *RSC Adv.* **2014**, *4*, 41271-41276.
109. Mahato, T. H.; Prasad, G. K.; Singh, B.; Srivastava, A. R.; Ganesan, K.; Acharya, J.; Vijayaraghavan, R. Reactions of sulphur mustard and sarin on V<sub>1.02</sub>O<sub>2.98</sub> nanotubes. *J. Hazard. Mater.* **2009**, *166*, 1545-1549.
110. Hay, R. W.; Clifford, T.; Govan, N. Selective manganese(III) and vanadium(IV) catalysts for the oxidation of dialkyl sulfides in microemulsion media. *Transition Met. Chem.* **1998**, *23*, 619-624.

111. Sheldon, R. A.; Kochi, J. K., *Metal-Catalyzed Oxidations of Organic Compounds: Mechanistic Principles and Synthetic Methodology Including Biochemical Processes*. Academic Press, Inc: New York, NY, 1981.
112. Chatgililoglu, C.; Crich, D.; Komatsu, M.; Ryu, I. Chemistry of Acyl Radicals. *Chem. Rev.* **1999**, *99*, 1991-2070.
113. Liu, M.; Wang, H.; Zeng, H.; Li, C.-J. Silver(I) as a widely applicable, homogeneous catalyst for aerobic oxidation of aldehydes toward carboxylic acids in water—"silver mirror": From stoichiometric to catalytic. *Sci. Adv.* **2015**, *1*.
114. Dumont, V.; Oliviero, L.; Mauge, F.; Houalla, M. Oxidation of dibenzothiophene by a metal–oxygen–aldehyde system. *Catal. Today* **2008**, *130*, 195-198.
115. Song, G.; Wang, F.; Zhang, H.; Lu, X.; Wang, C. Efficient Oxidation of Sulfides Catalyzed by Transition Metal Salts with Molecular Oxygen in the Presence of Aldehydes. *Synth. Commun.* **1998**, *28*, 2783-2787.
116. Dell'Anna, M. M.; Mastrorilli, P.; Nobile, C. F. Aerobic oxidation of sulfides catalysed by cobalt(II) complexes under homogeneous and heterogeneous conditions. *J. Mol. Catal. A: Chem.* **1996**, *108*, 57-62.
117. Murata, S.; Murata, K.; Kidena, K.; Nomura, M. A Novel Oxidative Desulfurization System for Diesel Fuels with Molecular Oxygen in the Presence of Cobalt Catalysts and Aldehydes. *Energy Fuels* **2004**, *18*, 116-121.
118. El Amrani, I.; Atlamsani, A.; Dakkach, M.; Rodríguez, M.; Romero, I.; Amthiou, S. Efficient and selective oxidation of aldehydes with dioxygen catalysed by vanadium-containing heteropolyanions. *C. R. Chim.* **2017**, *20*, 888-895.
119. Mastrorilli, P.; Nobile, C. F. Catalytic activity of a polymerizable tris( $\beta$ -ketoesterate)iron(III) complex towards the oxidation of organic substrates. *Tetrahedron Lett.* **1994**, *35*, 4193-4196.
120. Nam, W.; Kim, H. J.; Kim, S. H.; Ho, R. Y. N.; Valentine, J. S. Metal Complex-Catalyzed Epoxidation of Olefins by Dioxygen with Co-Oxidation of Aldehydes. A Mechanistic Study. *Inorg. Chem.* **1996**, *35*, 1045-1049.

121. Suzuki, M.; Ishikawa, T.; Harada, A.; Ohba, S.; Sakamoto, M.; Nishida, Y. Chemical mechanism of dioxygen activation by manganese(III) Schiff base compound in the presence of aliphatic aldehydes. *Polyhedron* **1997**, *16*, 2553-2561.
122. Komiya, N.; Naota, T.; Oda, Y.; Murahashi, S.-I. Aerobic oxidation of alkanes and alkenes in the presence of aldehydes catalyzed by copper salts and copper-crown ether. *J. Mol. Catal. A: Chem.* **1997**, *117*, 21-37.
123. Tada, M.; Muratsugu, S.; Kinoshita, M.; Sasaki, T.; Iwasawa, Y. Alternative Selective Oxidation Pathways for Aldehyde Oxidation and Alkene Epoxidation on a SiO<sub>2</sub>-Supported Ru-Monomer Complex Catalyst. *J. Am. Chem. Soc.* **2010**, *132*, 713-724.
124. Joergensen, K. A. Transition-metal-catalyzed epoxidations. *Chem. Rev.* **1989**, *89*, 431-458.
125. Selvaraj, M.; Song, S. W.; Kawi, S. Epoxidation of styrene over mesoporous Zr-Mn-MCM-41. *Microporous Mesoporous Mater.* **2008**, *110*, 472-479.
126. Carlin, D. A.; Bertolani, S. J.; Siegel, J. B. Biocatalytic conversion of ethylene to ethylene oxide using an engineered toluene monooxygenase. *Chem. Commun.* **2015**, *51*, 2283-2285.
127. Mimoun, H. Oxygen Transfer from Inorganic and Organic Peroxides to Organic Substrates: A Common Mechanism? *Angew. Chem. Int. Ed. Engl.* **1982**, *21*, 734-750.
128. Kwart, H.; Hoffman, D. M. Observations Regarding the Mechanism of Olefin Epoxidation with Per Acids. *J. Org. Chem.* **1966**, *31*, 419-425.
129. Mimoun, H.; Seree de Roch, I.; Sajus, L. Epoxydation des olefines par les complexes peroxydiques covalents du molybdene—VI. *Tetrahedron* **1970**, *26*, 37-50.
130. Nunes, C. D.; Vaz, P. D.; Felix, V.; Veiros, L. F.; Moniz, T.; Rangel, M.; Realista, S.; Mourato, A. C.; Calhorda, M. J. Vanadyl cationic complexes as catalysts in olefin oxidation. *Dalton Trans.* **2015**, *44*, 5125-5138.

131. Sharpless, K. B.; Michaelson, R. C. High stereo- and regioselectivities in the transition metal catalyzed epoxidations of olefinic alcohols by tert-butyl hydroperoxide. *J. Am. Chem. Soc.* **1973**, *95*, 6136-6137.
132. Sharpless, K. B.; Townsend, J. M.; Williams, D. R. Mechanism of epoxidation of olefins by covalent peroxides of molybdenum(VI). *J. Am. Chem. Soc.* **1972**, *94*, 295-296.
133. Bingham, K. D.; Meakins, G. D.; Whitham, G. H. The mechanism of epoxide formation by peroxy-acids. *Chem. Commun. (London)* **1966**, 445-446.
134. Chong, A. O.; Sharpless, K. B. Mechanism of the molybdenum and vanadium catalyzed epoxidation of olefins by alkyl hydroperoxides. *J. Org. Chem.* **1977**, *42*, 1587-1590.
135. Housecroft, C. E.; Sharpe, A. G., *Inorganic Chemistry*. 2nd ed.; Pearson Education Limited: Harlow, England, 2005; p 182-188.
136. El-Nahhal, I. M.; Chehimi, M.; Selmane, M. Synthesis and Structural Characterization of G-SBA-IDA, G-SBA-EDTA and G-SBA-DTPA Modified Mesoporous SBA-15 Silica and Their Application for Removal of Toxic Metal Ions Pollutants. *Silicon* **2018**, *10*, 981-993.
137. Gomes, A. J.; Espreafico, E. M.; Tfouni, E. trans-[Ru(NO)Cl(cyclam)](PF<sub>6</sub>)<sub>2</sub> and [Ru(NO)(Hedta)] Incorporated in PLGA Nanoparticles for the Delivery of Nitric Oxide to B16–F10 Cells: Cytotoxicity and Phototoxicity. *Molecular Pharmaceutics* **2013**, *10*, 3544-3554.
138. Liu, Y.; Fu, R.; Sun, Y.; Zhou, X.; Baig, S. A.; Xu, X. Multifunctional nanocomposites Fe<sub>3</sub>O<sub>4</sub>@SiO<sub>2</sub>-EDTA for Pb(II) and Cu(II) removal from aqueous solutions. *Applied Surface Science* **2016**, *369*, 267-276.
139. Madarang, C. J.; Kim, H. Y.; Gao, G.; Wang, N.; Zhu, J.; Feng, H.; Gorring, M.; Kasner, M. L.; Hou, S. Adsorption Behavior of EDTA-Graphene Oxide for Pb (II) Removal. *ACS Appl. Mater. Interfaces* **2012**, *4*, 1186-1193.
140. Egli, T. Biodegradation of metal-complexing aminopolycarboxylic acids. *J. Biosci. Bioeng.* **2001**, *92*, 89-97.

141. Kroll, H.; Korman, S.; Siegel, E.; Hart, H. E.; Rosoff, B.; Spencer, H.; Laszlo, D. Excretion of Yttrium and Lanthanum Chelates of Cyclohexane 1,2-Trans Diamine Tetraacetic Acid and Diethylenetriamine Pentaacetic Acid in Man. *Nature* **1957**, *180*, 919.
142. Lohrke, J.; Frenzel, T.; Endrikat, J.; Alves, F. C.; Grist, T. M.; Law, M.; Lee, J. M.; Leiner, T.; Li, K.-C.; Nikolaou, K.; Prince, M. R.; Schild, H. H.; Weinreb, J. C.; Yoshikawa, K.; Pietsch, H. 25 Years of Contrast-Enhanced MRI: Developments, Current Challenges and Future Perspectives. *Adv. Ther.* **2016**, *33*, 1-28.
143. Yang, D.; Yang, G.; Gai, S.; He, F.; Lv, R.; Dai, Y.; Yang, P. Imaging-Guided and Light-Triggered Chemo-/Photodynamic/Photothermal Therapy Based on Gd (III) Chelated Mesoporous Silica Hybrid Spheres. *ACS Biomater. Sci. Eng.* **2016**, *2*, 2058-2071.
144. Zhang, C.; Zhang, F.; Wang, W.; Liu, J.; Xu, M.; Wu, D.; Shuai, X.; Shen, J.; Cao, Z. Chitosan coated gold nanorod chelating gadolinium for MRI-visible photothermal therapy of cancer. *RSC Adv.* **2016**, *6*, 111337-111344.
145. Jiang, B.; Liu, M.; Zhang, K.; Zu, G.; Dong, J.; Cao, Y.; Zhang, L.; Pei, R. Oligoethylenimine grafted PEGylated poly(aspartic acid) as a macromolecular contrast agent: properties and in vivo studies. *J. Mater. Chem. B* **2016**, *4*, 3324-3330.
146. Cooper, M. S.; Ma, M. T.; Sunassee, K.; Shaw, K. P.; Williams, J. D.; Paul, R. L.; Donnelly, P. S.; Blower, P. J. Comparison of <sup>64</sup>Cu-Complexing Bifunctional Chelators for Radioimmunoconjugation: Labeling Efficiency, Specific Activity, and in Vitro/in Vivo Stability. *Bioconjugate Chem.* **2012**, *23*, 1029-1039.
147. Laprise-Pelletier, M.; Bouchoucha, M.; Lagueux, J.; Chevallier, P.; Lecomte, R.; Gossuin, Y.; Kleitz, F.; Fortin, M.-A. Metal chelate grafting at the surface of mesoporous silica nanoparticles (MSNs): physico-chemical and biomedical imaging assessment. *J. Mater. Chem. B* **2015**, *3*, 748-758.
148. Laurent, S.; Henoumont, C.; Vander Elst, L.; Muller, R. N. Synthesis and Physicochemical Characterisation of Gd-DTPA Derivatives as Contrast Agents for MRI. *Eur. J. Inorg. Chem.* **2012**, *2012*, 1889-1915.

149. Liu, Y.; Zhang, N. Gadolinium loaded nanoparticles in theranostic magnetic resonance imaging. *Biomaterials* **2012**, *33*, 5363-5375.
150. Boehm-Sturm, P.; Haeckel, A.; Hauptmann, R.; Mueller, S.; Kuhl, C. K.; Schellenberger, E. A. Low-Molecular-Weight Iron Chelates May Be an Alternative to Gadolinium-based Contrast Agents for T1-weighted Contrast-enhanced MR Imaging. *Radiology* **2018**, *286*, 537-546.
151. Pniok, M.; Kubíček, V.; Havlíčková, J.; Kotek, J.; Sabatie-Gogová, A.; Plutnar, J.; Huclier-Markai, S.; Hermann, P. Thermodynamic and Kinetic Study of Scandium(III) Complexes of DTPA and DOTA: A Step Toward Scandium Radiopharmaceuticals. *Chem. - Eur. J.* **2014**, *20*, 7944-7955.
152. Lu, Y.; Ngo Ndjock Mbong, G.; Liu, P.; Chan, C.; Cai, Z.; Weinrich, D.; Boyle, A. J.; Reilly, R. M.; Winnik, M. A. Synthesis of Polyglutamide-Based Metal-Chelating Polymers and Their Site-Specific Conjugation to Trastuzumab for Auger Electron Radioimmunotherapy. *Biomacromolecules* **2014**, *15*, 2027-2037.
153. Liu, M.; Xu, W.; Xu, L.-j.; Zhong, G.-r.; Chen, S.-l.; Lu, W.-y. Synthesis and Biological Evaluation of Diethylenetriamine Pentaacetic acid–Polyethylene Glycol–Folate: A New Folate-Derived, <sup>99m</sup>Tc-Based Radiopharmaceutical. *Bioconjugate Chem.* **2005**, *16*, 1126-1132.
154. Liu, P.; Boyle, A. J.; Lu, Y.; Adams, J.; Chi, Y.; Reilly, R. M.; Winnik, M. A. Metal-Chelating Polymers (MCPs) with Zwitterionic Pendant Groups Complexed to Trastuzumab Exhibit Decreased Liver Accumulation Compared to Polyanionic MCP Immunoconjugates. *Biomacromolecules* **2015**, *16*, 3613-3623.
155. Liu, S.; Edwards, D. S. Bifunctional Chelators for Therapeutic Lanthanide Radiopharmaceuticals. *Bioconjugate Chem.* **2001**, *12*, 7-34.
156. Zhang, N.-n.; Yu, R.-s.; Xu, M.; Cheng, X.-y.; Chen, C.-m.; Xu, X.-l.; Lu, C.-y.; Lu, K.-j.; Chen, M.-j.; Zhu, M.-l.; Weng, Q.-y.; Hui, J.-g.; Zhang, Q.; Du, Y.-Z.; Ji, J.-s. Visual targeted therapy of hepatic cancer using homing peptide modified calcium phosphate nanoparticles loading doxorubicin guided by T1 weighted MRI. *Nanomedicine* **2018**, *14*, 2167-2178.

157. Li, S.; Wang, F.; He, X.-W.; Li, W.-Y.; Zhang, Y.-K. One-pot hydrothermal preparation of gadolinium-doped silicon nanoparticles as a dual-modal probe for multicolor fluorescence and magnetic resonance imaging. *J. Mater. Chem. B* **2018**, *6*, 3358-3365.
158. Pourmanouchehri, Z.; Jafarzadeh, M.; Kakaei, S.; Khameneh, E. S. Magnetic Nanocarrier Containing  $^{68}\text{Ga}$ -DTPA Complex for Targeted Delivery of Doxorubicin. *J. Inorg. Organomet. Polym. Mater.* **2018**, *28*, 1980-1990.
159. Wu, B.; Lu, S.-T.; Yu, H.; Liao, R.-F.; Li, H.; Lucie Zafitatsimo, B. V.; Li, Y.-S.; Zhang, Y.; Zhu, X.-L.; Liu, H.-G.; Xu, H.-B.; Huang, S.-W.; Cheng, Z. Gadolinium-chelate functionalized bismuth nanotheranostic agent for in vivo MRI/CT/PAI imaging-guided photothermal cancer therapy. *Biomaterials* **2018**, *159*, 37-47.
160. Zhang, C.; Wu, D.; Lu, L.; Duan, X.; Liu, J.; Xie, X.; Shuai, X.; Shen, J.; Cao, Z. Multifunctional Hybrid Liposome as a Theranostic Platform for Magnetic Resonance Imaging Guided Photothermal Therapy. *ACS Biomater. Sci. Eng.* **2018**, *4*, 2597-2605.
161. Bernhard, Y.; Winckler, P.; Perrier-Cornet, J.-M.; Decreau, R. A. Harnessing medically relevant metals onto water-soluble subphthalocyanines: towards bimodal imaging and theranostics. *Dalton Trans.* **2015**, *44*, 3200-3208.
162. Bouchoucha, M.; C.-Gaudreault, R.; Fortin, M.-A.; Kleitz, F. Mesoporous Silica Nanoparticles: Selective Surface Functionalization for Optimal Relaxometric and Drug Loading Performances. *Adv. Funct. Mater.* **2014**, *24*, 5911-5923.
163. Kaur, M.; Zhang, H.; Martin, L.; Todd, T.; Qiang, Y. Conjugates of Magnetic Nanoparticle—Actinide Specific Chelator for Radioactive Waste Separation. *Environ. Sci. Technol.* **2013**, *47*, 11942-11959.
164. Tian, G.; Zhang, Z.; Martin, L. R.; Rao, L. Complexation of Curium(III) with DTPA at 10–70 °C: Comparison with Eu(III)–DTPA in Thermodynamics, Luminescence, and Coordination Modes. *Inorg. Chem.* **2015**, *54*, 1232-1239.
165. Shkrob, I. A.; Marin, T. W.; Jensen, M. P. Ionic Liquid Based Separations of Trivalent Lanthanide and Actinide Ions. *Ind. Eng. Chem. Res.* **2014**, *53*, 3641-3653.

166. Yang, B.; Liao, L.; Zeng, Y.; Zhu, X.; Wan, Y. A simple and recyclable copper/DTPA catalyst system for amination of aryl halides with aqueous ammonia in water. *Catal. Commun.* **2014**, *45*, 100-103.
167. Bouriazos, A.; Sotiriou, S.; Stathis, P.; Papadogianakis, G. Superior aqueous-phase catalytic hydrogenation activity of palladium modified with nitrogen-containing ligands compared with the TPPTS benchmark modifier in micellar nanoreactors. *Appl. Catal. B* **2014**, *150-151*, 345-353.
168. Shao, D.; Li, Y. Preparation of polycarboxylic acid-functionalized silica supported Pt catalysts and their applications in alkene hydrosilylation. *RSC Adv.* **2018**, *8*, 20379-20393.
169. Díaz-de Alba, M.; Galindo-Riaño, M. D.; Casanueva-Marenco, M. J.; García-Vargas, M.; Kosore, C. M. Assessment of the metal pollution, potential toxicity and speciation of sediment from Algeciras Bay (South of Spain) using chemometric tools. *J. Hazard. Mater.* **2011**, *190*, 177-187.
170. Lottermoser, B. G. Colonisation of the rehabilitated Mary Kathleen uranium mine site (Australia) by *Calotropis procera*: Toxicity risk to grazing animals. *J. Geochem. Explor.* **2011**, *111*, 39-46.
171. Kosore, C. M.; Galindo-Riaño, M. D.; Díaz-de-Alba, M. Assessing trace-element mobility in Algeciras Bay (Spain) sediments by acid and complexing screening. *Arabian J. Chem.* **2015**.
172. Tsadilas, C. D.; Shaheen, S. M. Distribution of Total and Ammonium Bicarbonate-DTPA-Extractable Soil Vanadium From Greece and Egypt and Their Correlation To Soil Properties. *Soil Sci.* **2010**, *175*, 535-543.
173. Pinto, E.; Almeida, A. A.; Ferreira, I. M. P. L. V. O. Assessment of metal(loid)s phytoavailability in intensive agricultural soils by the application of single extractions to rhizosphere soil. *Ecotoxicol. Environ. Saf.* **2015**, *113*, 418-424.
174. Chen, B.; Shan, X.-q.; Qian, J. Bioavailability index for quantitative evaluation of plant availability of extractable soil trace elements. *Plant Soil* **1996**, *186*, 275-283.

175. Domingo, J. L.; Gomez, M.; Llobet, J. M.; Corbella, J. Chelating agents in the treatment of acute vanadyl sulphate intoxication in mice. *Toxicology* **1990**, *62*, 203-211.
176. Hamada, T. A new experimental system of using fertile chick eggs to evaluate vanadium absorption and antidotal effectiveness to prevent vanadium uptake. *J. Nutr. Biochem.* **1994**, *5*, 382-388.
177. Majlesi, K.; Rezaieejad, S.; Balali, S. Speciation and Stability of Dioxovanadium(V) Complexes with Diethylenetriaminepentaacetic Acid at Different Ionic Strengths. *J. Solution Chem.* **2013**, *42*, 1729-1747.
178. Chen, Z.; Naidu, R. On-column complexation and simultaneous separation of vanadium(IV) and vanadium(V) by capillary electrophoresis with direct UV detection. *Anal. Bioanal. Chem.* **2002**, *374*, 520-525.
179. Pozdniakova, S. Speciation of metals in different oxidation states by capillary electrophoresis using pre-capillary complexation with complexones. *Analyst* **1998**, *123*, 1497-1500.
180. Inoue, K.; Yoshizuka, K.; Ohto, K. Adsorptive separation of some metal ions by complexing agent types of chemically modified chitosan. *Anal. Chim. Acta* **1999**, *388*, 209-218.
181. Lee, M.-H.; O, T.-S. Carbon-13 and Vanadium-51 Nuclear Magnetic Resonance Studies of Vanadium(v)-Aminopolycarboxylic Acids (I). *J. Korean Chem. Soc.* **1983**, *27*, 117-126.
182. Kanamori, K.; Ino, K.; Maeda, H.; Miyazaki, K.; Fukagawa, M.; Kumada, J.; Eguchi, T.; Okamoto, K.-i. Relationship between Oxo-Bridged Dimer Formation and Structure of Vanadium(III) amino polycarboxylates. *Inorg. Chem.* **1994**, *33*, 5547-5554.
183. Chen, J. W.; Belford, R. L.; Clarkson, R. B. Second-Sphere and Outer-Sphere Proton Relaxation of Paramagnetic Complexes: From EPR to NMRD. *J. Phys. Chem. A* **1998**, *102*, 2117-2130.

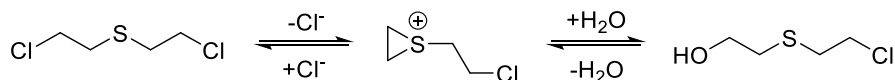
184. Rehder, D., *Bioinorganic vanadium chemistry*. John Wiley & Sons: West Sussex, England, 2008; Vol. 30.
185. Sing, K. S. W.; Everett, D. H.; Haul, R. A. W.; Moscou, L.; Pierotti, R. A.; Rouquerol, J.; Siemieniewska, T. Reporting Physisorption Data for Gas/Solid Systems With Special Reference to the Determination of Surface Area and Porosity. *Pure Appl. Chem.* **1985**, *57*, 603-619.
186. Brunauer, S.; Emmett, P. H.; Teller, E. Adsorption of Gases in Multimolecular Layers. *J. Am. Chem. Soc.* **1938**, *60*, 309–319.
187. Thommes, M. Physical Adsorption Characterization of Nanoporous Materials. *Chem. Ing. Tech.* **2010**, *82*, 1059-1073.
188. Cohan, L. H. Hysteresis and the Capillary Theory of Adsorption of Vapors. *J. Am. Chem. Soc.* **1944**, *66*, 98-105.
189. Cohan, L. H. Sorption Hysteresis and the Vapor Pressure of Concave Surfaces. *J. Am. Chem. Soc.* **1938**, *60*, 433-435.
190. Barrett, E. P.; Joyner, L. G.; Halenda, P. P. The Determination of Pore Volume and Area Distributions in Porous Substances. I. Computations from Nitrogen Isotherms. *J. Am. Chem. Soc.* **1951**, *73*, 373–380.
191. Lowell, S.; Shields, J. E.; Thomas, M. A.; Thommes, M., *Characterization of Porous Solids and Powders: Surface Area, Pore Size and Density*. Kluwer Academic Publishers: Dordrecht, The Netherlands, 2004; p 347.
192. Weil, J. A.; Bolton, J. R.; Wertz, J. E., *Electron Paramagnetic Resonance: Elementary Theory and Practical Applications*. John Wiley & Sons, Inc: New York, NY, 1994.
193. Palmer, G., Electron Paramagnetic Resonance of Metalloproteins. In *Physical Methods in Bioinorganic Chemistry Spectroscopy and Magnetism*, Que, L., Ed. University Science Books: Sausalito, CA, 2000; pp 121-185.

194. Ebsworth, E. A. V.; Rankin, D. W.; Cradock, S., *Structural Methods in Inorganic Chemistry*. Blackwell Scientific Publications: Oxford, England, 1987.
195. Ball, D. W., *Physical Chemistry*. Brooks/Cole- Thomson Learning: Pacific Grove, CA, 2003; p 519-559.
196. Stoll, S.; Schweiger, A. EasySpin, a comprehensive software package for spectral simulation and analysis in EPR. *J. Magn. Reson.* **2006**, *178*, 42-55.
197. Neese, F. The ORCA program system. *Wiley Interdiscip. Rev.: Comput. Mol. Sci.* **2012**, *2*, 73-78.
198. Petrenko, T.; Sturhahn, W.; Neese, F. First-principles calculation of nuclear resonance vibrational spectra. *Hyperfine Interactions* **2007**, *175*, 165-174.

## CHAPTER 2: VO(dtpa) IMMOBILIZED ON MESOPOROUS SILICA: STRUCTURAL CHARACTERIZATION AND SULFIDE OXIDATION

### 2.1 Introduction

New materials and methods designed to react with bis(2-chloroethyl) sulfide, commonly known as sulfur mustard or mustard gas, are of interest because this compound is a vesicant, leading to blistering and injury upon contact.<sup>1</sup> As a chemical warfare agent, concerns remain about the decontamination of chemical stockpiles and treatment of chemical exposures to sulfur mustard. Oxidative processes involving conversion of this sulfide to its corresponding sulfoxide or sulfone are important because its blistering properties arise as a result of hydrolysis of the C-Cl bond to form HCl,<sup>2</sup> a process that mechanistically involves cyclization to form a cyclic thioether (**Scheme 2.1**); this pathway is not available in the oxidized forms.



**Scheme 2.1.** Hydrolysis of bis(2-chloroethyl) sulfide.

Large-scale oxidation of sulfur mustard can be accomplished by reaction with bulk commodities such as hydrogen peroxide or bleach.<sup>3-5</sup> However, transport, corrosion, and toxicity concerns limit the practical use of these strong oxidants. Additionally, as oxidants are quantitative, they must be constantly supplied. Catalytic processes are therefore preferable; in particular, vanadium complexed in solution or distributed on solid supports has been shown to be an excellent catalyst for the oxidation of sulfides.<sup>6-14</sup> Heterogeneous systems are more practically useful, cost-effective, and environmentally friendly. Several systems have been developed involving vanadium. To begin, vanadium

oxide nanomaterials<sup>15,16</sup> and mixed oxide materials which include vanadium<sup>17</sup> have demonstrated their catalytic ability towards the degradation of mustard. An example of such material is work by Prasad.<sup>15</sup> Prasad developed a catalytic process based on  $V_{1.02}O_{2.98}$  nanotubes which were prepared by heating  $V_2O_5$  with dodecylamine, ethanol, and water for 7 days at 180 °C. These nanotubes were effective at degrading sulfur mustard into three degradation products through interaction with the catalyst's surface. Two of the products were not oxidative degradation pathways. The sulfur mustard could react with physisorbed water to form thiodiglycols and the sulfur mustard could also react with the surface hydroxyls to form covalently bonded products. The third product, sulfoxide, which is from an oxidative degradation pathway, was produced with molecular oxygen as the oxidant.<sup>15</sup> Although the idea of molecular oxygen as an oxidant is appealing, these reactions took approximately 40 hours to degrade mustard.<sup>15</sup> Similarly, heterogeneous catalysts can be made that produce oxidative products from photoinduced radical surface hydroxyls.<sup>18-20</sup> One example of this is a heterogeneous catalyst made by immobilizing  $VO(acac)_2$  onto  $TiO_2$  nanocatalysts.<sup>19</sup> The catalyst degraded mustard through three pathways: elimination, oxidation and hydrolysis. Using dimethylsulfoxide as a probe, the reaction produced methanesulfonic acid ethyl ester and methanesulfonic acid. These products result from hydroxyl radicals created on the surface from the exposure to visible light. Although activation by light produces a faster catalysis than simple vanadium catalysts with molecular oxygen, the reactions take 180 min which is still quite a long time. Also, this catalyst was only able to be recycled three times due to catalyst poisoning from alkoxy species,  $H_2SO_4$  and  $HCl$  on the surface.<sup>19</sup> Finally, another series of catalysts involve polyoxometalates or POMS which are often homogeneous<sup>21,22</sup>

and have been showed to oxidize sulfides with molecular oxygen.<sup>3,23-25</sup> In order to use POMS heterogeneously, hybrid materials must be synthesized.<sup>24,26</sup> An example of such a material is by Jiao.<sup>24</sup> They prepared a vanadium polyoxometalate ( $H_{3+n}PMo_{12-n}VnO_{40} \cdot xH_2O$  and  $H_3PW_{12}O_{40} \cdot xH_2O$  n = 1, 2, 3), electrospun it with nylon-6 to make a catalytic fiber, and then showed that it was effective at degrading sulfur mustard by oxidation with molecular oxygen.<sup>16</sup> Their catalyst was quite slow, taking six hours to degrade 41.55% of the mustard gas to which the fabric was exposed.<sup>24</sup> Another example is embedding a POM,  $H_5PV_2Mo_{10}O_{40}$ , into a metal organic frameworks (MOFs), which in this study was MIL-101(Cr).<sup>26</sup> The MOF without the POM decontaminates through adsorption but when the POM is embedded, oxidation products are also observed. The degradation took a little over 2 hours.

We recently showed that V-doped porous silica nanoparticles are active catalysts for the rapid oxidative decontamination of a commonly used sulfur mustard analogue, 2-chloroethyl ethyl sulfide (CEES), in aldehydes using only  $O_2$  from air as the oxidant source at room temperature.<sup>6</sup> As a heterogeneous system operating at ambient conditions, using an aldehyde as the solvent and producing only propionic acid as a byproduct, this process is particularly attractive for oxidation of sulfur compounds. Mechanistic studies indicated that the vanadium performs a dual catalytic role.<sup>6</sup> First, it rapidly converts the aldehyde to the corresponding peroxyacid using dissolved  $O_2$ , a process that has been observed for aldehydes but that is commonly slow. Once the peroxyacid is formed, the vanadium catalytically transfers an oxygen atom to the sulfide, forming the sulfoxide and carboxylic acid as products. The sulfoxide can then react at the vanadium site with a second equivalent of peroxyacid to form the sulfone, but this process is significantly

slower; thus, the sulfone appears only after all of the sulfide has reacted. One problem with this system was that because the vanadium was distributed onto the porous silica support by ion exchange and calcination, under humid conditions or when water was a contaminant the vanadium would leach from the solid, leading to decreased or no catalytic activity.

In this study, we sought to chelate vanadium within the porous silica by covalently linking the multi-dentate chelator diethylenetriamine pentaacetate (dtpa) onto the surface through peptide coupling of one of the acetate groups to 3-aminopropyltriethoxysilane (APTES), condensing the dtpa-APTES molecule onto the mesoporous silica surface, and then exchanging a vanadyl salt into the resulting solid. In addition to being easily modified through peptide coupling, dtpa has been shown to be an effective chelator for transition metals in a variety of applications.<sup>27</sup> For example, it has been used in the detection and/or removal of first-row transition metal ions from soil and wastewater, including  $\text{Sc}^{3+}$ ,  $\text{Cr}^{3+}$ ,  $\text{Cr}^{4+}$ ,  $\text{Cr}^{6+}$ ,  $\text{Ni}^{2+}$ ,  $\text{Cu}^{2+}$ , and  $\text{Zn}^{2+}$ .<sup>28-35</sup> Dtpa is also an effective chelator in biological conditions<sup>36</sup> and has been used to complex  $^{47}\text{Sc}^{3+}$ ,  $^{45}\text{Sc}^{3+}$ , and  $^{45}\text{Ti}^{3+}$  in radiopharmaceutical applications.<sup>37-39,40</sup> With respect to vanadium, dtpa has been used in similar applications, such as metal extraction,<sup>41-44</sup> measuring vanadium phytoavailability,<sup>45,46</sup> and for the chelation of vanadium in biological systems.<sup>47,48</sup> Some researchers have used dtpa to investigate the stability constants for  $\text{VO}_2^+$  ions in solution,<sup>49</sup> and others have determined vanadium speciation using chelation with dtpa and capillary electrophoresis.<sup>50-52</sup> These applications have relied on the chelation of vanadium and formation of a  $\text{VO}(\text{dtpa})$  complex, but they have not explored the actual structure of the complex. To our knowledge, only three studies have attempted to define the structure

of the VO(dtpa) complex.<sup>53-55</sup> Each group used a different vanadium source and different spectroscopic techniques, proposing various hexacoordinate or heptacoordinate structures without consistency.

Because very few examples of V complexes with dtpa exist, and because the structural information from those studies has produced inconsistent results, we sought as part of our study to define the coordination environment of the vanadium in the immobilized complex. Then, we used it in the same aldehyde-O<sub>2</sub> sulfide oxidation system described above<sup>6</sup> to show that the vanadium remained active in this type of process after chelation.

## **2.2 Experimental Section**

### **2.2.1 Materials and methods**

(3-aminopropyl)triethoxysilane was obtained from Gelest, Inc. All other chemicals were obtained from Sigma Aldrich. Porosity and surface area measurements were obtained at 77 K on a Micromeritics TriStar 3000 surface area and porosity analyzer. Samples were degassed on a Micromeritics FlowPrep 060 Sample Degas System. Surface areas and pore size distributions were calculated using the BET and BJH theories. Thermogravimetric analysis was completed on a Perkin Elmer Pyris 1 TGA. Elemental analysis via inductively-coupled plasma optical emission spectroscopy (ICP-OES) was completed on a PerkinElmer Optima 7000DV ICP optical emission spectrometer with a CCD array detector, a PerkinElmer S10 autosampler, and WinLab32 software. Cross polarization magic angle spinning (CP MAS) Solid-State Nuclear Magnetic Resonance was completed on a Bruker AXR 500 MHz spectrometer with a

solid state probe (MAS DVT 500SB BL3.2 N-P/H). Electron Paramagnetic Resonance was done at 4K on a Bruker. EPR was modeled with EasySpin.<sup>56</sup>

### **2.2.2 Synthesis of Acid Prepared Mesoporous Spheres (APMS)**

APMS was synthesized from a previously published protocol.<sup>57-58</sup> Briefly, cetyltrimethylammonium bromide (CTAB, 3.6 g, 9.88 mmol) was added to a solution of H<sub>2</sub>O (79.2 g), EtOH (200 proof, 22.2 g, 0.482 mol) and HCl (37 wt%, 8.8 g, 89 mmol) at room temperature. The solution was stirred for approximately 10 min, and then Si(OEt)<sub>4</sub> (TEOS, 8.0 g, 38 mmol) was added and stirring was continued for another 10 min. A solution of NaF (0.5 M, 9.52 g, 4.76 mmol) was then added. Precipitation occurred after 1.5 min, and stirring was continued for an additional 0.5 min, after which the mixture was transferred to a Teflon container that was sealed and placed in an oven at 373 K for 120 min. The mixture was then cooled to room temperature while stirring in an ice bath, and the precipitate was collected via vacuum filtration, rinsed with H<sub>2</sub>O and EtOH to remove adsorbed surfactant, and dried overnight. Surfactant was removed by calcination using the following program: the sample was heated from 298 K to 723 K at a rate of 2 K/min, followed by a 240 min hold at 723 K. The sample was then ramp to 823 K at a rate of 10 K/min with a hold time of 480 min at 823 K before cooling to room temperature.

### **2.2.3 Synthesis of dtpa-APMS**

Diethylenetriaminepentaacetic dianhydride (dtpa, 0.07 g, 0.2 mmol), N-(3-dimethylaminopropyl)-N'-ethylcarbodiimide hydrochloride (EDC, 0.038 g, 0.2 mmol) and N-hydroxysuccinimide (NHS, 0.023 g, 0.2 mmol) were dissolved in 5 mL of dry DMSO in a sealed round bottomed flask under N<sub>2</sub>. After 1 h, 3-aminopropyltriethoxysilane (APTES, 31.2  $\mu$ L, 0.13 mmol, 1:1.5 molar ratio to dtpa) was

added, and the solution was stirred for 24 h at room temperature. In a separate vial, 0.2 g of APMS was stirred in 15 mL H<sub>2</sub>O for 24 h. The APMS was collected by centrifugation and vacuum filtration, and then suspended in 10 mL toluene in a 25 mL round bottom flask. The DMSO solution was then added via direct addition to the toluene mixture, and the resulting mixture was refluxed for approximately 18 h. After cooling to room temperature, the modified APMS was collected by centrifugation and vacuum filtration, and washed with DMSO, toluene, EtOH, and NaOAc buffer (10 μM, pH = 6.5), and dried overnight.

#### **2.2.4 Chelation of vanadium to dtpa-APMS and exchanged vanadium APMS (V-APMS-exch)**

dtpa-APMS or APMS (0.10 g) was placed in a 4 dram scintillation vial and sonicated briefly in NaOAc buffer (10 mL, 10 μM, pH = 6.5). In a separate vial, VOSO<sub>4</sub> • xH<sub>2</sub>O (x = 3-5, 0.03 g, excess) was dissolved in H<sub>2</sub>O (5 mL), and then added to the APMS mixture. After stirring for 4 h at room temperature, the resulting material was collected by centrifugation and vacuum filtration, washed with H<sub>2</sub>O and NaOAc buffer (10 μM, pH = 6.5), and dried in a vacuum oven at room temperature overnight.

#### **2.2.5 Synthesis of incipient wetness prepared vanadium APMS (V-APMS-incip)**

V-APMS-incip was synthesized from a previously published protocol.<sup>6</sup> Briefly, NH<sub>4</sub>VO<sub>3</sub> (0.011 g, 0.09 mmol) was dissolved in H<sub>2</sub>O (10 mL), and APMS (0.1 g) was added. The mixture was stirred to dryness and calcined using the calcination program for APMS as described above.

### **2.2.6 Catalytic oxidation of sulfide to sulfoxide**

The catalysis protocol was modified from a previously published procedure. 2-chloroethyl ethylsulfide (CEES, 5  $\mu\text{L}$ , 1.07 g/mL, 42.9  $\mu\text{mol}$ ) and propionaldehyde (61.9  $\mu\text{L}$ , 0.805 g/mL, 858  $\mu\text{mol}$ ) were placed in a 3 mL volumetric flask, which was filled with  $\text{C}_4\text{F}_9\text{OCH}_3$  (3M™ Novec™ 7100 Engineered Fluid, HFE-7100). 1,2,4-trimethylbenzene (1  $\mu\text{L}$ , 0.876 g/mL, 7.88  $\mu\text{mol}$ ) was added as a GC reference. Catalysis was initiated by simply adding one of the vanadium-loaded catalysts prepared above (20 mg) to this solution. Aliquots (200  $\mu\text{L}$ ) were removed with a 2 mL plastic syringe, the solid catalyst was filtered out using a 0.22  $\mu\text{m}$  Millipore syringe filter, and the resulting filtrate was analyzed by gas chromatography with mass spectrometric detection using a HP-5 (length 30 m, i.d. 0.32 mm) column.

### **2.2.7 Determination of leaching**

Vanadium-loaded material (20 mg) was stirred in  $\text{H}_2\text{O}$  (3 mL) for 8 h. The resulting material was collected by centrifugation, washed with  $\text{H}_2\text{O}$ , and dried under vacuum at room temperature.

### **2.2.8 Recycling of the catalyst**

2-Chloroethyl ethyl sulfide (CEES, 41.7  $\mu\text{L}$ , 1.07 g/mL, 358  $\mu\text{mol}$ ) and 1,2,4-trimethylbenzene (8.33  $\mu\text{L}$ , 0.876 g/mL, 60.7  $\mu\text{mol}$ ) were mixed into 25 mL stock solutions with  $\text{C}_4\text{F}_9\text{OCH}_3$  (3M™ Novec™ 7100 Engineered Fluid, HFE-7100) as a solvent. For reaction 0x, 3mL of stock with mixed with propionaldehyde (61.9  $\mu\text{L}$ , 0.805 g/mL, 858  $\mu\text{mol}$ ) and then added to a VO(dtpa)-APMS (20 mg). At the same time, a recycle pot of 66 mg of VO(dtpa) were mixed with CEES (16.55  $\mu\text{L}$ , 1.07 g/mL, 142  $\mu\text{mol}$ ), 1,2,4-trimethylbenzene (3.31  $\mu\text{L}$ , 0.876 g/mL, 24.1  $\mu\text{mol}$ ) and propionaldehyde

(205  $\mu\text{L}$ , 0.805 g/mL, 2.84 mmol). Aliquots (200  $\mu\text{L}$ ) were removed with a 2 mL plastic syringe, the solid catalyst was filtered out using a 0.22  $\mu\text{m}$  Millipore syringe filter, and the resulting filtrate was analyzed by gas chromatography with mass spectrometric detection using a ZB-5 (length 30 m, i.d. 0.25 mm) column. The recycle pot was centrifuged, washed with 10 mL  $\text{C}_4\text{F}_9\text{OCH}_3$ , dried for 1 hour at 110  $^\circ\text{C}$  and then dried under vacuum overnight. This cycle was repeated 3 more times.

## 2.3 Results and Discussion

### 2.3.1 Physical characterization of materials containing grafted dtpa and VO(dtpa) complexes

Of the many types of porous silica supports that could be used for these experiments, acid-prepared mesoporous silica (APMS) were prepared due to their facile and low-cost synthesis, high thermal stability,<sup>59</sup> and large internal surface area.<sup>60</sup> This material is easily and rapidly prepared by the polymerization of a silicon alkoxide source in the presence of surfactants in acidic solutions. Once prepared, the particles were calcined to remove the surfactant and provide access to the internal porosity. Scanning electron microscopy (**Figure 2.1**) showed that the particles were monodisperse and had a spherical morphology, consistent with our previous results. Because calcination tends to reduce the number of silanol groups on the silica surface by dehydration reactions, and because a post-synthetic grafting method was used to attach the chelating ligands to the surface, the calcined material was stirred in water for an extended period of time to rehydrate the surface. This step, which has been employed previously for this purpose,<sup>61</sup>

was important to maximize the number of metal complexes, and therefore the amount of catalyst, in the solid.

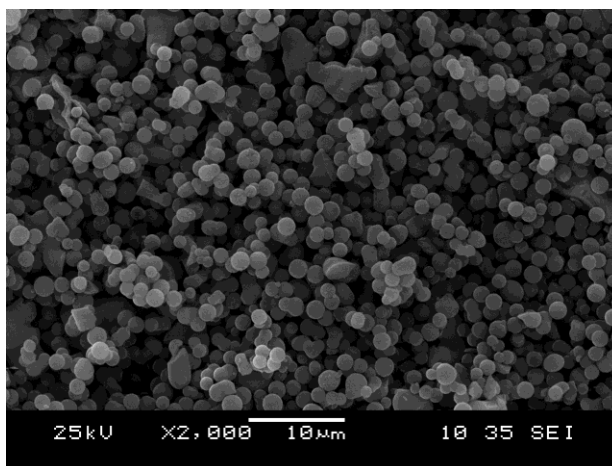
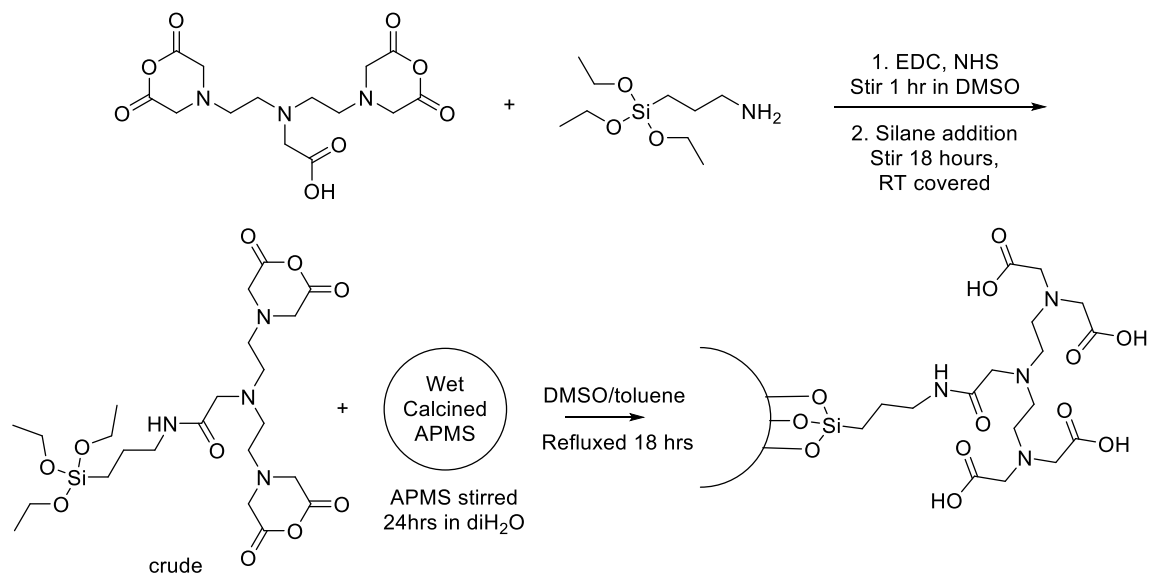


**Figure 2.1.** Scanning electronic microscope (SEM) image of VO(dtpa)-APMS.

To prepare the ligand to be immobilized onto the porous substrate, diethylenetriamine pentaacetic anhydride (dtpa) was modified with 3-aminopropyltriethoxysilane (APTES) by coupling to the free carboxylic acid group on the dtpa (**Scheme 2.2**). Initially, a two-step modification process was used, first condensing APTES to the surface, then isolating the product and coupling dtpa to the amine-modified surface. However, this procedure led to a more complicated and less defined surface because the peptide coupling of the dtpa to the APTES was never complete. The free amines that were left behind on the surface could form complexes with the vanadyl ions, complicating the catalytic results. In addition, any anhydrides that had reacted with residual water within the APMS to form carboxylates could lead to the reaction of a single molecule of dtpa with several APTES molecules, preventing it from fully complexing to a vanadyl group. Coupling the dtpa to APTES before grafting to

APMS afforded the most synthetic control and maximized the amount of complex immobilized on the solid.



**Scheme 2.2.** Synthesis procedure used to prepare dtpa-APMS.

During the surface grafting step, APMS that was slightly wet from the rehydration process was used to not only ensure that as many surface silanol groups as possible were open but also to react with the anhydrides to form carboxylates and to prevent any excess coupling reagents from binding to the surface. After isolating the product and washing to remove adventitious dtpa silane that had not reacted, modified APMS was placed in NaOAc buffer and an aqueous solution of vanadyl sulfate was added to form the vanadyl complexes on the surface. Thermogravimetric analysis (TGA) prior to vanadyl complexation showed that 0.364 mmol/g of dtpa silane had been grafted.

N<sub>2</sub> physisorption was used to characterize the porosity of the solid at each stage of modification (**Table 2.1**). The as-synthesized material analyzed after calcination was highly porous, with a pore volume of approximately 1.0 cm<sup>3</sup>/g, surface area of 573 m<sup>2</sup>/g

and moderately large pores of 71 Å. Synthesis conditions were used to produce a material with this pore diameter to ensure that complexes could be formed within the pores and to maximize molecular diffusion. After grafting with the dtpa silane, the pore diameter and pore volume decreased, indicating successful modification of the pore surfaces. The change in these parameters is also due to silica restructuring during the aqueous treatment to rehydrate the surface. However, the material remained very porous after grafting and did not change significantly upon complexation with vanadyl sulfate.

**Table 2.1.** Physical Characterization of the Porous Solids.

Material	$d_{\text{pore}}$ (Å)	$S_{\text{ABET}}$ (m <sup>2</sup> /g)	$V_{\text{pore}}$ (cm <sup>3</sup> /g)
APMS	71	573	0.999
after dtpa grafting	58	500	0.688
after V complexation	52	506	0.640

Initial structural characterization of the grafted dtpa-silane was performed by solid-state NMR spectroscopy (**Figure 2.2**). <sup>29</sup>Si CPMAS NMR of the rehydrated APMS showed that the material was uncondensed, with a large Q<sup>3</sup>, HOSi(OSi)<sub>3</sub> and Q<sup>2</sup>, (HO)<sub>2</sub>Si(OSi)<sub>2</sub> peaks at approximately -100 and -90 ppm as well as a smaller Q<sup>4</sup>, Si(OSi)<sub>4</sub>, peak at -110 ppm. The lack of condensation indicated that many silanol groups were available for surface modification. After the dtpa-silane was grafted, the Q<sup>2</sup> peak decreased and the Q<sup>4</sup> peak increased in intensity, both of which were indications that the silane had been successfully coupled to the surface. More importantly, the appearance of T<sup>2</sup>, RSi(OH)(OSi)<sub>2</sub>, and T<sup>3</sup>, RSi(OSi)<sub>3</sub>, peaks at -55 and -65 ppm confirmed that the silane had been grafted to the APMS surface. <sup>13</sup>C CPMAS NMR was used to examine the dtpa structure. A comparison of the <sup>13</sup>C NMR spectra of pure dtpa (acid form) and pure

APTES with the grafted material showed that the dtpa environment was quite regular after immobilization and that the anhydride had been successfully opened to the acid. The APTES and dtpa carbon atoms are both visible in the spectrum, and the peak at 174 ppm is consistent with the carboxylic acid groups. A ninhydrin test<sup>62</sup> of this material showed that there were no free amines, so coordination to the vanadyl ions must come exclusively from the dtpa.

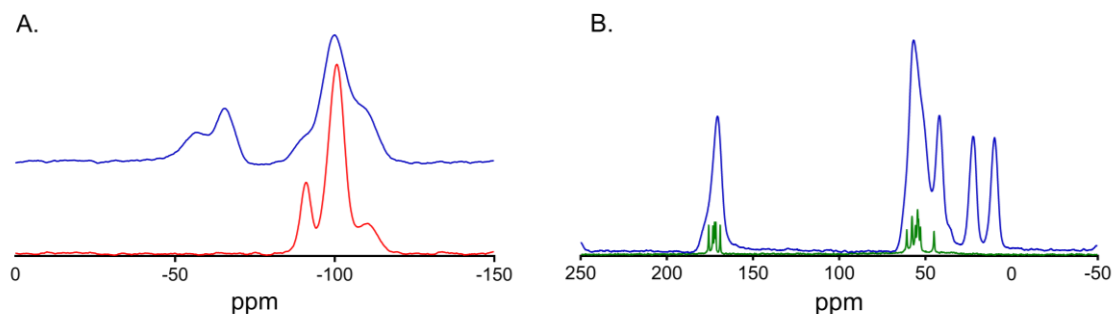


**Figure 2.2.** Characterization of materials by solid-state NMR. (A) <sup>29</sup>Si CPMAS NMR spectra of rehydrated APMS (red) and the same material after dtpa silane was grafted (blue). (B) <sup>13</sup>C CPMAS NMR spectrum of the grafted material (blue) and pure dtpa (green).

Although there are no published X-ray crystallographic structures of vanadium complexed to dtpa, several spectroscopic studies exist. Chen prepared VO(dtpa) complexes from vanadyl sulfate, and used EPR to show that the resulting complexes deviated from axial symmetry.<sup>55</sup> Although they did not suggest a geometry, they concluded that the complex would have three unchelated acid groups because they observed second sphere water ligands via analysis of their proton relaxation profiles.<sup>55</sup> Another study used NH<sub>4</sub>VO<sub>3</sub> as the vanadium source, with the V<sup>5+</sup> ion complexed by dtpa.<sup>53</sup> Characterization by <sup>13</sup>C and <sup>51</sup>V solution NMR led these researchers to conclude that the vanadium had a hexacoordinate environment, with three uncoordinated acetates.

The two axial positions were occupied by dtpa acetates. Of the four equatorial coordination sites, two were occupied by two separate double-bonded oxygen. Of the final two sites, one was occupied by a nitrogen atom bound to the binding dtpa acetate and an unbound dtpa acetate. The final site was the central N in the ligand, also bound to a binding dtpa acetate but two carbons away from the other binding N and two carbons away from unbound N and two unbound dtpa acetates. In a third study,  $V_2(SO_4)_3$ ,<sup>54</sup> containing the  $V^{3+}$  ion, was the vanadium source and IR and UV/Visible spectroscopies were used as characterization tools. The researchers proposed a heptacoordinate vanadium environment without a double-bonded oxygen, with one unbound acetate, four bound acetates, one labile bound  $H_2O$ , and two N atoms bound to the vanadium ion.

The confusion and lack of information about  $VO(dtpa)$  complexes, and the availability of improved spectroscopic and computational methods, led us to investigate the structure of the immobilized  $VO(dtpa)$  complex. Due to the paramagnetic nature of the vanadyl ion, solid-state electron paramagnetic resonance (EPR) spectroscopy was used (**Figure 2.3**). The hyperfine structure in the EPR spectrum is characteristic of a  $V^{4+}$  ( $d^1$ ) species, combined with the V nuclear spin of  $I = 7/2$ . Curve-fitting of the experimental data using EasySpin gave tensors that indicated the vanadium was in a distorted five-coordinate environment. The pattern of the tensors in relation to one another can be related to orbital diagrams through spin-orbit interactions and rotational relationships. Trigonal bipyramidal and square pyramidal geometries have an orbital diagram in which an electron can rotate into a degenerate orbital. Typically, when an electron rotates into a degenerate orbital, the resulting g tensor deviates more than our experimental value of 1.93. This could indicate that the ligand field around the vanadium

is distorted in a way such that the orbital degeneracy is no longer present. To further investigate and support the proposed geometry, DFT computational studies with a program called ORCA are being conducted.<sup>63</sup> After computationally optimizing predicted geometries, ORCA will allow us to derive theoretical values of the  $g$  and  $A$  tensors to compare to the experimental EPR spectra. This study is ongoing, but currently, the complex shown in **Figure 2.4** illustrates the geometry that best fits the experimental data. The complex is 5-coordinate with a mixture of a distorted trigonal bipyramidal and distorted square pyramidal geometry.

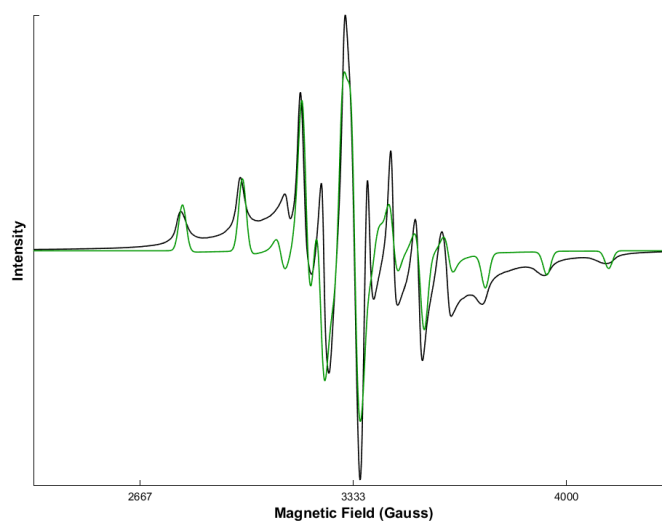


**Figure 2.3.** EPR spectra of the immobilized VO(dtpa) complex. The experimental data is shown in black, and the simulated spectrum used to derive  $g$  and  $A$  tensors is shown in green. Tensors calculated from EasySpin:  $g_{\perp} = 1.98, 1.99$ ,  $g_{\parallel} = 1.93$ ;  $A_x = -200.8$ ,  $A_y = -71.43$ ,  $A_z = -515.4$ .

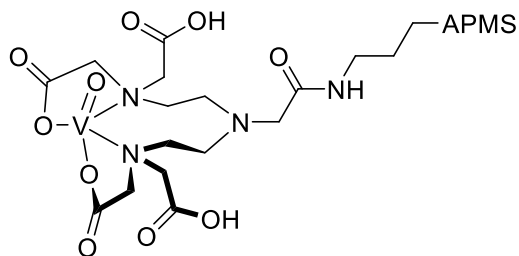


**Figure 2.4.** Potential geometry of VO(dtpa) based on computational studies.

### 2.3.2 Comparison of the properties of materials containing grafted vanadyl complexes and exchanged vanadium species

For comparison, two materials containing vanadium that was not grafted to the silica surface were also synthesized. One material (V-APMS-exch) was prepared by exchanging vanadyl ions into calcined APMS from aqueous  $\text{VO}_2^{+}$ , followed by centrifugation and drying. The other material (V-APMS-incip) was prepared using the incipient wetness technique as in our previously published work,<sup>7</sup> by stirring APMS in an aqueous solution of  $\text{NH}_4\text{VO}_3$  to dryness, followed by calcination. The degree of hydration of the silica in each case was somewhat different, and the oxidation states of the V ion in each as-prepared material were also different.

**Table 2.2** summarizes some of the physical properties of these materials in comparison to the material containing grafted VO(dtpa) complexes. V-APMS-exch, which was treated the least relative to as-prepared APMS, was the most porous of the three materials. V-APMS-incip, in contrast, spent more time exposed to aqueous solution, and was calcined afterwards, leading to a decreased porosity and pore diameter as a result of restructuring of the silica surface. Comparison of the abilities of the three materials to retain vanadium were performed by measuring their V contents by ICP-OES before and

after stirring in water for 8 hours. V-APMS-exch did not start out with much vanadium, and only retained 36% of the original amount after the leaching test.

**Table 2.2.** Comparison of Physical Properties and Vanadium Retention Capabilities of V-APMS Materials.

Material	$d_{\text{pore}}$ (Å)	$S_{\text{ABET}}$ ( $\text{m}^2/\text{g}$ )	$V_{\text{pore}}$ ( $\text{cm}^3/\text{g}$ )	Chelator (mmol/g)	Mass of $V_{\text{initial}}$ ( $\mu\text{g}$ )	Mass of $V_{\text{final}}$ ( $\mu\text{g}$ )	remaining (%)
V-APMS-exch	70	609	1.03	-	$102 \pm 2$	$36.5 \pm 0.5$	36
V-APMS-incip	40	702	0.537	-	$667 \pm 10$	$42.7 \pm 1.0$	6.4
VO(dtpa)-APMS	52	506	0.640	0.364	$429 \pm 11$	$393 \pm 5$	92

V-APMS-incip began with more vanadium, because the incipient wetness technique left a large amount of physisorbed vanadium on the silica surface; however, this material ended up retaining approximately the same amount of vanadium as V-APMS-exch, losing nearly 94% of the initially loaded amount. In contrast, VO(dtpa)-APMS lost only 8% of the initial amount, indicating that dtpa was an effective ligand for the vanadyl ion.

### 2.3.3 CEES oxidation

Oxidative decontamination of half-mustard (CEES) was performed in methoxyperfluorobutane (HFE-7100), with CEES, an approximately 20-fold excess of propionaldehyde, and 20 mg of catalyst after washing for 8 h in water (**Table 2.3**). The progress of the reaction was followed by gas chromatography with mass spectrometric detection (**Figure 2.5**). The results demonstrate the stepwise nature of the sulfur oxidation, with the sulfide first consumed to make the sulfoxide, which is then reacted to the sulfone. Under these conditions, the oxidation of the sulfide is complete in less than 15 minutes; because the system is heterogeneous, the reaction can be stopped at this point

to isolate the sulfoxide. The VO(dtpa)-APMS catalyst shows excellent ability to be recycled and even improves upon recycling.

**Table 2.3.** Kinetic Data for the Oxidation of CEES in HFE-7100 Under Ambient Conditions.

Material	Rate ( $\mu\text{mol/hr}$ )	TOF (mol CEES/mol V)/hr	TON (mol CEES/mol V)	V (mass %)
V-APMS-exch	173	244.78	65.41	0.183
V-APMS-incip	61.5	29.21	11.09	0.324
VO(dtpa)-APMS	422	38.16	6.36	1.89

TON calculated at 20 min.

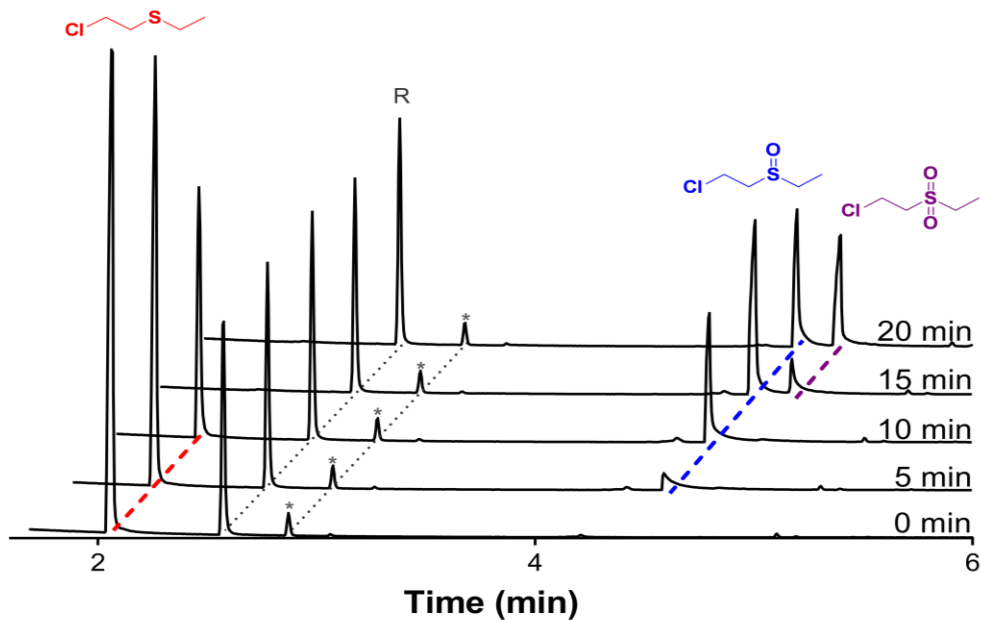


**Figure 2.5.** Progress of the oxidation of CEES using VO(dtpa)-APMS as the catalyst, monitored by gas chromatography. R is an internal reference and \* is an impurity.

A comparison of catalysts prepared by different synthetic methods shows that VO(dtpa)-APMS is the fastest and is more active than the V-APMS-incip. V-APMS-exch

is more active but it is slower than VO(dtpa)-APMS. The activity of each catalyst varied due to the fact that they are operating with different catalytic mechanisms. For VO(dtpa)-APMS, the ligand may hinder substrates from accessing the metal center. In addition, the mechanism for VO(dtpa)-APMS could involve interaction with the ligand and therefore would be different than a catalyst without the ligand. Both V-APMS-incip and V-APMS-exch have no bulky ligand around the catalytic VO center and therefore the substrate can easily diffuse to the metal. Investigation into the mechanism of how VO(dtpa)-APMS oxidizes sulfides is discussed in Chapter 3.

## 2.4 Conclusion

A new catalytic system for sulfide oxidation has been prepared. The system uses a VO(dtpa) complex immobilized on a highly porous silica substrate. Physical characterization of the material confirmed that the substrate retained its porosity after modification, and that the leaching of vanadium was greatly reduced, in contrast to samples that did not contain dtpa. Solid-state EPR spectroscopy, combined with ongoing computational modeling, indicated that the vanadium was in a distorted five-coordinate environment. The catalytic system effectively oxidizes CEES at room temperature in less than 15 minutes, using a fluorocarbon solvent and oxygen as the oxidant source, consistent with our previous results. Experiments to define the catalytic mechanism are described in Chapter 3.

## 2.5 References

1. Marrs, T. C.; Maynard, R. L.; Sidell, F. R., *Chemical Warfare Agents: Toxicology and Treatment*. John Wiley & Sons: New York, 1996; p 243.
2. Wang, Q.-Q.; Begum, R. A.; Day, V. W.; Bowman-James, K. Sulfur, oxygen, and nitrogen mustards: stability and reactivity. *Org. Biomol. Chem.* **2012**, *10*, 8786-8793.
3. Dong, J.; Hu, J.; Chi, Y.; Lin, Z.; Zou, B.; Yang, S.; Hill, C. L.; Hu, C. A Polyoxoniobate–Polyoxovanadate Double-Anion Catalyst for Simultaneous Oxidative and Hydrolytic Decontamination of Chemical Warfare Agent Simulants. *Angew. Chem. Int. Ed.* **2017**, *56*, 4473-4477.
4. Stone, H.; See, D.; Smiley, A.; Ellingson, A.; Schimmoeller, J.; Oudejans, L. Surface decontamination for blister agents Lewisite, sulfur mustard and agent yellow, a Lewisite and sulfur mustard mixture. *J. Hazard. Mater.* **2016**, *314*, 59-66.
5. Ramakrishna, C.; Krishna, R.; Saini, B.; Gopi, T.; Swetha, G.; Chandra Shekar, S. A simple and controlled oxidative decontamination of sulfur mustard and its simulants using ozone gas. *Phosphorus Sulfur Silicon Relat Elem* **2016**, *191*, 965-970.
6. Livingston, S. R.; Landry, C. C. Oxidation of a Mustard Gas Analogue Using an Aldehyde/O<sub>2</sub> System Catalyzed by V-Doped Mesoporous Silica. *J. Am. Chem. Soc.* **2008**, *130*, 13214-13215.
7. Livingston, S. R.; Kumar, D.; Landry, C. C. Oxidation of 2-chloroethyl ethyl sulfide using V-APMS. *J. Mol. Catal. A: Chem.* **2008**, *283*, 52-59.
8. Ringenbach, C. R.; Livingston, S. R.; Kumar, D.; Landry, C. C. Vanadium-Doped Acid-Prepared Mesoporous Silica: Synthesis, Characterization, and Catalytic Studies on the Oxidation of a Mustard Gas Analogue. *Chem. Mater.* **2005**, *17*, 5580-5586.

9. Wang, K.; Niu, Y.; Zhao, D.; Zhao, Y.; Ma, P.; Zhang, D.; Wang, J.; Niu, J. The Polyoxovanadate-Based Carboxylate Derivative  $K_6H[V_{17}^{V}V_{12}^{IV}(OH)_4O_{60}(OOC(CH_2)_4COO)_8] \cdot nH_2O$ : Synthesis, Crystal Structure, and Catalysis for Oxidation of Sulfides. *Inorg. Chem.* **2017**, *56*, 14053-14059.
10. Negi, S. S.; Sivaranjani, K.; Singh, A. P.; Gopinath, C. S. Disordered mesoporous V/TiO<sub>2</sub> system for ambient oxidation of sulfides to sulfoxides. *Appl. Catal., A* **2013**, *452*, 132-138.
11. Hu, Y.-L.; Liu, X.-B.; Fang, D. Efficient and convenient oxidation of sulfides to sulfones using H<sub>2</sub>O<sub>2</sub> catalyzed by V<sub>2</sub>O<sub>5</sub> in ionic liquid [C<sub>12</sub>mim][HSO<sub>4</sub>]. *Catal. Sci. Technol.* **2014**, *4*, 38-42.
12. Karpyshev, N. N.; Yakovleva, O. D.; Talsi, E. P.; Bryliakov, K. P.; Tolstikova, O. V.; Tolstikov, A. G. Effect of portionwise addition of oxidant in asymmetric vanadium-catalyzed sulfide oxidation. *J. Mol. Catal. A: Chem.* **2000**, *157*, 91-95.
13. Fuerte, A.; Iglesias, M.; Sánchez, F.; Corma, A. Chiral dioxomolybdenum(VI) and oxovanadium(V) complexes anchored on modified USY-zeolite and mesoporous MCM-41 as solid selective catalysts for oxidation of sulfides to sulfoxides or sulfones. *J. Mol. Catal. A: Chem.* **2004**, *211*, 227-235.
14. Ben Zid, T.; Khedher, I.; Ghorbel, A. Chiral vanadyl salen catalyst immobilized on mesoporous silica as support for asymmetric oxidation of sulfides to sulfoxides. *React. Kinet., Mech. Catal.* **2010**, *100*, 131-143.
15. Mahato, T. H.; Prasad, G. K.; Singh, B.; Srivastava, A. R.; Ganesan, K.; Acharya, J.; Vijayaraghavan, R. Reactions of sulphur mustard and sarin on V<sub>1.02</sub>O<sub>2.98</sub> nanotubes. *J. Hazard. Mater.* **2009**, *166*, 1545-1549.
16. Singh, B.; Mahato, T. H.; Srivastava, A. K.; Prasad, G. K.; Ganesan, K.; Vijayaraghavan, R.; Jain, R. Significance of porous structure on degradation of 2,2'-dichloro diethyl sulphide and 2-chloroethyl ethyl sulphide on the surface of vanadium oxide nanostructure. *J. Hazard. Mater.* **2011**, *190*, 1053-1057.
17. Prasad, G. K. Decontamination of 2-chloroethyl phenyl sulphide using mixed metal oxide nanocrystals. *J. Sci. Ind. Res.* **2010**, *69*, 835-840.

18. Ramacharyulu, P. V. R. K.; Kumar, J. P.; Prasad, G. K.; Kumar, G. P.; Dwivedi, K. Mesoporous Vanadium Ion Doped Titania Nanocatalysts for the Photocatalytic Degradation of Sulfur Mustard. *Advanced Porous Materials* **2013**, *1*, 286-293.
19. Ramacharyulu, P. V. R. K.; Praveen Kumar, J.; Prasad, G. K.; Singh, B.; Sreedhar, B.; Dwivedi, K. Sunlight assisted photocatalytic detoxification of sulfur mustard on vanadium ion doped titania nanocatalysts. *J. Mol. Catal. A: Chem.* **2014**, *387*, 38-44.
20. Neațu, Ș.; Pârvulescu, V. I.; Epure, G.; Preda, E.; Șomoghi, V.; Damin, A.; Bordiga, S.; Zecchina, A. Photo-degradation of yperite over V, Fe and Mn-doped titania–silica photocatalysts. *Phys. Chem. Chem. Phys.* **2008**, *10*, 6562-6570.
21. Weinstock, I. A. Homogeneous-Phase Electron-Transfer Reactions of Polyoxometalates. *Chem. Rev.* **1998**, *98*, 113-170.
22. Long, D.-L.; Tsunashima, R.; Cronin, L. Polyoxometalates: Building Blocks for Functional Nanoscale Systems. *Angew. Chem. Int. Ed.* **2010**, *49*, 1736-1758.
23. Hill, C. L.; Gall, R. D. The first combinatorially prepared and evaluated inorganic catalysts. Polyoxometalates for the aerobic oxidation of the mustard analog tetrahydrothiophene (THT). *J. Mol. Catal. A: Chem.* **1996**, *114*, 103-111.
24. Liu, F.; Lu, Q.; Jiao, X.; Chen, D. Fabrication of nylon-6/POMs nanofibrous membranes and the degradation of mustard stimulant research. *RSC Adv.* **2014**, *4*, 41271-41276.
25. Gall, R. D.; Faraj, M.; Hill, C. L. Role of Water in Polyoxometalate-Catalyzed Oxidations in Nonaqueous Media. Scope, Kinetics, and Mechanism of Oxidation of Thioether Mustard (HD) Analogs by tert-Butyl Hydroperoxide Catalyzed by H<sub>5</sub>PV<sub>2</sub>Mo<sub>10</sub>O<sub>40</sub>. *Inorg. Chem.* **1994**, *33*, 5015-5021.
26. Li, Y.; Gao, Q.; Zhang, L.; Zhou, Y.; Zhong, Y.; Ying, Y.; Zhang, M.; Huang, C.; Wang, Y. a. H<sub>5</sub>PV<sub>2</sub>Mo<sub>10</sub>O<sub>40</sub> encapsulated in MIL-101(Cr): facile synthesis and characterization of rationally designed composite materials for efficient decontamination of sulfur mustard. *Dalton Trans.* **2018**, *47*, 6394-6403.

27. Durham, E. J.; Ryskiewich, D. P. The Acid Dissociation Constants of Diethylenetriaminepentaacetic Acid and the Stability Constants of Some of its Metal Chelates1. *J. Am. Chem. Soc.* **1958**, *80*, 4812-4817.
28. Jianping, L.; Shangwang, L.; Qiuyan, L.; Xuehong, Z. A New Chromium(III) Microelectrode Based on Self-Assembled Diethylenetriaminepentaacetic Acid-Poly(fuchsin basic) Modified Electrode. *Electroanalysis* **2009**, *21*, 831-836.
29. Andrzej, B.; Paweł, K.; Jerzy, Z. Catalytic Adsorptive Stripping Chronopotentiometric Determination of Hexavalent Chromium at a Silver Amalgam Film Electrode of Prolonged Application. *Electroanalysis* **2011**, *23*, 2265-2269.
30. Dib, S.; Boufatit, M.; Chelouaou, S.; Sadi-Hassaine, F.; Croissant, J.; Long, J.; Raehm, L.; Charnay, C.; Durand, J. O. Versatile heavy metals removal via magnetic mesoporous nanocontainers. *RSC Adv.* **2014**, *4*, 24838-24841.
31. Zhao, S.; Shen, Z.; Duo, L. Heavy metal uptake and leaching from polluted soil using permeable barrier in DTPA-assisted phytoextraction. *Environ. Sci. Pollut. Res.* **2015**, *22*, 5263-5270.
32. Bhatt, R.; Sreedhar, B.; Padmaja, P. Adsorption of chromium from aqueous solutions using crosslinked chitosan–diethylenetriaminepentaacetic acid. *Int. J. Biol. Macromol.* **2015**, *74*, 458-466.
33. Li, P.; Hong, Y.; Feng, H.; Li, S. F. Y. An efficient "off-on" carbon nanoparticle-based fluorescent sensor for recognition of chromium(vi) and ascorbic acid based on the inner filter effect. *J. Mater. Chem. B* **2017**, *5*, 2979-2988.
34. Roosen, J.; Van Roosendael, S.; Borra, C. R.; Van Gerven, T.; Mullens, S.; Binnemans, K. Recovery of scandium from leachates of Greek bauxite residue by adsorption on functionalized chitosan-silica hybrid materials. *Green Chem.* **2016**, *18*, 2005-2013.
35. Li, X.; Wang, S.; Liu, Y.; Jiang, L.; Song, B.; Li, M.; Zeng, G.; Tan, X.; Cai, X.; Ding, Y. Adsorption of Cu(II), Pb(II), and Cd(II) Ions from Acidic Aqueous Solutions by Diethylenetriaminepentaacetic Acid-Modified Magnetic Graphene Oxide. *J. Chem. Eng. Data* **2017**, *62*, 407-416.

36. Parker Siburt, C. J.; Lin, E. M.; Brandt, S. J.; Tinoco, A. D.; Valentine, A. M.; Crumbliss, A. L. Redox potentials of Ti(IV) and Fe(III) complexes provide insights into titanium biodistribution mechanisms. *J. Inorg. Biochem.* **2010**, *104*, 1006-1009.
37. Pniok, M.; Kubíček, V.; Havlíčková, J.; Kotek, J.; Sabatie-Gogová, A.; Plutnar, J.; Huclier-Markai, S.; Hermann, P. Thermodynamic and Kinetic Study of Scandium(III) Complexes of DTPA and DOTA: A Step Toward Scandium Radiopharmaceuticals. *Chem. - Eur. J.* **2014**, *20*, 7944-7955.
38. Huclier-Markai, S.; Alliot, C.; Sebti, J.; Brunel, B.; Aupiais, J. A comparative thermodynamic study of the formation of scandium complexes with DTPA and DOTA. *RSC Adv.* **2015**, *5*, 99606-99617.
39. Połosak, M.; Piotrowska, A.; Krajewski, S.; Bilewicz, A. Stability of <sup>47</sup>Sc-complexes with acyclic polyamino-polycarboxylate ligands. *J. Radioanal. Nucl. Chem.* **2013**, *295*, 1867-1872.
40. Ishiwata, K.; Ido, T.; Monma, M.; Murakami, M.; Fukuda, H.; Kameyama, M.; Yamada, K.; Endo, S.; Yoshioka, S.; Sato, T.; Matsuzawa, T. Potential radiopharmaceuticals labeled with titanium-45. *Int. J. Radiat. Appl. Instrum., Part A* **1991**, *42*, 707-712.
41. Díaz-de Alba, M.; Galindo-Riaño, M. D.; Casanueva-Marengo, M. J.; García-Vargas, M.; Kosore, C. M. Assessment of the metal pollution, potential toxicity and speciation of sediment from Algeciras Bay (South of Spain) using chemometric tools. *J. Hazard. Mater.* **2011**, *190*, 177-187.
42. Lottermoser, B. G. Colonisation of the rehabilitated Mary Kathleen uranium mine site (Australia) by *Calotropis procera*: Toxicity risk to grazing animals. *J. Geochem. Explor.* **2011**, *111*, 39-46.
43. Kosore, C. M.; Galindo-Riaño, M. D.; Díaz-de-Alba, M. Assessing trace-element mobility in Algeciras Bay (Spain) sediments by acid and complexing screening. *Arabian J. Chem.* **2015**.
44. Tsadilas, C. D.; Shaheen, S. M. Distribution of Total and Ammonium Bicarbonate-DTPA-Extractable Soil Vanadium From Greece and Egypt and Their Correlation To Soil Properties. *Soil Sci.* **2010**, *175*, 535-543.

45. Pinto, E.; Almeida, A. A.; Ferreira, I. M. P. L. V. O. Assessment of metal(loid)s phytoavailability in intensive agricultural soils by the application of single extractions to rhizosphere soil. *Ecotoxicol. Environ. Saf.* **2015**, *113*, 418-424.
46. Chen, B.; Shan, X.-q.; Qian, J. Bioavailability index for quantitative evaluation of plant availability of extractable soil trace elements. *Plant Soil* **1996**, *186*, 275-283.
47. Domingo, J. L.; Gomez, M.; Llobet, J. M.; Corbella, J. Chelating agents in the treatment of acute vanadyl sulphate intoxication in mice. *Toxicology* **1990**, *62*, 203-211.
48. Hamada, T. A new experimental system of using fertile chick eggs to evaluate vanadium absorption and antidotal effectiveness to prevent vanadium uptake. *J. Nutr. Biochem.* **1994**, *5*, 382-388.
49. Majlesi, K.; Rezaiejad, S.; Balali, S. Speciation and Stability of Dioxovanadium(V) Complexes with Diethylenetriaminepentaacetic Acid at Different Ionic Strengths. *J. Solution Chem.* **2013**, *42*, 1729-1747.
50. Chen, Z.; Naidu, R. On-column complexation and simultaneous separation of vanadium(IV) and vanadium(V) by capillary electrophoresis with direct UV detection. *Anal. Bioanal. Chem.* **2002**, *374*, 520-525.
51. Pozdniakova, S. Speciation of metals in different oxidation states by capillary electrophoresis using pre-capillary complexation with complexones. *Analyst* **1998**, *123*, 1497-1500.
52. Inoue, K.; Yoshizuka, K.; Ohto, K. Adsorptive separation of some metal ions by complexing agent types of chemically modified chitosan. *Anal. Chim. Acta* **1999**, *388*, 209-218.
53. Lee, M.-H.; O, T.-S. Carbon-13 and Vanadium-51 Nuclear Magnetic Resonance Studies of Vanadium(v)-Aminopolycarboxylic Acids (I). *J. Korean Chem. Soc.* **1983**, *27*, 117-126.

54. Kanamori, K.; Ino, K.; Maeda, H.; Miyazaki, K.; Fukagawa, M.; Kumada, J.; Eguchi, T.; Okamoto, K.-i. Relationship between Oxo-Bridged Dimer Formation and Structure of Vanadium(III) amino polycarboxylates. *Inorg. Chem.* **1994**, *33*, 5547-5554.
55. Chen, J. W.; Belford, R. L.; Clarkson, R. B. Second-Sphere and Outer-Sphere Proton Relaxation of Paramagnetic Complexes: From EPR to NMRD. *J. Phys. Chem. A* **1998**, *102*, 2117-2130.
56. Stoll, S.; Schweiger, A. EasySpin, a comprehensive software package for spectral simulation and analysis in EPR. *J. Magn. Reson.* **2006**, *178*, 42-55.
57. Solberg, S.; Landry, C. Adsorption of DNA into Mesoporous Silica. *J. Phys. Chem. B* **2006**, *110*, 15261-15268.
58. Gallis, K. W.; Landry, C. C. Mesoporous Silica Production for Liquid Chromatography. U.S. Patent 6,334,988, August 20, 1999.
59. Jin, Y.; Li, A.; Hazelton, S. G.; Liang, S.; John, C. L.; Selid, P. D.; Pierce, D. T.; Zhao, J. X. Amorphous silica nanohybrids: Synthesis, properties and applications. *Coord. Chem. Rev.* **2009**, *253*, 2998-3014.
60. Gallis, K. W.; Araujo, J. T.; Duff, K. J.; Moore, J. G.; Landry, C. C. The Use of Mesoporous Silica in Liquid Chromatography. *Adv. Mater.* **1999**, *11*, 1452-1455.
61. Zhuravlev, L. T. The surface chemistry of amorphous silica. Zhuravlev model. *Colloids Surf., A* **2000**, *173*, 1-38.
62. Kaiser, E.; Colescott, R. L.; Bossinger, C. D.; Cook, P. I. Color test for detection of free terminal amino groups in the solid-phase synthesis of peptides. *Anal. Biochem.* **1970**, *34*, 595-598.
63. Bal, H. E.; Kaashoek, M. F.; Tanenbaum, A. S. Orca: a language for parallel programming of distributed systems. *IEEE Trans. Softw. Eng.* **1992**, *18*, 190-205.

## CHAPTER 3: MECHANISTIC INVESTIGATION OF SULFIDE OXIDATION WITH PEROXYACID AND AN IMMOBILIZED VANADYL COMPLEX

### 3.1 Introduction

Oxovanadium complexes are used to catalyze a variety of oxidation reactions. For example, they have been shown to oxidize alkanes, alkenes, alcohols, aromatic compounds, and sulfides.<sup>1-3</sup> Sulfide oxidation is of particular interest due to its applicability in a range of applications. For example, vanadium dependent peroxidases, which can be found in marine algae, lichen and fungus, have been the subject of several modeling and mechanistic studies.<sup>4-7</sup> This family of enzymes oxidizes halides in nature and it is thought that algae oxidized products are used as a defense system while fungi use them to degrade plant cell walls.<sup>8</sup> Scientists have been able to exploit vanadium bromoperoxidase, a type of vanadium dependent peroxidase, as a biocatalyst for the oxidation of sulfides.<sup>9,10</sup> Another example is asymmetric sulfide oxidation using vanadium complexes which is useful in organic synthesis and in the pharmaceutical industry.<sup>11-14,15</sup> Also, desulfurization of petrochemicals through oxidative catalysis has been an important field of study for many years.<sup>16,17</sup> The broad applicability of heterogeneous vanadium oxidation catalysts lend them a special advantage in terms of environmental friendliness and allow them to be used in a variety of industrial and biochemical applications.<sup>18-25</sup>

Although the most common oxidants used in the oxidation of sulfides are peroxides such as  $\text{H}_2\text{O}_2$  or  $^t\text{BuOOH}$ , we have recently developed a novel heterogeneous system for sulfide oxidation at ambient conditions. This system uses a vanadium catalyst immobilized onto a porous silica substrate to catalyze the oxidation of an aldehyde to the

corresponding peroxyacid with O<sub>2</sub>, followed by catalysis of the peroxyacid with an organic sulfide to yield a sulfoxide. The oxidation of aldehydes is often performed using H<sub>2</sub>O<sub>2</sub> as the oxidant.<sup>26-28</sup> Molecular oxygen has also been used in this capacity both with<sup>29-38</sup> and without<sup>39</sup> transition metals, but there are only a few examples using a vanadium catalyst.<sup>40-42</sup> Transition metals can perform this oxidation either through formation of an acyl radical, or by forming a transition metal oxygen radical species.<sup>43</sup>

There have been numerous studies of the mechanism of sulfide oxidation by vanadium complexes.<sup>3,44-51</sup> Very often, the studied mechanisms use H<sub>2</sub>O<sub>2</sub> as the oxidant source. One of the potential mechanistic pathways for the oxidation of sulfides is a direct mechanism, meaning that the sulfide directly attacks the oxidant and does not coordinate with the transition metal catalyst. Smith and Pecoraro experimentally studied the mechanism of sulfide oxidation by vanadium haloperoxidases using ligands such as N-(2-hydroxyethyl)iminodiacetic acid), N,N-bis(2-pyridylmethyl)glycine, N-(2-amidomethyl)-iminodiacetic acid and nitrilotriacetic acid.<sup>48</sup> They determined that the sulfide was directly attacking the oxidant and that protonation of the vanadium-peroxide intermediate was an important part of the catalytic process. Using density functional theory (DFT), De Gioia studied the reactivity of peroxo forms of vanadium haloperoxidase cofactor.<sup>52</sup> In the study, they determined that the sulfide attacks the peroxo ligand directly without coordination to the vanadium. They went further into their investigation to determine from which direction the sulfide attacks. In their system, the model compound was a strongly distorted trigonal bipyramidal structure, a vanadium with an imidazole and one peroxo atom in axial position ([ImVO<sub>4</sub>]<sup>-</sup>). It was determined that the sulfide attacks the axial oxygen in the peroxo ligand, rather than attacking the equatorial positioned

oxygen.<sup>52</sup> In a separate computational study, they performed a detailed DFT investigation using 2,2-[(2-hydroxyethyl)imino]diacetate as a ligand to model the vanadium haloperoxidase active site, and illustrated a direct mechanism.<sup>53</sup> Maseras used DFT to model sulfide oxidation.<sup>51</sup> The focus of these studies was oxo transfer from H<sub>2</sub>O<sub>2</sub> to a sulfide using a simplified version of a bulky tridentate Schiff base as the ligand for a vanadium catalyst and dimethyl disulfide as the substrate. From their DFT calculations, they determined that the direct mechanism was the most likely.

In addition to using an *in situ* generated peroxyacid as the oxidant source, our previous work differs from these studies in several regards. First, diethylenetriamine pentaacetic acid (dtpa) was chosen as the ligand, due to its strong chelating ability.<sup>54</sup> Second, the VO(dtpa) complex was immobilized onto a highly porous silica support to create a heterogeneous catalytic system, which is more environmentally friendly and allowed a large amount of catalyst to be supported on a nanoparticulate solid. Finally, we are particularly interested in the reaction chemistry of 2-chloroethyl ethylsulfide (CEES), which we and others have studied for many years as an analogue of mustard gas, bis(2-chloroethyl)sulfide. The latter compound is a chemical warfare agent, a vesicant that is still present in military stockpiles around the world; thus, there is a need for the development of new catalytic systems for its decontamination. In this work, we expand on our recent synthetic and catalytic study to investigate details of the catalysis mechanism, including both the aldehyde oxidation using O<sub>2</sub> and the sulfide oxidation using the peroxyacid thus generated *in situ*.

## 3.2 Experimental Section

### 3.2.1 Materials and methods

(3-aminopropyl)triethoxysilane was obtained from Gelest, Inc. 4-Fluorothioanisole was obtained from Alfa Aesar. All other chemicals were obtained from Sigma Aldrich. Porosity and surface area measurements were obtained at 77 K on a Micromeritics TriStar 3000 surface area and porosity analyzer. Samples were degassed on a Micromeritics FlowPrep 060 Sample Degas System. Surface areas and pore size distributions were calculated using the BET and BJH theories. Thermogravimetric analysis was completed on a Perkin Elmer Pyris 1 TGA. Elemental analysis via inductively-coupled plasma optical emission spectroscopy (ICP-OES) was completed on a PerkinElmer Optima 7000DV ICP optical emission spectrometer with a CCD array detector, a PerkinElmer S10 autosampler, and WinLab32 software.

### 3.2.2 Synthesis of Acid Prepared Mesoporous Spheres (APMS)

APMS was synthesized from a previously published protocol.<sup>55,56</sup> Briefly, cetyltrimethylammonium bromide (CTAB, 3.6 g, 9.88 mmol) was added to a solution of H<sub>2</sub>O (79.2 g), EtOH (200 proof, 22.2 g, 0.482 mol) and HCl (37 wt%, 8.8 g, 0.089 mol) at room temperature. The solution was stirred for approximately 10 min, and then Si(OEt)<sub>4</sub> (TEOS, 8.0 g, 38 mmol) was added and stirring was continued for another 10 min. A solution of NaF (0.5 M, 9.52 g, 4.76 mmol) was then added. Precipitation occurred after 1.5 min, and stirring was continued for an additional 0.5 min, after which the mixture was transferred to a Teflon container that was sealed and placed in an oven at 373 K for 120 min. The mixture was then cooled to room temperature while stirring in an ice bath, and the precipitate was collected via vacuum filtration, rinsed with H<sub>2</sub>O and

EtOH to remove adsorbed surfactant, and dried overnight. Surfactant was removed by calcination using the following program: the sample was heated from 298 K to 723 K at a rate of 2 K/min, followed by a 240 min hold at 723 K. The sample was then ramp to 823 K at a rate of 10 K/min with a hold time of 480 min at 823 K before cooling to room temperature.

### 3.2.3 Synthesis of dtpa-APMS

Diethylenetriaminepentaacetic dianhydride (dtpa, 0.07 g, 0.2 mmol), N-(3-dimethylaminopropyl)-N'-ethylcarbodiimide hydrochloride (EDC, 0.038 g, 0.2 mmol) and N-hydroxysuccinimide (NHS, 0.023 g, 0.2 mmol) were dissolved in 5 mL of dry DMSO in a sealed round bottomed flask under N<sub>2</sub>. After 1 h, 3-aminopropyltriethoxysilane (APTES, 31.2  $\mu$ L, 0.13 mmol, 1:1.5 molar ratio to dtpa) was added, and the solution was stirred for 24 h at room temperature. In a separate 4 dram scintillation vial, 0.2 g of APMS was stirred in 15 mL H<sub>2</sub>O for 24 h to rehydrate the material prior to attachment of dtpa-APTES. The APMS was collected by centrifugation and vacuum filtration, and then suspended in 10 mL toluene in a 25 mL round bottom flask. The DMSO solution was then added to the toluene mixture, and the resulting mixture was refluxed for approximately 18 h. After cooling to room temperature, the modified APMS was collected by centrifugation and vacuum filtration, and washed with DMSO, toluene, EtOH and NaOAc buffer (10  $\mu$ M, pH = 6.5), and dried overnight.

### 3.2.4 Chelation of vanadium to dtpa-APMS

dtpa-APMS (0.10 g) was placed in a 4 dram scintillation vial and sonicated briefly in NaOAc buffer (10 mL, 10  $\mu$ M, pH = 6.5). In a separate vial, VOSO<sub>4</sub> • xH<sub>2</sub>O (x = 3-5, 0.03 g, excess) was dissolved in H<sub>2</sub>O (5 mL), and this solution was then added to

the APMS mixture. After stirring for 4 h at room temperature, the resulting material was collected by centrifugation and vacuum filtration, washed with H<sub>2</sub>O and NaOAc buffer (10  $\mu$ M, pH = 6.5), and dried in a vacuum oven at room temperature overnight.

### 3.2.5 Catalytic oxidation of CEES

The catalysis protocol was modified from a previously published procedure. 2-chloroethyl ethylsulfide (CEES, 5  $\mu$ L, 1.07 g/mL, 42.9  $\mu$ mol) and propionaldehyde (61.9  $\mu$ L, 0.805 g/mL, 858  $\mu$ mol) were placed in a 3 mL volumetric flask, which was filled with C<sub>4</sub>F<sub>9</sub>OCH<sub>3</sub> (3M™ Novec™ 7100 Engineered Fluid, HFE-7100). 1,2,4-trimethylbenzene (1  $\mu$ L, 0.876 g/mL, 7.88  $\mu$ mol) was added as a GC reference. Catalysis was initiated by simply adding one of the vanadium-loaded catalysts prepared above (20 mg) to this solution. Aliquots (200  $\mu$ L) were removed with a 2 mL plastic syringe, the solid catalyst was filtered out using a 0.22  $\mu$ m Millipore syringe filter, and the resulting filtrate was analyzed by gas chromatography with mass spectrometric detection using a HP-5 (length 30 m, i.d. 0.32 mm) column and ZB-5 (length 30 m, i.d. 0.25 mm) column. For reactions where a radical trap was present, a stock solution of diphenylamine (0.01206 M in HFE-7100) was prepared and added to the reaction solution (3  $\mu$ L or 36.2 nmol; 6  $\mu$ L or 72.3 nmol; and 12  $\mu$ L or 144.7 nmol) before the catalyst was added.

### 3.2.6 Eyring Plot catalysis

CEES (16.67  $\mu$ L, 1.07 g/mL, 143  $\mu$ mol) and 1,2,4-trimethylbenzene (3.33  $\mu$ L, 0.876 g/mL, 26.27  $\mu$ mol) were mixed into six 10 mL stock solutions with HFE-7100 as a solvent. Stock solutions and aliquots of propionaldehyde were adjusted to appropriate temperatures using either a refrigerator or a temperature-controlled oven. Catalysts were adjusted to temperature for 10 min in 10 mL round bottom flasks before addition of

reactants. To perform the analysis, a stock solution (3 mL) and propionaldehyde (61.9  $\mu\text{L}$ , 0.805 g/mL, 858  $\mu\text{mol}$ ) were pre-mixed before being poured onto the vanadium catalyst in a 10 mL round-bottom flask to initiate the oxidation reaction. Temperatures below room temperature were achieved using cold or ice water, and temperatures above room temperature used a sand bath or heating mantle. Temperatures were monitored throughout the reactions with an *in situ* thermometer. Aliquots (200  $\mu\text{L}$ ) for analysis were removed with a 2 mL plastic syringe, the solid catalyst was filtered out using a 0.22  $\mu\text{m}$  Millipore syringe filter, and the resulting filtrate was analyzed by gas chromatography with mass spectrometric detection using a HP-5 (length 30 m, i.d. 0.32 mm) column.

### **3.2.7 Hammett Plot catalytic experiments**

Reaction conditions were identical to those used for oxidation of CEES, except various sulfides were used in its place.

## **3.3 Results**

In previous work, we showed that a simple catalyst prepared by doping mesoporous silica nanoparticles with vanadium (V-APMS) was capable of oxidizing half mustard, 2-chloroethyl ethyl sulfide or CEES, using aldehydes under ambient conditions with a commercially available hydrofluorocarbon solvent, HFE-7100.<sup>40,57</sup> However, in the presence of water or under humid conditions, the vanadium leached from the solid, interfering with or stopping the oxidation reaction. This was the source of our interest in binding a vanadium complex to the support instead of free vanadium. In Chapter 2, we used diethylenetriamine pentaacetate (dtpa) to chelate the vanadyl ion, and the VO(dtpa) complex was immobilized onto the porous silica support. Solid-state NMR experiments

showed that the dtpa was covalently bound to the silica surface through a peptide link to 3-aminopropyltriethoxysilane (APTES). Solid-state EPR spectroscopy, combined with ongoing computational modeling, indicated that the vanadium was in a distorted five-coordinate environment. In the oxidation of CEES, the immobilized VO(dtpa) complex was effective under the same conditions (aldehyde, HFE-7100) as the unchelated vanadium prepared through incipient wetness technique, with a faster turnover frequency. The ligand remained intact during the oxidation process. This preliminary work indicated a similar stepwise oxidation process to the one that had been defined for the unchelated vanadium catalyst,<sup>57</sup> but detailed mechanistic studies were not completed.

Preliminary studies indicated that porous silica nanoparticles with a pore diameter of 7 nm allowed the maximum amount of VO(dtpa) to be bound to the pore surfaces. Materials with smaller pores prevented the complex from binding, and materials with larger pores had less surface area and showed decreased amounts of complex on the surface. Additional optimization tests indicated that a four-fold excess of V used during the complexation process provided materials with the highest activity, as measured by turnover number and turnover frequency. By varying the amount of catalyst and the ratios of each reagent, it was determined that 20 mg of the VO(dtpa) solid catalyst, 5  $\mu$ L of CEES, and a 20-fold excess of aldehyde provided the best conditions to study the catalytic process.

The oxidation of aldehydes to peroxyacids with O<sub>2</sub> proceeds through formation of acyl radicals and peroxyacid radicals.<sup>58</sup> This reaction proceeds slowly without a catalyst but can be accelerated with transition metals such as Ag<sup>+</sup><sup>36</sup> or V<sup>4+</sup>.<sup>26</sup> In our previous catalytic studies using immobilized vanadium, radical trapping was used to confirm that

radicals were also present. To confirm their presence in the VO(dtpa) catalytic system, diphenylamine was added to the system as a radical trap.<sup>59</sup> Without diphenylamine, the conversion of CEES was rapid and began immediately, but in the presence of diphenylamine an induction period was observed before CEES began to react (**Figure 3.1**). The length of the induction period was related to the amount of diphenylamine in the system. This confirmed that radicals were formed during the aldehyde oxidation. When diphenylamine was present, the radicals were quenched before forming the peroxyacid, so CEES did not react until all of the diphenylamine was used (note that there was a large excess of aldehyde present in the system relative to CEES). When <sup>t</sup>BuOOH was used as the oxidant, the addition of diphenylamine had no effect on the oxidation of CEES, further confirming that radicals were produced during the oxidation of the aldehyde and not during the sulfide oxidation.

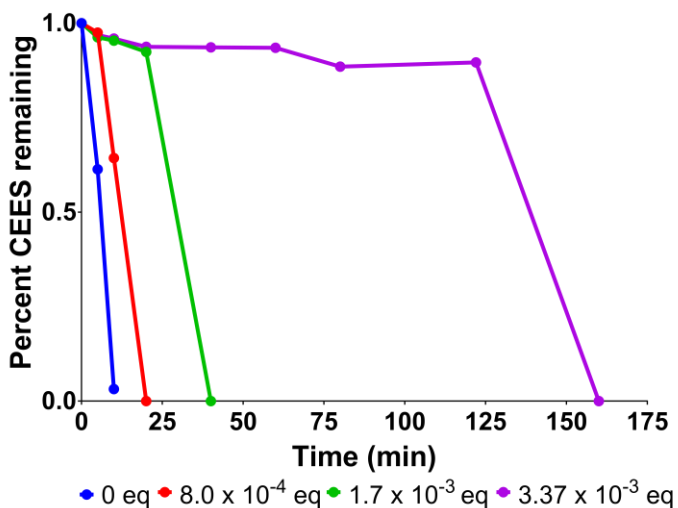


**Figure 3.1.** Radical trap experiments using diphenylamine.

To abstract thermodynamic parameters for our reaction, the reaction temperature was varied to generate an Eyring plot ( $\ln(k/T)$  versus  $1/T$ , **Figure 3.2a** and **Table A1**).

First order kinetics were observed for the peroxyacid catalysis. Rate constants were obtained through the following relationship (**Equation 3.1**):

$$\ln [\text{sulfide}]_t = -kt + \ln [\text{sulfide}]_0 \quad (3.1)$$

In contrast to our previous work using unchelated vanadium, the slope of the Eyring plot was not the same over the entire temperature range, changing from a negative value at lower temperatures to a positive value at higher temperatures. A non-linear Eyring plot indicated that the mechanism of the reaction was dependent on the reaction temperature. This can be related to the presence of peroxyacid  $[\text{R}(\text{C}=\text{O})\text{OO}^*]$  radicals in the system. At lower temperatures, these radicals can bind to the vanadium complex and participate in sulfide oxidation, but at higher temperatures they can react with themselves,<sup>60</sup> reducing the amount of oxidant available to react with CEES. As in the radical trapping experiment above, the importance of radical reaction was studied by repeating the oxidation using  $^t\text{BuOOH}$  as the oxidant source, which does not proceed through a radical mechanism. For the  $^t\text{BuOOH}$  reaction, second order kinetics were observed. The rate constants were obtained through the following relationship (**Equation 2.2**):

$$\frac{1}{[\text{sulfide}]_t} = kt + \frac{1}{[\text{sulfide}]_0} \quad (2.2)$$

The Eyring plot from this reaction (**Figure 3.2b**) is linear over the entire temperature range, supporting the conclusion that radical quenching was an important part of the reaction when the oxidant is the *in situ* generated peroxyacid.

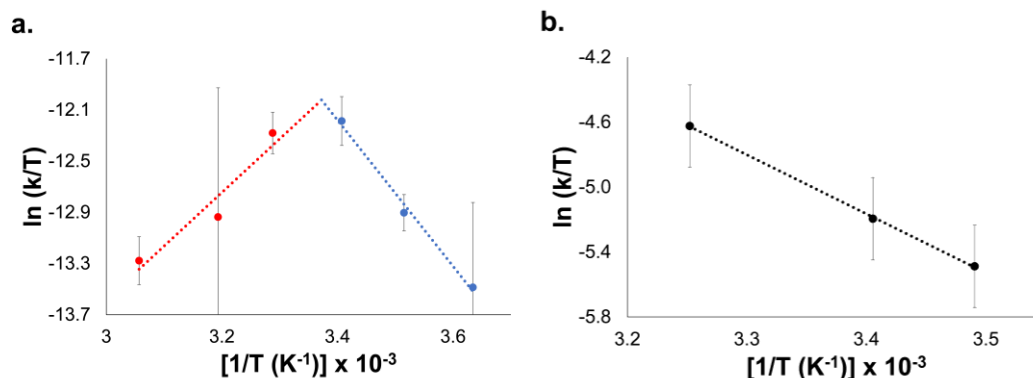


**Figure 3.2.** Eyring Plot from kinetic temperature runs of the oxidation of CEES with **a.** aldehyde/O<sub>2</sub> as oxidant **b.** <sup>t</sup>BuOOH as oxidant.

The Eyring plots in **Figure 3.2** were used to calculate thermodynamic parameters for the sulfide oxidation using VO(dtpa). Parameters are shown in **Table 3.1**. The entropy of activation ( $\Delta S^\ddagger$ ) was negative at all temperatures and regardless of the identity of the oxidant.  $\Delta S^\ddagger$  can be affected by solvation, but often a negative value of  $\Delta S^\ddagger$  is representative of the combination of two molecules through the decrease of translational and rotational degrees of freedom and can indicate an associative mechanism.<sup>61,62</sup>

**Table 3.1.** Entropy and Enthalpy of Reaction.

Temperature Range (°C)	$\Delta H^\ddagger$ (kcal/mol)	$\Delta S^\ddagger$ (cal/K mol)
2-11-20	10.43	-125.82
31-40-54	-8.93	-190.82
<i>t</i> BuOOH: 13-20-34	6.32	-125.72

This is consistent with a process where both the sulfide and the peroxyacid react at the vanadium center. The change in the slope of the Eyring plot in **Figure 3.2a** at higher temperatures results in a change in the sign of  $\Delta H^\ddagger$  for those temperatures. The negative enthalpy of activation found at high temperatures has been observed in other cases as a

result of the combination of radicals.<sup>61</sup> It can also be indicative of a reversible formation of complexes that have lower energy profiles than that of the normal reaction pathway.<sup>63</sup>

In order to gain insight into the electronics of the transition state, electronic effects on the mechanism were studied using methyl phenyl sulfide and para-substituted derivatives as model compounds. The oxidation reaction was repeated using the *in situ* generated peroxyacid as the oxidant and the compounds methyl phenyl sulfide, 4-fluorophenyl methyl sulfide, 4-bromophenyl methyl sulfide, and 4-methoxythioanisole as substrates, and the kinetic data was used to generate a Hammett plot (**Figure 3.4** and **Table A3**). Hammett parameters ( $\sigma$ ) were obtained from the literature.<sup>64</sup> The Hammett plot was originally based on benzoic acid and can be made using equilibrium constants or rate constants. The following relationship is in terms of rate constants (**Equation 3.3**):

$$\log\left(\frac{k_x}{k_H}\right) = \rho\sigma_x \quad (3.3)$$

where  $k_x$  is the rate constant for any substituted methyl phenyl sulfide and  $k_H$  is the rate constant for methyl phenyl sulfide. The Hammett parameter ( $\sigma_x$ ) changes depending on where the substituent is located. Since our substituents were in the para position,  $\sigma_p$  was used. Rho ( $\rho$ ) is equivalent to the slope of  $\log\left(\frac{k_x}{k_H}\right)$  versus the Hammett parameters ( $\sigma_p$ ). The sign of the slope ( $\rho$ ), and its magnitude, can be used to gain information about electronic effects in the reaction mechanism. The positive value of  $\rho$ , ( $\rho = 1.47$ ), for our reaction is an interesting result. In sulfide oxidations, positive value of  $\rho$ , where rate increases when the substituents have increasingly electron withdrawing character, can indicate that the oxidant is acting as a nucleophile and the sulfide as an electrophile.<sup>50,65</sup> Conversely, a typical nucleophilic attack by a sulfide onto an oxidant may be expected to

give a negative value of  $\rho$ .<sup>66-67</sup> In other studies exploring electrophilic and nucleophilic oxygen transfer reactions with aryl sulfoxides, researchers have found that the sign of  $\rho$  changes when aryl sulfoxides reacted with protonated versus deprotonated peroxyacids.<sup>68</sup> Using DFT calculations, it was determined that the difference was due to the electrostatic component of the reaction dominating over orbital components in the latter case.<sup>68</sup> With this information, and with the data from the Eyring plot, we interpret the Hammett plot to indicate that sulfide reacts with an oxygen atom on the peroxyacid with a partial negative charge, due to the concerted reaction of the sulfide with the peroxyacid.

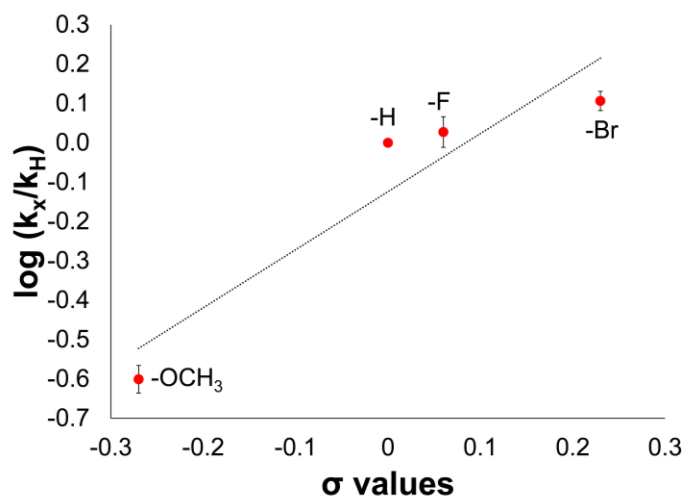


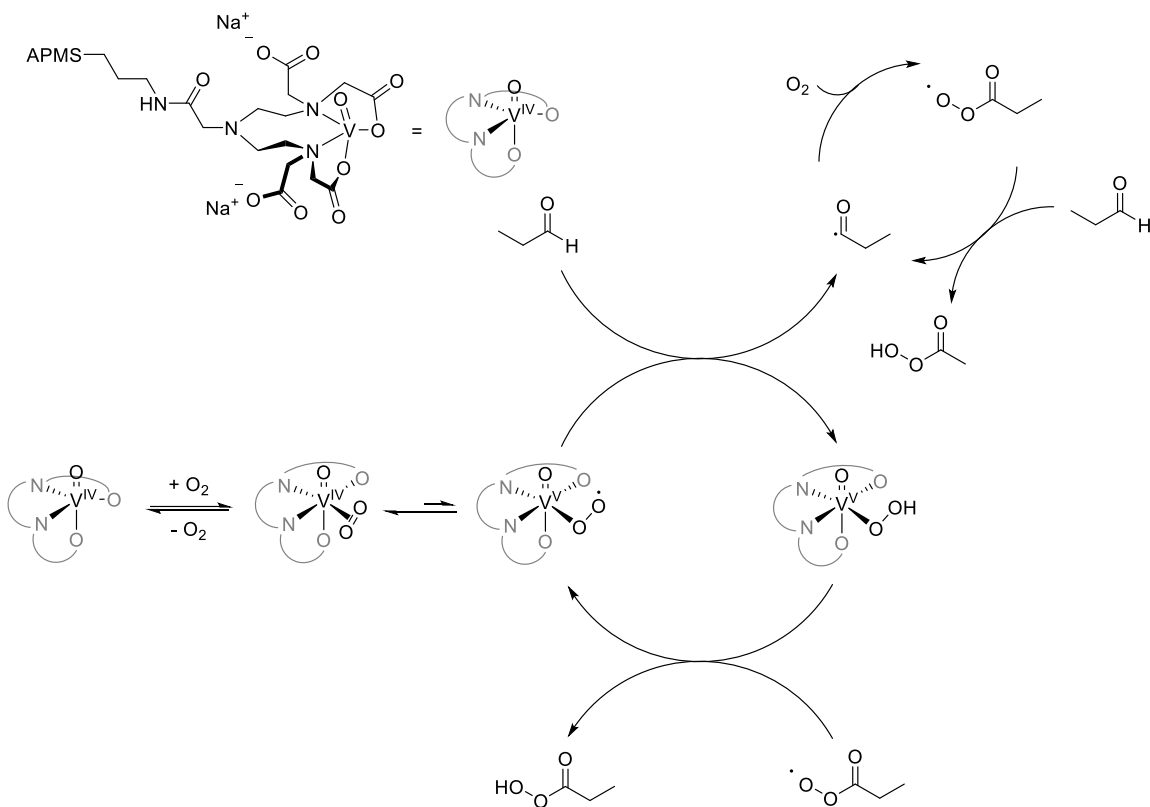
**Figure 3.3.** Hammett Plot for methyl phenyl sulfide, 4-fluorophenyl methyl sulfide, 4-bromophenyl methyl sulfide, and 4-methoxythioanisole.

### 3.4 Discussion

In previous work, we found that vanadium-doped mesoporous silica performed a dual catalytic role in the oxidation of CEES using this system. First, the vanadium catalyzed the oxidation of aldehyde to the corresponding peroxyacid with O<sub>2</sub>, and then it catalyzed the oxidation of CEES using the peroxyacid that had been generated *in situ*.<sup>40</sup>

In these studies where vanadium complexed with dtpa was used as the catalyst, we have found a similar dual catalytic role.

The catalytic formation of peroxyacid from aldehyde requires O<sub>2</sub> to bind at the metal center. O<sub>2</sub> can bind to vanadium complexes in either a superoxo ( $\eta^1$ ) or peroxy ( $\eta^2$ ) fashion.<sup>69</sup> Molecular oxygen has been studied less frequently than hydrogen peroxide, which is frequently used in oxidation reactions using vanadium complexes and commonly binds in an  $\eta^2$  manner.<sup>70-77</sup> Most studies have shown that O<sub>2</sub> also binds in an  $\eta^2$ , supported by X-ray diffraction, <sup>18</sup>O labeling, and FT-IR techniques as well as DFT calculations.<sup>77-79</sup> In some cases,  $\eta^1$  and  $\eta^2$  binding were both proposed,<sup>69,80,81</sup> and an equilibrium between dioxygen and superoxo O<sub>2</sub> ligands has also been proposed.<sup>69,82,83</sup> This equilibrium is important, because the  $\eta^1$  superoxo O<sub>2</sub> has also been implicated as a reaction site for the abstraction of a hydrogen atom from an aldehyde to form an aldehyde radical during peroxyacid formation reactions.<sup>43,80-82</sup> Based on these studies, it is likely that in our system, O<sub>2</sub> binds initially to VO(dtpa) as dioxygen and then undergoes a reversible redox reaction to form the superoxo  $\eta^1$ -bound O<sub>2</sub>. The superoxo oxygen can then abstract a hydrogen atom from propionaldehyde to form an acyl radical and vanadium-bound,  $\eta^1$  hydroperoxide. The acyl radical can then react with O<sub>2</sub> directly to form a peroxyacid radical. This in turn forms peroxyacid by reacting either with aldehyde or with the  $\eta^1$  hydroperoxide, feeding either acyl radicals or vanadium peroxyacid radicals back into the catalytic cycle. A proposed mechanism for the formation of the peroxyacid is shown in **Scheme 3.1**.



**Scheme 3.1.** Proposed mechanism for the formation of peroxyacid from aldehyde and O<sub>2</sub> using VO(dtpa) as the catalyst. VO(dtpa)-APMS drawn as suggested by DFT data.

The peroxyacid produced in this manner can then react with a sulfide in a process also catalyzed by the VO(dtpa) complex. Three reaction pathways<sup>3,51</sup> have been proposed for the sulfide oxidation catalyzed by vanadium complexes: (1) direct transfer, in which the sulfide interacts directly with the oxidant; (2) a radical mechanism, in which the oxidant forms radicals that perform a nucleophilic attack on the sulfide; (3) indirect transfer, in which the sulfide and oxidant both coordinate to the metal center, which facilitates the reaction.

Information that can help in establishing the reaction pathway includes a determination of whether the oxidant is nucleophilic or electrophilic. Theoretically, when

presented with the choice of oxidizing either a sulfide or a sulfoxide, a nucleophilic oxidant will oxidize the sulfoxide to the sulfone while an electrophilic oxidant will oxidize the sulfide to the sulfoxide. This is because sulfoxides are known to be weaker nucleophiles than sulfides.<sup>84</sup> Reaction assays have been developed to determine the nature of a system's oxidant by probing the rate of sulfide versus sulfoxide oxidation.<sup>85</sup> In a radical mechanism, the oxidant acts as a nucleophile.<sup>2</sup> In our case, we observed a two-step oxidative process:  $\text{CEES} \rightarrow \text{CEESO} \rightarrow \text{CEESO}_2$ . That is, we did not observe the formation of any sulfone until after all of the sulfide had been consumed. This would imply that the sulfide is the preferred substrate, indicating that the oxidant in our system is electrophilic. Therefore, our oxidant cannot undergo a radical mechanism. Additional reactions were performed to measure the rates of oxidation of diphenyl sulfide and diphenyl sulfoxide in our system (**Figure A1**). Although the rates are somewhat similar in this case, the sulfide does have a faster rate of oxidation than the sulfoxide, providing further evidence for an electrophilic oxidant in our reaction system.

There are only a few examples of the indirect oxidation pathway. Steric effects can be used to determine whether an indirect pathway is occurring, for example because molecular crowding at the metal center in a complex can decrease the rate of an indirect process. Several researchers have used Schiff base complexes of vanadium to illustrate such processes,<sup>46,50,45</sup> which makes sense because their systems have an open axial coordination site to which sulfide can bind. Schiff base complexes of vanadium are known to produce enantioselective oxidations of sulfides and researchers have intentionally designed ligands to direct sulfides to coordinate in certain orientations in order to produce enantioselective products. In our system, there was no observable

hindrance in rate when CEES, methyl phenyl sulfide, or diphenyl sulfide were used as the substrate (**Table A4**). Therefore, sterics do not appear to play a significant role in our mechanism, and the indirect pathway is not likely for our catalytic system.

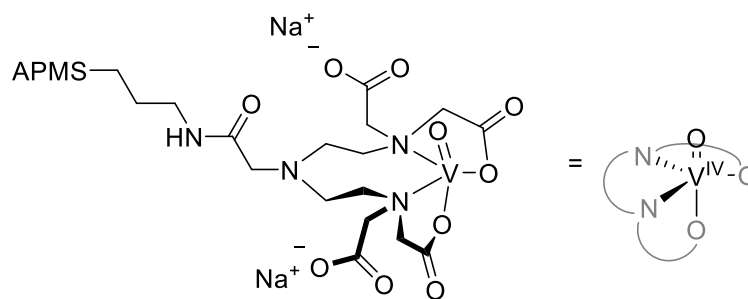
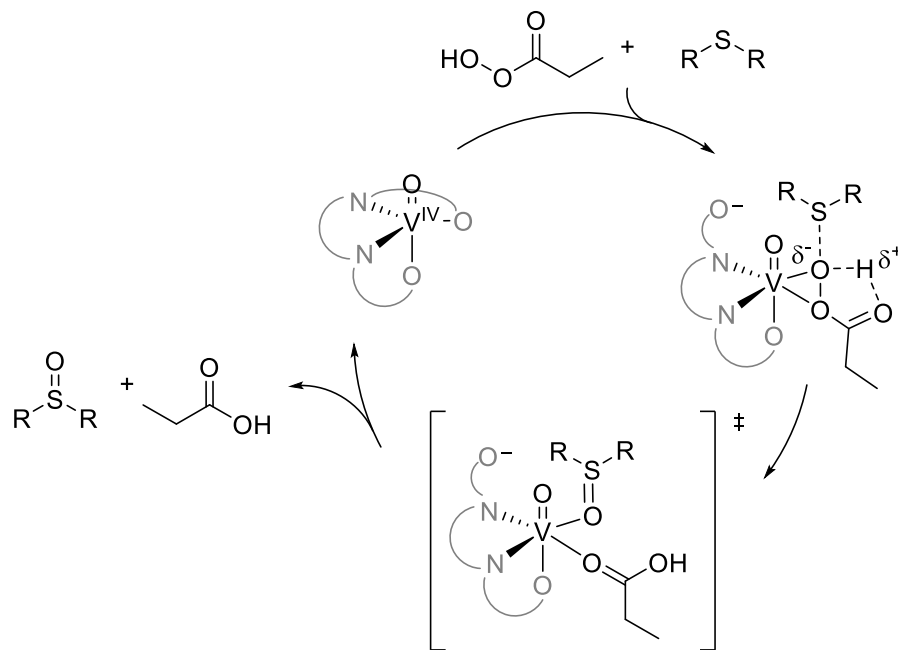
On the other hand, there is substantial evidence to support a direct oxidation pathway, although the examples use hydrogen peroxide as the oxidant source rather than a peroxyacid. Some examples of direct oxidation pathways can be found in computational work done with a bulky tridentate Schiff base vanadium catalyst on dimethyl disulfide<sup>51,86</sup> or with experimental and theoretical work with salophen and salen oxo vanadium complexes on methyl phenyl sulfide.<sup>47</sup> In terms of our work, our ligand looks very similar to model vanadium haloperoxidase ligands. Pecoraro investigated sulfide oxidation using models of the active site of vanadium haloperoxidase, with ligands such as N-(2-hydroxyethyl)iminodiacetic acid), N,N-bis(2-pyridylmethyl)glycine, N-(2-amidomethyl)-iminodiacetic acid and nitrilotriacetic acid.<sup>48</sup> These vanadium haloperoxidase model compounds look similar to our system in that they are multidentate ligands composed of carbonyl acetates and tertiary nitrogens. Vanadium haloperoxidase are known to oxidize halides in nature. The focus of Pecoraro's work was to investigate the ability for these vanadium haloperoxidase models to oxidize sulfides, in particular methyl phenyl sulfide, and compare the efficiency of the oxidation to that of halide oxidation. What they found was the best catalyst for halides was also the best catalyst for sulfides, catalyzing methyl phenyl sulfide for 1000 turnovers in 3 h. More importantly, in their work, a direct oxidation mechanism was observed.<sup>48</sup> Along the same lines, De Gioia performed a computational study of the oxidation of bromides and sulfides with peroxo forms of the vanadium haloperoxidase cofactor.<sup>52</sup> They found evidence for a direct

oxidation pathway, where an oxygen atom is bound in a pseudoaxial position at the vanadium center. In a separate study, a detailed investigation was performed using 2,2-[(2-hydroxyethyl)imino]diacetate as a vanadium ligand to model the haloperoxidase cofactor and it was again found that a direct oxidation pathway was preferred.<sup>53</sup>

Given this evidence, the fact that steric effects of sulfide substrates do not inhibit the rate of oxidation, and that VO(dtpa) is most similar to the nitrilotriacetic acid complex that was proposed to participate in a direct pathway,<sup>48</sup> a direct oxidation pathway is most likely occurring in our system. Details of our proposed reaction mechanism are shown in **Scheme 3.2**. There is substantial experimental support in the literature for an electrophilic oxidant at a vanadium catalyst interacting with a nucleophilic sulfide.<sup>3</sup> The Hammett plot in **Figure 3.4** suggests that sulfide reacts with an oxygen atom on the peroxyacid with a partial negative charge, due to the concerted reaction of the sulfide with the peroxyacid. After the sulfide reacts with the oxygen of the peroxyacid, an intermediate is formed prior to the release of sulfoxide and propionic acid products to regenerate the VO(dtpa) complex. It is possible that this intermediate is 6-coordinate, with one of the labile acetate ligands decoupled from the vanadium center.

As previously mentioned, we observed a two-step oxidative process: CEES  $\rightarrow$  CEESO  $\rightarrow$  CEESO<sub>2</sub>. That is, we did not observe the formation of any sulfone until after all of the sulfide had been consumed. We have determined that the sulfide is the nucleophile in our system and therefore in the oxidation of sulfoxide to sulfones, the sulfoxide would remain the nucleophile. Sulfoxides are known to be weaker nucleophiles than sulfides.<sup>84</sup> Therefore it is expected to have a slower rate of oxidation of a sulfoxide to sulfone than that of sulfide to sulfoxide. Since the mechanism is a direct oxidation, the

sulfide bonding directly to the oxidant, we expect the mechanism to be similar for the sulfoxide as there should be no steric hindrance and minimal electronic repulsion since the oxidant should be freely accessible.



**Scheme 3.2.** Proposed mechanism for the oxidation of sulfides using  $VO(dtpa)$  as the catalyst and peroxyacid as the oxidant.  $VO(dtpa)$ -APMS drawn as suggested by DFT data.

### 3.5 Conclusion

In this work, the details of the mechanism for the oxidation of aldehyde using  $O_2$  and the oxidation of sulfide using the peroxyacid generated *in situ*, were investigated. Kinetic experiments with varied temperatures indicated that the mechanism of the

reaction was dependent on the reaction temperature. This can be related to the presence of peroxyacid radicals in the system. At lower temperatures, these radicals can form peroxyacids, bind to the vanadium complex and participate in sulfide oxidation, but at higher temperatures they can react with themselves, reducing the amount of oxidant available to react with CEES. To confirm the presence of radicals, a radical trap, diphenylamine, was used. Upon addition of the radical trap, an induction period was observed which otherwise was not present. Kinetic experiments using methyl phenyl sulfide and para-substituted derivatives provided insight into the transition state of the mechanism. A Hammett plot constructed from this data gave a positive value of  $\rho$ , indicating a negatively charged center in the transition state of the mechanism.

Two catalytic cycles for VO(dtpa)-APMS have been proposed. To begin, O<sub>2</sub> binds initially to VO(dtpa) as dioxygen and then undergoes a reversible redox reaction to form the superoxo  $\eta^1$ -bound O<sub>2</sub>. The superoxo oxygen can then abstract a hydrogen atom from propionaldehyde to form an acyl radical and vanadium-bound,  $\eta^1$  hydroperoxide. The acyl radical can then react with O<sub>2</sub> directly to form a peroxyacid radical. This in turn forms peroxyacid by reacting either with aldehyde or with the  $\eta^1$  hydroperoxide, feeding either acyl radicals or vanadium peroxyacid radicals back into the catalytic cycle. The peroxyacid produced in this manner can then react with a sulfide in a process also catalyzed by the VO(dtpa) complex. In this step, a direct oxidation pathway is most likely occurring in the system. The Hammett plot suggests that sulfide reacts with an oxygen atom on the peroxyacid with a partial negative charge. After the sulfide attacks the peroxyacid, a 6-coordinate intermediate is formed prior to the release of sulfoxide and propionic acid products to regenerate the VO(dtpa) complex.

### 3.6 References

1. da Silva, J. A. L.; da Silva, J. J. R. F.; Pombeiro, A. J. L. Oxovanadium complexes in catalytic oxidations. *Coord. Chem. Rev.* **2011**, *255*, 2232-2248.
2. Butler, A.; Clague, M. J.; Meister, G. E. Vanadium Peroxide Complexes. *Chem. Rev.* **1994**, *94*, 625-638.
3. Conte, V.; Coletti, A.; Floris, B.; Licini, G.; Zonta, C. Mechanistic aspects of vanadium catalysed oxidations with peroxides. *Coord. Chem. Rev.* **2011**, *255*, 2165-2177.
4. Wu, P.; Santoni, G.; Fröba, M.; Rehder, D. Modelling the Sulfoxxygenation Activity of Vanadate-Dependent Peroxidases. *Chem. Biodiversity* **2008**, *5*, 1913-1926.
5. Rehder, D.; Ebel, M.; Wikete, C.; Santoni, G.; Gätjens, J. Modeling the active site structures of vanadate-dependent peroxidases and vanadate-inhibited phosphatases. In *Pure Appl. Chem.*, 2005; Vol. 77, p 1607.
6. Maurya, M. R.; Arya, A.; Kumar, A.; Pessoa, J. C. Polystyrene bound oxidovanadium(IV) and dioxidovanadium(V) complexes of histamine derived ligand for the oxidation of methyl phenyl sulfide, diphenyl sulfide and benzoin. *Dalton Trans.* **2009**, 2185-2195.
7. de Azevedo Marques, A. P.; Dockal, E. R.; Skrobot, F. C.; Viana Rosa, I. L. Synthesis, characterization and catalytic study of [N,N'-bis(3-ethoxysalicylidene)-m-xylylenediamine]oxovanadium(IV) complex. *Inorg. Chem. Commun.* **2007**, *10*, 255-261.
8. Rehder, D., *Bioinorganic vanadium chemistry*. John Wiley & Sons: West Sussex, England, 2008; Vol. 30.
9. Andersson, M.; Willetts, A.; Allenmark, S. Asymmetric Sulfoxidation Catalyzed by a Vanadium-Containing Bromoperoxidase. *J. Org. Chem.* **1997**, *62*, 8455-8458.

10. ten Brink, H. B.; Tuynman, A.; Dekker, H. L.; Hemrika, W.; Izumi, Y.; Oshiro, T.; Schoemaker, H. E.; Wever, R. Enantioselective Sulfoxidation Catalyzed by Vanadium Haloperoxidases. *Inorg. Chem.* **1998**, *37*, 6780-6784.
11. Ben Zid, T.; Khedher, I.; Ksibi, Z.; Fraile, J. M. Vanadium-Schiff base complex covalently bonded on modified MCM-41 as catalyst for asymmetric oxidation of methyl phenyl sulfide. *J. Porous Mater.* **2016**, *23*, 507-516.
12. Ben Zid, T.; Fadhli, M.; Khedher, I.; Fraile, J. M. New bis(oxazoline)-vanadyl complexes, supported by electrostatic interaction in Laponite clay, as heterogeneous catalysts for asymmetric oxidation of methyl phenyl sulfide. *Microporous Mesoporous Mater.* **2017**, *239*, 167-172.
13. Ben Zid, T.; Khedher, I.; Ghorbel, A. Chiral vanadyl salen catalyst immobilized on mesoporous silica as support for asymmetric oxidation of sulfides to sulfoxides. *React. Kinet., Mech. Catal.* **2010**, *100*, 131-143.
14. Bryliakov, K. P. Catalytic Asymmetric Oxygenations with the Environmentally Benign Oxidants H<sub>2</sub>O<sub>2</sub> and O<sub>2</sub>. *Chem. Rev.* **2017**, *117*, 11406-11459.
15. Shen, C.; Qiao, J.; Zhao, L.; Zheng, K.; Jin, J.; Zhang, P. An efficient silica supported Chitosan@vanadium catalyst for asymmetric sulfoxidation and its application in the synthesis of esomeprazole. *Catal. Commun.* **2017**, *92*, 114-118.
16. Gao, J.; Lu, L.; Zhou, W.; Gao, G.; He, M. Synthesis, characterization and sulfide oxidation activity of vanadyl Schiff base complexes anchored on MCM-41. *J. Porous Mater.* **2008**, *15*, 127-132.
17. Hulea, V.; Maciuca, A.-L.; Cojocariu, A.-M.; Ciocan, C.-E.; Dumitriu, E. New heterogeneous catalysts for mild oxidation of S-containing organic compounds. *C. R. Chim.* **2009**, *12*, 723-730.
18. Zolfigol, M. A.; Khazaei, A.; Safaiee, M.; Mokhlesi, M.; Rostamian, R.; Bagheri, M.; Shiri, M.; Kruger, H. G. Application of silica vanadic acid as a heterogeneous, selective and highly reusable catalyst for oxidation of sulfides at room temperature. *J. Mol. Catal. A: Chem.* **2013**, *370*, 80-86.

19. Tamoradi, T.; Ghadermazi, M.; Ghorbani-Choghamarani, A.; Molaei, S. Synthesis and characterization of oxo-vanadium complex anchored onto SBA-15 as a green, novel and reusable nanocatalyst for the oxidation of sulfides and oxidative coupling of thiols. *Res. Chem. Intermed.* **2018**.
20. Norouzi, M.; Ghorbani-Choghamarani, A. Mild and highly efficient method for the oxidation of sulfides and protection of alcohols catalyzed by oxovanadium(IV) supported on modified magnetic nanoparticles as recyclable catalyst. *React. Kinet., Mech. Catal.* **2016**, *119*, 537-554.
21. Noori, N.; Nikoorazm, M.; Ghorbani-Choghamarani, A. Oxo-vanadium immobilized on L-cysteine-modified MCM-41 as catalyst for the oxidation of sulfides and oxidative coupling of thiols. *Microporous Mesoporous Mater.* **2016**, *234*, 166-175.
22. Nikoorazm, M.; Ghorbani-Choghamarani, A.; Noori, N. Oxo-vanadium(IV) Schiff base complex supported on modified MCM-41: a reusable and efficient catalyst for the oxidation of sulfides and oxidative S–S coupling of thiols. *Appl. Organomet. Chem.* **2015**, *29*, 328-333.
23. Kantam, M. L.; Neelima, B.; Reddy, C. V.; Chaudhuri, M. K.; Dehury, S. K. VO(acac)<sub>2</sub> Supported on Titania: A Heterogeneous Protocol for the Selective Oxidation of Sulfides Using TBHP. *Catal. Lett.* **2004**, *95*, 19-22.
24. Gregori, F.; Nobili, I.; Bigi, F.; Maggi, R.; Predieri, G.; Sartori, G. Selective oxidation of sulfides to sulfoxides and sulfones using 30% aqueous hydrogen peroxide and silica-vanadia catalyst. *J. Mol. Catal. A: Chem.* **2008**, *286*, 124-127.
25. Eftekhari-Sis, B.; Akbari, M.; Akbari, A.; Amini, M. Vanadium (V) and Tungsten (VI) Oxoperoxo-Complexes Anchored on Fe<sub>3</sub>O<sub>4</sub> Magnetic Nanoparticles: Versatile and Efficient Catalysts for the Oxidation of Alcohols and Sulfides. *Catal. Lett.* **2017**, *147*, 2106-2115.
26. Talukdar, D.; Sharma, K.; Bharadwaj, S. K.; Thakur, A. J. VO(acac)<sub>2</sub>: An Efficient Catalyst for the Oxidation of Aldehydes to the Corresponding Acids in the Presence of Aqueous H<sub>2</sub>O<sub>2</sub>. *Synlett* **2013**, *24*, 963-966.
27. Pokutsa, A.; Kubaj, Y.; Zaborovskyi, A.; Sobkowiak, A.; Muzart, J. Oxalic acid-improved mild cyclohexane oxidation catalyzed by VO(acac)<sub>2</sub>: non-radical versus radical mechanism. *React. Kinet., Mech. Catal.* **2017**, *122*, 757-774.

28. Yao, X.; Peng, C.; Shi, Z. Reaction Mechanism for Selective Oxidation of Anethole to Anisaldehyde by Hydrogen Peroxide in Presence of Ferric Vanadate. *Asian J. Chem* **2014**, *26*.
29. Vincent, S.; Lion, C.; Hedayatullah, M.; Challier, A.; Delmas, G.; Magnaud, G. Selective Oxidation of Sulfides to Sulfoxides by Atmospheric Oxygen and Aldehyde Catalysed by Ni<sup>II</sup> Complexes. *Phosphorus Sulfur Silicon Relat Elem* **1994**, *92*, 189-192.
30. Song, G.; Wang, F.; Zhang, H.; Lu, X.; Wang, C. Efficient Oxidation of Sulfides Catalyzed by Transition Metal Salts with Molecular Oxygen in the Presence of Aldehydes. *Synth. Commun.* **1998**, *28*, 2783-2787.
31. Murata, S.; Murata, K.; Kidena, K.; Nomura, M. A Novel Oxidative Desulfurization System for Diesel Fuels with Molecular Oxygen in the Presence of Cobalt Catalysts and Aldehydes. *Energy Fuels* **2004**, *18*, 116-121.
32. Kiyomi, I.; Takushi, N.; Tohru, Y.; Teruaki, M. Asymmetric Oxidation of Sulfides with Molecular Oxygen Catalyzed by  $\beta$ -Oxo Aldiminato Manganese(III) Complexes. *Chem. Lett.* **1995**, *24*, 335-336.
33. Das, P.; Saha, D.; Saha, D.; Guin, J. Aerobic Direct C(sp<sup>2</sup>)-H Hydroxylation of 2-Arylpyridines by Palladium Catalysis Induced with Aldehyde Auto-Oxidation. *ACS Catal.* **2016**, *6*, 6050-6054.
34. Komiya, N.; Naota, T.; Oda, Y.; Murahashi, S.-I. Aerobic oxidation of alkanes and alkenes in the presence of aldehydes catalyzed by copper salts and copper-crown ether. *J. Mol. Catal. A: Chem.* **1997**, *117*, 21-37.
35. Yu, H.; Ru, S.; Zhai, Y.; Dai, G.; Han, S.; Wei, Y. An Efficient Aerobic Oxidation Protocol of Aldehydes to Carboxylic Acids in Water Catalyzed by an Inorganic-Ligand-Supported Copper Catalyst. *ChemCatChem* **2018**, *10*, 1253-1257.
36. Liu, M.; Wang, H.; Zeng, H.; Li, C.-J. Silver(I) as a widely applicable, homogeneous catalyst for aerobic oxidation of aldehydes toward carboxylic acids in water—"silver mirror": From stoichiometric to catalytic. *Sci. Adv.* **2015**, *1*.

37. Nam, W.; Kim, H. J.; Kim, S. H.; Ho, R. Y. N.; Valentine, J. S. Metal Complex-Catalyzed Epoxidation of Olefins by Dioxygen with Co-Oxidation of Aldehydes. A Mechanistic Study. *Inorg. Chem.* **1996**, *35*, 1045-1049.
38. Tada, M.; Muratsugu, S.; Kinoshita, M.; Sasaki, T.; Iwasawa, Y. Alternative Selective Oxidation Pathways for Aldehyde Oxidation and Alkene Epoxidation on a SiO<sub>2</sub>-Supported Ru-Monomer Complex Catalyst. *J. Am. Chem. Soc.* **2010**, *132*, 713-724.
39. Rao, T. V.; Sain, B.; Kumar, K.; Murthy, P. S.; Rao, T. S. R. P.; Joshi, G. C. Oxidation of Sulphides by Molecular Oxygen - Aldehyde System in the Absence of Metal Catalyst. *Synth. Commun.* **1998**, *28*, 319-326.
40. Livingston, S. R.; Landry, C. C. Oxidation of a Mustard Gas Analogue Using an Aldehyde/O<sub>2</sub> System Catalyzed by V-Doped Mesoporous Silica. *J. Am. Chem. Soc.* **2008**, *130*, 13214-13215.
41. Khavrutskii, I. V.; Maksimov, G. M.; Kholdeeva, O. A. Oxidation of methyl phenyl sulfide with molecular oxygen in the presence of isobutyraldehyde and transition metal monosubstituted heteropolytungstates. *React. Kinet. Catal. Lett.* **1999**, *66*, 325-330.
42. El Amrani, I.; Atlamsani, A.; Dakkach, M.; Rodríguez, M.; Romero, I.; Anthiou, S. Efficient and selective oxidation of aldehydes with dioxygen catalysed by vanadium-containing heteropolyanions. *C. R. Chim.* **2017**, *20*, 888-895.
43. Chatgililoglu, C.; Crich, D.; Komatsu, M.; Ryu, I. Chemistry of Acyl Radicals. *Chem. Rev.* **1999**, *99*, 1991-2070.
44. Hall, N.; Orio, M.; Jorge-Robin, A.; Gennaro, B.; Marchi-Delapierre, C.; Duboc, C. Vanadium Thiolate Complexes for Efficient and Selective Sulfoxidation Catalysis: A Mechanistic Investigation. *Inorg. Chem.* **2013**, *52*, 13424-13431.
45. Romanowski, G. Synthesis, characterization and catalytic activity in the oxidation of sulfides and styrene of vanadium(V) complexes with tridentate Schiff base ligands. *J. Mol. Catal. A: Chem.* **2013**, *368-369*, 137-144.

46. Zeng, Q.; Wang, H.; Weng, W.; Lin, W.; Gao, Y.; Huang, X.; Zhao, Y. Substituent effects and mechanism elucidation of enantioselective sulfoxidation catalyzed by vanadium Schiff base complexes. *New J. Chem.* **2005**, *29*, 1125-1127.
47. Coletti, A.; Galloni, P.; Sartorel, A.; Conte, V.; Floris, B. Salophen and salen oxo vanadium complexes as catalysts of sulfides oxidation with H<sub>2</sub>O<sub>2</sub>: Mechanistic insights. *Catal. Today* **2012**, *192*, 44-55.
48. Smith, T. S.; Pecoraro, V. L. Oxidation of Organic Sulfides by Vanadium Haloperoxidase Model Complexes. *Inorg. Chem.* **2002**, *41*, 6754-6760.
49. Curci, R.; Di Furia, F.; Testi, R.; Modena, G. Metal catalysis in oxidation by peroxides. Vanadium catalysed oxidation of organosulphur compounds by t-butyl hydroperoxide. *J. Chem. Soc., Perkin Trans. 2* **1974**, 752-757.
50. Jeong, Y.-C.; Kang, E. J.; Ahn, K.-H. Electronic effects of substituents in sulfides: mechanism elucidation of vanadium catalyzed sulfoxidation. *Bull. Korean Chem. Soc.* **2009**, *30*, 2795-2798.
51. Balcells, D.; Maseras, F.; Lledós, A. Density Functional Study on the Mechanism of the Vanadium-Catalyzed Oxidation of Sulfides by Hydrogen Peroxide. *J. Org. Chem.* **2003**, *68*, 4265-4274.
52. Zampella, G.; Fantucci, P.; Pecoraro, V. L.; De Gioia, L. Reactivity of Peroxo Forms of the Vanadium Haloperoxidase Cofactor. A DFT Investigation. *J. Am. Chem. Soc.* **2005**, *127*, 953-960.
53. Schneider, C. J.; Zampella, G.; Greco, C.; Pecoraro, V. L.; De Gioia, L. Mechanistic Analysis of Nucleophilic Substrates Oxidation by Functional Models of Vanadium-Dependent Haloperoxidases: A Density Functional Theory Study. *Eur. J. Inorg. Chem.* **2007**, *2007*, 515-523.
54. Lattuada, L.; Barge, A.; Cravotto, G.; Giovenzana, G. B.; Tei, L. The synthesis and application of polyamino polycarboxylic bifunctional chelating agents. *Chem. Soc. Rev.* **2011**, *40*, 3019-3049.
55. Solberg, S.; Landry, C. Adsorption of DNA into Mesoporous Silica. *J. Phys. Chem. B* **2006**, *110*, 15261-15268.

56. Gallis, K. W.; Landry, C. C. Mesoporous Silica Production for Liquid Chromatography. U.S. Patent 6,334,988, August 20, 1999.
57. Livingston, S. R.; Kumar, D.; Landry, C. C. Oxidation of 2-chloroethyl ethyl sulfide using V-APMS. *J. Mol. Catal. A: Chem.* **2008**, *283*, 52-59.
58. Sheldon, R. A.; Kochi, J. K., *Metal-Catalyzed Oxidations of Organic Compounds: Mechanistic Principles and Synthetic Methodology Including Biochemical Processes*. Academic Press, Inc: New York, NY, 1981.
59. Haidasz, E. A.; Shah, R.; Pratt, D. A. The Catalytic Mechanism of Diarylamine Radical-Trapping Antioxidants. *J. Am. Chem. Soc.* **2014**, *136*, 16643-16650.
60. Dumont, V.; Oliviero, L.; Maugé, F.; Houalla, M. Oxidation of dibenzothiophene by a metal–oxygen–aldehyde system. *Catal. Today* **2008**, *130*, 195-198.
61. Anslyn, E. V.; Dougherty, D. A., *Modern Physical Organic Chemistry*. 1st ed.; University Science Books: Sausalito, California, 2006.
62. Housecroft, C. E.; Sharpe, A. G., *Inorganic Chemistry*. 2nd ed.; Pearson Education Limited: Harlow, England, 2005; p 765-766.
63. Houk, K. N.; Rondan, N. G.; Mareda, J. Theoretical studies of halocarbene cycloaddition selectivities: A new interpretation of negative activation energies and entropy control of selectivity. *Tetrahedron* **1985**, *41*, 1555-1563.
64. Hansch, C.; Leo, A.; Taft, R. W. A survey of Hammett substituent constants and resonance and field parameters. *Chem. Rev.* **1991**, *91*, 165-195.
65. Neu, H. M.; Yang, T.; Baglia, R. A.; Yosca, T. H.; Green, M. T.; Quesne, M. G.; de Visser, S. P.; Goldberg, D. P. Oxygen-Atom Transfer Reactivity of Axially Ligated Mn(V)–Oxo Complexes: Evidence for Enhanced Electrophilic and Nucleophilic Pathways. *J. Am. Chem. Soc.* **2014**, *136*, 13845-13852.
66. Du, G.; Espenson, J. H. Oxidation of Triarylphosphines and Aryl Methyl Sulfides with Hydrogen Peroxide Catalyzed by Dioxovanadium(V) Ion. *Inorg. Chem.* **2005**, *44*, 2465-2471.

67. Yamaura, T.; Kamata, K.; Yamaguchi, K.; Mizuno, N. Efficient sulfoxidation with hydrogen peroxide catalyzed by a divanadium-substituted phosphotungstate. *Catal. Today* **2013**, *203*, 76-80.
68. Licini, G.; Zonta, C. Revisiting the Hammett  $\rho$  Parameter for the Determination of Philicity: Nucleophilic Substitution with Inverse Charge Interaction. *Angew. Chem.* **2013**, *125*, 2983-2986.
69. Cozzolino, A. F.; Tofan, D.; Cummins, C. C.; Temprado, M.; Palluccio, T. D.; Rybak-Akimova, E. V.; Majumdar, S.; Cai, X.; Captain, B.; Hoff, C. D. Two-Step Binding of O<sub>2</sub> to a Vanadium(III) Trisanilide Complex To Form a Non-Vanadyl Vanadium(V) Peroxo Complex. *J. Am. Chem. Soc.* **2012**, *134*, 18249-18252.
70. Islam, N. S.; Boruah, J. J. Macromolecular peroxo complexes of Vanadium(V) and Molybdenum(VI): Catalytic activities and biochemical relevance. *J. Chem. Sci* **2015**, *127*, 777-795.
71. Maurya, M. R.; Bisht, M.; Avecilla, F. Synthesis, characterization and catalytic activities of vanadium complexes containing ONN donor ligand derived from 2-aminoethylpyridine. *J. Mol. Catal. A: Chem.* **2011**, *344*, 18-27.
72. Mimoun, H.; Saussine, L.; Daire, E.; Postel, M.; Fischer, J.; Weiss, R. Vanadium(V) peroxy complexes. New versatile biomimetic reagents for epoxidation of olefins and hydroxylation of alkanes and aromatic hydrocarbons. *J. Am. Chem. Soc.* **1983**, *105*, 3101-3110.
73. Ballistreri, F. P.; Fortuna, C. G.; Pappalardo, A.; Tomaselli, G. A.; Toscano, R. M. Oxidation of organic sulfides by a vanadium(5+) oxo-monoperoxo-picolate complex: Kinetics and mechanism. *J. Mol. Catal. A: Chem.* **2009**, *308*, 56-60.
74. Colpas, G. J.; Hamstra, B. J.; Kampf, J. W.; Pecoraro, V. L. Functional Models for Vanadium Haloperoxidase: Reactivity and Mechanism of Halide Oxidation. *J. Am. Chem. Soc.* **1996**, *118*, 3469-3478.
75. Stomberg, R. The Crystal Structures of Potassium Bis (oxalato) oxoperoxovanadate (V) Hemihydrate, K<sub>3</sub> [VO(O<sub>2</sub>)(C<sub>2</sub>O<sub>4</sub>)<sub>2</sub>] 1/2 H<sub>2</sub>O, and Potassium Bis (oxalato) dioxovanadate (V) Trihydrate K<sub>3</sub> [VO<sub>2</sub>(C<sub>2</sub>O<sub>4</sub>)<sub>2</sub>] 3H<sub>2</sub>O. *Acta Chem. Scand.* **1986**, *40*, 168-176.

76. Pacigová, S.; Gyepes, R.; Tatiersky, J.; Sivák, M. Interpretation of the multiple vanadium-oxygen bonds in the central  $\text{VO}(\eta^2\text{-O}_2)^+$  group. Synthesis, structure, supramolecular interactions and DFT studies for complexes with 2,2'-bipyridine, 1,10-phenanthroline, pyrazinato(1-) and pyrazinamide ligands. *Dalton Trans.* **2008**, 121-130.
77. Gutsev, G. L.; Rao, B. K.; Jena, P. Systematic Study of Oxo, Peroxo, and Superoxo Isomers of 3d-Metal Dioxides and Their Anions. *J. Phys. Chem. A* **2000**, *104*, 11961-11971.
78. Kosugi, M.; Hikichi, S.; Akita, M.; Moro-oka, Y. The first evidence for activation of exogenous  $\text{O}_2$  on a vanadium(IV) center: synthesis and characterization of a peroxo vanadium(V) complex with hydrotris(3,5-diisopropylpyrazol-1-yl)borate. *J. Chem. Soc., Dalton Trans.* **1999**, 1369-1372.
79. Waidmann, C. R.; DiPasquale, A. G.; Mayer, J. M. Synthesis and Reactivity of Oxo-Peroxo-Vanadium(V) Bipyridine Compounds. *Inorg. Chem.* **2010**, *49*, 2383-2391.
80. Zhang, J.; Yang, H.; Sun, T.; Chen, Z.; Yin, G. Nonredox Metal-Ions-Enhanced Dioxygen Activation by Oxidovanadium(IV) Complexes toward Hydrogen Atom Abstraction. *Inorg. Chem.* **2017**, *56*, 834-844.
81. Tyagi, S.; Cook, C. D.; DiDonato, D. A.; Key, J. A.; McKillican, B. P.; Eberle, W. J.; Carlin, T. J.; Hunt, D. A.; Marshall, S. J.; Bow, N. L. Bioinspired Synthesis of a Sedaxane Metabolite Using Catalytic Vanadyl Acetylacetonate and Molecular Oxygen. *J. Org. Chem.* **2015**, *80*, 11941-11947.
82. Kelm, H.; Krüger, H.-J. A Superoxovanadium(V) Complex Linking the Peroxide and Dioxygen Chemistry of Vanadium. *Angew. Chem. Int. Ed.* **2001**, *40*, 2344-2348.
83. Kirk Egdal, R.; Bond, A. D.; McKenzie, C. J. Air oxidation of divanadium(IV) complexes. *Dalton Trans.* **2009**, 3833-3839.
84. Ballistreri, F. P.; Tomaselli, G. A.; Toscano, R. M.; Conte, V.; Di Furia, F. Application of the thianthrene 5-oxide mechanistic probe to peroxometal complexes. *J. Am. Chem. Soc.* **1991**, *113*, 6209-6212.

85. Adam, W.; Haas, W.; Sieker, G. Thianthrene 5-oxide as mechanistic probe in oxygen-transfer reactions: the case of carbonyl oxides vs. dioxiranes. *J. Am. Chem. Soc.* **1984**, *106*, 5020-5022.
86. Balcells, D.; Maseras, F.; Ujaque, G. Computational Rationalization of the Dependence of the Enantioselectivity on the Nature of the Catalyst in the Vanadium-Catalyzed Oxidation of Sulfides by Hydrogen Peroxide. *J. Am. Chem. Soc.* **2005**, *127*, 3624-3634.

## CHAPTER 4: OXIDATION OF CYCLOALKENES USING VO(dtpa) IMMOBILIZED ON A POROUS SILICA SUBSTRATE

### 4.1 Introduction

Vanadium catalysts participate in the oxidation, halogenation, and carboxylation of a variety of organic compounds.<sup>1-3</sup> Alkene oxidation, especially epoxidation, is of particular interest due to the value of epoxides in organic synthesis<sup>4,5</sup> and industrial production,<sup>6,7</sup> and homogeneous catalysis using vanadium complexes can be used for epoxidation.<sup>2</sup> Vanadium oxidation catalysts have also been immobilized onto solid supports, generating heterogeneous catalysts that are easier to recycle and can be used in "green" systems that generate less solvent waste than homogeneous systems.<sup>8-10</sup> These supports include zeolite Y,<sup>11</sup> boehmite nanoparticles,<sup>12</sup> carbon nanotubes<sup>13</sup> and nanostructured carbon materials,<sup>14</sup> magnetic nanoparticles,<sup>15</sup> polymers,<sup>16</sup> silica gel,<sup>17</sup> and mesoporous silica.<sup>10,18-20</sup> Of these, mesoporous silica is a desirable support due to its simple and low-cost synthesis, its structural stability in organic solvents,<sup>20</sup> and its large internal surface area, which can exceed 1000 m<sup>2</sup>/g. In addition, the pore diameter of mesoporous silica can be synthetically controlled, providing a measure of influence over the catalytic process.

Many silica-supported vanadium catalysts used in alkene oxidations are traditional heterogeneous catalysts, in the sense that vanadium ions are included in the silica through a variety of techniques such as including vanadium during the sol-gel synthesis of silica,<sup>21</sup> post-synthetic impregnation,<sup>22</sup> (i.e. aqueous solutions of metal precursors stirred with the silica materials until dryness and then calcined to 773 K for 5 hours), grafting followed by calcination<sup>23,24</sup> or kneading (i.e. aqueous vanadium and chromium oxide poured into a

silica sol and then the mixture kneaded for 6 hours at 80 °C, dried and then calcined at 450 °C for 5 hours).<sup>25,26</sup> Polyoxometalates that incorporate vanadium have also been immobilized by similar methods onto silica.<sup>20,27-30</sup> Examples of organometallic vanadium catalysts immobilized onto silica also exist. In one case, the metal-organic framework V-MIL-101 was tethered to silica-coated iron oxide nanoparticles through peptide coupling.<sup>31,32</sup> These researchers then surveyed the oxidation of allylic alcohols and alkenes using <sup>t</sup>BuOOH as the oxidant. Some challenges with this catalyst were observed; for example, oxidation of *cis*-cyclooctene was only 50% complete after 24 hours in refluxing MeCN. In another study, VO(acac)<sub>2</sub> was immobilized on the mesoporous silica MCM-41, also using peptide coupling, and alkene oxidation was examined.<sup>10</sup> Using <sup>t</sup>BuOOH as the oxidant, 90% of *cis*-cyclooctene was oxidized after 24 hours. Finally, there are two examples of systems using silica-tethered Schiff base ligands for alkene oxidation. In the first, a hydrazine Schiff base ligand on silica gel was synthesized by grafting N-(triethoxysilylpropyl)salicylaldehyde to the silica surface and then complexing VO(acac)<sub>2</sub> with the grafted salicylaldehyde and (E)-N<sup>0</sup>-(2-hydroxybenzylidene)benzohydrazide). The catalyst, with H<sub>2</sub>O<sub>2</sub> as the oxidant and sodium bicarbonate as an activator for the H<sub>2</sub>O<sub>2</sub>, was used to oxidize a variety of alkenes in refluxing MeCN. After 5 hours, the oxidation of *cis*-cyclooctene was 96% complete.<sup>17</sup> In the second example, a vanadium Schiff base complex prepared from salicylaldehyde and diethylenetriamine (two salicylaldehyde bound to diethylenetriamine through an imine bond on the nitrogen atoms of the diethylenetriamine) was tethered to MCM-41 and H<sub>2</sub>O<sub>2</sub> and sodium bicarbonate were used to oxidize *cis*-cyclooctene.<sup>18</sup> After 8 hours at room temperature, 82% of the *cis*-cyclooctene had been oxidized.

We have recently shown that VO(dtpa) (dtpa = diethylenetriamine pentaacetate) can be easily tethered to mesoporous silica with peptide coupling reactions, and is an effective catalyst for the oxidation of sulfides. In that system, the oxidant was peroxyacid that was generated *in situ* through the reaction of O<sub>2</sub> with aldehyde, which was included in the reaction mixture. An investigation of the catalytic mechanism of this process showed VO(dtpa)-APMS performs two catalytic oxidations: first, the oxidation of propionaldehyde to make the peroxyacid; then the oxidation of sulfides. For the oxidation of propionaldehyde, it has been proposed that O<sub>2</sub> binds initially to the vanadium metal center as dioxygen and then undergoes a reversible redox reaction to form the superoxo  $\eta^1$ -bound O<sub>2</sub>. The superoxo oxygen can then abstract a hydrogen atom from propionaldehyde to form an acyl radical and vanadium-bound,  $\eta^1$  hydroperoxide. The acyl radical reacts with O<sub>2</sub> directly to form a peroxyacid radical. This in turn forms peroxyacid by reacting either with propionaldehyde or with the  $\eta^1$  hydroperoxide, feeding either acyl radicals or vanadium peroxyacid radicals back into the catalytic cycle. The peroxyacid produced in this manner can then react with a sulfide in a process also catalyzed by the VO(dtpa) complex. The peroxyacid coordinates with the vanadium center at which point a sulfide then directly reacts with the peroxyacid without coordination to the vanadium metal center. A 6-coordinate catalyst intermediate is formed prior to the release of sulfoxide and propionic acid to regenerate the VO(dtpa) complex. Considering the utility of a system using an oxidant that was generated *in situ* and the previous reactions showing the capability of vanadium catalysts in epoxidation, in this study we use immobilized VO(dtpa) in the

oxidation of alkenes. We also investigate the reaction mechanism and compared to our previous study on sulfide oxidation.

## **4.2 Experimental Section**

### **4.2.1 Materials and methods**

(3-aminopropyl)triethoxysilane was obtained from Gelest, Inc. Cyclododecene was obtained from TCI America. 4-Fluorostyrene and p-Methylstyrene were obtained from ACROS Organics. 4-Methoxystyrene, *cis*-cyclooctene, cyclohexene were obtained from Alfa Aesar. All other chemicals were obtained from Sigma Aldrich. Porosity and surface area measurements were obtained at 77 K on a Micromeritics TriStar 3000 surface area and porosity analyzer. Samples were degassed on a Micromeritics FlowPrep 060 Sample Degas System. Surface areas and pore size distributions were calculated using the BET and BJH theories. Thermogravimetric analysis was completed on a Perkin Elmer Pyris 1 TGA. Elemental analysis via inductively-coupled plasma optical emission spectroscopy (ICP-OES) was completed on a PerkinElmer Optima 7000DV ICP optical emission spectrometer with a CCD array detector, a PerkinElmer S10 autosampler, and WinLab32 software.

### **4.2.2 Synthesis of (VO)dtpa-APMS**

The immobilized VO(dtpa) catalyst was synthesized as described in Chapter 2.

### **4.2.3 Catalytic oxidation of cycloalkene to cycloalkene oxide**

The catalysis protocol was modified from a previously published procedure. Cycloalkene (42.9  $\mu\text{mol}$ ) and propionaldehyde (61.9  $\mu\text{L}$ , 0.805 g/mL, 858  $\mu\text{mol}$ ) were placed in a 3 mL volumetric flask, which was filled with acetonitrile. 1,2,4-trimethylbenzene (1  $\mu\text{L}$ , 0.876 g/mL, 7.88  $\mu\text{mol}$ ) was added as a GC reference. Catalysis

was initiated by simply adding one of the vanadium-loaded catalysts prepared above (20 mg) to this solution. Aliquots (200  $\mu$ L) were removed with a 2 mL plastic syringe, the solid catalyst was filtered out using a 0.22  $\mu$ m Millipore syringe filter, and the resulting filtrate was analyzed by gas chromatography with mass spectrometric detection using a ZB-5 (length 30 m, i.d. 0.25 mm) column.

#### 4.2.4 Eyring Plot catalysis

*cis*-Cyclooctene (18.63  $\mu$ L, 0.846 g/mL, 143  $\mu$ mol) and 1,2,4-trimethylbenzene (3.33  $\mu$ L, 0.876 g/mL, 26.27  $\mu$ mol) were mixed into three 10 mL stock solutions with acetonitrile as a solvent. For 15  $^{\circ}$ C reactions, two stock solution were chilled to 2-8  $^{\circ}$ C in the refrigerator. For 21  $^{\circ}$ C reaction, a stock solution was left at room temperature (19-21  $^{\circ}$ C). Finally, 40  $^{\circ}$ C reaction, the stock solution was heated in a 40  $^{\circ}$ C oven. Aliquots of propionaldehyde were also adjusted to specific temperatures. Each vanadium catalyst was adjusted to temperatures for 10 min in 4 dram scintillation vials before addition of reactants. 3 mL of stock solution were measured in a 3 mL volumetric flask. To the stock solution, propionaldehyde (61.9  $\mu$ L, 0.805 g/mL, 858  $\mu$ mol) was added. The oxidation reaction was initiated once the reactants were poured onto the vanadium catalyst. The cold reactions were completed in scintillation vials a beaker condenser filled with cold water. The warm reactions were completed in a scintillation vial with glass wool and a heating mantle. The room temperature reactions were completed at room temperature inside a scintillation vial Temperature was monitored throughout the reaction with an *in situ* thermometer. Aliquots (200  $\mu$ L) were removed with a 2 mL plastic syringe, the solid catalyst was filtered out using a 0.22  $\mu$ m Millipore syringe filter, and the resulting filtrate

was analyzed by gas chromatography with mass spectrometric detection using a ZB-5 (length 30 m, i.d. 0.25 mm) column.

#### 4.2.5 Hammett Plot catalytic experiments

Reaction conditions were identical to those used for oxidation of *cis*-cyclooctene, except various para-substituted styrenes were used in its place.

### 4.3 Results and Discussion

In Chapter 2 will be found the description of the synthesis and characterization of the immobilized VO(dtpa) complex used in the studies reported here. Briefly, mesoporous silica nanoparticles with diameters of 1-2  $\mu\text{m}$  were prepared and calcined. Separately, dtpa was reacted with 3-aminopropyltriethoxysilane using standard peptide bond-forming techniques, and the dtpa-silane was grafted onto the silica nanoparticles, confirmed using solid-state NMR spectroscopy. Exposure of the grafted solid to VO(SO<sub>4</sub>) produced the immobilized VO(dtpa) catalyst. Solid-state EPR spectroscopy, combined with ongoing computational modeling, indicated that the vanadium was in a distorted five-coordinate environment. N<sub>2</sub> physisorption of the nanoparticles used for these experiments showed that the pore diameter was 52 Å, the surface area was 506 m<sup>2</sup>/g, and the pore volume was 0.640 cm<sup>3</sup>/g, indicating a highly porous material.

The oxidation of alkenes has been extensively studied, but one area that is still a challenge is large cyclic alkenes.<sup>33</sup> Titanium Silicalite-1 (TS-1), which is industrially used to oxidize propylene with H<sub>2</sub>O<sub>2</sub> as an oxidant, consists of pores with a 5 Å diameter,<sup>34</sup> which are too small to allow for the diffusion of large cyclic alkenes such as *cis*-cyclooctene.<sup>34,33</sup> As a result, the only available sites for catalysis on TS-1 for large cyclic

alkenes are the outer surface. *cis*-Cyclooctene was chosen to illustrate the versatility of VO(dtpa)-APMS. In contrast to TS-1, VO(dtpa)-APMS has 52 Å pore diameters, which allows for the diffusion of much bulkier alkenes.

Our earlier catalytic studies using immobilized VO(dtpa) involved sulfide oxidation. In those studies, the oxidant, peroxyacid, was generated *in situ* through the oxidation of an aldehyde with O<sub>2</sub>. The solvent in those studies was methoxyperfluorobutane (3M™ Novec™ 7100 Engineered Fluid or HFE-7100), which was selected for its ability to solubilize O<sub>2</sub> effectively but also because one goal of those studies was decontamination of sulfides from polymers or other materials, and HFE-7100 is ideal in cleaning and degreasing applications. Here, we initially tested a range of solvents including HFE-7100, which were selected based on literature precedents and the ability to solubilize *cis*-cyclooctene.<sup>10,35,36</sup> For these tests, propionaldehyde was added to a solution containing *cis*-cyclooctene, and the amount of *cis*-cyclooctene remaining after 4 hours was determined using GC-MS. Oxidation of *cis*-cyclooctene to cyclooctene oxide took place at a reasonable rate in acetonitrile, chloroform, dichloromethane, acetone, and HFE-7100. Of these solvents, the reaction was fastest in acetonitrile, with only 41% of the *cis*-cyclooctene remaining after 4 hours. This is consistent with the literature results. For this reason, acetonitrile was used in our subsequent catalytic tests.

#### **4.3.1 Investigation of reaction mechanism using *cis*-cyclooctene**

To abstract thermodynamic parameters for the alkene oxidation reaction, the reaction was repeated at a variety of temperatures. First order kinetics were observed, allowing us to identify the first order rate constant *k*. An Eyring plot, based on the

relationship below, was then prepared (**Equation 4.1, Figure 4.1**).

$$\ln\left(\frac{k}{T}\right) = \frac{-\Delta H^\ddagger}{RT} + \ln\left(\frac{k'}{h}\right) + \frac{\Delta S^\ddagger}{R} \quad (4.1)$$

In this equation,  $k$  = the first order rate constant,  $T$  = temperature,  $\Delta H^\ddagger$  = enthalpy of activation,  $\Delta S^\ddagger$  = entropy of activation,  $R$  = the gas constant,  $k'$  = the Boltzman constant, and  $h$  = Planck's constant. On a plot of  $\ln(k/T)$  vs.  $1/T$ , the slope is equal to  $-\Delta H^\ddagger/R$  and  $y$  intercept is equal to  $\ln(k'/h) + \Delta S^\ddagger/R$ . Using the Eyring plot,  $\Delta H^\ddagger$  and  $\Delta S^\ddagger$  were found to be 43.24 kJ/mol and -0.5545 kJ/mol, respectively. A large negative entropy of activation is usually an indication of an associative mechanism.<sup>37-39</sup> A positive enthalpy of activation indicates the bond strengths of the activated complex are lower than the starting material.<sup>37</sup> Interestingly, the values of  $\Delta H^\ddagger$  and  $\Delta S^\ddagger$  were similar to that of the sulfide oxidation reaction, indicating that the activation energies and mechanisms for both reactions were similar. This is likely due at least in part to the use of the same *in situ* peroxyacid oxidant.

The influence of electronic effects on the mechanism were studied by performing the reaction with a variety of para-substituted styrenes as model compounds: styrene, 4-methylstyrene, 4-fluorostyrene, and 4-methoxystyrene. The first order rate constant  $k$  was again used in a Hammett plot, which is based on the following relationship (**Equation 4.2**):

$$\log\left(\frac{k_x}{k_H}\right) = \rho\sigma_x \quad (4.2)$$

where  $k_x$  = the rate constant of the specific styrene being reacted,  $k_H$  = the rate constant of styrene,  $\sigma_p$  = the Hammett parameter for para substituents, obtained from literature,<sup>40</sup> and  $\rho$  = the reaction constant or the sensitivity constant.<sup>37</sup> Plotting  $\log(k_x/k_H)$  vs.  $\sigma_p$  gives a line with a slope of  $\rho$ . The sign and magnitude of  $\rho$  provide an indication of the influence of electronic effects on the reaction mechanism. For this reaction, the small value of  $\rho$  (0.645)

indicates that the system is not very sensitive to electronic effects. Similar values of  $\rho$  have been obtained in other related catalytic systems for alkene oxidation. For example,  $\rho = -0.67$  for a  $\text{Mn}^{2+}$  complex ( $\text{Mn}(\text{CF}_3\text{SO}_3)_2(\text{H,MePyTACN})$ ) where  $\text{H,MePyTACN} = 1$ -(2-pyridylmethyl)-4,7-dimethyl-1,4,7-triazacyclononane) using peracetic acid as the oxidant,<sup>41</sup>  $\rho = -0.99$  for a porphyrin oxo  $\text{Mn}^{4+}$  complex with  $\text{O}_2$  as the oxidant;<sup>42</sup> and  $\rho = -0.92$  for the diperoxorhenium complex  $\text{CH}_3\text{Re}(\text{O})(\eta^2\text{-O}_2)_2(\text{H}_2\text{O})$  with  $\text{H}_2\text{O}_2$  as the oxidant.<sup>43</sup> On the other hand, the positive sign of  $\rho$  in our case is distinct from these systems, and can indicate a small negative charge in the transition state. While alkene oxidation reactions have a positive charge in the transition state due to a carbocation,<sup>44</sup> we propose that the negative charge of the transition state is a result of the deprotonation of the peroxyacid occurring at the same time as the alkene oxidation (see below).

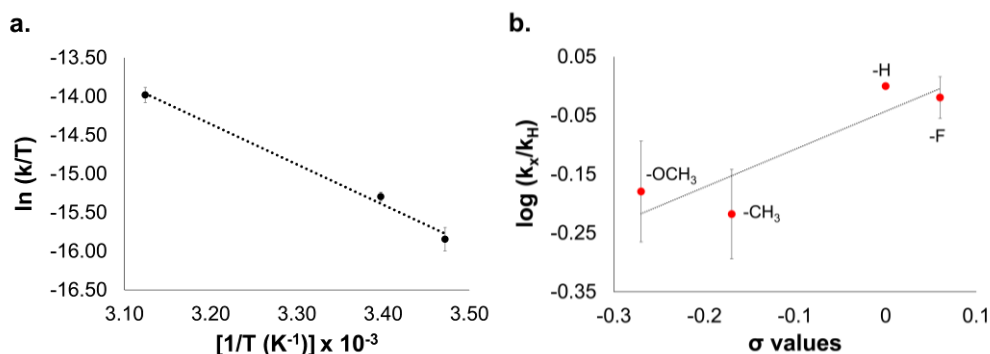


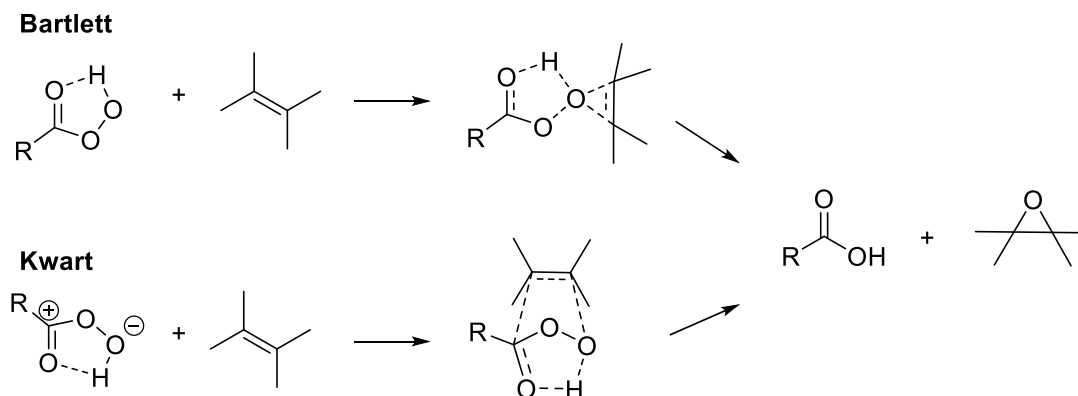
**Figure 4.1.** a. Eyring Plot of *cis*-cyclooctene oxidation using VO(dtpa)-APMS *in situ* generated peroxyacid. b. Hammett Plot for 4-methoxystyrene, p-methylstyrene, 4-fluorostyrene, and styrene.

The formation of the peroxyacid, catalyzed by the VO(dtpa) complex, was described in our previous study. Briefly,  $\text{O}_2$  binds to the complex as dioxygen and then undergoes a reversible redox reaction to form the superoxo  $\eta^1$ -bound  $\text{O}_2$ .<sup>45,46</sup> In the  $\eta^1$

form, the O<sub>2</sub> can abstract a hydrogen from the aldehyde to form an acyl radical,<sup>47</sup> which can in turn react with free O<sub>2</sub> to produce a peroxyacid radical. Reaction of this radical with the complex containing the η<sup>1</sup> OOH ligand regenerates the catalyst and produces the peroxyacid.

The peroxyacid formed in this manner can then react with an alkene in a process that is also catalyzed by the VO(dtpa) complex. Although the mechanism of catalytic alkene oxidation with peroxyacids has not been studied previously in detail, three reaction pathways have been proposed for transition metal catalyzed alkene oxidation using H<sub>2</sub>O<sub>2</sub>. These are an inner sphere mechanism proposed by Mimoun,<sup>39,48</sup> an outer sphere mechanism proposed by Sharpless,<sup>39,49</sup> and a biradical mechanism proposed by Sams and Jørgensen.<sup>50</sup> The last mechanism is unlikely due to recent computational studies on V(salan) (salan = [V<sup>4+</sup>(=O)(L)(H<sub>2</sub>O)]( L = (CH<sub>2</sub>NHCH<sub>2</sub>CH=CHO<sup>-</sup>)<sub>2</sub>) complexes which showed that the energies of the transition states in the biradical mechanism were higher than in the Sharpless mechanism.<sup>51</sup> In the inner sphere mechanism, the alkene coordinates to the metal and a 5-membered cyclic transition state with the peroxide is formed, while in the outer sphere mechanism, the alkene directly reacts with the peroxide to form a 3-membered transition state. Density Functional Theory (DFT) calculations using related vanadium catalysts, such as VO(acac)<sub>2</sub>, have shown that the outer sphere mechanism is most likely because the 3-membered structure has a lower energy.<sup>51,52</sup> This is also consistent with our conclusions using the immobilized VO(dtpa) complex in sulfide oxidations. For these reasons, we propose that the Sharpless mechanism is operating here.<sup>53,54</sup>

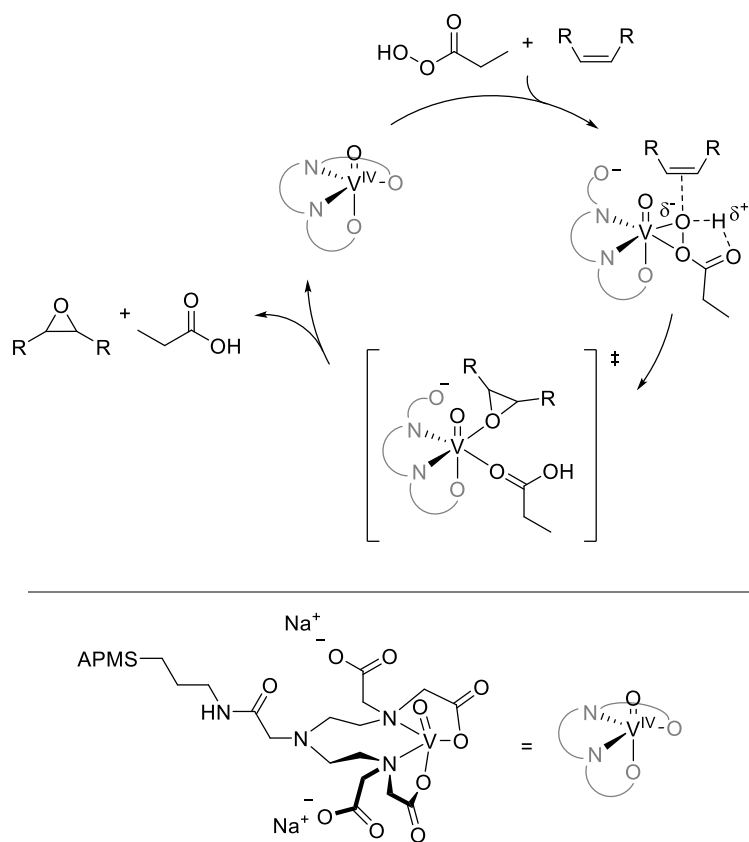
Because peroxyacids are more electrophilic than  $\text{H}_2\text{O}_2$  or  $\eta^2\text{-O}_2$  ligands, results from previous experiments must be applied cautiously to our results.<sup>55</sup> Additional insight can be gained from reactions of peroxyacids with alkenes in the absence of transition metal catalysts. For these reactions, two mechanisms have been proposed (**Scheme 4.1**). First, Bartlett proposed a butterfly mechanism that includes a direct interaction between the peroxyacid and the alkene, leading to a 3-membered ring in the intermediate.<sup>56</sup> This is similar to the Sharpless mechanism for the metal-catalyzed reaction of alkenes and peroxides. In the second peroxyacid mechanism, Kwart proposed the formation of a zwitterionic peroxyacid, which reacts with the alkene through the carbonyl carbon and the terminal oxygen of the peroxyacid, resulting in a unique 5-membered intermediate.<sup>57</sup> Computational studies,<sup>58</sup> including *ab initio* calculations,<sup>59</sup> using peroxyformic acid and ethylene led to the conclusion that Bartlett's mechanism is more probable.



**Scheme 4.1.** Bartlett and Kwart pathways for the oxidation of an alkene by a peroxyacid.

This background leads to the proposal that in our experiments, the mechanism includes the direct interaction between a vanadium-bound peroxyacid and an alkene,

leading to a 3-membered ring in the catalytic intermediate. Additional support for this conclusion comes from a study using alkene substrates with various sizes (see **Table 4.1** below); the lack of a rate dependence on steric effects indicates that the alkene does not coordinate with the metal center but instead directly reacts with the oxidant. An additional mechanistic insight comes from the positive value of the Hammett parameter  $\rho$ , indicating a negatively charged transition state. This is an indication that the peroxyacid is being deprotonated while it reacts with the alkene. A summary of the proposed mechanism is shown in **Scheme 4.2**.



**Scheme 4.2.** Proposed mechanism for the oxidation of alkenes using VO(dtpa)-APMS as the catalyst and peroxyacid as the oxidant. VO(dtpa)-APMS drawn as suggested by DFT data.

### 4.3.2 Exploration of the reaction scope using other cyclic alkenes

Part of the usefulness of mounting transition metal catalysts within a porous substrate is the potential for size selectivity among similar substrates.<sup>60</sup> Consequently, we chose several relatively bulky cyclic alkene substrates for comparison in our system: cyclohexene, *cis*-cyclooctene, cyclododecene, 1,2-dihydronaphthalene, and indene. Obviously, one additional consideration was solubility in acetonitrile, which somewhat limited our selection of substrates. All substrates showed at least some reactivity. The three non-aromatic substrates all resulted in the epoxide as the major product (**Table 4.2**), while the other two substrates resulted in a more complicated set of oxidized products. Because *cis*-cyclooctene was specifically used as the substrate for the mechanistic studies, the epoxide was the only product of the oxidation reaction. At room temperature, 35% of the initial concentration of *cis*-cyclooctene remained after 4 hours; at 47 °C, 14 % of the initial concentration remained after 2 hours. On the other hand, a mixture of *cis* and *trans* isomers of cyclododecene was used as a substrate, as determined by GC-MS. Similar to *cis*-cyclooctene, the epoxide was the only product. Based on peak areas, it was evident that one isomer oxidized much faster than the other; based on steric consideration and on literature,<sup>61</sup> it is probably that the *cis*-cyclododecene oxidized faster than the *trans* form. As expected based on its size, this substrate reacted more slowly than *cis*-cyclooctene. The difference in rate can be partly attributed to diffusion into the pores of the catalyst. The two slowest and most rigid cyclic alkenes, indene and 1,2-dihydronaphthalene are also the largest molecules at approximately 4.2 Å and 5 Å in diameter. Cyclododecene, 5.3 Å, is of a similar size but is much more flexible than the rigid fused aromatic rings. The pore

diameter of VO(dpta)-APMS is 52 Å and therefore should easily be able to catalyze the substrates both in and outside of the pores.

**Table 4.1.** Comparison of Reaction Rates for the Oxidation of Various Cycloalkenes.

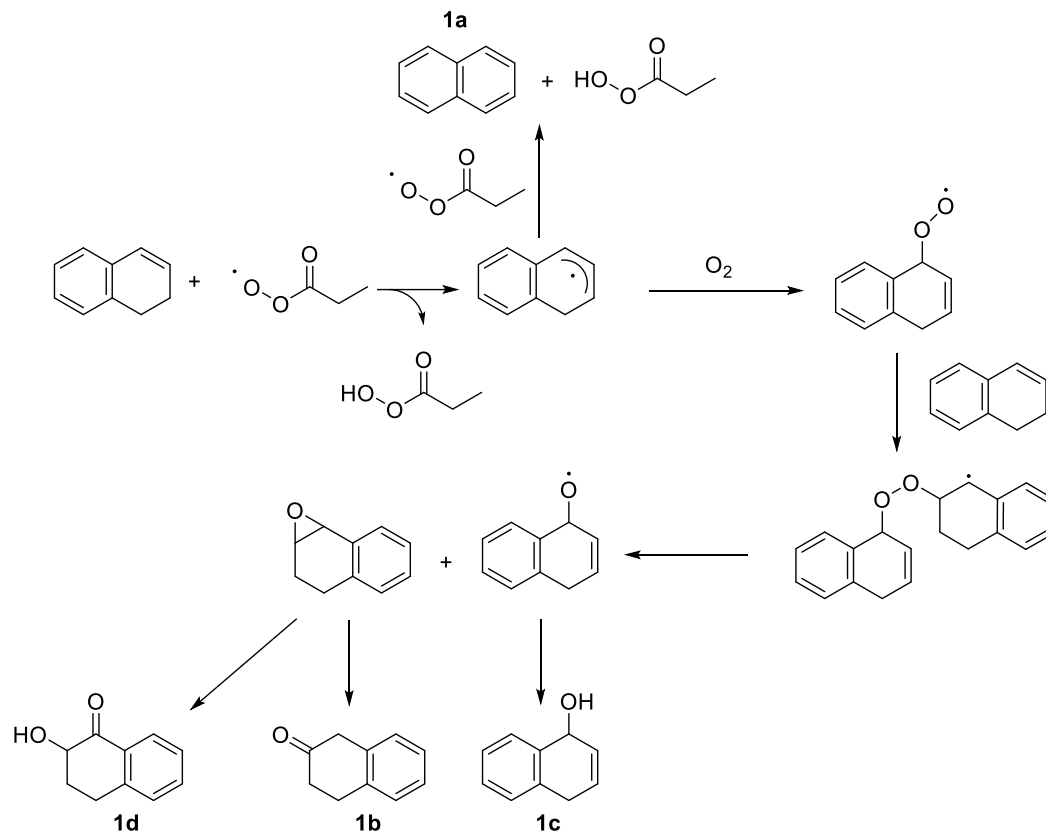
Substrate	Rate (μmol/hr) <sup>a</sup>	Concentration Remaining <sup>b</sup> (%)	Major Product <sup>b</sup>
Cyclohexene	9.9 ± 1	53	Cyclohexene oxide
<i>cis</i> -Cyclooctene	9.4 ± 1	35	Cyclooctene oxide
Cyclododecene <sup>c</sup>	8.4 ± 0.9	40	1,2-Epoxycyclododecane
1,2-Dihydronaphthalene	4.19 ± 0.5	73	2-Tetralone & 1,4-Dihydronaphthalenol
Indene	4.73 ± 0.2	74	2-Indanone

<sup>a</sup>Cyclohexene rate calculated at 2 h; all others at 4 h. <sup>b</sup>After 4 h for all substrates. <sup>c</sup>Racemic mixture

The major product (78%) of the cyclohexene oxidation is cyclohexene oxide, but 2-cyclohexenone was also observed as a minor product. This is likely the result of an allylic oxidation, which is a known reaction of cyclohexene with dioxygen radicals.<sup>62,63</sup> The two possible reaction pathways of alkenes with peroxyacid radicals are proton abstraction or addition; the major pathway is determined by the structure of the alkene.<sup>64</sup> At 70 °C, cyclohexene has been shown to favor abstraction by a ratio of 19:1. In our system, peroxyacid radicals are present, as was demonstrated in our previous work by radical trapping. Here, abstraction occurs on the allylic carbon, which then reacts with another equivalent of peroxyacid radical to form a transient organic peroxyacyl species, ultimately producing 2-cyclohexenone and the carboxylic acid as products.

With more complicated cyclic alkenes, a larger range of reaction pathways exist, and a variety of reaction products were identified (**Figure 4.2**). As with cyclohexene, these products are the result of either abstraction or addition. In the reaction of 1,2-dihydronaphthalene, two major products were observed after 4 hours: the oxidized

products 42% 2-tetralone (**1b**) and 44% 1,4-dihydronaphthalenol (**1c**). 2-Hydroxy-1-tetralone (**1d**) was observed as a minor product (14%) and after 24 hours, the hydrogen abstraction product naphthalene (**1a**) was observed. 2-tetralone is a ring-opening product of the corresponding epoxide.<sup>65</sup> This reaction pattern is similar to what has been previously reported for the oxidation of indene and 1,2-dihydronaphthalene with Mn-substituted polyoxotungstates using H<sub>2</sub>O<sub>2</sub> as the oxidant.<sup>66</sup> Martan explored the oxidation of dihydronaphthalenes with molecular O<sub>2</sub> and found that hydrogen abstraction to form the dihydronaphthalene radical was the key step to further reactivity.<sup>65</sup> That radical could react in one of two ways. First, a second hydrogen abstraction could take place to form naphthalene. Alternatively, reaction with molecular oxygen could lead to the formation of a peroxy-bridged dihydronaphthalene radical, which could decompose to form the epoxide and an oxygen radical species. Protonation of the latter compound would lead to compound **1c**, while ring-opening of the epoxide would lead to compounds **1b** and **1d**. With this in mind, a possible set of pathways for the formation of these products is shown in **Scheme 3**. Although **1d** and **1b** can be produced through this radical pathway, based on the product distribution, it is likely that the epoxide product from which they are produced is made from participating in the catalytic cycle proposed for *cis*-cyclooctene (**Scheme 4.2**) and only **1c**, a minor product, is formed from this radical pathway. After the epoxide product is formed, the product **1d** is a result of further oxidation after ring-opening by a peroxyacid radical species, but not as a result of the pathway described in **Scheme 4.2**.



**Scheme 4.5.** Possible pathways for the reaction of 1,2- dihydronaphthalene with peroxyacid radicals.

Indene is known to autoxidize with molecular oxygen to result in the abstraction of the allylic hydrogen.<sup>64</sup> When adding another carbon into the ring of indene, 1,2-dihydronaphthalene, that abstraction of the allylic hydrogen can result in the formation of naphthalene.<sup>66</sup>

When indene was the substrate, three products were observed. The major products 2-indanone (54%) and 2-hydroxy-1-indanone (34%), are products from the ring-opening of indene epoxide. A minor product, (11%) 1-propionylindane is the result of a hydrogen abstraction from indene followed by reaction with an acyl radical. As the major products are derived from epoxides, they are most likely reacting in the same mechanism as *cis*-

cyclooctene (**Scheme 4.2**) while the minor side product is a result of a radical pathway. The ring-opening epoxide products found in the aromatic cyclic alkenes, not found in the non-aromatic cyclic alkenes, are due to their ability to stabilize carbocations that form upon the ring opening of the epoxide.<sup>67</sup>

#### 4.4 Conclusion

In this work, the mechanism for the oxidation of alkenes using the peroxyacid generated *in situ* was investigated. *cis*-Cyclooctene was chosen as a model alkene to illustrate the ability of VO(dtpa)-APMS to catalyze bulky substituents. The catalytic system can function in a variety of solvents, with optimal rates and epoxide production in acetonitrile at room temperature.

Kinetic experiments with varied temperatures demonstrated that the rate of alkene oxidation was proportional to heat and that the reaction entropy remains relatively the same as it was for the oxidation of sulfides while the enthalpy is similar to the colder kinetic data points of the oxidation of sulfides. Kinetic experiments with varied para-substituted styrenes indicated a negative charge in the transition state and that the reaction was not very susceptible to electronic effects.

In the end, a plausible mechanism for the oxidation of cycloalkenes with VO(dtpa)-APMS was proposed. The reaction proceeds through two cycles. The catalyst first initiates the autoxidation of the propionaldehyde to form *in situ* peroxyacids. The peroxyacid then coordinates with the vanadium at which point the cycloalkene reacts through an outer sphere mechanism while the peroxyacid is being deprotonated. The cycloalkene does not coordinate to the vanadium. In the main reaction, there are two products are formed:

cycloalkene oxide and propionic acid. When introducing fused aromatic cycloalkenes into the system, the radical peroxyacids in the system produce additional side products beyond the epoxide.

#### 4.5 References

1. da Silva, J. A. L.; da Silva, J. J. R. F.; Pombeiro, A. J. L. Oxovanadium complexes in catalytic oxidations. *Coord. Chem. Rev.* **2011**, *255*, 2232-2248.
2. Butler, A.; Clague, M. J.; Meister, G. E. Vanadium Peroxide Complexes. *Chem. Rev.* **1994**, *94*, 625-638.
3. Conte, V.; Coletti, A.; Floris, B.; Licini, G.; Zonta, C. Mechanistic aspects of vanadium catalysed oxidations with peroxides. *Coord. Chem. Rev.* **2011**, *255*, 2165-2177.
4. Joergensen, K. A. Transition-metal-catalyzed epoxidations. *Chem. Rev.* **1989**, *89*, 431-458.
5. Matsuo, J.-i.; Takeuchi, K.; Ishibashi, H. Stereocontrolled Formal Synthesis of ( $\pm$ )-Platensimycin. *Org. Lett.* **2008**, *10*, 4049-4052.
6. Selvaraj, M.; Song, S. W.; Kawi, S. Epoxidation of styrene over mesoporous Zr-Mn-MCM-41. *Microporous Mesoporous Mater.* **2008**, *110*, 472-479.
7. Carlin, D. A.; Bertolani, S. J.; Siegel, J. B. Biocatalytic conversion of ethylene to ethylene oxide using an engineered toluene monooxygenase. *Chem. Commun.* **2015**, *51*, 2283-2285.
8. Maurya, M. R.; Kumar, A.; Costa Pessoa, J. Vanadium complexes immobilized on solid supports and their use as catalysts for oxidation and functionalization of alkanes and alkenes. *Coord. Chem. Rev.* **2011**, *255*, 2315-2344.

9. Kosslick, H.; Mönnich, I.; Paetzold, E.; Fuhrmann, H.; Fricke, R.; Müller, D.; Oehme, G. Suzuki reaction over palladium-complex loaded MCM-41 catalysts. *Microporous Mesoporous Mater.* **2001**, *44-45*, 537-545.
10. Bhunia, S.; Koner, S. Functionalization of oxo-vanadium(IV) acetylacetonate over modified MCM-41: an efficient reusable catalyst for epoxidation reaction. *J. Porous Mater.* **2011**, *18*, 399-407.
11. Modi, C. K.; Vithalani, R. S.; Patel, D. S.; Som, N. N.; Jha, P. K. Zeolite-Y entrapped metallo-pyrazolone complexes as heterogeneous catalysts: Synthesis, catalytic aptitude and computational investigation. *Microporous Mesoporous Mater.* **2018**, *261*, 275-285.
12. Mirzaee, M.; Bahramian, B.; Gholizadeh, J.; Feizi, A.; Gholami, R. Acetylacetonate complexes of vanadium and molybdenum supported on functionalized boehmite nano-particles for the catalytic epoxidation of alkenes. *Chem. Eng. J.* **2017**, *308*, 160-168.
13. Salavati-Niasari, M.; Badieli, A.; Saberyan, K. Oxovanadium(IV) salophen complex covalently anchored to multi-wall carbon nanotubes (MWNTs) as heterogeneous catalyst for oxidation of cyclooctene. *Chem. Eng. J.* **2011**, *173*, 651-658.
14. Dorbes, S.; Pereira, C.; Andrade, M.; Barros, D.; Pereira, A. M.; Rebelo, S. L. H.; Araújo, J. P.; Pires, J.; Carvalho, A. P.; Freire, C. Oxidovanadium(IV) acetylacetonate immobilized onto CMK-3 for heterogeneous epoxidation of geraniol. *Microporous Mesoporous Mater.* **2012**, *160*, 67-74.
15. Hamidipour, L.; Farzaneh, F. Immobilized VOsalpr on modified Fe<sub>3</sub>O<sub>4</sub> nanoparticles as a magnetically separable epoxidation catalyst. *C. R. Chim.* **2014**, *17*, 927-933.
16. Hsiao, M.-C.; Liu, S.-T. Polymer Supported Vanadium Complexes as Catalysts for the Oxidation of Alkenes in Water. *Catal. Lett.* **2010**, *139*, 61-66.
17. Monfared, H. H.; Abbasi, V.; Rezaei, A.; Ghorbanloo, M.; Aghaei, A. A heterogenized vanadium oxo-aryylhydrazone catalyst for efficient and selective oxidation of hydrocarbons with hydrogen peroxide. *Transition Met. Chem.* **2012**, *37*, 85-92.

18. Parida, K. M.; Singha, S.; Sahoo, P. C. A facile method for promoting activities of vanadium–schiffbase complex anchored on organically modified MCM-41 in epoxidation reaction. *J. Mol. Catal. A: Chem.* **2010**, *325*, 40-47.
19. Kalilur Rahiman, A.; Shanmuga Bharathi, K.; Sreedaran, S.; Rajesh, K.; Narayanan, V. Cationic vanadyl porphyrin-encapsulated mesoporous Al/V-MCM-41 as heterogeneous catalysts for the oxidation of alkenes. *Inorg. Chim. Acta* **2009**, *362*, 1810-1818.
20. Kala Raj, N. K.; Deshpande, S. S.; Ingle, R. H.; Raja, T.; Manikandan, P. Heterogenized Molybdovanadophosphoric Acid on Amine-Functionalized SBA-15 for Selective Oxidation of Alkenes. *Catal. Lett.* **2004**, *98*, 217-224.
21. Jurado, M. J.; Gracia, M. D.; Campelo, J. M.; Luque, R.; Marinas, J. M.; Romero, A. A. Selective epoxidation of alkenes using highly active V-SBA-15 materials: microwave vs. conventional heating. *J. Mater. Chem.* **2009**, *19*, 8603-8609.
22. Amano, F.; Yamaguchi, T.; Tanaka, T. Photocatalytic Oxidation of Propylene with Molecular Oxygen over Highly Dispersed Titanium, Vanadium, and Chromium Oxides on Silica. *J. Phys. Chem. B* **2006**, *110*, 281-288.
23. Thornburg, N. E.; Thompson, A. B.; Notestein, J. M. Periodic Trends in Highly Dispersed Groups IV and V Supported Metal Oxide Catalysts for Alkene Epoxidation with H<sub>2</sub>O<sub>2</sub>. *ACS Catal.* **2015**, *5*, 5077-5088.
24. D. Oldroyd, R.; Sankar, G.; Meurig Thomas, J.; Hunnius, M.; F. Maier, W. Creation, characterisation and performance of vanadyl active sites in microporous and mesoporous silica-based catalysts for the selective oxidation of hydrocarbons. *J. Chem. Soc., Faraday Trans.* **1998**, *94*, 3177-3182.
25. Takehira, K.; Hayakawa, T.; Ishikawa, T. Heterogeneous Catalysis in the Liquid-phase Oxidation of Olefins. IV. The Activity of a Supported Vanadium or Chromium Oxide Catalyst in the Decomposition of t-Butyl Hydroperoxide. *Bull. Chem. Soc. Jpn.* **1980**, *53*, 2103-2110.
26. Katsuomi, T.; Takashi, H.; Toshio, I. Heterogeneous Catalysis in the Liquid-phase Oxidation of Olefins. III. Activity of Supported Vanadium–Chromium Binary Oxide Catalyst for the Oxidation of Cyclohexene. *Bull. Chem. Soc. Jpn.* **1979**, *52*, 697-705.

27. Kasai, J.; Nakagawa, Y.; Uchida, S.; Yamaguchi, K.; Mizuno, N. [ $\gamma$ -1,2- $\text{H}_2\text{SiV}_2\text{W}_{10}\text{O}_{40}$ ] Immobilized on Surface-Modified  $\text{SiO}_2$  as a Heterogeneous Catalyst for Liquid-Phase Oxidation with  $\text{H}_2\text{O}_2$ . *Chem. - Eur. J.* **2006**, *12*, 4176-4184.
28. Tangestaninejad, S.; Mirkhani, V.; Moghadam, M.; Mohammadpoor-Baltork, I.; Shams, E.; Salavati, H. Hydrocarbon oxidation catalyzed by vanadium polyoxometalate supported on mesoporous MCM-41 under ultrasonic irradiation. *Ultrason. Sonochem.* **2008**, *15*, 438-447.
29. Salavati, H.; Teimouri, A. Efficient Epoxidation of Alkenes with Hydrogen Peroxide and Electrochemical Behavior in Water Over Heteropolymolybdate/Silica Nanocomposite. *Int. J. Electrochem. Sci.* **2017**, *12*, 7829-7843.
30. Kala Raj, N. K.; Deshpande, S. S.; Ingle, R. H.; Raja, T.; Manikandan, P., Immobilized molybdovanadophosphoric acids on SBA-15 for selective oxidation of alkenes. In *Studies in Surface Science and Catalysis*, Sayari, A.; Jaroniec, M., Eds. Elsevier: 2005; Vol. 156, pp 769-778.
31. Farzaneh, F.; Sadeghi, Y. Immobilized V-MIL-101 on modified  $\text{Fe}_3\text{O}_4$  nanoparticles as heterogeneous catalyst for epoxidation of allyl alcohols and alkenes. *J. Mol. Catal. A: Chem.* **2015**, *398*, 275-281.
32. Serre, C.; Millange, F.; Thouvenot, C.; Noguès, M.; Marsolier, G.; Louër, D.; Férey, G. Very Large Breathing Effect in the First Nanoporous Chromium(III)-Based Solids: MIL-53 or  $\text{Cr}^{\text{III}}(\text{OH}) \cdot \{\text{O}_2\text{C}-\text{C}_6\text{H}_4-\text{CO}_2\} \cdot \{\text{HO}_2\text{C}-\text{C}_6\text{H}_4-\text{CO}_2\text{H}\}_x \cdot \text{H}_2\text{O}_y$ . *J. Am. Chem. Soc.* **2002**, *124*, 13519-13526.
33. Zhao, Y.; Zhou, D.; Zhang, T.; Yang, Y.; Zhan, K.; Liu, X.; Min, H.; Lu, X.; Nie, R.; Xia, Q. High-Rota Synthesis of Single-/Double-/Multi-Unit-Cell Ti-HSZ Nanosheets To Catalyze Epoxidation of Large Cycloalkenes Efficiently. *ACS Appl. Mater. Interfaces* **2018**, *10*, 6390-6397.
34. Clerici, M. G. The activity of titanium silicalite-1 (TS-1): Some considerations on its origin. *Kinet. Catal.* **2015**, *56*, 450-455.

35. Neumann, R.; Levin-Elad, M. Vanadium silicate xerogels in hydrogen peroxide catalyzed oxidations. *Appl. Catal. A* **1995**, *122*, 85-97.
36. Rayati, S.; Koliaei, M.; Ashouri, F.; Mohebbi, S.; Wojtczak, A.; Kozakiewicz, A. Oxovanadium(IV) Schiff base complexes derived from 2,2'-dimethylpropanediamine: A homogeneous catalyst for cyclooctene and styrene oxidation. *Appl. Catal. A* **2008**, *346*, 65-71.
37. Anslyn, E. V.; Dougherty, D. A., *Modern Physical Organic Chemistry*. 1st ed.; University Science Books: Sausalito, California, 2006.
38. Housecroft, C. E.; Sharpe, A. G., *Inorganic Chemistry*. 2nd ed.; Pearson Education Limited: Harlow, England, 2005; p 765-766.
39. Nunes, C. D.; Vaz, P. D.; Felix, V.; Veiros, L. F.; Moniz, T.; Rangel, M.; Realista, S.; Mourato, A. C.; Calhorda, M. J. Vanadyl cationic complexes as catalysts in olefin oxidation. *Dalton Trans.* **2015**, *44*, 5125-5138.
40. Hansch, C.; Leo, A.; Taft, R. W. A survey of Hammett substituent constants and resonance and field parameters. *Chem. Rev.* **1991**, *91*, 165-195.
41. Garcia-Bosch, I.; Company, A.; Fontrodona, X.; Ribas, X.; Costas, M. Efficient and Selective Peracetic Acid Epoxidation Catalyzed by a Robust Manganese Catalyst. *Org. Lett.* **2008**, *10*, 2095-2098.
42. Arasasingham, R. D.; He, G. X.; Bruice, T. C. Mechanism of manganese porphyrin-catalyzed oxidation of alkenes. Role of manganese(IV)-oxo species. *J. Am. Chem. Soc.* **1993**, *115*, 7985-7991.
43. Al-Ajlouni, A. M.; Espenson, J. H. Kinetics and Mechanism of the Epoxidation of Alkyl-Substituted Alkenes by Hydrogen Peroxide, Catalyzed by Methylrhodium Trioxide. *J. Org. Chem.* **1996**, *61*, 3969-3976.
44. Al-Ajlouni, A. M.; Sağlam, Ö.; Diafla, T.; Kühn, F. E. Kinetic studies on phenylphosphopolyperoxotungstates catalyzed epoxidation of olefins with hydrogen peroxide. *J. Mol. Catal. A: Chem.* **2008**, *287*, 159-164.

45. Tyagi, S.; Cook, C. D.; DiDonato, D. A.; Key, J. A.; McKillican, B. P.; Eberle, W. J.; Carlin, T. J.; Hunt, D. A.; Marshall, S. J.; Bow, N. L. Bioinspired Synthesis of a Sedaxane Metabolite Using Catalytic Vanadyl Acetylacetonate and Molecular Oxygen. *J. Org. Chem.* **2015**, *80*, 11941-11947.
46. Zhang, J.; Yang, H.; Sun, T.; Chen, Z.; Yin, G. Nonredox Metal-Ions-Enhanced Dioxygen Activation by Oxidovanadium(IV) Complexes toward Hydrogen Atom Abstraction. *Inorg. Chem.* **2017**, *56*, 834-844.
47. Kelm, H.; Krüger, H.-J. A Superoxovanadium(V) Complex Linking the Peroxide and Dioxygen Chemistry of Vanadium. *Angew. Chem. Int. Ed.* **2001**, *40*, 2344-2348.
48. Mimoun, H.; Sere de Roch, I.; Sajus, L. Epoxydation des olefines par les complexes peroxydiques covalents du molybdene—VI. *Tetrahedron* **1970**, *26*, 37-50.
49. Sharpless, K. B.; Townsend, J. M.; Williams, D. R. Mechanism of epoxidation of olefins by covalent peroxides of molybdenum(VI). *J. Am. Chem. Soc.* **1972**, *94*, 295-296.
50. Sams, C. K.; Jorgensen, K. A. Mechanistic Aspects of Vanadium-Catalysed Oxygen Transfer Reactions. *Acta Chem. Scand.* **1995**, *49*, 839-839.
51. Kuznetsov, M. L.; Pessoa, J. C. Epoxidation of olefins catalysed by vanadium–salan complexes: a theoretical mechanistic study. *Dalton Trans.* **2009**, 5460-5468.
52. Vandichel, M.; Leus, K.; Van Der Voort, P.; Waroquier, M.; Van Speybroeck, V. Mechanistic insight into the cyclohexene epoxidation with VO(acac)<sub>2</sub> and tert-butyl hydroperoxide. *J. Catal.* **2012**, *294*, 1-18.
53. Adão, P.; Costa Pessoa, J.; Henriques, R. T.; Kuznetsov, M. L.; Avecilla, F.; Maurya, M. R.; Kumar, U.; Correia, I. Synthesis, Characterization, and Application of Vanadium–Salan Complexes in Oxygen Transfer Reactions. *Inorg. Chem.* **2009**, *48*, 3542-3561.

54. Bühl, M.; Schurhammer, R.; Imhof, P. Peroxovanadate Imidazole Complexes as Catalysts for Olefin Epoxidation: Density Functional Study of Dynamics,  $^{51}\text{V}$  NMR Chemical Shifts, and Mechanism. *J. Am. Chem. Soc.* **2004**, *126*, 3310-3320.
55. Macchi, P.; Schultz, A. J.; Larsen, F. K.; Iversen, B. B. Experimental and Theoretical Electron Density Study of the Peroxo Function in Oxoperoxo(pyridine-2,6-dicarboxylato)(hexamethylphosphoramide)molybdenum(VI): Implications for Olefin Epoxidation by Peroxo Transition Metal Complexes. *J. Phys. Chem. A* **2001**, *105*, 9231-9242.
56. Mimoun, H. Oxygen Transfer from Inorganic and Organic Peroxides to Organic Substrates: A Common Mechanism? *Angew. Chem. Int. Ed. Engl.* **1982**, *21*, 734-750.
57. Kwart, H.; Hoffman, D. M. Observations Regarding the Mechanism of Olefin Epoxidation with Per Acids. *J. Org. Chem.* **1966**, *31*, 419-425.
58. Ottenbacher, R. V.; Samsonenko, D. G.; Talsi, E. P.; Bryliakov, K. P. Enantioselective Epoxidations of Olefins with Various Oxidants on Bioinspired Mn Complexes: Evidence for Different Mechanisms and Chiral Additive Amplification. *ACS Catal.* **2016**, *6*, 979-988.
59. Yamabe, S.; Kondou, C.; Minato, T. A Theoretical Study of the Epoxidation of Olefins by Peracids. *J. Org. Chem.* **1996**, *61*, 616-620.
60. Chen, C.; Shen, P.; Wan, M.; Ding, N.; Shi, X.; Wang, X.; Zhang, N. Size-selective epoxidation of olefins in two new metal-organic framework constructed from six-coordinated tetranuclear Cu(II) SBUs. *Microporous Mesoporous Mater.* **2016**, *232*, 167-173.
61. Prasad, M. R.; Madhavi, G.; Rao, A. R.; Kulkarni, S. J.; Raghavan, K. V. Synthesis, characterization of high Ti-containing Ti-MCM-41 catalysts and their activity evaluation in oxidation of cyclohexene and epoxidation of higher olefins. *J. Porous Mater.* **2006**, *13*, 81-94.
62. Fraile, J. M.; García, J. I.; Mayoral, J. A.; Vispe, E. Optimization of cyclohexene epoxidation with dilute hydrogen peroxide and silica-supported titanium catalysts. *Appl. Catal. A* **2003**, *245*, 363-376.

63. Arzoumanian, H.; Blanc, A.; Hartig, U.; Metzger, J. Homogeneous bimetallic catalysis. The selective autoxidation of cyclohexene. *Tetrahedron Lett.* **1974**, *15*, 1011-1014.
64. Sheldon, R. A.; Kochi, J. K., *Metal-Catalyzed Oxidations of Organic Compounds: Mechanistic Principles and Synthetic Methodology Including Biochemical Processes*. Academic Press, Inc: New York, NY, 1981.
65. Martan, M.; Manassen, J.; Vofsi, D. Liquid Phase Oxidation of 1, 4 and 1, 2-Dihydronaphthalene. *Isr. J. Chem.* **1969**, *7*, 751-767.
66. Estrada, A. C.; Simões, M. M. Q.; Santos, I. C. M. S.; Neves, M. G. P. M. S.; Silva, A. M. S.; Cavaleiro, J. A. S.; Cavaleiro, A. M. V. Transition Metal Substituted Polyoxotungstates in the Catalytic Oxidation of 1H-Indene and 1,2-Dihydronaphthalene with Hydrogen Peroxide. *Catal. Lett.* **2009**, *128*, 281-289.
67. Carey, F. A.; Sundberg, R. J., *Advanced Organic Chemistry Part A: Structure and Mechanisms*. 5th ed.; Springer Science+Business Media: New York, NY, 2007; p 511-515.

## CHAPTER 5: CONCLUSIONS

### 5.1 Conclusions

It was recently shown that V-doped acid-prepared mesoporous silica (APMS) nanoparticles are active catalysts for the oxidation of the mustard gas analogue 2-chloroethyl ethyl sulfide (CEES) under ambient conditions in the presence of aldehydes, using O<sub>2</sub> from air as the oxidation source. One problem with this system was that because the vanadium was distributed onto the porous silica support by ion exchange and calcination, under humid conditions or when water was a contaminant, the vanadium would leach from the solid, leading to decreased or no catalytic activity.

In this work, a new catalytic system for sulfide and alkene oxidation has been prepared. The vanadium is immobilized onto mesoporous silica nanoparticles, using diethylenetriamine pentaacetic acid (dtpa) as a ligand and anchoring it to the surface, to investigate its effect on vanadium's ability to perform oxidation reactions. The system uses a VO(dtpa) complex immobilized on a highly porous silica substrate. Physical characterization of the material confirmed that the substrate retained its porosity after modification, and that the vanadium did not leach from the solid, in contrast to samples that did not contain dtpa. Solid-state EPR spectroscopy, combined with ongoing computational modeling, indicated that the vanadium was in a distorted five-coordinate environment. To further understand the catalyst's ability to perform oxidation reactions, the mechanisms, including both the aldehyde oxidation using O<sub>2</sub> and the sulfide/alkene oxidation using the peroxyacid thus generated *in situ*, were studied. Two model substrates were chosen for the investigation: CEES and *cis*-cyclooctene. The sulfide oxidation

occurs through a two-step oxidative process:  $\text{CEES} \rightarrow \text{CEESO} \rightarrow \text{CEESO}_2$ . The formation of sulfone does not occur until after all of the sulfide has been consumed. Sulfoxides are known to be weaker nucleophiles than sulfides. Therefore, it is expected to have a slower rate of oxidation of a sulfoxide to sulfone than that of sulfide to sulfoxide. The catalytic system effectively oxidizes CEES at room temperature in less than 15 minutes and *cis*-cyclooctene at 47 °C within 3 hours, using a peroxyacid generated *in situ* as the oxidant source. Kinetic experiments with varied temperatures demonstrated that the reaction with CEES is dependent on temperature while the reaction with *cis*-cyclooctene produces a rate of oxidation that is directly proportional to temperature. Kinetic experiments on various para-substituted methyl phenyl sulfides and styrenes illustrated that the mechanism has a negatively charged transition state. This data was interpreted as the substrate reacting with an oxygen atom on the peroxyacid with a partial negative charge, due to the concerted reaction of the substrate with the peroxyacid. The confirmation of radical formation in the mechanism was experimentally shown by the appearance of an induction period when diphenylamine, a radical trap, was introduced into the reaction.

The generation of epoxides with the VO(dtpa) complex are the resulting products for non-aromatic cyclic alkenes. When introducing fused aromatic cycloalkenes into the system, the radical peroxyacids in the system produce additional side products beyond the epoxides. These side products are likely not catalyzed by VO(dtpa) and therefore are not in the catalytic cycle.

The catalytic cycles of both the aldehyde oxidation using  $\text{O}_2$  and the

sulfide/alkene oxidation using the peroxyacid generated *in situ* were proposed. To begin, O<sub>2</sub> binds initially to VO(dtpa) as dioxygen and then undergoes a reversible redox reaction to form the superoxo  $\eta^1$ -bound O<sub>2</sub>. The superoxo oxygen can then abstract a hydrogen atom from propionaldehyde to form an acyl radical and vanadium-bound,  $\eta^1$  hydroperoxide. The acyl radical can then react with O<sub>2</sub> directly to form a peroxyacid radical. This in turn forms peroxyacid by reacting either with aldehyde or with the  $\eta^1$  hydroperoxide, feeding either acyl radicals or vanadium peroxyacid radicals back into the catalytic cycle.

The peroxyacid produced in this manner can then react with a sulfide or an alkene in a process also catalyzed by the VO(dtpa) complex. In this step, a direct oxidation pathway is most likely occurring for the sulfide oxidation and an outer sphere mechanism for the cis-cyclooctene. The combination of kinetic data and Hammett parameters showed that sulfides and alkenes react with oxygen atoms on the peroxyacids with partial negative charges, due to the concerted reaction of the sulfides and alkenes with the peroxyacids. A 6-coordinate intermediate is formed prior to the release of sulfoxide or epoxide and propionic acid products to regenerate the VO(dtpa) complex.

In conclusion, changing the environment around the vanadium did not hinder vanadium's ability to perform oxidation reactions. The new catalyst was able to oxidize both sulfides and alkenes and a mechanism was proposed for both oxidations. New ligand geometry information of VO(dtpa) was gained from EPR and ongoing computational studies.

## COMPREHENSIVE BIBLIOGRAPHY

Adam, W.; Haas, W.; Sieker, G. Thianthrene 5-oxide as mechanistic probe in oxygen-transfer reactions: the case of carbonyl oxides vs. dioxiranes. *J. Am. Chem. Soc.* **1984**, *106*, 5020-5022.

Adão, P.; Costa Pessoa, J.; Henriques, R. T.; Kuznetsov, M. L.; Avecilla, F.; Maurya, M. R.; Kumar, U.; Correia, I. Synthesis, Characterization, and Application of Vanadium–Salan Complexes in Oxygen Transfer Reactions. *Inorg. Chem.* **2009**, *48*, 3542-3561.

Adkins, H.; Krsek, G. Preparation of Aldehydes from Alkenes by the Addition of Carbon Monoxide and Hydrogen with Cobalt Carbonyls as Intermediates. *J. Am. Chem. Soc.* **1948**, *70*, 383-386.

Al-Ajlouni, A. M.; Espenson, J. H. Kinetics and Mechanism of the Epoxidation of Alkyl-Substituted Alkenes by Hydrogen Peroxide, Catalyzed by Methylrhenum Trioxide. *J. Org. Chem.* **1996**, *61*, 3969-3976.

Al-Ajlouni, A. M.; Sağlam, Ö.; Diafla, T.; Kühn, F. E. Kinetic studies on phenylphosphopolyperoxotungstates catalyzed epoxidation of olefins with hydrogen peroxide. *J. Mol. Catal. A: Chem.* **2008**, *287*, 159-164.

Allothman, Z. A. A Review: Fundamental Aspects of Silicate Mesoporous Materials. *Materials* **2012**, *5*, 2874-2902.

Alvaro, M.; Corma, A.; Das, D.; Fornés, V.; García, H. Single-step preparation and catalytic activity of mesoporous MCM-41 and SBA-15 silicas functionalized with perfluoroalkylsulfonic acid groups analogous to Nafion®. *Chem. Commun.* **2004**, 956-957.

Amano, F.; Yamaguchi, T.; Tanaka, T. Photocatalytic Oxidation of Propylene with Molecular Oxygen over Highly Dispersed Titanium, Vanadium, and Chromium Oxides on Silica. *J. Phys. Chem. B* **2006**, *110*, 281-288.

Andersson, M.; Willetts, A.; Allenmark, S. Asymmetric Sulfoxidation Catalyzed by a Vanadium-Containing Bromoperoxidase. *J. Org. Chem.* **1997**, *62*, 8455-8458.

Andrzej, B.; Paweł, K.; Jerzy, Z. Catalytic Adsorptive Stripping Chronopotentiometric Determination of Hexavalent Chromium at a Silver Amalgam Film Electrode of Prolonged Application. *Electroanalysis* **2011**, *23*, 2265-2269.

Anslyn, E. V.; Dougherty, D. A., *Modern Physical Organic Chemistry*. 1st ed.; University Science Books: Sausalito, California, 2006.

Anwander, R. SOMC@PMS. Surface Organometallic Chemistry at Periodic Mesoporous Silica. *Chem. Mater.* **2001**, *13*, 4419-4438.

Arasasingham, R. D.; He, G. X.; Bruice, T. C. Mechanism of manganese porphyrin-catalyzed oxidation of alkenes. Role of manganese(IV)-oxo species. *J. Am. Chem. Soc.* **1993**, *115*, 7985-7991.

Ariga, K.; Vinu, A.; Hill, J. P.; Mori, T. Coordination chemistry and supramolecular chemistry in mesoporous nanospace. *Coord. Chem. Rev.* **2007**, *251*, 2562-2591.

Arzoumanian, H.; Blanc, A.; Hartig, U.; Metzger, J. Homogeneous bimetallic catalysis. The selective autoxidation of cyclohexene. *Tetrahedron Lett.* **1974**, *15*, 1011-1014.

Azizi, T. S.; Gholamhossein, G.; Dehno, K. A. Six-coordinated vanadium(IV) complexes with tridentate task-specific ionic liquid Schiff base ligands: Synthesis, characterization and effect of ionic nature on catalytic activity. *Appl. Organomet. Chem.* **2018**, *32*, 4078.

Bal, H. E.; Kaashoek, M. F.; Tanenbaum, A. S. Orca: a language for parallel programming of distributed systems. *IEEE Trans. Softw. Eng.* **1992**, *18*, 190-205.

Balcells, D.; Maseras, F.; Lledós, A. Density Functional Study on the Mechanism of the Vanadium-Catalyzed Oxidation of Sulfides by Hydrogen Peroxide. *J. Org. Chem.* **2003**, *68*, 4265-4274.

Balcells, D.; Maseras, F.; Ujaque, G. Computational Rationalization of the Dependence of the Enantioselectivity on the Nature of the Catalyst in the Vanadium-Catalyzed Oxidation of Sulfides by Hydrogen Peroxide. *J. Am. Chem. Soc.* **2005**, *127*, 3624-3634.

Ball, D. W., *Physical Chemistry*. Brooks/Cole- Thomson Learning: Pacific Grove, CS, 2003; p 519-559.

Ballistreri, F. P.; Fortuna, C. G.; Pappalardo, A.; Tomaselli, G. A.; Toscano, R. M. Oxidation of organic sulfides by a vanadium(5+) oxo-monoperoxo-picolinate complex: Kinetics and mechanism. *J. Mol. Catal. A: Chem.* **2009**, *308*, 56-60.

Ballistreri, F. P.; Tomaselli, G. A.; Toscano, R. M.; Conte, V.; Di Furia, F. Application of the thianthrene 5-oxide mechanistic probe to peroxometal complexes. *J. Am. Chem. Soc.* **1991**, *113*, 6209-6212.

Barrett, E. P.; Joyner, L. G.; Halenda, P. P. The Determination of Pore Volume and Area Distributions in Porous Substances. I. Computations from Nitrogen Isotherms. *J. Am. Chem. Soc.* **1951**, *73*, 373-380.

Beck, J. S.; Vartuli, J. C.; Kennedy, G. J.; Kresge, C. T.; Roth, W. J.; Schramm, S. E. Molecular or Supramolecular Templating: Defining the Role of Surfactant Chemistry in the Formation of Microporous and Mesoporous Molecular Sieves. *Chem. Mater.* **1994**, *6*, 1816-1821.

Beck, J. S.; Vartuli, J. C.; Roth, W. J.; Leonowicz, M. E.; Kresge, C. T.; Schmitt, K. D.; Chu, C. T.-W.; Olson, D. H.; Sheppard, E. W.; McCullen, S. B.; Higgins, J. B.; Schlenkert, J. L. A New Family of Mesoporous Molecular Sieves Prepared with Liquid Crystal Templates. *J. Am. Chem. Soc.* **1992**, *114*, 10834-10843.

Ben Zid, T.; Fadhli, M.; Khedher, I.; Fraile, J. M. New bis(oxazoline)-vanadyl complexes, supported by electrostatic interaction in Laponite clay, as heterogeneous catalysts for asymmetric oxidation of methyl phenyl sulfide. *Microporous Mesoporous Mater.* **2017**, *239*, 167-172.

Ben Zid, T.; Fadhli, M.; Khedher, I.; Fraile, J. M. New bis(oxazoline)-vanadyl complexes, supported by electrostatic interaction in Laponite clay, as heterogeneous

catalysts for asymmetric oxidation of methyl phenyl sulfide. *Microporous Mesoporous Mater.* **2017**, *239*, 167-172.

Ben Zid, T.; Khedher, I.; Ghorbel, A. Chiral vanadyl salen catalyst immobilized on mesoporous silica as support for asymmetric oxidation of sulfides to sulfoxides. *React. Kinet., Mech. Catal.* **2010**, *100*, 131-143.

Ben Zid, T.; Khedher, I.; Ksibi, Z.; Fraile, J. M. Vanadium-Schiff base complex covalently bonded on modified MCM-41 as catalyst for asymmetric oxidation of methyl phenyl sulfide. *J. Porous Mater.* **2016**, *23*, 507-516.

Bernhard, Y.; Winckler, P.; Perrier-Cornet, J.-M.; Decreau, R. A. Harnessing medically relevant metals onto water-soluble subphthalocyanines: towards bimodal imaging and theranostics. *Dalton Trans.* **2015**, *44*, 3200-3208.

Bhatt, R.; Sreedhar, B.; Padmaja, P. Adsorption of chromium from aqueous solutions using crosslinked chitosan–diethylenetriaminepentaacetic acid. *Int. J. Biol. Macromol.* **2015**, *74*, 458-466.

Bhattacharyya, S.; Lelong, G.; Saboungi, M. L. Recent progress in the synthesis and selected applications of MCM-41: a short review. *J. Exp. Nanosci.* **2006**, *1*, 375-395.

Bhunja, S.; Koner, S. Functionalization of oxo-vanadium(IV) acetylacetonate over modified MCM-41: an efficient reusable catalyst for epoxidation reaction. *J. Porous Mater.* **2011**, *18*, 399-407.

Bikas, R.; Ghorbanloo, M.; Jafari, S.; Eigner, V.; Dusek, M. Catalytic oxidation of olefins and sulfides in the presence of hydrazone-oxidovanadium(V) complex containing  $\text{VOCl}_2^+$  core. *Inorg. Chim. Acta* **2016**, *453*, 78-85.

Bingham, K. D.; Meakins, G. D.; Whitham, G. H. The mechanism of epoxide formation by peroxy-acids. *Chem. Commun. (London)* **1966**, 445-446.

Boehm-Sturm, P.; Haeckel, A.; Hauptmann, R.; Mueller, S.; Kuhl, C. K.; Schellenberger, E. A. Low-Molecular-Weight Iron Chelates May Be an Alternative to

Gadolinium-based Contrast Agents for T1-weighted Contrast-enhanced MR Imaging. *Radiology* **2018**, *286*, 537-546.

Bouchoucha, M.; C.-Gaudreault, R.; Fortin, M.-A.; Kleitz, F. Mesoporous Silica Nanoparticles: Selective Surface Functionalization for Optimal Relaxometric and Drug Loading Performances. *Adv. Funct. Mater.* **2014**, *24*, 5911-5923.

Bouriazos, A.; Sotiriou, S.; Stathis, P.; Papadogianakis, G. Superior aqueous-phase catalytic hydrogenation activity of palladium modified with nitrogen-containing ligands compared with the TPPTS benchmark modifier in micellar nanoreactors. *Appl. Catal. B* **2014**, *150-151*, 345-353.

Brinker, C. J., Sol—Gel Processing of Silica. In *The Colloid Chemistry of Silica*, American Chemical Society: 1994; Vol. 234, pp 361-401.

Brunauer, S.; Emmett, P. H.; Teller, E. Adsorption of Gases in Multimolecular Layers. *J. Am. Chem. Soc.* **1938**, *60*, 309–319.

Bryliakov, K. P. Catalytic Asymmetric Oxygenations with the Environmentally Benign Oxidants H<sub>2</sub>O<sub>2</sub> and O<sub>2</sub>. *Chem. Rev.* **2017**, *117*, 11406-11459.

Bühl, M.; Schurhammer, R.; Imhof, P. Peroxovanadate Imidazole Complexes as Catalysts for Olefin Epoxidation: Density Functional Study of Dynamics, <sup>51</sup>V NMR Chemical Shifts, and Mechanism. *J. Am. Chem. Soc.* **2004**, *126*, 3310-3320.

Butler, A.; Clague, M. J.; Meister, G. E. Vanadium Peroxide Complexes. *Chem. Rev.* **1994**, *94*, 625-638.

Carey, F. A.; Sundberg, R. J., *Advanced Organic Chemistry Part A: Structure and Mechanisms*. 5th ed.; Springer Science+Business Media: New York, NY, 2007; p 511-515.

Carlin, D. A.; Bertolani, S. J.; Siegel, J. B. Biocatalytic conversion of ethylene to ethylene oxide using an engineered toluene monooxygenase. *Chem. Commun.* **2015**, *51*, 2283-2285.

Carlin, D. A.; Bertolani, S. J.; Siegel, J. B. Biocatalytic conversion of ethylene to ethylene oxide using an engineered toluene monooxygenase. *Chem. Commun.* **2015**, *51*, 2283-2285.

Chanquía, C. M.; Cánepa, A. L.; Winkler, E. L.; Rodríguez-Castellón, E.; Casuscelli, S. G.; Eimer, G. A. Nature of active vanadium nanospecies in MCM-41 type catalysts for olefins oxidation. *Mater. Chem. Phys.* **2016**, *175*, 172-179.

Chatgililoglu, C.; Crich, D.; Komatsu, M.; Ryu, I. Chemistry of Acyl Radicals. *Chem. Rev.* **1999**, *99*, 1991-2070.

Chen, B.; Shan, X.-q.; Qian, J. Bioavailability index for quantitative evaluation of plant availability of extractable soil trace elements. *Plant Soil* **1996**, *186*, 275-283.

Chen, C.; Shen, P.; Wan, M.; Ding, N.; Shi, X.; Wang, X.; Zhang, N. Size-selective epoxidation of olefins in two new metal-organic framework constructed from six-coordinated tetranuclear Cu(II) SBUs. *Microporous Mesoporous Mater.* **2016**, *232*, 167-173.

Chen, J. W.; Belford, R. L.; Clarkson, R. B. Second-Sphere and Outer-Sphere Proton Relaxation of Paramagnetic Complexes: From EPR to NMRD. *J. Phys. Chem. A* **1998**, *102*, 2117-2130.

Chen, Z.; Naidu, R. On-column complexation and simultaneous separation of vanadium(IV) and vanadium(V) by capillary electrophoresis with direct UV detection. *Anal. Bioanal. Chem.* **2002**, *374*, 520-525.

Cheng, K.; Blumen, S. R.; MacPherson, M. B.; Steinbacher, J. L.; Mossman, B. T.; Landry, C. C. Enhanced Uptake of Porous Silica Microparticles by Bifunctional Surface Modification with a Targeting Antibody and a Biocompatible Polymer. *ACS Appl. Mater. Interfaces* **2010**, *2*, 2489-2495.

Chong, A. O.; Sharpless, K. B. Mechanism of the molybdenum and vanadium catalyzed epoxidation of olefins by alkyl hydroperoxides. *J. Org. Chem.* **1977**, *42*, 1587-1590.

Clerici, M. G. The activity of titanium silicalite-1 (TS-1): Some considerations on its origin. *Kinet. Catal.* **2015**, *56*, 450-455.

Cohan, L. H. Hysteresis and the Capillary Theory of Adsorption of Vapors. *J. Am. Chem. Soc.* **1944**, *66*, 98-105.

Cohan, L. H. Sorption Hysteresis and the Vapor Pressure of Concave Surfaces. *J. Am. Chem. Soc.* **1938**, *60*, 433-435.

Coletti, A.; Galloni, P.; Sartorel, A.; Conte, V.; Floris, B. Salophen and salen oxo vanadium complexes as catalysts of sulfides oxidation with H<sub>2</sub>O<sub>2</sub>: Mechanistic insights. *Catal. Today* **2012**, *192*, 44-55.

Colpas, G. J.; Hamstra, B. J.; Kampf, J. W.; Pecoraro, V. L. Functional Models for Vanadium Haloperoxidase: Reactivity and Mechanism of Halide Oxidation. *J. Am. Chem. Soc.* **1996**, *118*, 3469-3478.

Conte, V.; Coletti, A.; Floris, B.; Licini, G.; Zonta, C. Mechanistic aspects of vanadium catalysed oxidations with peroxides. *Coord. Chem. Rev.* **2011**, *255*, 2165-2177.

Cooper, M. S.; Ma, M. T.; Sunassee, K.; Shaw, K. P.; Williams, J. D.; Paul, R. L.; Donnelly, P. S.; Blower, P. J. Comparison of <sup>64</sup>Cu-Complexing Bifunctional Chelators for Radioimmunoconjugation: Labeling Efficiency, Specific Activity, and in Vitro/in Vivo Stability. *Bioconjugate Chem.* **2012**, *23*, 1029-1039.

Corma, A.; Garcia, H. Silica-Bound Homogenous Catalysts as Recoverable and Reusable Catalysts in Organic Synthesis. *Adv. Synth. Catal.* **2006**, *348*, 1391-1412.

Corma, A.; Garcia, H. Supramolecular Host-Guest Systems in Zeolites Prepared by Ship-in-a-Bottle Synthesis. *Eur. J. Inorg. Chem.* **2004**, *2004*, 1143-1164.

Cozzolino, A. F.; Tofan, D.; Cummins, C. C.; Temprado, M.; Palluccio, T. D.; Rybak-Akimova, E. V.; Majumdar, S.; Cai, X.; Captain, B.; Hoff, C. D. Two-Step Binding of O<sub>2</sub> to a Vanadium(III) Trisanilide Complex To Form a Non-Vanadyl Vanadium(V) Peroxo Complex. *J. Am. Chem. Soc.* **2012**, *134*, 18249-18252.

Curci, R.; Di Furia, F.; Testi, R.; Modena, G. Metal catalysis in oxidation by peroxides. Vanadium catalysed oxidation of organosulphur compounds by t-butyl hydroperoxide. *J. Chem. Soc., Perkin Trans. 2* **1974**, 752-757.

D. Oldroyd, R.; Sankar, G.; Meurig Thomas, J.; Hunnius, M.; F. Maier, W. Creation, characterisation and performance of vanadyl active sites in microporous and mesoporous silica-based catalysts for the selective oxidation of hydrocarbons. *J. Chem. Soc., Faraday Trans.* **1998**, 94, 3177-3182.

da Silva, J. A. L.; da Silva, J. J. R. F.; Pombeiro, A. J. L. Oxovanadium complexes in catalytic oxidations. *Coord. Chem. Rev.* **2011**, 255, 2232-2248.

Das, P.; Saha, D.; Saha, D.; Guin, J. Aerobic Direct C(sp<sup>2</sup>)-H Hydroxylation of 2-Arylpyridines by Palladium Catalysis Induced with Aldehyde Auto-Oxidation. *ACS Catal.* **2016**, 6, 6050-6054.

de Azevedo Marques, A. P.; Dockal, E. R.; Skrobot, F. C.; Viana Rosa, I. L. Synthesis, characterization and catalytic study of [N,N'-bis(3-ethoxysalicylidene)-m-xylylenediamine]oxovanadium(IV) complex. *Inorg. Chem. Commun.* **2007**, 10, 255-261.

Dell'Anna, M. M.; Mastrorilli, P.; Nobile, C. F. Aerobic oxidation of sulfides catalysed by cobalt(II) complexes under homogeneous and heterogeneous conditions. *J. Mol. Catal. A: Chem.* **1996**, 108, 57-62.

Díaz-de Alba, M.; Galindo-Riaño, M. D.; Casanueva-Marenco, M. J.; García-Vargas, M.; Kosore, C. M. Assessment of the metal pollution, potential toxicity and speciation of sediment from Algeciras Bay (South of Spain) using chemometric tools. *J. Hazard. Mater.* **2011**, 190, 177-187.

Dib, S.; Boufatit, M.; Chelouaou, S.; Sadi-Hassaine, F.; Croissant, J.; Long, J.; Raehm, L.; Charnay, C.; Durand, J. O. Versatile heavy metals removal via magnetic mesoporous nanocontainers. *RSC Adv.* **2014**, 4, 24838-24841.

Domingo, J. L.; Gomez, M.; Llobet, J. M.; Corbella, J. Chelating agents in the treatment of acute vanadyl sulphate intoxication in mice. *Toxicology* **1990**, 62, 203-211.

Dong, J.; Hu, J.; Chi, Y.; Lin, Z.; Zou, B.; Yang, S.; Hill, C. L.; Hu, C. A Polyoxoniobate–Polyoxovanadate Double-Anion Catalyst for Simultaneous Oxidative and Hydrolytic Decontamination of Chemical Warfare Agent Simulants. *Angew. Chem. Int. Ed.* **2017**, *56*, 4473-4477.

Dorbes, S.; Pereira, C.; Andrade, M.; Barros, D.; Pereira, A. M.; Rebelo, S. L. H.; Araújo, J. P.; Pires, J.; Carvalho, A. P.; Freire, C. Oxidovanadium(IV) acetylacetonate immobilized onto CMK-3 for heterogeneous epoxidation of geraniol. *Microporous Mesoporous Mater.* **2012**, *160*, 67-74.

Du, G.; Espenson, J. H. Oxidation of Triarylphosphines and Aryl Methyl Sulfides with Hydrogen Peroxide Catalyzed by Dioxovanadium(V) Ion. *Inorg. Chem.* **2005**, *44*, 2465-2471.

Dumont, V.; Oliviero, L.; Maugé, F.; Houalla, M. Oxidation of dibenzothiophene by a metal–oxygen–aldehyde system. *Catal. Today* **2008**, *130*, 195-198.

Duncan, A. K.; Klemm, P. J.; Raymond, K. N.; Landry, C. C. Silica Microparticles as a Solid Support for Gadolinium Phosphonate Magnetic Resonance Imaging Contrast Agents. *J. Am. Chem. Soc.* **2012**, *134*, 8046-8049.

Durham, E. J.; Ryskiewich, D. P. The Acid Dissociation Constants of Diethylenetriaminepentaacetic Acid and the Stability Constants of Some of its Metal Chelates. *J. Am. Chem. Soc.* **1958**, *80*, 4812-4817.

Ebsworth, E. A. V.; Rankin, D. W.; Cradock, S., *Structural Methods in Inorganic Chemistry*. Blackwell Scientific Publications: Oxford, England, 1987.

Eftekhari-Sis, B.; Akbari, M.; Akbari, A.; Amini, M. Vanadium (V) and Tungsten (VI) Oxoperoxo-Complexes Anchored on Fe<sub>3</sub>O<sub>4</sub> Magnetic Nanoparticles: Versatile and Efficient Catalysts for the Oxidation of Alcohols and Sulfides. *Catal. Lett.* **2017**, *147*, 2106-2115.

Eftekhari-Sis, B.; Akbari, M.; Akbari, A.; Amini, M. Vanadium (V) and Tungsten (VI) Oxoperoxo-Complexes Anchored on Fe<sub>3</sub>O<sub>4</sub> Magnetic Nanoparticles: Versatile and Efficient Catalysts for the Oxidation of Alcohols and Sulfides. *Catal. Lett.* **2017**, *147*, 2106-2115.

- Egli, T. Biodegradation of metal-complexing aminopolycarboxylic acids. *J. Biosci. Bioeng.* **2001**, *92*, 89-97.
- El Amrani, I.; Atlamsani, A.; Dakkach, M.; Rodríguez, M.; Romero, I.; Amthiou, S. Efficient and selective oxidation of aldehydes with dioxygen catalysed by vanadium-containing heteropolyanions. *C. R. Chim.* **2017**, *20*, 888-895.
- El-Faham, A.; Albericio, F. Peptide Coupling Reagents, More than a Letter Soup. *Chem. Rev.* **2011**, *111*, 6557-6602.
- El-Nahhal, I. M.; Chehimi, M.; Selmane, M. Synthesis and Structural Characterization of G-SBA-IDA, G-SBA-EDTA and G-SBA-DTPA Modified Mesoporous SBA-15 Silica and Their Application for Removal of Toxic Metal Ions Pollutants. *Silicon* **2018**, *10*, 981-993.
- Erathodiyil, N.; Ying, J. Y. Functionalization of Inorganic Nanoparticles for Bioimaging Applications. *Acc. Chem. Res.* **2011**, *44*, 925-935.
- Estrada, A. C.; Simões, M. M. Q.; Santos, I. C. M. S.; Neves, M. G. P. M. S.; Silva, A. M. S.; Cavaleiro, J. A. S.; Cavaleiro, A. M. V. Transition Metal Substituted Polyoxotungstates in the Catalytic Oxidation of 1H-Indene and 1,2-Dihydronaphthalene with Hydrogen Peroxide. *Catal. Lett.* **2009**, *128*, 281-289.
- Everett, D. H. Manual of Symbols and Terminology for Physicochemical Quantities and Units, Appendix II: Definitions, Terminology and Symbols in Colloid and Surface Chemistry. *Pure Appl. Chem.* **1972**, *31*, 577-638.
- Farzaneh, F.; Sadeghi, Y. Immobilized V-MIL-101 on modified Fe<sub>3</sub>O<sub>4</sub> nanoparticles as heterogeneous catalyst for epoxidation of allyl alcohols and alkenes. *J. Mol. Catal. A: Chem.* **2015**, *398*, 275-281.
- Farzaneh, F.; Zamanifar, E.; Williams, C. D. V-MCM-41 as selective catalyst for epoxidation of olefins and trans-2-hexene-1-ol. *J. Mol. Catal. A: Chem.* **2004**, *218*, 203-209.

Fazaeli, R.; Mohagheghian, Z. Vanadium oxide supported on mesocellulose silica foams (MCF): An efficient and reusable catalyst for selective oxidation of sulfides. *Iran. Chem. Commun.* **2016**, *4*, 198-206.

Firouzi, A.; Kumar, D.; Bull, L. M.; Besier, T.; Sieger, P.; Huo, Q.; Walker, S. A.; Zasadzinski, J. A.; Glinka, C.; Nicol, J.; Margolese, D.; Stucky, G. D.; Chemelka, B. F. Cooperative organization of inorganic-surfactant and biomimetic assemblies. *Science* **1995**, *267*, 1138-1143.

Fraile, J. M.; García, J. I.; Mayoral, J. A.; Vispe, E. Optimization of cyclohexene epoxidation with dilute hydrogen peroxide and silica-supported titanium catalysts. *Appl. Catal. A* **2003**, *245*, 363-376.

Fuerte, A.; Iglesias, M.; Sánchez, F.; Corma, A. Chiral dioxomolybdenum(VI) and oxovanadium(V) complexes anchored on modified USY-zeolite and mesoporous MCM-41 as solid selective catalysts for oxidation of sulfides to sulfoxides or sulfones. *J. Mol. Catal. A: Chem.* **2004**, *211*, 227-235.

Gall, R. D.; Faraj, M.; Hill, C. L. Role of Water in Polyoxometalate-Catalyzed Oxidations in Nonaqueous Media. Scope, Kinetics, and Mechanism of Oxidation of Thioether Mustard (HD) Analogs by tert-Butyl Hydroperoxide Catalyzed by  $H_5PV_2Mo_{10}O_{40}$ . *Inorg. Chem.* **1994**, *33*, 5015-5021.

Gallis, K. W.; Araujo, J. T.; Duff, K. J.; Moore, J. G.; Landry, C. C. The Use of Mesoporous Silica in Liquid Chromatography. *Adv. Mater.* **1999**, *11*, 1452-1455.

Gallis, K. W.; Landry, C. C. Mesoporous Silica Production for Liquid Chromatography. U.S. Patent 6,334,988, August 20, 1999.

Gao, J.; Lu, L.; Zhou, W.; Gao, G.; He, M. Synthesis, characterization and sulfide oxidation activity of vanadyl Schiff base complexes anchored on MCM-41. *J. Porous Mater.* **2008**, *15*, 127-132.

Garcia-Bosch, I.; Company, A.; Fontrodona, X.; Ribas, X.; Costas, M. Efficient and Selective Peracetic Acid Epoxidation Catalyzed by a Robust Manganese Catalyst. *Org. Lett.* **2008**, *10*, 2095-2098.

- Gawande, M. B.; Monga, Y.; Zboril, R.; Sharma, R. K. Silica-decorated magnetic nanocomposites for catalytic applications. *Coord. Chem. Rev.* **2015**, *288*, 118-143.
- Genna, D. T.; Wong-Foy, A. G.; Matzger, A. J.; Sanford, M. S. Heterogenization of Homogeneous Catalysts in Metal–Organic Frameworks via Cation Exchange. *J. Am. Chem. Soc.* **2013**, *135*, 10586-10589.
- Ghosh, D.; Febriansyah, B.; Gupta, D.; Ng, L. K.-S.; Xi, S.; Du, Y.; Baikie, T.; Dong, Z.; Soo, H. S. Hybrid Nanomaterials with Single-Site Catalysts by Spatially Controllable Immobilization of Nickel Complexes via Photoclick Chemistry for Alkene Epoxidation. *ACS Nano* **2018**, *12*, 5903-5912.
- Gibson, L. T. Mesosilica materials and organic pollutant adsorption: part A removal from air. *Chem. Soc. Rev.* **2014**, *43*, 5163-5172.
- Gomes, A. J.; Espreafico, E. M.; Tfouni, E. trans-[Ru(NO)Cl(cyclam)](PF<sub>6</sub>)<sub>2</sub> and [Ru(NO)(Hedta)] Incorporated in PLGA Nanoparticles for the Delivery of Nitric Oxide to B16–F10 Cells: Cytotoxicity and Phototoxicity. *Molecular Pharmaceutics* **2013**, *10*, 3544-3554.
- Graham, T. XXXV.—On the properties of silicic acid and other analogous colloidal substances. *J. Chem. Soc.* **1864**, *17*, 318-327.
- Gregori, F.; Nobili, I.; Bigi, F.; Maggi, R.; Predieri, G.; Sartori, G. Selective oxidation of sulfides to sulfoxides and sulfones using 30% aqueous hydrogen peroxide and silica-vanadia catalyst. *J. Mol. Catal. A: Chem.* **2008**, *286*, 124-127.
- Grivani, G.; Tahmasebi, V.; Khalaji, A. D.; Fejfarová, K.; Dušek, M. Synthesis, characterization and crystal structure determination of a new vanadium(IV) Schiff base complex (VOL<sub>2</sub>) and investigation of its catalytic activity in the epoxidation of cyclooctene. *Polyhedron* **2013**, *51*, 54-60.
- Gutsev, G. L.; Rao, B. K.; Jena, P. Systematic Study of Oxo, Peroxo, and Superoxo Isomers of 3d-Metal Dioxides and Their Anions. *J. Phys. Chem. A* **2000**, *104*, 11961-11971.

Haber, F.; van Oordt, G. Über die Bildung von Ammoniak den Elementen. *Z. Anorg. Allg. Chem.* **1905**, *44*, 341-378.

Haidasz, E. A.; Shah, R.; Pratt, D. A. The Catalytic Mechanism of Diarylamine Radical-Trapping Antioxidants. *J. Am. Chem. Soc.* **2014**, *136*, 16643-16650.

Hall, N.; Orio, M.; Jorge-Robin, A.; Gennaro, B.; Marchi-Delapierre, C.; Duboc, C. Vanadium Thiolate Complexes for Efficient and Selective Sulfoxidation Catalysis: A Mechanistic Investigation. *Inorg. Chem.* **2013**, *52*, 13424-13431.

Hamada, T. A new experimental system of using fertile chick eggs to evaluate vanadium absorption and antidotal effectiveness to prevent vanadium uptake. *J. Nutr. Biochem.* **1994**, *5*, 382-388.

Hamidipour, L.; Farzaneh, F. Immobilized VOsalpr on modified Fe<sub>3</sub>O<sub>4</sub> nanoparticles as a magnetically separable epoxidation catalyst. *C. R. Chim.* **2014**, *17*, 927-933.

Hansch, C.; Leo, A.; Taft, R. W. A survey of Hammett substituent constants and resonance and field parameters. *Chem. Rev.* **1991**, *91*, 165-195.

Hartwig, J. F., *Organotransition Metal Chemistry: From Bonding to Catalysis*. University Science Books: Sausalito, CA, 2010.

Hay, R. W.; Clifford, T.; Govan, N. Selective manganese(III) and vanadium(IV) catalysts for the oxidation of dialkyl sulfides in microemulsion media. *Transition Met. Chem.* **1998**, *23*, 619-624.

Heveling, J. Heterogeneous Catalytic Chemistry by Example of Industrial Applications. *J. Chem. Educ.* **2012**, *89*, 1530-1536.

Hill, C. L.; Gall, R. D. The first combinatorially prepared and evaluated inorganic catalysts. Polyoxometalates for the aerobic oxidation of the mustard analog tetrahydrothiophene (THT). *J. Mol. Catal. A: Chem.* **1996**, *114*, 103-111.

Hillegass, J. M.; Blumen, S. R.; Cheng, K.; MacPherson, M. B.; Alexeeva, V.; Lathrop, S. A.; Beuschel, S. L.; Steinbacher, J. L.; Butnor, K. J.; Ramos-Niño, M. E.; Shukla, A.; James, T. A.; Weiss, D. J.; Taatjes, D. J.; Pass, H. I.; Carbone, M.; Landry, C. C.;

Mossman, B. T. Increased efficacy of doxorubicin delivered in multifunctional microparticles for mesothelioma therapy. *Int. J. Cancer* **2011**, *129*, 233-244.

Houk, K. N.; Rondan, N. G.; Mareda, J. Theoretical studies of halocarbene cycloaddition selectivities: A new interpretation of negative activation energies and entropy control of selectivity. *Tetrahedron* **1985**, *41*, 1555-1563.

Housecroft, C. E.; Sharpe, A. G., *Inorganic Chemistry*. 2nd ed.; Pearson Education Limited: Harlow, England, 2005; p 182-188.

Housecroft, C. E.; Sharpe, A. G., *Inorganic Chemistry*. 2nd ed.; Pearson Education Limited: Harlow, England, 2005; p 765-766.

Hsiao, M.-C.; Liu, S.-T. Polymer Supported Vanadium Complexes as Catalysts for the Oxidation of Alkenes in Water. *Catal. Lett.* **2010**, *139*, 61-66.

Hu, Y.-L.; Liu, X.-B.; Fang, D. Efficient and convenient oxidation of sulfides to sulfones using H<sub>2</sub>O<sub>2</sub> catalyzed by V<sub>2</sub>O<sub>5</sub> in ionic liquid [C<sub>12</sub>mim][HSO<sub>4</sub>]. *Catal. Sci. Technol.* **2014**, *4*, 38-42.

Huang, Z.; Brookhart, M.; Goldman, A. S.; Kundu, S.; Ray, A.; Scott, S. L.; Vicente, B. C. Highly Active and Recyclable Heterogeneous Iridium Pincer Catalysts for Transfer Dehydrogenation of Alkanes. *Adv. Synth. Catal.* **2009**, *351*, 188-206.

Huclier-Markai, S.; Alliot, C.; Sebti, J.; Brunel, B.; Aupiais, J. A comparative thermodynamic study of the formation of scandium complexes with DTPA and DOTA. *RSC Adv.* **2015**, *5*, 99606-99617.

Hulea, V.; Maciucă, A.-L.; Cojocariu, A.-M.; Ciocan, C.-E.; Dumitriu, E. New heterogeneous catalysts for mild oxidation of S-containing organic compounds. *C. R. Chim.* **2009**, *12*, 723-730.

Inoue, K.; Yoshizuka, K.; Ohto, K. Adsorptive separation of some metal ions by complexing agent types of chemically modified chitosan. *Anal. Chim. Acta* **1999**, *388*, 209-218.

Ishiwata, K.; Ido, T.; Monma, M.; Murakami, M.; Fukuda, H.; Kameyama, M.; Yamada, K.; Endo, S.; Yoshioka, S.; Sato, T.; Matsuzawa, T. Potential radiopharmaceuticals labeled with titanium-45. *Int. J. Radiat. Appl. Instrum., Part A* **1991**, *42*, 707-712.

Islam, N. S.; Boruah, J. J. Macromolecular peroxo complexes of Vanadium(V) and Molybdenum(VI): Catalytic activities and biochemical relevance. *J. Chem. Sci* **2015**, *127*, 777-795.

Jeong, Y.-C.; Kang, E. J.; Ahn, K.-H. Electronic effects of substituents in sulfides: mechanism elucidation of vanadium catalyzed sulfoxidation. *Bull. Korean Chem. Soc.* **2009**, *30*, 2795-2798.

Jiang, B.; Liu, M.; Zhang, K.; Zu, G.; Dong, J.; Cao, Y.; Zhang, L.; Pei, R. Oligoethylenimine grafted PEGylated poly(aspartic acid) as a macromolecular contrast agent: properties and in vivo studies. *J. Mater. Chem. B* **2016**, *4*, 3324-3330.

Jianping, L.; Shangwang, L.; Qiuyan, L.; Xuehong, Z. A New Chromium(III) Microelectrode Based on Self-Assembled Diethylenetriaminepentaacetic Acid-Poly(fuchsin basic) Modified Electrode. *Electroanalysis* **2009**, *21*, 831-836.

Jin, Y.; Li, A.; Hazelton, S. G.; Liang, S.; John, C. L.; Selid, P. D.; Pierce, D. T.; Zhao, J. X. Amorphous silica nanohybrids: Synthesis, properties and applications. *Coord. Chem. Rev.* **2009**, *253*, 2998-3014.

Jing, D.; Jufang, H.; Yingnan, C.; Zhengguo, L.; Bo, Z.; Song, Y.; L., H. C.; Changwen, H. A Polyoxoniobate-Polyoxovanadate Double-Anion Catalyst for Simultaneous Oxidative and Hydrolytic Decontamination of Chemical Warfare Agent Simulants. *Angew. Chem. Int. Ed.* **2017**, *56*, 4473-4477.

Joergensen, K. A. Transition-metal-catalyzed epoxidations. *Chem. Rev.* **1989**, *89*, 431-458.

Jung, H.; Lee, H. W.; Jeong, E. A. Enhanced thermal degradation of 2,2'-dichlorodiethyl sulfide (sulfur mustard, HD) with the presence of metal oxides. *Phosphorus Sulfur Silicon Relat Elem* **2016**, *191*, 1137-1141.

Jurado, M. J.; Gracia, M. D.; Campelo, J. M.; Luque, R.; Marinas, J. M.; Romero, A. A. Selective epoxidation of alkenes using highly active V-SBA-15 materials: microwave vs. conventional heating. *J. Mater. Chem.* **2009**, *19*, 8603-8609.

Kaiser, E.; Colescott, R. L.; Bossinger, C. D.; Cook, P. I. Color test for detection of free terminal amino groups in the solid-phase synthesis of peptides. *Anal. Biochem.* **1970**, *34*, 595-598.

Kala Raj, N. K.; Deshpande, S. S.; Ingle, R. H.; Raja, T.; Manikandan, P. Heterogenized Molybdovanadophosphoric Acid on Amine-Functionalized SBA-15 for Selective Oxidation of Alkenes. *Catal. Lett.* **2004**, *98*, 217-224.

Kala Raj, N. K.; Deshpande, S. S.; Ingle, R. H.; Raja, T.; Manikandan, P., Immobilized molybdovanadophosphoric acids on SBA-15 for selective oxidation of alkenes. In *Studies in Surface Science and Catalysis*, Sayari, A.; Jaroniec, M., Eds. Elsevier: 2005; Vol. 156, pp 769-778.

Kalilur Rahiman, A.; Shanmuga Bharathi, K.; Sreedaran, S.; Rajesh, K.; Narayanan, V. Cationic vanadyl porphyrin-encapsulated mesoporous Al/V-MCM-41 as heterogeneous catalysts for the oxidation of alkenes. *Inorg. Chim. Acta* **2009**, *362*, 1810-1818.

Kanamori, K.; Ino, K.; Maeda, H.; Miyazaki, K.; Fukagawa, M.; Kumada, J.; Eguchi, T.; Okamoto, K.-i. Relationship between Oxo-Bridged Dimer Formation and Structure of Vanadium(III) amino polycarboxylates. *Inorg. Chem.* **1994**, *33*, 5547-5554.

Kantam, M. L.; Neelima, B.; Reddy, C. V.; Chaudhuri, M. K.; Dehury, S. K. VO(acac)<sub>2</sub> Supported on Titania: A Heterogeneous Protocol for the Selective Oxidation of Sulfides Using TBHP. *Catal. Lett.* **2004**, *95*, 19-22.

Karpyshev, N. N.; Yakovleva, O. D.; Talsi, E. P.; Bryliakov, K. P.; Tolstikova, O. V.; Tolstikov, A. G. Effect of portionwise addition of oxidant in asymmetric vanadium-catalyzed sulfide oxidation. *J. Mol. Catal. A: Chem.* **2000**, *157*, 91-95.

Kasai, J.; Nakagawa, Y.; Uchida, S.; Yamaguchi, K.; Mizuno, N. [ $\gamma$ -1,2-H<sub>2</sub>SiV<sub>2</sub>W<sub>10</sub>O<sub>40</sub>] Immobilized on Surface-Modified SiO<sub>2</sub> as a Heterogeneous Catalyst for Liquid-Phase Oxidation with H<sub>2</sub>O<sub>2</sub>. *Chem. - Eur. J.* **2006**, *12*, 4176-4184.

Katsuomi, T.; Takashi, H.; Toshio, I. Heterogeneous Catalysis in the Liquid-phase Oxidation of Olefins. III. Activity of Supported Vanadium–Chromium Binary Oxide Catalyst for the Oxidation of Cyclohexene. *Bull. Chem. Soc. Jpn.* **1979**, *52*, 697-705.

Kaur, M.; Zhang, H.; Martin, L.; Todd, T.; Qiang, Y. Conjugates of Magnetic Nanoparticle—Actinide Specific Chelator for Radioactive Waste Separation. *Environ. Sci. Technol.* **2013**, *47*, 11942-11959.

Kelm, H.; Krüger, H.-J. A Superoxovanadium(V) Complex Linking the Peroxide and Dioxygen Chemistry of Vanadium. *Angew. Chem. Int. Ed.* **2001**, *40*, 2344-2348.

Khavrutskii, I. V.; Maksimov, G. M.; Kholdeeva, O. A. Oxidation of methyl phenyl sulfide with molecular oxygen in the presence of isobutyraldehyde and transition metal monosubstituted heteropolytungstates. *React. Kinet. Catal. Lett.* **1999**, *66*, 325-330.

Kirk Egdal, R.; Bond, A. D.; McKenzie, C. J. Air oxidation of divanadium(IV) complexes. *Dalton Trans.* **2009**, 3833-3839.

Kiyomi, I.; Takushi, N.; Tohru, Y.; Teruaki, M. Asymmetric Oxidation of Sulfides with Molecular Oxygen Catalyzed by  $\beta$ -Oxo Aldiminato Manganese(III) Complexes. *Chem. Lett.* **1995**, *24*, 335-336.

Komiya, N.; Naota, T.; Oda, Y.; Murahashi, S.-I. Aerobic oxidation of alkanes and alkenes in the presence of aldehydes catalyzed by copper salts and copper-crown ether. *J. Mol. Catal. A: Chem.* **1997**, *117*, 21-37.

Kosore, C. M.; Galindo-Riaño, M. D.; Díaz-de-Alba, M. Assessing trace-element mobility in Algeciras Bay (Spain) sediments by acid and complexing screening. *Arabian J. Chem.* **2015**.

Kosslick, H.; Mönnich, I.; Paetzold, E.; Fuhrmann, H.; Fricke, R.; Müller, D.; Oehme, G. Suzuki reaction over palladium-complex loaded MCM-41 catalysts. *Microporous Mesoporous Mater.* **2001**, *44-45*, 537-545.

Kosugi, M.; Hikichi, S.; Akita, M.; Moro-oka, Y. The first evidence for activation of exogenous O<sub>2</sub> on a vanadium(IV) center: synthesis and characterization of a peroxy

vanadium(V) complex with hydrotris(3,5-diisopropylpyrazol-1-yl)borate. *J. Chem. Soc., Dalton Trans.* **1999**, 1369-1372.

Kresge, C. T.; Leonowicz, M. E.; Roth, W. J.; Vartuli, J. C.; Beck, J. S. Ordered mesoporous molecular sieves synthesized by a liquid-crystal template mechanism. *Nature* **1992**, *359*, 710.

Kresge, C. T.; Roth, W. J. The discovery of mesoporous molecular sieves from the twenty year perspective. *Chem. Soc. Rev.* **2013**, *42*, 3663-3670.

Kroll, H.; Korman, S.; Siegel, E.; Hart, H. E.; Rosoff, B.; Spencer, H.; Laszlo, D. Excretion of Yttrium and Lanthanum Chelates of Cyclohexane 1,2-Trans Diamine Tetraacetic Acid and Diethylenetriamine Pentaacetic Acid in Man. *Nature* **1957**, *180*, 919.

Kumar, R.; Chaudhary, N.; Sankar, M.; Maurya, M. R. Electron deficient nonplanar  $\beta$ -octachlorovanadylporphyrin as a highly efficient and selective epoxidation catalyst for olefins. *Dalton Trans.* **2015**, *44*, 17720-17729.

Kuznetsov, M. L.; Pessoa, J. C. Epoxidation of olefins catalysed by vanadium–salan complexes: a theoretical mechanistic study. *Dalton Trans.* **2009**, 5460-5468.

Kwart, H.; Hoffman, D. M. Observations Regarding the Mechanism of Olefin Epoxidation with Per Acids. *J. Org. Chem.* **1966**, *31*, 419-425.

Laprise-Pelletier, M.; Bouchoucha, M.; Lagueux, J.; Chevallier, P.; Lecomte, R.; Gossuin, Y.; Kleitz, F.; Fortin, M.-A. Metal chelate grafting at the surface of mesoporous silica nanoparticles (MSNs): physico-chemical and biomedical imaging assessment. *J. Mater. Chem. B* **2015**, *3*, 748-758.

Lattuada, L.; Barge, A.; Cravotto, G.; Giovenzana, G. B.; Tei, L. The synthesis and application of polyamino polycarboxylic bifunctional chelating agents. *Chem. Soc. Rev.* **2011**, *40*, 3019-3049.

Laurent, S.; Henoumont, C.; Vander Elst, L.; Muller, R. N. Synthesis and Physicochemical Characterisation of Gd-DTPA Derivatives as Contrast Agents for MRI. *Eur. J. Inorg. Chem.* **2012**, 2012, 1889-1915.

Lee, M.-H.; O, T.-S. Carbon-13 and Vanadium-51 Nuclear Magnetic Resonance Studies of Vanadium(v)-Aminopolycarboxylic Acids (I). *J. Korean Chem. Soc.* **1983**, 27, 117-126.

Li, P.; Hong, Y.; Feng, H.; Li, S. F. Y. An efficient "off-on" carbon nanoparticle-based fluorescent sensor for recognition of chromium(vi) and ascorbic acid based on the inner filter effect. *J. Mater. Chem. B* **2017**, 5, 2979-2988.

Li, S.; Wang, F.; He, X.-W.; Li, W.-Y.; Zhang, Y.-K. One-pot hydrothermal preparation of gadolinium-doped silicon nanoparticles as a dual-modal probe for multicolor fluorescence and magnetic resonance imaging. *J. Mater. Chem. B* **2018**, 6, 3358-3365.

Li, W.; Zhao, D. Extension of the Stöber Method to Construct Mesoporous SiO<sub>2</sub> and TiO<sub>2</sub> Shells for Uniform Multifunctional Core–Shell Structures. *Adv. Mater.* **2013**, 25, 142-149.

Li, X.; Wang, S.; Liu, Y.; Jiang, L.; Song, B.; Li, M.; Zeng, G.; Tan, X.; Cai, X.; Ding, Y. Adsorption of Cu(II), Pb(II), and Cd(II) Ions from Acidic Aqueous Solutions by Diethylenetriaminepentaacetic Acid-Modified Magnetic Graphene Oxide. *J. Chem. Eng. Data* **2017**, 62, 407-416.

Li, Y.; Gao, Q.; Zhang, L.; Zhou, Y.; Zhong, Y.; Ying, Y.; Zhang, M.; Huang, C.; Wang, Y. a. H<sub>5</sub>PV<sub>2</sub>Mo<sub>10</sub>O<sub>40</sub> encapsulated in MIL-101(Cr): facile synthesis and characterization of rationally designed composite materials for efficient decontamination of sulfur mustard. *Dalton Trans.* **2018**, 47, 6394-6403.

Li, Z.; Wu, S.; Zheng, D.; Liu, H.; Hu, J.; Su, H.; Sun, J.; Wang, X.; Huo, Q.; Guan, J.; Kan, Q. Enhanced alkenes epoxidation reactivity of discrete bis(8-quinolinol)oxovanadium(IV) or bis(8-quinolinol)dioxomolybdenum(VI) tethered to graphene oxide by a metal-template/metal-exchange method. *Appl. Catal. A* **2014**, 470, 104-114.

Licini, G.; Zonta, C. Revisiting the Hammett  $\rho$  Parameter for the Determination of Philicity: Nucleophilic Substitution with Inverse Charge Interaction. *Angew. Chem.* **2013**, *125*, 2983-2986.

Liu, F.; Lu, Q.; Jiao, X.; Chen, D. Fabrication of nylon-6/POMs nanofibrous membranes and the degradation of mustard stimulant research. *RSC Adv.* **2014**, *4*, 41271-41276.

Liu, M.; Wang, H.; Zeng, H.; Li, C.-J. Silver(I) as a widely applicable, homogeneous catalyst for aerobic oxidation of aldehydes toward carboxylic acids in water—"silver mirror": From stoichiometric to catalytic. *Sci. Adv.* **2015**, *1*.

Liu, M.; Xu, W.; Xu, L.-j.; Zhong, G.-r.; Chen, S.-l.; Lu, W.-y. Synthesis and Biological Evaluation of Diethylenetriamine Pentaacetic acid–Polyethylene Glycol–Folate: A New Folate-Derived,  $^{99m}\text{Tc}$ -Based Radiopharmaceutical. *Bioconjugate Chem.* **2005**, *16*, 1126-1132.

Liu, P.; Boyle, A. J.; Lu, Y.; Adams, J.; Chi, Y.; Reilly, R. M.; Winnik, M. A. Metal-Chelating Polymers (MCPs) with Zwitterionic Pendant Groups Complexed to Trastuzumab Exhibit Decreased Liver Accumulation Compared to Polyanionic MCP Immunoconjugates. *Biomacromolecules* **2015**, *16*, 3613-3623.

Liu, S.; Edwards, D. S. Bifunctional Chelators for Therapeutic Lanthanide Radiopharmaceuticals. *Bioconjugate Chem.* **2001**, *12*, 7-34.

Liu, Y.; Fu, R.; Sun, Y.; Zhou, X.; Baig, S. A.; Xu, X. Multifunctional nanocomposites  $\text{Fe}_3\text{O}_4@ \text{SiO}_2$ -EDTA for Pb(II) and Cu(II) removal from aqueous solutions. *Applied Surface Science* **2016**, *369*, 267-276.

Liu, Y.; Zhang, N. Gadolinium loaded nanoparticles in theranostic magnetic resonance imaging. *Biomaterials* **2012**, *33*, 5363-5375.

Livingston, S. R.; Kumar, D.; Landry, C. C. Oxidation of 2-chloroethyl ethyl sulfide using V-APMS. *J. Mol. Catal. A: Chem.* **2008**, *283*, 52-59.

Livingston, S. R.; Landry, C. C. Oxidation of a Mustard Gas Analogue Using an Aldehyde/O<sub>2</sub> System Catalyzed by V-Doped Mesoporous Silica. *J. Am. Chem. Soc.* **2008**, *130*, 13214-13215.

Lohrke, J.; Frenzel, T.; Endrikat, J.; Alves, F. C.; Grist, T. M.; Law, M.; Lee, J. M.; Leiner, T.; Li, K.-C.; Nikolaou, K.; Prince, M. R.; Schild, H. H.; Weinreb, J. C.; Yoshikawa, K.; Pietsch, H. 25 Years of Contrast-Enhanced MRI: Developments, Current Challenges and Future Perspectives. *Adv. Ther.* **2016**, *33*, 1-28.

Long, D.-L.; Tsunashima, R.; Cronin, L. Polyoxometalates: Building Blocks for Functional Nanoscale Systems. *Angew. Chem. Int. Ed.* **2010**, *49*, 1736-1758.

Lottermoser, B. G. Colonisation of the rehabilitated Mary Kathleen uranium mine site (Australia) by *Calotropis procera*: Toxicity risk to grazing animals. *J. Geochem. Explor.* **2011**, *111*, 39-46.

Lowell, S.; Shields, J. E.; Thomas, M. A.; Thommes, M., *Characterization of Porous Solids and Powders: Surface Area, Pore Size and Density*. Kluwer Academic Publishers: Dordrecht, The Netherlands, 2004; p 347.

Lu, Y.; Ngo Ndjock Mbong, G.; Liu, P.; Chan, C.; Cai, Z.; Weinrich, D.; Boyle, A. J.; Reilly, R. M.; Winnik, M. A. Synthesis of Polyglutamide-Based Metal-Chelating Polymers and Their Site-Specific Conjugation to Trastuzumab for Auger Electron Radioimmunotherapy. *Biomacromolecules* **2014**, *15*, 2027-2037.

Macchi, P.; Schultz, A. J.; Larsen, F. K.; Iversen, B. B. Experimental and Theoretical Electron Density Study of the Peroxo Function in Oxoperoxo(pyridine-2,6-dicarboxylato)(hexamethylphosphoramidate)molybdenum(VI): Implications for Olefin Epoxidation by Peroxo Transition Metal Complexes. *J. Phys. Chem. A* **2001**, *105*, 9231-9242.

Madadrang, C. J.; Kim, H. Y.; Gao, G.; Wang, N.; Zhu, J.; Feng, H.; Gorring, M.; Kasner, M. L.; Hou, S. Adsorption Behavior of EDTA-Graphene Oxide for Pb (II) Removal. *ACS Appl. Mater. Interfaces* **2012**, *4*, 1186-1193.

Mahato, T. H.; Prasad, G. K.; Singh, B.; Srivastava, A. R.; Ganesan, K.; Acharya, J.; Vijayaraghavan, R. Reactions of sulphur mustard and sarin on  $V_{1.02}O_{2.98}$  nanotubes. *J. Hazard. Mater.* **2009**, *166*, 1545-1549.

Majlesi, K.; Rezaiejad, S.; Balali, S. Speciation and Stability of Dioxovanadium(V) Complexes with Diethylenetriaminepentaacetic Acid at Different Ionic Strengths. *J. Solution Chem.* **2013**, *42*, 1729-1747.

Marrs, T. C.; Maynard, R. L.; Sidell, F. R., *Chemical Warfare Agents: Toxicology and Treatment*. John Wiley & Sons: New York, 1996; p 243.

Martan, M.; Manassen, J.; Vofsi, D. Liquid Phase Oxidation of 1, 4 and 1, 2-Dihydronaphthalene. *Isr. J. Chem.* **1969**, *7*, 751-767.

Mastrorilli, P.; Nobile, C. F. Catalytic activity of a polymerizable tris( $\beta$ -ketoesterate)iron(III) complex towards the oxidation of organic substrates. *Tetrahedron Lett.* **1994**, *35*, 4193-4196.

Matsuo, J.-i.; Takeuchi, K.; Ishibashi, H. Stereocontrolled Formal Synthesis of ( $\pm$ )-Platensimycin. *Org. Lett.* **2008**, *10*, 4049-4052.

Maurya, M. R.; Arya, A.; Kumar, A.; Pessoa, J. C. Polystyrene bound oxidovanadium(IV) and dioxidovanadium(V) complexes of histamine derived ligand for the oxidation of methyl phenyl sulfide, diphenyl sulfide and benzoin. *Dalton Trans.* **2009**, 2185-2195.

Maurya, M. R.; Bisht, M.; Avecilla, F. Synthesis, characterization and catalytic activities of vanadium complexes containing ONN donor ligand derived from 2-aminoethylpyridine. *J. Mol. Catal. A: Chem.* **2011**, *344*, 18-27.

Maurya, M. R.; Kumar, A.; Costa Pessoa, J. Vanadium complexes immobilized on solid supports and their use as catalysts for oxidation and functionalization of alkanes and alkenes. *Coord. Chem. Rev.* **2011**, *255*, 2315-2344.

Mimoun, H. Oxygen Transfer from Inorganic and Organic Peroxides to Organic Substrates: A Common Mechanism? *Angew. Chem. Int. Ed. Engl.* **1982**, *21*, 734-750.

Mimoun, H.; Saussine, L.; Daire, E.; Postel, M.; Fischer, J.; Weiss, R. Vanadium(V) peroxy complexes. New versatile biomimetic reagents for epoxidation of olefins and hydroxylation of alkanes and aromatic hydrocarbons. *J. Am. Chem. Soc.* **1983**, *105*, 3101-3110.

Mimoun, H.; Sere de Roch, I.; Sajus, L. Epoxydation des olefines par les complexes peroxydiques covalents du molybdene—VI. *Tetrahedron* **1970**, *26*, 37-50.

Mirzaee, M.; Bahramian, B.; Gholizadeh, J.; Feizi, A.; Gholami, R. Acetylacetonate complexes of vanadium and molybdenum supported on functionalized boehmite nanoparticles for the catalytic epoxidation of alkenes. *Chem. Eng. J.* **2017**, *308*, 160-168.

Modi, C. K.; Vithalani, R. S.; Patel, D. S.; Som, N. N.; Jha, P. K. Zeolite-Y entrapped metallo-pyrazolone complexes as heterogeneous catalysts: Synthesis, catalytic aptitude and computational investigation. *Microporous Mesoporous Mater.* **2018**, *261*, 275-285.

Monfared, H. H.; Abbasi, V.; Rezaei, A.; Ghorbanloo, M.; Aghaei, A. A heterogenized vanadium oxo-aryldiazine catalyst for efficient and selective oxidation of hydrocarbons with hydrogen peroxide. *Transition Met. Chem.* **2012**, *37*, 85-92.

Murata, S.; Murata, K.; Kidena, K.; Nomura, M. A Novel Oxidative Desulfurization System for Diesel Fuels with Molecular Oxygen in the Presence of Cobalt Catalysts and Aldehydes. *Energy Fuels* **2004**, *18*, 116-121.

Nam, W.; Kim, H. J.; Kim, S. H.; Ho, R. Y. N.; Valentine, J. S. Metal Complex-Catalyzed Epoxidation of Olefins by Dioxygen with Co-Oxidation of Aldehydes. A Mechanistic Study. *Inorg. Chem.* **1996**, *35*, 1045-1049.

Nassivera, T.; Eklund, A. G.; Landry, C. C. Size-exclusion chromatography of low-molecular-mass polymers using mesoporous silica. *J. Chromatogr. A* **2002**, *973*, 97-101.

Neațu, Ș.; Pârvulescu, V. I.; Epure, G.; Preda, E.; Șomoghi, V.; Damin, A.; Bordiga, S.; Zecchina, A. Photo-degradation of yperite over V, Fe and Mn-doped titania-silica photocatalysts. *Phys. Chem. Chem. Phys.* **2008**, *10*, 6562-6570.

Neese, F. The ORCA program system. *Wiley Interdiscip. Rev.: Comput. Mol. Sci.* **2012**, *2*, 73-78.

Negi, S. S.; Sivaranjani, K.; Singh, A. P.; Gopinath, C. S. Disordered mesoporous V/TiO<sub>2</sub> system for ambient oxidation of sulfides to sulfoxides. *Appl. Catal., A* **2013**, *452*, 132-138.

Neu, H. M.; Yang, T.; Baglia, R. A.; Yosca, T. H.; Green, M. T.; Quesne, M. G.; de Visser, S. P.; Goldberg, D. P. Oxygen-Atom Transfer Reactivity of Axially Ligated Mn(V)–Oxo Complexes: Evidence for Enhanced Electrophilic and Nucleophilic Pathways. *J. Am. Chem. Soc.* **2014**, *136*, 13845-13852.

Neumann, R.; Levin-Elad, M. Vanadium silicate xerogels in hydrogen peroxide catalyzed oxidations. *Appl. Catal. A* **1995**, *122*, 85-97.

Nikoorazm, M.; Ghorbani-Choghamarani, A.; Noori, N. Oxo-vanadium(IV) Schiff base complex supported on modified MCM-41: a reusable and efficient catalyst for the oxidation of sulfides and oxidative S–S coupling of thiols. *Appl. Organomet. Chem.* **2015**, *29*, 328-333.

Noori, N.; Nikoorazm, M.; Ghorbani-Choghamarani, A. Oxo-vanadium immobilized on L-cysteine-modified MCM-41 as catalyst for the oxidation of sulfides and oxidative coupling of thiols. *Microporous Mesoporous Mater.* **2016**, *234*, 166-175.

Norouzi, M.; Ghorbani-Choghamarani, A. Mild and highly efficient method for the oxidation of sulfides and protection of alcohols catalyzed by oxovanadium(IV) supported on modified magnetic nanoparticles as recyclable catalyst. *React. Kinet., Mech. Catal.* **2016**, *119*, 537-554.

Nunes, C. D.; Vaz, P. D.; Felix, V.; Veiros, L. F.; Moniz, T.; Rangel, M.; Realista, S.; Mourato, A. C.; Calhorda, M. J. Vanadyl cationic complexes as catalysts in olefin oxidation. *Dalton Trans.* **2015**, *44*, 5125-5138.

Okemoto, A.; Ueyama, K.; Taniya, K.; Ichihashi, Y.; Nishiyama, S. Direct oxidation of benzene with molecular oxygen in liquid phase catalysed by heterogeneous copper complexes encapsulated in Y-type zeolite. *Catal. Commun.* **2017**, *100*, 29-32.

Ottenbacher, R. V.; Samsonenko, D. G.; Talsi, E. P.; Bryliakov, K. P. Enantioselective Epoxidations of Olefins with Various Oxidants on Bioinspired Mn Complexes: Evidence for Different Mechanisms and Chiral Additive Amplification. *ACS Catal.* **2016**, *6*, 979-988.

Pacigová, S.; Gyepes, R.; Tatiersky, J.; Sivák, M. Interpretation of the multiple vanadium-oxygen bonds in the central VO( $\eta^2$ -O<sub>2</sub>)<sup>+</sup> group. Synthesis, structure, supramolecular interactions and DFT studies for complexes with 2,2'-bipyridine, 1,10-phenanthroline, pyrazinato(1<sup>-</sup>) and pyrazinamide ligands. *Dalton Trans.* **2008**, 121-130.

Palmer, G., Electron Paramagnetic Resonance of Metalloproteins. In *Physical Methods in Bioinorganic Chemistry Spectroscopy and Magnetism*, Que, L., Ed. University Science Books: Sausalito, CA, 2000; pp 121-185.

Pang, J.; Zhao, L.; Zhang, L.; Li, Z.; Luan, Y. Folate-conjugated hybrid SBA-15 particles for targeted anticancer drug delivery. *J. Colloid Interface Sci.* **2013**, 31-39.

Parida, K. M.; Singha, S.; Sahoo, P. C. A facile method for promoting activities of vanadium-schiffbase complex anchored on organically modified MCM-41 in epoxidation reaction. *J. Mol. Catal. A: Chem.* **2010**, *325*, 40-47.

Parker Siburt, C. J.; Lin, E. M.; Brandt, S. J.; Tinoco, A. D.; Valentine, A. M.; Crumbliss, A. L. Redox potentials of Ti(IV) and Fe(III) complexes provide insights into titanium biodistribution mechanisms. *J. Inorg. Biochem.* **2010**, *104*, 1006-1009.

Petrenko, T.; Sturhahn, W.; Neese, F. First-principles calculation of nuclear resonance vibrational spectra. *Hyperfine Interactions* **2007**, *175*, 165-174.

Petrucci, M. G. L.; Kakkar, A. K. Heterogenizing homogeneous catalysis. *Adv. Mater.* **1996**, *8*, 251-253.

Pinto, E.; Almeida, A. A.; Ferreira, I. M. P. L. V. O. Assessment of metal(loid)s phytoavailability in intensive agricultural soils by the application of single extractions to rhizosphere soil. *Ecotoxicol. Environ. Saf.* **2015**, *113*, 418-424.

Pniok, M.; Kubíček, V.; Havlíčková, J.; Kotek, J.; Sabatie-Gogová, A.; Plutnar, J.; Huclier-Markai, S.; Hermann, P. Thermodynamic and Kinetic Study of Scandium(III)

Complexes of DTPA and DOTA: A Step Toward Scandium Radiopharmaceuticals. *Chem. - Eur. J.* **2014**, *20*, 7944-7955.

Pokutsa, A.; Kubaj, Y.; Zaborovskyi, A.; Sobkowiak, A.; Muzart, J. Oxalic acid-improved mild cyclohexane oxidation catalyzed by VO(acac)<sub>2</sub>: non-radical versus radical mechanism. *React. Kinet., Mech. Catal.* **2017**, *122*, 757-774.

Połosak, M.; Piotrowska, A.; Krajewski, S.; Bilewicz, A. Stability of <sup>47</sup>Sc-complexes with acyclic polyamino-polycarboxylate ligands. *J. Radioanal. Nucl. Chem.* **2013**, *295*, 1867-1872.

Pourmanouchehri, Z.; Jafarzadeh, M.; Kakaei, S.; Khameneh, E. S. Magnetic Nanocarrier Containing <sup>68</sup>Ga-DTPA Complex for Targeted Delivery of Doxorubicin. *J. Inorg. Organomet. Polym. Mater.* **2018**, *28*, 1980-1990.

Pozdniakova, S. Speciation of metals in different oxidation states by capillary electrophoresis using pre-capillary complexation with complexones. *Analyst* **1998**, *123*, 1497-1500.

Prasad, G. K. Decontamination of 2 chloro ethyl phenyl sulphide using mixed metal oxide nanocrystals. *J. Sci. Ind. Res.* **2010**, *69*, 835-840.

Prasad, M. R.; Madhavi, G.; Rao, A. R.; Kulkarni, S. J.; Raghavan, K. V. Synthesis, characterization of high Ti-containing Ti-MCM-41 catalysts and their activity evaluation in oxidation of cyclohexene and epoxidation of higher olefins. *J. Porous Mater.* **2006**, *13*, 81-94.

Ramacharyulu, P. V. R. K.; Praveen Kumar, J.; Prasad, G. K.; Singh, B.; Sreedhar, B.; Dwivedi, K. Sunlight assisted photocatalytic detoxification of sulfur mustard on vanadium ion doped titania nanocatalysts. *J. Mol. Catal. A: Chem.* **2014**, *387*, 38-44.

Ramakrishna, C.; Krishna, R.; Saini, B.; Gopi, T.; Swetha, G.; Chandra Shekar, S. A simple and controlled oxidative decontamination of sulfur mustard and its simulants using ozone gas. *Phosphorus Sulfur Silicon Relat Elem* **2016**, *191*, 965-970.

Rao, T. V.; Sain, B.; Kumar, K.; Murthy, P. S.; Rao, T. S. R. P.; Joshi, G. C. Oxidation of Sulphides by Molecular Oxygen - Aldehyde System in the Absence of Metal Catalyst. *Synth. Commun.* **1998**, *28*, 319-326.

Rayati, S.; Koliaei, M.; Ashouri, F.; Mohebbi, S.; Wojtczak, A.; Kozakiewicz, A. Oxovanadium(IV) Schiff base complexes derived from 2,2'-dimethylpropanediamine: A homogeneous catalyst for cyclooctene and styrene oxidation. *Appl. Catal. A* **2008**, *346*, 65-71.

Rehder, D., *Bioinorganic vanadium chemistry*. John Wiley & Sons: West Sussex, England, 2008; Vol. 30.

Rehder, D.; Ebel, M.; Wikete, C.; Santoni, G.; Gätjens, J. Modeling the active site structures of vanadate-dependent peroxidases and vanadate-inhibited phosphatases. In *Pure Appl. Chem.*, 2005; Vol. 77, p 1607.

Ringenbach, C. R.; Livingston, S. R.; Kumar, D.; Landry, C. C. Vanadium-Doped Acid-Prepared Mesoporous Silica: Synthesis, Characterization, and Catalytic Studies on the Oxidation of a Mustard Gas Analogue. *Chem. Mater.* **2005**, *17*, 5580-5586.

Romanowski, G. Synthesis, characterization and catalytic activity in the oxidation of sulfides and styrene of vanadium(V) complexes with tridentate Schiff base ligands. *J. Mol. Catal. A: Chem.* **2013**, *368-369*, 137-144.

Romanowski, G.; Kira, J.; Wera, M. Five- and six-coordinate vanadium(V) complexes with tridentate Schiff base ligands derived from S(+)-isoleucinol: Synthesis, characterization and catalytic activity in the oxidation of sulfides and olefins. *Polyhedron* **2014**, *67*, 529-539.

Romanowski, G.; Kira, J.; Wera, M. Vanadium(V) complexes with chiral tridentate Schiff base ligands derived from 1S,2R(+)-2-amino-1,2-diphenylethanol and with acetohydroxamate co-ligand: Synthesis, characterization and catalytic activity in the oxidation of prochiral sulfides and olefins. *J. Mol. Catal. A: Chem.* **2014**, *381*, 148-160.

Roosen, J.; Van Roosendaal, S.; Borra, C. R.; Van Gerven, T.; Mullens, S.; Binnemans, K. Recovery of scandium from leachates of Greek bauxite residue by adsorption on functionalized chitosan-silica hybrid materials. *Green Chem.* **2016**, *18*, 2005-2013.

Roy, A.; Srivastava, A. K.; Singh, B.; Shah, D.; Mahato, T. H.; Srivastava, A. Kinetics of degradation of sulfur mustard and sarin simulants on HKUST-1 metal organic framework. *Dalton Trans.* **2012**, *41*, 12346-12348.

Salavati, H.; Teimouri, A. Efficient Epoxidation of Alkenes with Hydrogen Peroxide and Electrochemical Behavior in Water Over Heteropolymolybdate/Silica Nanocomposite. *Int. J. Electrochem. Sci.* **2017**, *12*, 7829-7843.

Salavati-Niasari, M.; Badiei, A.; Saberyan, K. Oxovanadium(IV) salophen complex covalently anchored to multi-wall carbon nanotubes (MWNTs) as heterogeneous catalyst for oxidation of cyclooctene. *Chem. Eng. J.* **2011**, *173*, 651-658.

Sams, C. K.; Jorgensen, K. A. Mechanistic Aspects of Vanadium-Catalysed Oxygen Transfer Reactions. *Acta Chem. Scand.* **1995**, *49*, 839-839.

Schneider, C. J.; Zampella, G.; Greco, C.; Pecoraro, V. L.; De Gioia, L. Mechanistic Analysis of Nucleophilic Substrates Oxidation by Functional Models of Vanadium-Dependent Haloperoxidases: A Density Functional Theory Study. *Eur. J. Inorg. Chem.* **2007**, *2007*, 515-523.

Selvaraj, M.; Song, S. W.; Kawi, S. Epoxidation of styrene over mesoporous Zr–Mn-MCM-41. *Microporous Mesoporous Mater.* **2008**, *110*, 472-479.

Serre, C.; Millange, F.; Thouvenot, C.; Noguès, M.; Marsolier, G.; Louër, D.; Férey, G. Very Large Breathing Effect in the First Nanoporous Chromium(III)-Based Solids: MIL-53 or  $\text{Cr}^{\text{III}}(\text{OH}) \cdot \{\text{O}_2\text{C}-\text{C}_6\text{H}_4-\text{CO}_2\} \cdot \{\text{HO}_2\text{C}-\text{C}_6\text{H}_4-\text{CO}_2\text{H}\}_x \cdot \text{H}_2\text{O}_y$ . *J. Am. Chem. Soc.* **2002**, *124*, 13519-13526.

Shao, D.; Li, Y. Preparation of polycarboxylic acid-functionalized silica supported Pt catalysts and their applications in alkene hydrosilylation. *RSC Adv.* **2018**, *8*, 20379-20393.

Sharpless, K. B.; Michaelson, R. C. High stereo- and regioselectivities in the transition metal catalyzed epoxidations of olefinic alcohols by tert-butyl hydroperoxide. *J. Am. Chem. Soc.* **1973**, *95*, 6136-6137.

Sharpless, K. B.; Townsend, J. M.; Williams, D. R. Mechanism of epoxidation of olefins by covalent peroxides of molybdenum(VI). *J. Am. Chem. Soc.* **1972**, *94*, 295-296.

Sheldon, R. A.; Kochi, J. K., *Metal-Catalyzed Oxidations of Organic Compounds: Mechanistic Principles and Synthetic Methodology Including Biochemical Processes*. Academic Press, Inc: New York, NY, 1981.

Shen, C.; Qiao, J.; Zhao, L.; Zheng, K.; Jin, J.; Zhang, P. An efficient silica supported Chitosan@vanadium catalyst for asymmetric sulfoxidation and its application in the synthesis of esomeprazole. *Catal. Commun.* **2017**, *92*, 114-118.

Shkrob, I. A.; Marin, T. W.; Jensen, M. P. Ionic Liquid Based Separations of Trivalent Lanthanide and Actinide Ions. *Ind. Eng. Chem. Res.* **2014**, *53*, 3641-3653.

Sing, K. S. W.; Everett, D. H.; Haul, R. A. W.; Moscou, L.; Pierotti, R. A.; Rouquerol, J.; Siemieniewska, T. Reporting Physisorption Data for Gas/Solid Systems With Special Reference to the Determination of Surface Area and Porosity. *Pure Appl. Chem.* **1985**, *57*, 603-619.

Singh, B.; Mahato, T. H.; Srivastava, A. K.; Prasad, G. K.; Ganesan, K.; Vijayaraghavan, R.; Jain, R. Significance of porous structure on degradation of 2,2'-dichloro diethyl sulphide and 2-chloroethyl ethyl sulphide on the surface of vanadium oxide nanostructure. *J. Hazard. Mater.* **2011**, *190*, 1053-1057.

Smith, T. S.; Pecoraro, V. L. Oxidation of Organic Sulfides by Vanadium Haloperoxidase Model Complexes. *Inorg. Chem.* **2002**, *41*, 6754-6760.

Solberg, S.; Landry, C. Adsorption of DNA into Mesoporous Silica. *J. Phys. Chem. B* **2006**, *110*, 15261-15268.

Song, G.; Wang, F.; Zhang, H.; Lu, X.; Wang, C. Efficient Oxidation of Sulfides Catalyzed by Transition Metal Salts with Molecular Oxygen in the Presence of Aldehydes. *Synth. Commun.* **1998**, *28*, 2783-2787.

Sorensen, A. C.; Fuller, B. L.; Eklund, A. G.; Landry, C. C. Mo-Doped Mesoporous Silica for Thiophene Hydrodesulfurization: Comparison of Materials and Methods. *Chem. Mater.* **2004**, *16*, 2157-2164.

Sorensen, A. C.; Landry, C. C. Complete reduction of 2-chloroethylethylsulfide by hydrodesulfurization using mo-doped mesoporous substrates. *Catal. Lett.* **2005**, *100*, 135-138.

Steinbacher, J. L.; Lathrop, S. A.; Cheng, K.; Hillegass, J. M.; Butnor, K. J.; Kauppinen, R. A.; Mossman, B. T.; Landry, C. C. Gd-Labeled Microparticles in MRI: In vivo Imaging of Microparticles After Intraperitoneal Injection. *Small* **2010**, *6*, 2678-2682.

Stöber, W.; Fink, A.; Bohn, E. Controlled growth of monodisperse silica spheres in the micron size range. *J. Colloid Interface Sci.* **1968**, *26*, 62-69.

Stoll, S.; Schweiger, A. EasySpin, a comprehensive software package for spectral simulation and analysis in EPR. *J. Magn. Reson.* **2006**, *178*, 42-55.

Stomberg, R. The Crystal Structures of Potassium Bis (oxalato) oxoperoxovanadate (V) Hemihydrate,  $K_3 [VO(O_2)(C_2O_4)_2] \cdot \frac{1}{2} H_2O$ , and Potassium Bis (oxalato) dioxovanadate (V) Trihydrate  $K_3 [VO_2(C_2O_4)_2] \cdot 3H_2O$ . *Acta Chem. Scand.* **1986**, *40*, 168-176.

Stone, H.; See, D.; Smiley, A.; Ellingson, A.; Schimmoeller, J.; Oudejans, L. Surface decontamination for blister agents Lewisite, sulfur mustard and agent yellow, a Lewisite and sulfur mustard mixture. *J. Hazard. Mater.* **2016**, *314*, 59-66.

Sutradhar, M.; Martins, L. M. D. R. S.; Guedes da Silva, M. F. C.; Pombeiro, A. J. L. Vanadium complexes: Recent progress in oxidation catalysis. *Coord. Chem. Rev.* **2015**, *301-302*, 200-239.

Suzuki, M.; Ishikawa, T.; Harada, A.; Ohba, S.; Sakamoto, M.; Nishida, Y. Chemical mechanism of dioxygen activation by manganese(III) Schiff base compound in the presence of aliphatic aldehydes. *Polyhedron* **1997**, *16*, 2553-2561.

Tada, M.; Muratsugu, S.; Kinoshita, M.; Sasaki, T.; Iwasawa, Y. Alternative Selective Oxidation Pathways for Aldehyde Oxidation and Alkene Epoxidation on a SiO<sub>2</sub>-Supported Ru–Monomer Complex Catalyst. *J. Am. Chem. Soc.* **2010**, *132*, 713-724.

Takehira, K.; Hayakawa, T.; Ishikawa, T. Heterogeneous Catalysis in the Liquid-phase Oxidation of Olefins. IV. The Activity of a Supported Vanadium or Chromium Oxide Catalyst in the Decomposition of t-Butyl Hydroperoxide. *Bull. Chem. Soc. Jpn.* **1980**, *53*, 2103-2110.

Talukdar, D.; Sharma, K.; Bharadwaj, S. K.; Thakur, A. J. VO(acac)<sub>2</sub>: An Efficient Catalyst for the Oxidation of Aldehydes to the Corresponding Acids in the Presence of Aqueous H<sub>2</sub>O<sub>2</sub>. *Synlett* **2013**, *24*, 963-966.

Tamoradi, T.; Ghadermazi, M.; Ghorbani-Choghamarani, A.; Molaei, S. Synthesis and characterization of oxo-vanadium complex anchored onto SBA-15 as a green, novel and reusable nanocatalyst for the oxidation of sulfides and oxidative coupling of thiols. *Res. Chem. Intermed.* **2018**.

Tanaka, T.; Ooe, M.; Funabiki, T.; Yoshida, S. Formation of an epoxide intermediate in the photo-oxidation of alkenes over silica-supported vanadium oxide. *J. Chem. Soc., Faraday Trans. 1* **1986**, *82*, 35-43.

Tangestaninejad, S.; Mirkhani, V.; Moghadam, M.; Mohammadpoor-Baltork, I.; Shams, E.; Salavati, H. Hydrocarbon oxidation catalyzed by vanadium polyoxometalate supported on mesoporous MCM-41 under ultrasonic irradiation. *Ultrason. Sonochem.* **2008**, *15*, 438-447.

ten Brink, H. B.; Tuynman, A.; Dekker, H. L.; Hemrika, W.; Izumi, Y.; Oshiro, T.; Schoemaker, H. E.; Wever, R. Enantioselective Sulfoxidation Catalyzed by Vanadium Haloperoxidases. *Inorg. Chem.* **1998**, *37*, 6780-6784.

Thomas, J. M. Handbook Of Heterogeneous Catalysis. 2., completely revised and enlarged Edition. Vol. 1–8. Edited by G. Ertl, H. Knözinger, F. Schüth, and J. Weitkamp. *Angew. Chem. Int. Ed.* **2009**, *48*, 3390-3391.

Thommes, M. Physical Adsorption Characterization of Nanoporous Materials. *Chem. Ing. Tech.* **2010**, *82*, 1059-1073.

Thornburg, N. E.; Thompson, A. B.; Notestein, J. M. Periodic Trends in Highly Dispersed Groups IV and V Supported Metal Oxide Catalysts for Alkene Epoxidation with H<sub>2</sub>O<sub>2</sub>. *ACS Catal.* **2015**, *5*, 5077-5088.

Tian, G.; Zhang, Z.; Martin, L. R.; Rao, L. Complexation of Curium(III) with DTPA at 10–70 °C: Comparison with Eu(III)–DTPA in Thermodynamics, Luminescence, and Coordination Modes. *Inorg. Chem.* **2015**, *54*, 1232-1239.

Tsadilas, C. D.; Shaheen, S. M. Distribution of Total and Ammonium Bicarbonate-DTPA-Extractable Soil Vanadium From Greece and Egypt and Their Correlation To Soil Properties. *Soil Sci.* **2010**, *175*, 535-543.

Tyagi, S.; Cook, C. D.; DiDonato, D. A.; Key, J. A.; McKillican, B. P.; Eberle, W. J.; Carlin, T. J.; Hunt, D. A.; Marshall, S. J.; Bow, N. L. Bioinspired Synthesis of a Sedaxane Metabolite Using Catalytic Vanadyl Acetylacetonate and Molecular Oxygen. *J. Org. Chem.* **2015**, *80*, 11941-11947.

Uematsu, T.; Ogasawara, Y.; Suzuki, K.; Yamaguchi, K.; Mizuno, N. Platinum-supporting hollandite-type vanadium-chromium mixed oxides as efficient heterogeneous catalysts for deoxygenation of sulfoxides under atmospheric H<sub>2</sub> pressure. *Catal. Sci. Technol.* **2017**, *7*, 1912-1920.

Ullattil, S. G.; Periyat, P., Sol-Gel Synthesis of Titanium Dioxide. In *Sol-Gel Materials for Energy, Environment and Electronic Applications*, Pillai, S. C.; Hehir, S., Eds. Springer International Publishing: Cham, 2017; pp 271-283.

Vafaei, M.; Amini, M. M.; Najafi, E.; Sadeghi, O.; Amani, V. Modified nanoporous silicas for oral delivery of the water insoluble organotin compound: loading and release of methylphenyltin dichloride as an anti-tumor drug model. *J. Sol-Gel Sci. Technol.* **2012**, *64*, 411-417.

Vandichel, M.; Leus, K.; Van Der Voort, P.; Waroquier, M.; Van Speybroeck, V. Mechanistic insight into the cyclohexene epoxidation with VO(acac)<sub>2</sub> and tert-butyl hydroperoxide. *J. Catal.* **2012**, *294*, 1-18.

Vincent, S.; Lion, C.; Hedayatullah, M.; Challier, A.; Delmas, G.; Magnaud, G. Selective Oxidation of Sulfides to Sulfoxides by Atmospheric Oxygen and Aldehyde Catalysed by Ni<sup>II</sup> Complexes. *Phosphorus Sulfur Silicon Relat Elem* **1994**, *92*, 189-192.

Waidmann, C. R.; DiPasquale, A. G.; Mayer, J. M. Synthesis and Reactivity of Oxo-Peroxy-Vanadium(V) Bipyridine Compounds. *Inorg. Chem.* **2010**, *49*, 2383-2391.

Wang, K.; Niu, Y.; Zhao, D.; Zhao, Y.; Ma, P.; Zhang, D.; Wang, J.; Niu, J. The Polyoxovanadate-Based Carboxylate Derivative K<sub>6</sub>H[V<sup>V</sup><sub>17</sub>V<sup>IV</sup><sub>12</sub>(OH)<sub>4</sub>O<sub>60</sub>(OOC(CH<sub>2</sub>)<sub>4</sub>COO)<sub>8</sub>]·nH<sub>2</sub>O: Synthesis, Crystal Structure, and Catalysis for Oxidation of Sulfides. *Inorg. Chem.* **2017**, *56*, 14053-14059.

Wang, Q.-Q.; Begum, R. A.; Day, V. W.; Bowman-James, K. Sulfur, oxygen, and nitrogen mustards: stability and reactivity. *Org. Biomol. Chem.* **2012**, *10*, 8786-8793.

Wang, X.; Ma, X.; Song, C.; Locke, D. R.; Siefert, S.; Winans, R. E.; Möllmer, J.; Lange, M.; Möller, A.; Gläser, R. Molecular basket sorbents polyethylenimine–SBA-15 for CO<sub>2</sub> capture from flue gas: Characterization and sorption properties. *Microporous Mesoporous Mater.* **2013**, *169*, 103-111.

Weil, J. A.; Bolton, J. R.; Wertz, J. E., *Electron Paramagnetic Resonance: Elementary Theory and Practical Applications*. John Wiley & Sons, Inc: New York, NY, 1994.

Weinstock, I. A. Homogeneous-Phase Electron-Transfer Reactions of Polyoxometalates. *Chem. Rev.* **1998**, *98*, 113-170.

Wight, A. P.; Davis, M. E. Design and Preparation of Organic–Inorganic Hybrid Catalysts. *Chem. Rev.* **2002**, *102*, 3589-3614.

Wu, B.; Lu, S.-T.; Yu, H.; Liao, R.-F.; Li, H.; Lucie Zafitassimo, B. V.; Li, Y.-S.; Zhang, Y.; Zhu, X.-L.; Liu, H.-G.; Xu, H.-B.; Huang, S.-W.; Cheng, Z. Gadolinium-chelate functionalized bismuth nanotheranostic agent for in vivo MRI/CT/PAI imaging-guided photothermal cancer therapy. *Biomaterials* **2018**, *159*, 37-47.

- Wu, C.; Fan, W.; Chang, J. Functional mesoporous bioactive glass nanospheres: synthesis, high loading efficiency, controllable delivery of doxorubicin and inhibitory effect on bone cancer cells. *J. Mater. Chem. B* **2013**, *1*, 2710-2718.
- Wu, P.; Santoni, G.; Fröba, M.; Rehder, D. Modelling the Sulfoxxygenation Activity of Vanadate-Dependent Peroxidases. *Chem. Biodiversity* **2008**, *5*, 1913-1926.
- Yamabe, S.; Kondou, C.; Minato, T. A Theoretical Study of the Epoxidation of Olefins by Peracids. *J. Org. Chem.* **1996**, *61*, 616-620.
- Yamaura, T.; Kamata, K.; Yamaguchi, K.; Mizuno, N. Efficient sulfoxidation with hydrogen peroxide catalyzed by a divanadium-substituted phosphotungstate. *Catal. Today* **2013**, *203*, 76-80.
- Yang, B.; Liao, L.; Zeng, Y.; Zhu, X.; Wan, Y. A simple and recyclable copper/DTPA catalyst system for amination of aryl halides with aqueous ammonia in water. *Catal. Commun.* **2014**, *45*, 100-103.
- Yang, D.; Yang, G.; Gai, S.; He, F.; Lv, R.; Dai, Y.; Yang, P. Imaging-Guided and Light-Triggered Chemo-/Photodynamic/Photothermal Therapy Based on Gd (III) Chelated Mesoporous Silica Hybrid Spheres. *ACS Biomater. Sci. Eng.* **2016**, *2*, 2058-2071.
- Yao, X.; Peng, C.; Shi, Z. Reaction Mechanism for Selective Oxidation of Anethole to Anisaldehyde by Hydrogen Peroxide in Presence of Ferric Vanadate. *Asian J. Chem* **2014**, *26*.
- Yu, H.; Ru, S.; Zhai, Y.; Dai, G.; Han, S.; Wei, Y. An Efficient Aerobic Oxidation Protocol of Aldehydes to Carboxylic Acids in Water Catalyzed by an Inorganic-Ligand-Supported Copper Catalyst. *ChemCatChem* **2018**, *10*, 1253-1257.
- Yu, J.; Cui, Y.; Wu, C.; Yang, Y.; Wang, Z.; O'Keeffe, M.; Chen, B.; Qian, G. Second-Order Nonlinear Optical Activity Induced by Ordered Dipolar Chromophores Confined in the Pores of an Anionic Metal–Organic Framework. *Angew. Chem. Int. Ed.* **2012**, *51*, 10542-10545.

Zaera, F. Nanostructured materials for applications in heterogeneous catalysis. *Chem. Soc. Rev.* **2013**, *42*, 2746-2762.

Zampella, G.; Fantucci, P.; Pecoraro, V. L.; De Gioia, L. Reactivity of Peroxo Forms of the Vanadium Haloperoxidase Cofactor. A DFT Investigation. *J. Am. Chem. Soc.* **2005**, *127*, 953-960.

Zeng, Q.; Wang, H.; Weng, W.; Lin, W.; Gao, Y.; Huang, X.; Zhao, Y. Substituent effects and mechanism elucidation of enantioselective sulfoxidation catalyzed by vanadium Schiff base complexes. *New J. Chem.* **2005**, *29*, 1125-1127.

Zhang, C.; Wu, D.; Lu, L.; Duan, X.; Liu, J.; Xie, X.; Shuai, X.; Shen, J.; Cao, Z. Multifunctional Hybrid Liposome as a Theranostic Platform for Magnetic Resonance Imaging Guided Photothermal Therapy. *ACS Biomater. Sci. Eng.* **2018**, *4*, 2597-2605.

Zhang, C.; Zhang, F.; Wang, W.; Liu, J.; Xu, M.; Wu, D.; Shuai, X.; Shen, J.; Cao, Z. Chitosan coated gold nanorod chelating gadolinium for MRI-visible photothermal therapy of cancer. *RSC Adv.* **2016**, *6*, 111337-111344.

Zhang, J.; Yang, H.; Sun, T.; Chen, Z.; Yin, G. Nonredox Metal-Ions-Enhanced Dioxygen Activation by Oxidovanadium(IV) Complexes toward Hydrogen Atom Abstraction. *Inorg. Chem.* **2017**, *56*, 834-844.

Zhang, N.-n.; Yu, R.-s.; Xu, M.; Cheng, X.-y.; Chen, C.-m.; Xu, X.-l.; Lu, C.-y.; Lu, K.-j.; Chen, M.-j.; Zhu, M.-l.; Weng, Q.-y.; Hui, J.-g.; Zhang, Q.; Du, Y.-Z.; Ji, J.-s. Visual targeted therapy of hepatic cancer using homing peptide modified calcium phosphate nanoparticles loading doxorubicin guided by T1 weighted MRI. *Nanomedicine* **2018**, *14*, 2167-2178.

Zhao, A.; Samanta, A.; Sarkar, P.; Gupta, R. Carbon Dioxide Adsorption on Amine-Impregnated Mesoporous SBA-15 Sorbents: Experimental and Kinetics Study. *Ind. Eng. Chem. Res.* **2013**, *52*, 6480-6491.

Zhao, D.; Huo, Q.; Feng, J.; Chmelka, B. F.; Stucky, G. D. Nonionic Triblock and Star Diblock Copolymer and Oligomeric Surfactant Syntheses of Highly Ordered, Hydrothermally Stable, Mesoporous Silica Structures. *J. Am. Chem. Soc.* **1998**, *120*, 6024-6036.

Zhao, S.; Shen, Z.; Duo, L. Heavy metal uptake and leaching from polluted soil using permeable barrier in DTPA-assisted phytoextraction. *Environ. Sci. Pollut. Res.* **2015**, *22*, 5263-5270.

Zhao, Y.; Zhou, D.; Zhang, T.; Yang, Y.; Zhan, K.; Liu, X.; Min, H.; Lu, X.; Nie, R.; Xia, Q. High-Rota Synthesis of Single-/Double-/Multi-Unit-Cell Ti-HSZ Nanosheets To Catalyze Epoxidation of Large Cycloalkenes Efficiently. *ACS Appl. Mater. Interfaces* **2018**, *10*, 6390-6397.

Zhuravlev, L. T. The surface chemistry of amorphous silica. Zhuravlev model. *Colloids Surf., A* **2000**, *173*, 1-38.

Zolfigol, M. A.; Khazaei, A.; Safaiee, M.; Mokhlesi, M.; Rostamian, R.; Bagheri, M.; Shiri, M.; Kruger, H. G. Application of silica vanadic acid as a heterogeneous, selective and highly reusable catalyst for oxidation of sulfides at room temperature. *J. Mol. Catal. A: Chem.* **2013**, *370*, 80-86.

Zucca, P.; Sanjust, E. Inorganic Materials as Supports for Covalent Enzyme Immobilization: Methods and Mechanisms. *Molecules* **2014**, *19*, 14139-14194.

Zukal, A.; Pastva, J.; Čejka, J. MgO-modified mesoporous silicas impregnated by potassium carbonate for carbon dioxide adsorption. *Microporous Mesoporous Mater.* **2013**, *167*, 44-50.

## SECTION A. CHAPTER 3 APPENDIX

### A.1 Calculating k for Eyring Plots

Reactions were run in triplets at various temperatures. Measurements were taken every 5 minutes up until 20 minutes and one time point at 40 minutes. For the peroxyacid reactions, the data was treated for a 1<sup>st</sup> order reaction. The data was plotted time (seconds) versus  $\ln[\text{sulfide remaining, M}]$ . From that data, the following relationship holds true for a 1<sup>st</sup> order reaction (**Equation A1**):

$$\ln [\text{sulfide}]_t = -kt + \ln [\text{sulfide}]_0 \quad (\text{A1})$$

where slope is equivalent to  $-k$ . For the <sup>t</sup>BuOOH data, the reaction was treated as 2<sup>nd</sup> order as 1<sup>st</sup> order kinetic did not fit the data. For 2<sup>nd</sup> order, the data was plotted time (seconds) versus  $1/[\text{sulfide remaining, M}]$ . From that data, the following relationship holds true (**Equation A2**):

$$\frac{1}{[\text{sulfide}]_t} = kt + \frac{1}{[\text{sulfide}]_0} \quad (\text{A2})$$

where the slope is equivalent to  $k$ . These rate constants were then replotted to obtain kinetic data in an Eyring Plot. The data can be seen in **Table A1 and Table A2**.

**Table A1.** Kinetic Data for Eyring Plot of the Oxidation of CEES Using Aldehyde/O<sub>2</sub> as an Oxidant.

T (K)	k	1/T (K <sup>-1</sup> )	ln(k/T)
275.15	0.000425	0.003634	-13.3801
284.48	0.000713	0.003515	-12.8686
293.48	0.001514	0.003407	-12.1841
304.15	0.001422	0.003288	-12.2537
313.15	0.00095	0.003193	-12.7057
327.15	0.000565	0.003057	-13.296

**Table A2.** Kinetic Data for Eyring Plot of the Oxidation of CEES Using <sup>t</sup>BuOOH as an Oxidant.

T (K)	k	1/T (K <sup>-1</sup> )	ln(k/T)
286.48	1.3295	0.003491	-5.3728
293.65	1.7098	0.003405	-5.1460
307.48	3.0231	0.003252	-4.6221

## A.2 Calculating k for Hammett Plots

Reactions were run in triplets with varied sulfides. Two measurements were taken at 5 and 10 minutes and then every 10 minutes until 30 minutes. The reactions were treated with 1<sup>st</sup> order kinetics and followed the same relationship as rate constants obtained for the Eyring Plot. The data was plotted time (seconds) versus ln[sulfide remaining, M]. From that data, a 1<sup>st</sup> order reaction was observed (**Equation A1**). The k constant from **Equation A1** is equal to  $k_x$  for the different substituted methyl phenyl sulfides and  $k_H$  represents methyl phenyl sulfide. The  $\sigma_p$  values were obtained from the literature. The Hammett Plot is a type of linear free energy relationship. The original relationship is based off of work with benzoic acid but is heavily used for other systems as well. The relationship can be used with solubility constants (K) or rate constants (k) (**Equation A3**):

$$\log\left(\frac{K_x}{K_H}\right) = \rho\sigma_x \quad (\mathbf{A3})$$

$$\log\left(\frac{k_x}{k_H}\right) = \rho\sigma_x \quad (\mathbf{A4})$$

By plotting  $\log\left(\frac{k_x}{k_H}\right)$  versus the Hammett parameter, the reaction constant (also termed the sensitivity constant) is equivalent to the slope.

**Table A3. Kinetic Data for Hammett Plot Data.**

Sulfide	Rate (mmol/hr)	k	log (k <sub>x</sub> /k <sub>H</sub> )	σ <sub>p</sub> values
4-Fluorophenyl methyl sulfide	0.459 ± 0.03	0.285	0.02844	0.06
4-Methoxythioanisole	0.239 ± 0.03	0.067	-0.5999	-0.12
Methyl phenyl sulfide	0.453 ± 0.1	0.267		
4-Bromophenyl methyl sulfide	0.512 ± 0.04	0.342	0.10675	0.23

### A.3 Sterics and comparison of sulfide versus sulfoxide

In comparing the rates of CEES, methyl phenyl sulfide and diphenyl sulfide, there is no negative correlation of size upon the rate (**Table A4**). Therefore, there is no steric hindrance observed. In comparing the rate of diphenyl sulfide with diphenyl sulfoxide, the rate of oxidation for diphenyl sulfide was faster than diphenyl sulfoxide (**Figure A1**).

**Table A4. Steric Effects.**

Sulfide	Rate (mmol/hr)
2-Chloroethyl ethyl sulfide	0.242 ± 0.02
Methyl phenyl sulfide	0.453 ± 0.1
Diphenyl sulfide	0.373 ± 0.08

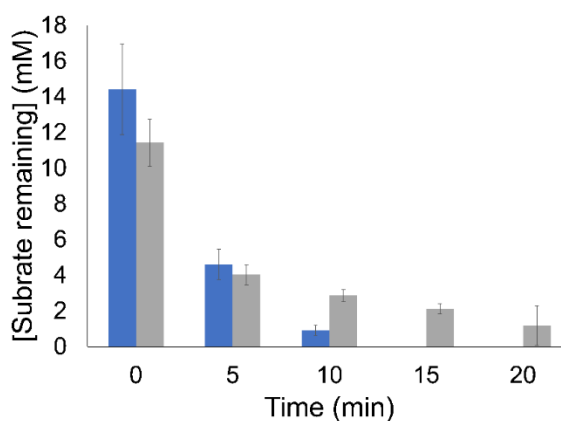


**Figure A1.** The oxidation of diphenyl sulfide (blue) versus the oxidation of diphenyl sulfoxide (grey).